SYSTEMS MODELLING AND ETHICAL DECISION ALGORITHMS FOR AUTONOMOUS VEHICLE COLLISIONS

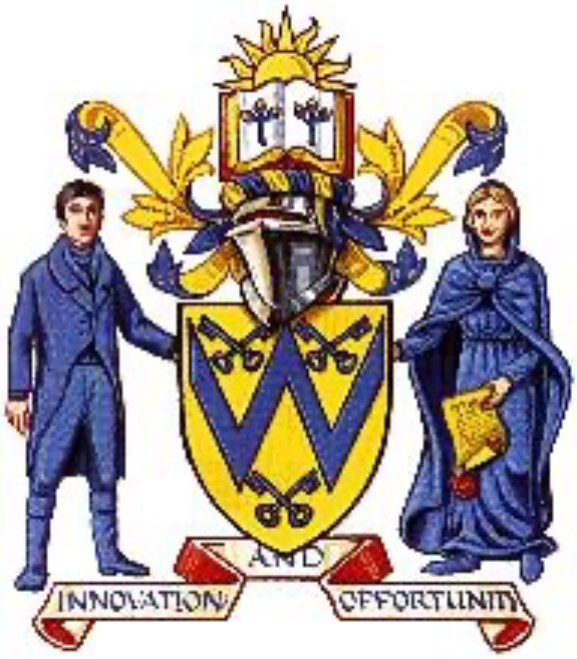

James Edward Pickering

University of Wolverhampton

August 2020

A Thesis submitted in partial fulfilment of the University's requirements for the degree of Doctor of Philosophy

ABSTRACT

There has been an increasing interest in autonomous vehicles (AVs) in recent years. Through the use of advanced safety systems (ASS), it is expected that driverless AVs will result in a reduced number of road traffic accidents (RTAs) and fatalities on the roads. However, until the technology matures, collisions involving AVs will inevitably take place. Herein lies the hub of the problem: if AVs are to be programmed to deal with a collision scenario, which set of ethically acceptable rules should be applied? The two main philosophical doctrines are the utilitarian and deontological approaches of Bentham and Kant, with the two competing societal actions being altruistic and selfish as defined by Hamilton. It is shown in simulation, that the utilitarian approach is likely to be the most favourable candidate to succeed as a serious contender for developments in the programming and decision making for control of AV technologies in the future.

At the heart of the proposed approach is the development of an ethical decision-maker (EDM), with this forming part of a model-to-decision (M2D) approach. Lumped parameter models (LPMs) are developed that capture the key features of AV collisions into an immovable rigid wall (IRW) or another AV, i.e. peak deformation and peak acceleration. The peak acceleration of the AV is then related to the accelerations experienced by the occupant(s) on-board the AV, e.g. peak head acceleration. Such information allows the M2D approach to decide on the collision target depending on the selected algorithm, e.g. utilitarian or altruistic. Alongside the EDM is an active collision system (ACS) which is able to change the AV structural stiffness properties. The ACS is able to compensate for situations when AVs are predicted to experience potentially severe and fatal injury severity levels.

ACKNOWLEDGEMENTS AND DEDICATION

I wish to acknowledge the following:

Keith James Burnham, supervisor, colleague and friend

Zena Joan Pickering, Mum

For their support throughout the journey of completing this thesis

I dedicate this thesis to Keith James Burnham, Keith's father – in memory

(1934 – 2018)

'He lived the life he loved and loved the life he lived'

CONTENTS

LIST OF TABLES

LIST OF FIGURES

NOMENCLATURE

ABREVIATIONS AND ACRONYMS

ABS	Anti-lock braking system
ACC	Adaptive cruise control
ACS	Active collision system
ADAS	Advanced driver assisted system
AEB	Automatic emergency braking
ASS	Active safety system
ATD	Anthropometric test device
AV	Autonomous Vehicle
CAN	Control area network
CCSA	Centre for Collision Safety and Analysis
CTAC	Control Theory and Applications Centre
DOF	Degrees of freedom
ECS	Ethical collision system
EDM	Ethical decision-making
EPAS	Electric power assisted steering
ESC	Electronic stability control
Euro NCAP	European New Car Assessment Programme
FE	Finite element
FMVSS	Federal Motor Vehicle Safety Standard
GPS	Global positioning satellite
GWU	George Washington University
HDV	Human driven vehicle

IMU	Inertia measurement unit
IRW	Immovable rigid wall
KF	Kalman filter
LIDAR	Laser imagining detection and ranging
LLS	Linear least squares
LPM	Lumped parameter model
LSTC	Livermore Software Technology Corporation
NCAC	National Crash Analysis Centre
NHTSA	National Highway Traffic Safety Administration
M2D	Model-to-decision
OEM	Original equipment manufacturer
OTS	On the spot
RADAR	Radio detection and ranging
RTA	Road traffic accidents
TYS	Toyota Yaris Sedan
US NCAP	United States New Car Assessment Programme
UK	United Kingdom
USA	United States of America
V2I	Vehicle to infrastructure
V2V	Vehicle to vehicle
V2X	General vehicle to anything
VBS	Vehicle body structure
VRU	Vulnerable road user
3D	3-dimensional

1. INTRODUCTION

1.1 INTRODUCTION

Over the past few years, there has been an increasing interest in autonomous vehicles (AVs). The advent of the AV is currently receiving attention from companies such as Apple, Google and Tesla, who are all developing their own AVs. In (Smith, 2013), it is stated that 90% of current road traffic accidents (RTAs) are caused by human error. This is a significant number considering that in 2019, there were 1870 deaths recorded on the roads in the UK (on average, just over 5 deaths per day), see (Dhani, 2019). It is estimated that collisions involving AVs are likely to be significantly reduced. However, the introduction of a fleet of AVs will not be completely without incidents (Crew, 2015). It is considered inevitable that collisions will take place between AVs and AVs and road infrastructure, e.g. immovable rigid walls (IRWs) and pedestrians, as well as non-AVs, particularly during the transition phase to AVs. With the introduction of AVs, this takes the human driver 'out of the loop' and entrusts a machine to make ethical decisions in the event of a collision. Such ethical decision-making issues have been considered by other authors, see for example (Lin, 2013), (Goodall, 2014) and (Bonnefon, Shariff and Rahwan, 2016).

1.2 MOTIVATION

Even with the transition from human-driven vehicles (HDVs) to AVs, it is expected that there will still be unavoidable collisions, especially in the phase prior to technology maturity. The research was initially motivated by the development of a system that minimises the number of serious injuries and fatalities of the occupants on-board an AV

in the event of an unavoidable collision. This involved the development of an active stiffness controller for the crumple zones of future AVs. The active stiffness controller has the ability to alter the crumple zone stiffness to minimise the injury severity, e.g. either to stiffen to reduce peak deformation or to soften to reduce occupant peak acceleration. The research was further motivated by work reported in (Goodall, 2014), where the need for AVs to make ethical decisions in terms of collision target selection was introduced. Considering Figure 1-1, where an AV will potentially collide into an IRW or a pedestrian (left) or another AV (right), it is postulated that the active stiffness controller would attempt to reduce the injury severity in both scenarios. The research question then focuses more on the collision target aspects, with the attendant ethical perplexities borrowing ideas from the classical trolley problem (Foot, 1967). The trolley problem involves a runaway trolley on course to kill five people on a track, unless action is taken to change the course of the trolley and instead kill only one person. The two possible outcomes to this problem correspond to two philosophical doctrines which are considered in this work. The deontological approach allows the trolley to take its natural course, i.e. killing five people. In contrast, the utilitarian approach aims to save as many people as possible, i.e. killing one person. Considering Figure 1-1, if a collision is unavoidable, the question is introduced: what 'target' should the AV steer into? In both of the scenarios illustrated in Figure 1-1 (left and right), there are two possible outcomes, and each will possess a degree of severity (injury levels and fatalities). Answering this question is the main motivation and focus of the research documented in this thesis – to generate a systematic approach that selects a path in the case of an unavoidable collision based on *a priori* knowledge, e.g. to reduce the injury severity levels and the number of fatalities. However, it should be noted that although the main motivation of this research is to minimise injuries and fatalities, users of AVs may not wish to subscribe to such an approach. Other AV decision making approaches will also be investigated, with these based on traits of human nature and referred to as the social

actions (Foster, Wenseleers and Ratnieks, 2001). At the time of writing, the utilitarian approach is currently viewed as being the likely approach for an AV ethical collision system, see (Bonnefon, Shariff and Rahwan, 2016).

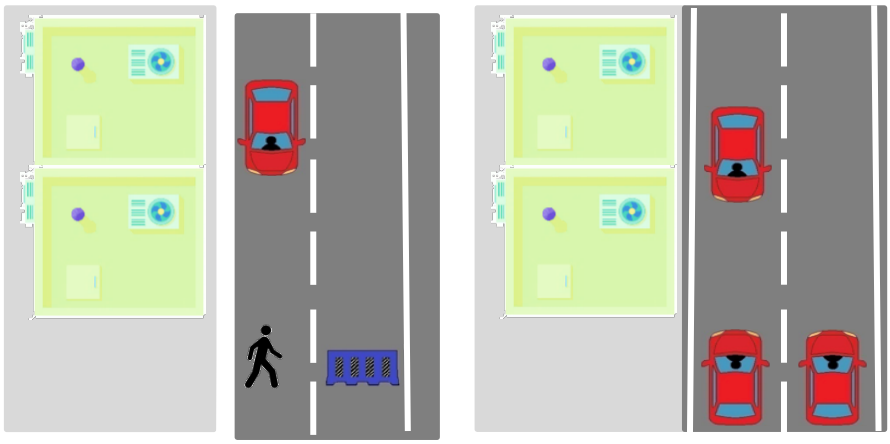

Figure 1-1: *Illustrating an Autonomous Vehicle (Upper Autonomous Vehicle, Left and Right) Making a Decision Between Swerving to Avoid 1 Pedestrians and to Collide into a Immoveable Rigid Wall (Left) and Making a Decision Between Swerving to Avoid a Given Autonomous Vehicle in the Path and to Collide Head-on with another Autonomous Vehicle (Right)*

1.3 AIM, OBJECTIVES AND STEPS

The **thesis aim** is to develop an ethical computation framework, known as the ethical collision system (ECS) to investigate the ethical decisions involved when AVs need to select the collision target. The collision cases considered in this work include an AV selecting either an immovable rigid wall (IRW) or pedestrian(s) as well as the case where an AV needs to select another target AV from potential multiple options. The ECS operates by making use of a model-to-decision (M2D) approach and involves two main stages. The first stages involves the use of a M2D approach for collision target selection, using an ethical decision maker (EDM) and lumped parameter model (LPM). The second stage involves an active stiffness controller will also be considered to reduce the severity of collisions into IRWs and other AVs. The act of an AV selecting the collision target and deploying stiffness control will form the active collision system (ACS). As with the EDM, the ACS operates by making use of a M2D approach, where information is extracted from an active LPMs that have been developed to capture the considered collision scenarios.

The **thesis objectives and steps** of this research are as follows:

1. Develop a computational ethical framework, known as the ECS that uses a M2D approach, which allows for the collision 'target' to be pre-determined based on a selected algorithm (philosophical approaches or social actions), and also for the considered collision scenarios to be improved using an active stiffness controller applied to the crumple zones of the AV
2. Investigate typical full-frontal collision properties through the use of finite element (FE) modelling involving a 2010 Toyota Yaris Sedan (TYS) over a range of collision velocities and vehicle laden mass values such that the FE model can then be taken as a realistic surrogate for the actual collision
3. Develop a second set of surrogate models in the form of single and two-vehicle LPMs that accurately capture the collision energy and the FE key structural

outputs (i.e. peak deformation, peak head and chest acceleration) and capture the values within look-up tables for subsequent interpolation

4. Investigate the effect of changing the structural stiffness of the single-vehicle collision LPM, forming look-up tables from the outputs and postulate concept of active stiffness control of AV crumple zones
5. Using the outputs from the LPMs (single and two-vehicle), develop levels of injury severity using existing standards of the European New Car Assessment Programme (Euro NCAP), Federal Motor Vehicle Safety Standard (FMVSS) and literature (i.e. for pedestrian safety) for the considered collision scenarios (AV to pedestrian/IRW/AV)
6. Develop a multi-layered interpolation method for interpolating between the stored points of the developed look-up tables based on using fuzzy logic
7. As part of the M2D collision 'target' selection approach/algorithm, for the EDM, develop algorithms which encompass the philosophical approaches and social actions
8. As part of the M2D active stiffness controller approach, develop an algorithm to emphasise injury severity to influence/avoid large utility costs to society
9. Simulate the determined collision scenarios using the developed EDM and ACS that utilises the LPMs and active LPMs, document results, undertake a quantification/verification analysis
10. To develop the basis of a simulation tool to allow a flexible MATLAB based design via simulation approach for investigating AV collision scenarios

1.5 OUTLINE OF THESIS

An outline of the research presented in each of the chapters is now given in the order they appear in the thesis. Each subsequent chapter builds upon the previous chapters to form a logical sequel.

Chapter 2 presents the background to AVs and the ethical issues that need to be addressed when considering the widespread launch of a fleet of AVs. In terms of computational ethics programming, the publicly available knowledge of the acceptance of AVs in terms of the utilitarian and deontological principles are reviewed. Further to these two philosophical doctrines (i.e. utilitarian and deontological approaches) that are viewed as viable solutions for AV collision target decision making, social actions are also considered. Emphasis is placed on the four basic social actions, these being: mutualism, altruism, selfishness and spite. However, mutualism and spite are ruled out in the context of programming for a fleet of AVs.

Chapter 3 presents a section summarising the problem statement, the scenarios to be considered and a proposed road map. An outline of the proposed ACS is then given that takes a nature-inspired M2D approach. Details of the required technology are given, e.g. vehicle-to-vehicle (V2V) communication, vehicle mass estimation and collision velocity prediction. A basic overview is then given of the collision target selection algorithm and the active crumple zone algorithm. To conclude, the working assumptions are presented for the development of the ECS.

Chapter 4 presents the background to current vehicle collision safety. It considers automotive vehicle crashworthiness design, describing the features of the vehicle crumple zones and passenger compartment and the full-width frontal impact test. In the absence of actual collision data, a FE simulation involving a Toyota Yaris Sedan (TYS) is implemented to obtain simulated crash data for single-vehicle collisions. The TYS output data of acceleration versus time is fed into a sled model to obtain occupant head and chest accelerations. Similar to the single-vehicle collision safety, the background into two multiple vehicle (two-vehicles) collision safety is then undertaken. Finally, sections

on the current developments in active collision structures and vulnerable road users (VRUs) are presented, with the emphasis of the latter being on pedestrian safety.

Chapter 5 presents single AV collision models and-in line with the United States Car Assessment Programme (US NCAP), with consideration given to full-frontal collisions with an IRW. In this Chapter, linear and nonlinear models are explored (both static and dynamic models). Dynamic models based on second-order lumped point mass and spring are developed, tuned and compared to the TYS FE simulation data. Based on the collision modelling, and the FE data forming an effective surrogate verification is undertaken to ensure the model behaves as expected.

Chapter 6 considers two AVs in a full-frontal collision and uses the same modelling approach as in Chapter 5, thus linear and nonlinear modelling approaches. A single linear lumped point mass and spring model is developed for each AV and a nodal three degree of freedom model of the connected two AV system is simulated. An equivalent modal model is also developed and simulated. The simplicity and transparency of the modal formulation make it an appealing choice as the eigenvalues corresponding to the stiffness to mass ratios are explicitly available. Based on the collision modelling, verification based on the fundamental laws of physics is undertaken to ensure the models nodal/modal behave as expected.

Chapters 7 and 8 present the method (Stages 1 and 2) used to pre-determine the collision injury severity levels for single-vehicle collisions (Chapter 7) and multiple vehicle collisions (Chapter 8). The AV collision injury severity levels of interest are peak deformation, peak head acceleration and peak chest acceleration, with these explored over a range of collision mass and velocity values. The injury severity levels of pedestrians is also of interest, with the effects of pedestrian impact velocity investigated.

A common utility cost unit for collision injury severity using a Euclidean metric is then developed, with this allowing the four features (peak deformation, peak head acceleration, peak chest acceleration and pedestrian impact velocity) to be compared. The collision target selection algorithms (Stage 3) are then developed and tested, along with the stiffness controller (Stage 4).

Chapter 9 presents the overall conclusions and further work.

Throughout the development of this research, various assumptions are made; with a full list being presented in Appendix 1.0.

1.6 CONTRIBUTIONS

The main research contributions within this thesis are summarised and listed in the order of importance as perceived by the author.

The development of a **computational ethics framework,** known as the **ECS** that permits AVs to make informed decisions in terms of **collision target selection**. At the hub of the developed ECS, pre-determined collision outcomes are used and a M2D approach. To capture the pre-determined collision outcomes, LPMs were developed that emulate the observed phenomenon of single AV (into IRW) and two AV collisions over a range of values for laden mass and collision velocity. Although the LPMs could be used onboard the AV, to reduce the computational time, look-up tables are developed based on the models over a range of laden mass and collision velocity values. Fuzzy logic is then used as an interpolation method to extract intermediate information between the pre-stored values of the look-up tables. Using the LPMs and pre-determined collision outcomes, injury severity levels could then be applied to collision outcomes. It was then possible to evaluate and relate various collision scenario outcomes via a common utility cost unit. With pre-determined collision injury severity levels, an EDM was developed, where philosophical doctrines (utilitarian and deontological) and social actions

(altruism and selfishness) algorithms were developed to test various collision scenarios, e.g. AV to 10 pedestrians/IRW or AV to AV/AV. The simulation findings over the given scenarios suggest the utilitarian and altruism algorithms are desirable in terms of the reduced cost to society, with the selfishness approach being the worst in terms of the largest cost to society when running the algorithms. The initially developed computational ethics framework has been very insightful in terms of how to programme future AVs. To the author's knowledge, this is the first attempt at applying an computational ethics framework to AV ethical problems, and no literature on this specific topic exists.

Further development to the **computational ethics framework** was on the topic of an **active stiffness controller** onboard future AVs, forming part of the ACS. The initial aim of the stiffness controller was to reduce the injury severities of a collision, hence improve safety. For this, the active LPMs for the collision target selection are used (where the stiffness value can be altered), along with fuzzy logic to obtain intermediate values from pre-determined stored points. The LPMs were used to demonstrate the effect of changing the structural stiffness properties, with an active stiffness control algorithm developed. In the case of the single vehicle, the potential benefit of the stiffness controller was demonstrated, initially with collision scenarios considering excessive peak deformation, i.e. beyond the design deformation length. Similarly, for the two-vehicle collision case, the stiffness controller algorithm was demonstrated to effectively transform that of a collision with two AVs experiencing excessive peak deformation, to two AVs where the peak deformation was within the design deformation length. The approach demonstrates the effectiveness of two colliding vehicles working together to create a better collision scenario for all involved. To the author's knowledge, the developed ECS and the accompanying controlled ACS represent

novel contributions to the field of automotive vehicle safety. The ACS forms a patent that has been granted in the UK and US, see Appendix 2.0.

A further contribution is the **bilinear modelling procedure** to create LPMs that accurately capture the deformation versus force characteristic from FE collision data. This has been developed for the single-vehicle collision case in Chapter 5 and the two-vehicle collision case in Chapter 6. The approach is extremely effective in capturing the key collision characteristics, i.e. peak deformation, peak acceleration and collision deformation energy and offers a relatively simplistic approach in terms of tuning the model. The nonlinear modelling approach has been successfully applied in nodal and modal form for single and two-vehicle collisions. There is very limited literature on the topic of nonlinear modelling of the deformation versus force characteristic, and to the knowledge of the author, the bilinear model in nodal and modal form presents a novel approach for modelling vehicle collision phenomenon.

2. AUTONOMOUS VEHICLE COLLISIONS: THE ETHICAL DILEMMA

2.1 INTRODUCTION

Whilst it is known that almost 90% of road traffic accidents (RTAs) are caused by human error (Smith, 2013), the introduction of a fleet of driverless autonomous vehicles (AVs) will not completely be without errors (Crew, 2015). Technology is continually evolving but it is predicted that there will still be human-driven vehicles (HDVs) and other anomalies to deal with. However, in general, it is considered that road safety will be improved with the advent of the AV. This Chapter introduces the current developments in AV's and focuses on the ethical dilemma when considering AV collisions. Current AV technology is presented and the five levels of vehicle automation defined by the United States National Highway Traffic Safety Administration (US NHTSA) are then described. Details are presented regarding the current cutting-edge AVs being developed today, i.e. the US NHTSA Level 2 Tesla S. It is expected that AVs will not operate entirely without system failures, especially in the early days of operation. With the human driver removed from the control loop, it becomes clear that should an unavoidable collision scenario arise, solutions to some very serious ethical questions are needed. For example, making an ethical decision between colliding into one pedestrian or a group of pedestrians or an immovable rigid wall (IRW). A possible solution to the AV collision ethical dilemma involves the well-known thought experiment known as the 'trolley problem' (Lin 2013). The trolley problem allows different and potentially conflicting philosophical views to be explored as the bases for an ethical decision algorithm for use

on-board an AV. This Chapter focuses on highlighting the issues and proposes potential computational ethical guidelines based on well-established philosophical foundations, namely those of Jeremy Bentham and Immanuel Kant, whose doctrines are known as the utilitarian and deontological approaches, respectively. Further to the detailed philosophical actions (i.e. the doctrines of Kant and Bentham), social actions based on nature will also be explored, i.e. mutualistic, selfish, altruistic or spiteful (Hamilton 1964a, 1964b). Such social actions are viewed as being a potential solution to how future AV's are programmed in the event of entering into an unavoidable collision.

2.2 CURRENT DEVELOPMENTS IN AUTONOMOUS VEHICLES

Advanced driver assisted systems (ADAS) on-board vehicles have evolved over the last two decades with the basic building block being that of adaptive cruise control (ACC). Other ADAS features include electronic stability control (ESC), anti-lock braking system (ABS), automatic emergency braking (AEB), electric power-assisted steering (EPAS), collision avoidance using a combination of EPAS and ABS, lane following and automatic parking. Vehicles equipped with ADAS make use of multiple sensors, actuators, control algorithms and microprocessors to execute the control functions (Belmonte et al., 2020). For road and lane accuracy, the ADAS uses a combination of radio detection and ranging (RADAR), laser imaging detection and ranging (LIDAR), ultrasonic, global positioning satellite (GPS) module, inertia measurement unit (IMU) and digital camera technologies. For an authoritative account of advances in ADAS, see (Lu, Wevers and Heijden, 2005) and (Gerónimo et al.,2017). It is envisaged that future ADAS systems will evolve to the point where there is no driver intervention; in effect becoming a full autonomous vehicle (AV), being defined by United States National Highway Traffic Safety Administration (US NHTSA) as a Level 5 AV, see Table 2-1.

As introduced above, techniques involving RADAR, LIDAR, GPS, IMU and cameras will be used to sense the surroundings, e.g. traffic lights, road signs, other vehicles and road

obstacles including pedestrians. Object recognition and tracking are already being developed for this purpose. The current techniques and technologies are rapidly evolving to provide continuous improvement. Using fast processors, intelligent control algorithms with decision-making abilities will need to be used for aspects of AV navigation, e.g. optimal gear choice, propulsion, conditions affecting operation such as the weather conditions and lane changing. In addition to the features introduced above, the system will be vulnerable to cyber-attacks and it is also likely that the AV will require some secure communication, i.e. vehicle to vehicle (V2V), vehicle to infrastructure (V2I) or in general, vehicle to anything (V2X), see (Yang et al., 2004) and (Litman, 2014).

Consequently, it is considered that realisation of the Level 5 AV will require a world-wide agreement among the original equipment manufacturers (OEMs) for a generic format and secure technology for V2X of a future AV fleet.

Table 2-1: *National Highway Traffic Safety Administration Road Autonomous Vehicle Levels (NHTSA, 2019)*

Level of Automation	Description
Level 0	The human driver is in full operation of the vehicle.
Level 1	An advanced driver assistance system (ADAS) on the vehicle can sometimes assist the human driver with either steering or braking/accelerating, but not both simultaneously.
Level 2	An ADAS on the vehicle can itself control both steering and braking/accelerating simultaneously under limited circumstances. The human driver must continue to pay full attention ("monitor the driving environment") at all times and perform the rest of the driving task.
Level 3	An Automated Driving System (ADS) on the vehicle can itself perform all aspects of the driving task under some circumstances. In those circumstances, the human driver must be ready to take back control at any time when an ADS requests the human driver to do so. In all other circumstances, the human driver performs the driving task.
Level 4	An ADS on the vehicle can itself perform all driving tasks and monitor the driving environment – essentially, do all the driving – in certain circumstances. The human need not pay attention in those circumstances.
Level 5	An ADS on the vehicle can do all the driving in all circumstances. The human occupants are just passengers and need never be involved in driving.

2.2.1 DEVELOPMENTS OF AUTONOMOUS VEHICLES

At the time of writing, a number of developments in AVs are beginning to emerge and highlights of some of these technologies are briefly described in this sub-section.

It is interesting to witness the development of the AV, with practical trials taking place in designated cities in the United Kingdom (UK), including Coventry, see (Sutcliffe, 2019). The trials in Coventry took place between 2015 and 2018 and involved a demonstration of autonomous driving in a busy mixed-use semi pedestrianised city centre. The project concluded and highlighted several challenges faced by AVs. Areas of particular interest include dealing with pedestrian detection and avoidance, dealing with potholes and relying on the use of GPS to keep the vehicle in the desired road lane.

In 2017, Audi A8 was claimed to be the first production vehicle to reach Level 3 of vehicle automation, see (McAleer, 2017). In the United States of America (USA), in 2018, Waymo (originating from Google) stated that its test AV had travelled 10,000,000 miles, with this increasing by 1,000,000 miles per month, see (Laris, 2018). More recently, in 2020, Waymo announced that its AV had driven 20,000,000 miles in 25 cities, see (Wiggers, 2020). Other OEMs have announced their plans to bring fully developed AVs to the market (i.e. NHTSA Level 5 of autonomy), such as Uber, Ford, Tesla, Baidu, Apple, Waymo, Mercedes and General Motors. At the Consumer Electronics Show of 2017, Ford executives stated that it would have fully AVs on the road with no steering wheel or pedals by 2021, see (Murphy, 2016) and (Ford, 2020). Tesla CEO Elon Musk claims that Tesla will have fully automated vehicles by the end of 2020, along with 'robo-taxis', see (Howard, 2019). Currently, Tesla is producing vehicles on today's roads with the required software and sensors to have limited to self-driving automation at NHTSA Level 2. In 2017, Las Vegas launched its first AV which provides an electric shuttle service on public roads, with the route taking the AV through congested traffic on the busy Las Vegas Boulevard to 8th Street. The AV had previously undergone test trials at the University of Michigan and the University's M-city testing ground; this being a simulated city for testing AVs, see (M-city, 2017). The pioneering work on the development of an electric AV named 'Navya', in which the University of Michigan in partnering with major OEMs has been witnessed when the author participated in an invited visit in April 2017. An image of the Navya AV in the M-city test ground is shown in Figure 2-1.

Automated shuttle buses and later driverless taxi services are considered by the author to be the next potential stepping stone towards the large-scale release of AVs. With the growing interests of many existing leading vehicle manufacturers and high-tech industries having multi-billion-dollar budgets, it seems highly likely that AVs in large

numbers will imminently appear on the roads soon, i.e. the next 10 – 20 years. In 2019, Uber (taxi service company) announced it's third-generation AV that has been developed in partnership with Volvo, see (O'Kane, 2019). Updates to the AV have been introduced since the second-generation AV collided and killed a pedestrian (more details are given in Section 2.2.2), see (Hawkins, 2019). Other recent developments include Mercedes-Benz and Bosch partnering together to develop an automated taxi service in San Jose, California, USA, see (Hawkins, 2019).

Also, the introduction of AVs could allow the elderly, disabled and visually impaired to travel using such a vehicle, see (Howard, 2014). It is also the view held by (Mladenović, Abbas and McPherson, 2014) that the widespread future introduction and uptake of AVs will revolutionise the very way in which human society evolves itself as the technological developments themselves continue to evolve. It is also claimed in (Friedrich, 2016) that the use of AVs should increase traffic efficiency of mobility, thus reducing pollution and the overall carbon footprint and reduced pollution to the environment.

Figure 2-1: *Electric AV named Navya being 'Driven' around the M-City Test Ground at the University of Michigan, see (M-city, 2017)*

2.2.2 AUTONOMOUS VEHICLE INCIDENTS AND FATALITIES

Since the introduction of AVs (at various Levels of automation, see Table 2-1 in Section 2.2) on public roads worldwide there have been a number of incidents and fatalities recorded. In 2016, since being in operation since 2009, Google's self-driving project, re-branded Waymo, exceeded 2 million miles self-driven on the public highway, see (Bhuiyan, 2016). In total, there were 20 recorded incidents, including at least one caused by the AV software, see (Google, 2016). This amounts to one accident on average every 100,000 miles. To add context, in 2015, data recorded from the NHTSA in the United States recorded an accident from a conventional human-driven vehicle (HDV) every 497,000 miles, see (Federal Highway Administration, 2016). Thus, this being over four times less abundant than recorded from the Waymo project to date. There have been several controversial incidents involving Tesla, i.e. the number of the Tesla AV fatalities due to technical faults. In 2014, Tesla introduced the 'Autopilot' mode of operation that gives Level 2 of automation. The introduction of such technology has been popular, but this has come with some failures/faults. The first recorded fatality in a Tesla that contains the 'Autopilot' mode came in 2016, see (Lambert, 2016), where the vehicle failed to slow down before the collision with a truck, see Figure 2-2. It is worth noting that due to the damage caused by the collision, it was not possible to transmit logged data to Tesla's servers to determine if the 'Autopilot' mode was engaged prior to the collision. Referring to the Tesla collision, if the AV had identified the truck, then the AV could have taken action to avoid the truck. However, this may then put the occupant at potential risk, e.g. steering into the path of oncoming vehicles in the next lane. In recent years, Tesla vehicles have been involved in a large number of collision scenarios involving parked vehicles/trucks, see (TeslaDeaths, 2020). In 2018, Uber's Level 3 AV collided and killed a pedestrian, see (Lee, 2019). The human driver, was not watching the road (this being a requirement of a Level 3 AV), and the sensors and algorithms only realised the collision would take place 1.2 seconds before impact, this being too late to

avoid colliding with the pedestrian, see Figure 2-3. Referring to the Uber collision, if the AV had identified the pedestrian, the AV could have taken action and swerved to avoid the pedestrian. However, this may then have put the operator at potential risk, e.g. steering into the path of an oncoming vehicle. A large number of the AV collision scenarios considered could have been avoided with 'better' software and sensors, however doing so may have resulted in a collision with another object/AV, which further highlights the need for ethical decision making. With the increasing number of AVs (at various autonomous levels) being introduced to the roads worldwide, it is the view of the author that there is an increasingly imminent need for ethical decision making, hence the motivation for the research presented in this thesis will be needed more and more.

Figure 2-2*: Tesla Vehicle not Identifying the Truck Ahead and Resulting in a Collision (Lambert, 2016)*

Figure 2-3: *Uber Vehicle Prior Failing to 'See' a Pedestrian (Lee, 2019)*

2.3 ETHICAL ISSUES WITH AUTONOMOUS VEHICLE COLLISIONS

It is considered inevitable that collisions will take place between AVs and AVs, AVs and pedestrian(s) and AVs and other road infrastructure, e.g. immovable rigid walls (IRWs). During the transition phase of introducing AVs at various levels of autonomy, there will be a mixed fleet with non-AVs, i.e. HDVs, and it is particularly during this early development phase where the technology is in its infancy where there are likely to be collisions. Therefore, the ethical issues are urgently required to be solved.

Such scenarios have been considered previously by other authors when discussing the ethical issues, see for example (Lin, 2013), (Goodall, 2014) and (Bonnefon, Shariff and Rahwan, 2016) and (Bonnefon, Shariff and Rahwan, 2019). Before the large-scale release of AVs, there are some major outstanding ethical issues to resolve. Even when the technology level matures to Level 5, the risk of AVs entering collisions at both the present time and in the future is inevitable (Goodall, 2014). If it is assumed that future AVs are likely to be involved in inevitable collisions, then vehicle collision safety measures will still be needed.

As stated above, it is anticipated, therefore, that AVs will inevitably be involved in collision scenarios requiring ethical decision making. To further emphasise the inevitable collisions that will occur with AVs, a scenario is illustrated in Figure 2.4. The scenario involves an AV having 'sight' of an IRW via on-board sensors (upper-left). The AV decides to maintain speed and steer around and thus avoid the IRW, however, a pedestrian then suddenly appears from behind a building (upper-right). The AV has the pedestrian in 'sight', however, based on the on-line calculations, the AV on the current course cannot avoid the pedestrian. A decision is therefore required to be needed regarding selection of the collision target, i.e. steering to collide into the IRW or to continue and collide with the pedestrian (lower).

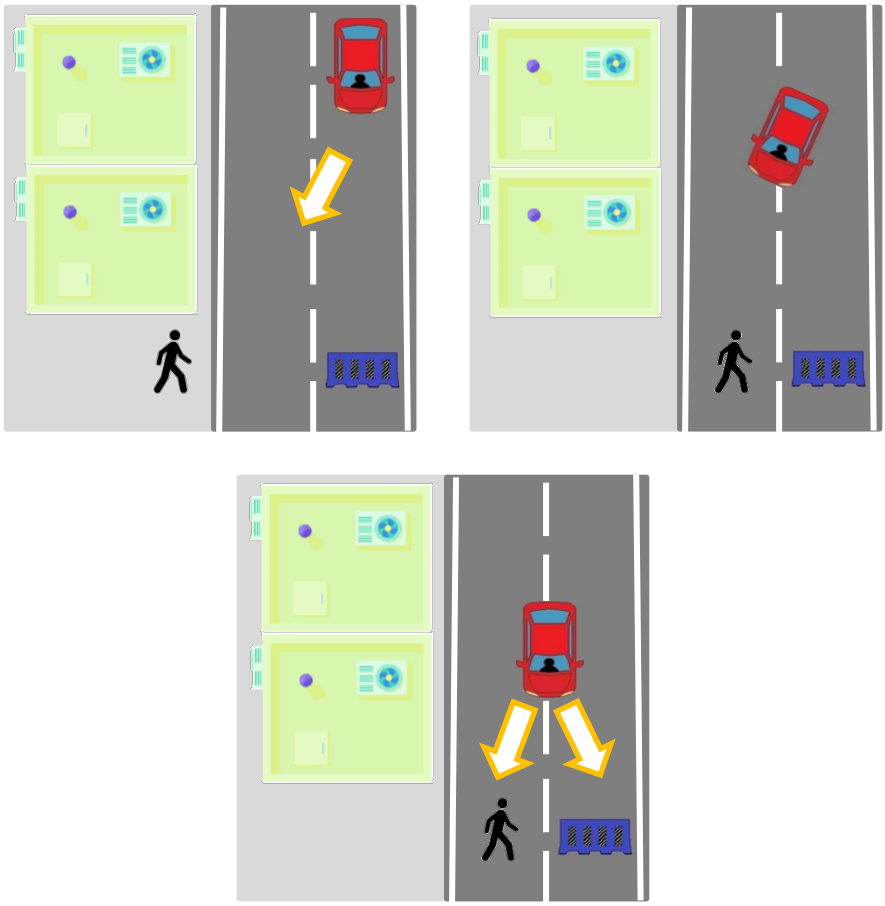

Figure 2-4: *Autonomous Vehicle Steering to avoid an Immovable Rigid Wall (Upper-Left), then taking Avoidance Action by Changing Paths but Steering into the Path of a Pedestrian that Steps into the Road from Behind a Building (Upper-Right) and then having to make a Decision in regards to the Collision Target (Lower)*

At present, there is a formidable debate taking place amongst OEMs and researchers concerning moral and ethical 'thinking' for AVs. Assuming passengers can not intervene, it is the authors view that it will be the AV manufacturers and not the passengers that decide on how to programme the AVs ethical decision-maker (EDM) algorithm, unless a user 'buy-in' option is permitted. AVs are certainly set to bring about a revolutionary societal change. However, the dichotomy is that before AVs are released on the roads, they will have to be programmed and this requires some serious ethical and legislative questions to be answered with onboard decision making and control algorithms being at the heart of this change. Proposing, debating and finally agreeing on what will

constitute a morally and ethically acceptable set of AV incident algorithms has been recognised as one of the most difficult challenges currently facing the transport technology industry today, see (Posadzki, 2016).

The following sub-sections introduce some of the ethical issues that have become apparent when presented with the introduction of AV technology. Some consideration is given to the 'thought experiments' that are currently of significant interest in the academic world, namely regarding the so-called 'trolley problem'. Current views on how an AV should be programmed in the event of a collision and public views of the ethical issues and the risks and unknowns, with reference to the trolley problem are also discussed.

2.3.1 THE TROLLEY PROBLEM

The trolley problem presents a philosophical thought experiment, see (Foot, 1967), (Thomson, 1985) and (Lin 2013), in which there is a runaway driverless trolley on course to collide and fatally kill five people who are trapped on the tracks unless a decision is taken to re-direct the trolley along a side track and instead kill only one person, see Figure 2-5. The most common response when posing this problem is for the trolley to be redirected so that five people are saved and only one person is fatally killed (Greene, 2013).

The trolley problem has been discussed in the literature of AV ethics, see for example (Lin, 2016) and (Bonnefon, Shariff and Rahwan, 2015) and (Bonnefon, Shariff and Rahwan, 2019). In these papers, the authors compare the ethics surrounding the development of 'accident-algorithms' for AVs to the runaway trolley problem. Lin (2016) states that the trolley problem is one of the most iconic thought-experiments and that such scenarios may now occur with the ever-closer introduction of AVs. However, (Kamm, 2015) questions why morally permitting scenarios are being presented where

a smaller number of people are killed to save a greater number. The author (Kamm) uses the example of why it is not permissible for a medical doctor to save five patients in need of transplants by 'harvesting' five organs from perfectly healthy patients who attended hospital for a routine check-up. The underlying decision in the background to the trolley problem is also said to be characterised as 'being made behind a veil of ignorance' as there are limited situations that can be considered, see (Rawls, 1971). For example, the five-people trapped on the track could be elderly or undesirables by society's standard, e.g. criminals and the one person trapped could be young or even a highly regarded member of the public.

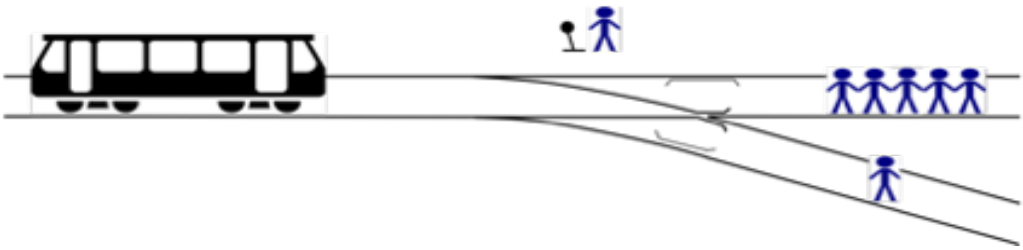

Figure 2-5: *Illustrating the Trolley Problem*

2.3.2 UTILITARIAN AND DEONTOLOGICAL APPROACHES

In (Nyholm and Smids, 2016), the authors present the following cases: should AVs be programmed to minimise the number of fatalities or should they be programmed to save a vehicle's occupants at all costs? The issue of how to programme AVs presents a significant ethical problem to be addressed. This is heightened with the rapid developments in the technology and the seriousness of the risks involved, i.e. the task of determining the most appropriate morally acceptable target in the case of an imminent collision. To highlight possible ethical issues, an example is presented here that is inspired by the work in (Goodall, 2014), (Dogan et al., 2016) and (Bonnefon, Shariff and Rahwan, 2016). The example involves an AV, in this case containing one healthy adult, with the AV having to make the decision between continuing its course to collide into ten pedestrians and causing ten fatalities, or to steer to avoid the ten pedestrians and instead collide into an IRW and cause one fatality, namely the occupant of the AV, as illustrated in Figure 2-6.

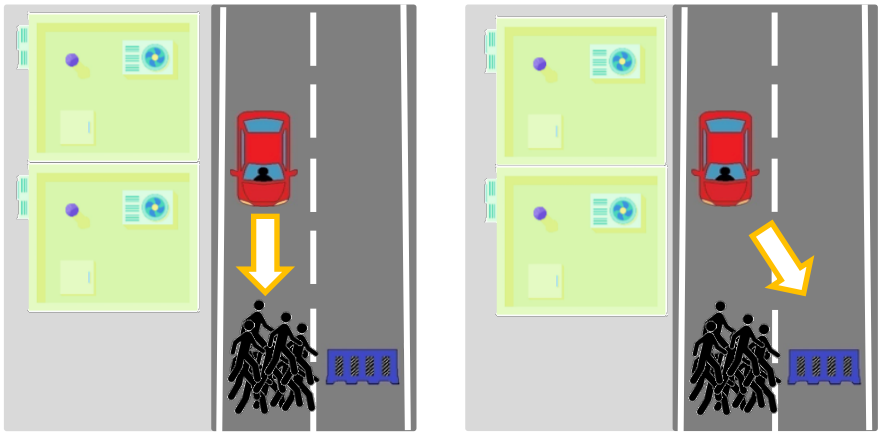

Figure 2-6: *Autonomous Vehicle Deciding Between Continuing On-Course to Collide into Ten Pedestrians or Steering and Colliding into a Solid Immoveable Wall*

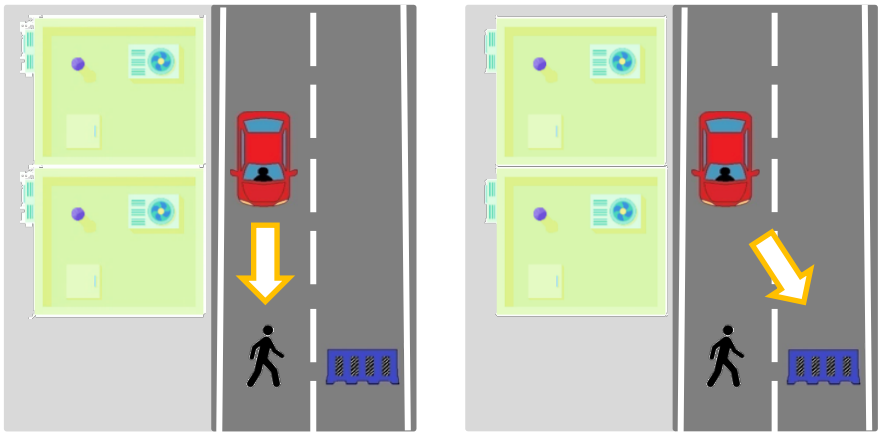

Figure 2-7: *Autonomous Vehicle Deciding Between Continuing On-Course to Collide into One Pedestrian or Steering and Colliding into a Solid Immoveable Wall*

There is currently much discussion on the ethics and decision making of AV collisions in the academic world, see for example references (Bonnefon, J.F., Shariff, A. and Rahwan, I., 2015), (Bonnefon, J.F., Shariff, A. and Rahwan, I., 2016), (Goodall, N.J., 2014), (Goodall, N.J., 2016), (Lin, P., 2013) and (Lin, P., 2016). Much of the literature details the philosophical doctrines of the English philosopher Jeremy Bentham and the German philosopher Immanuel Kant. The two philosophical doctrines are currently viewed as potential solutions to the AV ethics problem, see (Burns, J.H. and Hart, H.L.A., 1998) and (Kant, I., 2007). The philosophy of Bentham, known as the utilitarian approach involves minimising the cost to society via minimising loss of utility, or equivalently maximising utility, with all passengers within the AV representing an equal value to society. Therefore, the approach would involve saving as many lives as possible, even if this means deliberately sacrificing a small number of lives for the common good of the many. For the trolley problem presented in Section 2.3.1, Figure 2-5, a utilitarian approach would involve the runaway driverless trolley being re-directed away from the five-people trapped on the tracks to instead collide into the one person trapped. The deontological approach of Kant opposes that of Bentham, where such an approach requires that the AV obeys certain rules or duties, e.g. the AV could be programmed with the rule to always put the passengers of the AV at the lowest risk, even if more lives

would be lost. The deontological approach of philosopher Kant suggests that the AVs should follow their natural paths with no intention to take nor save any lives, i.e. if an action is not right for everyone involved to take, then it is not right for anyone.

Referring again to the trolley problem, illustrated in Figure 2-5, a deontological approach would mean the runaway driverless trolley would carry on-course and kill the five-trapped people. In likeness to the trolley problem, and referring to the example illustrated in Figure 2-6, the utilitarian approach would involve the AV steering to avoid the ten pedestrians (i.e. saving the ten pedestrians lives) and causing the fatality of the one occupant on-board the AV. The deontological approach, on the other hand, would involve the AV in Figure 2-6 to remain on its natural path and collide into the ten pedestrians (causing ten fatalities). A further interesting scenario is illustrated in Figure 2-7, where the AV contains one occupant and has the option of remaining on course to collide into one pedestrian or changing path and steering into the IRW. This introduces the need for a decision making process that can evaluate the collision severity of each outcome, especially so if steering into one collision path is less severe than the other. This introduces an interesting question, is it ethical for the AV to steer into the path of least severity?

Interestingly, the automotive vehicle manufacture Mercedes-Benz has stated that their designed AVs would run over a child rather than swerve and risk injuring the occupants on-board, see (Li and Cheer, 2016). The company insist that the technology on-board the AV would only be used to minimise the impact velocity, thus the severity of the collision.

2.3.3 PUBLIC VIEWS OF AUTONOMOUS VEHICLE ETHICAL ISSUES

In (Bonnefon, Shariff and Rahwan, 2015), a survey consisting of three separate studies involving independent groups of ordinary people is reported. The objective was to

assess their views on whether AVs should be programmed to be utilitarian, i.e. to minimise the number of fatalities in the case of an unavoidable collision. The outcome from Study 1 of the survey was that participants generally approved of utilitarian AVs making self-sacrifices to the same extent as they would approve for a HDV. The main deciding factor was the number of lives that would be saved. Participants agreed that it would be better to swerve to avoid a group of ten pedestrians and self-sacrifice, but not to swerve to save one pedestrian. Furthermore, the participants selected the option that the AV should swerve into one pedestrian to save another group of ten pedestrians. There was no evidence of the considerable influence of sex, age or religious belief among the participants. Participants were amenable to legally enforcing self-sacrifice for AVs, and there was greater comfort expressed of a utilitarian AV making this decision, rather than a human driver. From Study 2 of the survey, it was reported that participants generally supported others buying utilitarian AVs programmed for self-sacrifice, but they were less willing to buy such AVs themselves (even when the self-sacrificing AV would save ten lives). Most participants were in favour of saving ten lives but were not in favour of self-sacrifice to save the life of one pedestrian. When answering the question in Study 3 of which decision algorithm to choose between, a self-sacrificing AV, i.e. always swerve, a non-sacrificing AV, i.e. always stay on course, or a random decision, the score was split across the three. Whilst more than 75% of participants in Study 3 of the survey agreed that AVs should be self-sacrificial, i.e. utilitarian, less than 65% believed that AVs would be programmed this way. In other words, participants generally believed that AVs should be programmed for the greater good as far as pedestrians are concerned and less concerned about the safety of the occupants in the AV. However, they were less convinced that manufactures would programme AVs with this goal. Rather than being concerned about AVs being too utilitarian, they were generally wary that AVs would be programmed to protect their occupants at all costs. In a further survey paper by the same authors (Bonnefon, Shariff and Rahwan, 2016), a group was asked to

consider the scenarios like those described above, but when asked to imagine themselves as occupants within the AV they were also asked to imagine that a family relative was with them. Not surprisingly, this negatively affected the morality of the sacrifice compared to the person being alone. However, in all studies, participants expressed a moral preference for AVs sacrificing their occupants to save a greater number of pedestrians. Thus, the fundamental ethical question of whether AVs should behave in a utilitarian manner appears to be gaining public acceptance.

2.4 SOCIAL ACTIONS

Further to the detailed philosophical actions (i.e. the doctrines of Kant and Bentham) outlined in Section 2.3.2, social actions based on nature will now be explored. The topic of social actions has not yet been discussed in the literature of AV ethics, however, it is of interest to the author as a possible solution for resolving the ethical dilemma concerning decision making within algorithms of AVs. The subject of social actions in the natural world has been a hot topic for the last fifty years, e.g. ant colony policing of the workers and the social behaviour of penguins. Whilst traits of these instinctive behaviours exist in humans, the human moral and ethical judgmental actions can learn much directly from these other observations in nature. Such observations are of particular relevance when considering the ethical decision making and moral programming of the control algorithms for driverless AVs, and are considered when developing the proposed active collision system (ACS) in Chapter 3.

In a two-part paper published in 1964, the genetical evolution of social behaviour was hypothesised in (Hamilton 1964a, 1964b). Publications by the same author in the early 1970s, where the notions of selfish and spiteful behaviour (Hamilton, 1970) and the selection of selfish and altruistic behaviour (Hamilton, 1971) were originally expounded, were later to become recognised as authoritative seminal papers and were inspirational works for others to follow.

Figure 2-8 is an illustration taken from (Foster, Wenseleers and Ratnieks, 2001) and the interpretation is as follows. Considering the case in Figure 2-7 (i.e. an AV deciding between colliding into an immovable rigid barrier or one pedestrian), here the 'recipient' is the pedestrian, i.e. a vulnerable road user (VRU). The 'actor' here is the AV responsible for taking the action in terms of the 'collision target', with the action possible being either mutualistic, selfish, altruistic or spiteful. The AV carrying out the action can be programmed to take any of the four options. A benefit or 'gain' is indicated by a '+' and a dis-benefit or 'cost' is indicated by a '-'. Consequently, being mutualistic provides a benefit to both, selfish is beneficial to the selfish AV but at a cost to other AVs or VRUs, altruistic behaviour provides a benefit to other AVs or VRUs at a cost (or no cost, hence '0') to the AV responsible for the action and spiteful behaviour provides a cost (or dis-benefit) to other AVs or VRUs again at a cost or no cost to the AV responsible for the action.

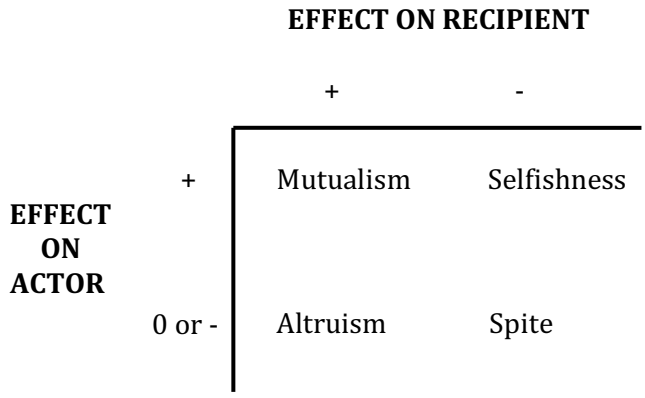

Figure 2-8: *Illustrating the Basic Four Social Actions taken by an Actor Affecting a Recipient (in Context of Autonomous Vehicles, the Actor is the Autonomous Vehicle Responsible for an Action and the Recipient is other Autonomous Vehicles or Vulnerable Road Users) – Diagram Taken from (Foster, Wenseleers and Ratnieks, 2001)*

Spite is briefly defined here in the Hamiltonian sense as it provides a basis for defining selfishness. It has also been described as the reverse of altruism. It was defined by Hamilton to be an action that harms the recipient but provides no benefit to the actor, i.e. placing this in context here the AV responsible for the action. In a redefinition by (Wilson, 1975), spite could provide benefit to a third party not directly involved in the action. It has been argued in (Keller et al., 1994), that spiteful animals are yet to be discovered. In (Foster, Wenseleers and Ratnieks, 2001), 'Spite: Hamilton's Unproven Theory' is discussed. It is argued that spite in the sense of Hamilton has not yet been discovered in the animal world and hints that it is only present in humans. Selfishness is like spite but there is a direct benefit to the actor responsible for the action. To be selfish means to harm others, i.e. in the context of AVs, to place others at risk to the benefit of the AV responsible for the action. There have been misleading characterisations of spite since the early definition of Hamilton. It is argued in (Foster, Wenseleers and Ratnieks, 2001), that most of the reported cases where actions of spite have been observed are better described as selfish rather than spiteful. In other words, there is a clear benefit to the individual at the expense of all the rest. Examples of selfishness in the animal world include cases where harm is done to others to conserve food for the benefit of one's self. For example, the behaviour of Vervet monkeys was originally described as spiteful. Vervet monkeys tend to destroy the competition's food source, this being to achieve a competitive gain to themselves and an energy/food loss to the recipient. Thus in the Hamilton sense, this is considered a selfish action rather than spiteful.

Altruism is the name given to describe the unselfishness concern for the welfare of others. The first publication on the topic is understood to be that of William Forster Lloyd in 1833, see (Lloyd, 1833) on a topic that in 1968 became known as 'the tragedy of the commons', see (Hardin, 1968). The tragedy of the commons involves a conflicting

situation whereby individuals act independently and rationally to each achieve the best interests of the whole group, whilst considering their self-interest in depleting a common resource. An example of a common group, considered in (Hardin, 1968), is where people graze their cattle on land which is common to all. Too much grazing of one individual's cattle ruins the common land resource for the other individuals. Altruism was first described mathematically in the work undertaken by W. D. Hamilton in 1963 and 1964, see for example (Hamilton, 1963), (Hamilton, 1964a) and (Hamilton, 1964b). This work was motivated by Charles Darwin's research on natural selection, commonly referred to as 'the survival of the fittest'. Hamilton questioned the approach of Darwin, suggesting that the hypothesis does not account for situations when living species behave in such a manner to promote the advantage of other members of the species at the expense of its own. A good example of altruistic behaviour within a species is that of the Vervet monkeys. In the event of a dangerous situation being identified, the monkey will give off an alarm call to warn other monkeys of the danger. A selfish approach would be for the monkey to stay silent and look after itself. However, studies have identified that a group of altruistically oriented monkeys have a much greater survival advantage over a group composed of selfish individuals. Taking this one step further, see (Dawkins, 2006), it has been discovered that a group of selfish organisms often isolate themselves and become extinct. As a result, they leave behind the altruistic organisms that go on to survive. Hamilton conjectures that if natural selection were true, species would not show any behaviour more positive towards each other than the coming together of the sexes and that of parenting. In his work, the altruistic behaviour is described in terms of parental care by 'fitness', where fitness effectively details the care and materials a parent can provide to its offspring, rather than being selfish and reserving these for their survival and further offspring. Hamilton states that the parents' gene which has the capability to give parental care will then leave more replica genes in the next generation. This is opposed to a parent with the opposite tendency, hence being selfish with their

care and materials. When two species exist in a relationship in which each benefit from the actions of the other, this is known as mutualism. In this situation, both the actor and recipient mutually benefit from an action.

2.5 SUMMARY

This Chapter has introduced the current development in autonomous vehicles (AVs), with details of the technology given and the five levels of autonomy defined. Examples of AV incidents and fatalities have been detailed that further highlight the potential issues with ethical decision making, e.g. steering away from one collision and potentially entering another collision. Such a scenario can be likened to the thought example, known as the trolley problem. Details of the trolley problem are given, with the current literature suggesting this can be applied to solve the current AV collision ethical dilemma, with philosophical views of utilitarian and deontological approaches being viewed as potential solutions. The literature on public views of AV ethical issues has been discussed, where it has been determined that the utilitarian approach is approved by those questioned. Details of further approaches to solving the current AV collision ethical dilemma are given, with social actions (utilitarian, selfish, mutualism and spite) have also been detailed.

3. PROBLEM STATEMENT AND PROPOSED ETHICAL COLLISION SYSTEM (ECS)

3.1 INTRODUCTION

Building on the autonomous vehicle (AV) collision ethical dilemma, this Chapter initially focuses attention on the problem statement and the proposed ethical collision system (ECS) for AVs involved in unavoidable collisions. The following two collision scenarios are considered in this research:

- AV to pedestrian(s)/wall
- AV to AV/AV

An approach is then detailed that outlines the stages to the ECS that is being proposed and developed (using simulation) in this piece of research. The ECS methodology adopted is one that is regarded as being 'inspired by nature'. A number of specific examples are drawn from nature to highlight the similarities and how the man-made machine-world can benefit from the natural world. The ECS approach to be developed is based on a model-to-decision (M2D) approach, where mathematical models of the collision scenarios are required, allowing the injury severity of the collision to be pre-determined, and then decisions to be made, e.g. collision target selection. In this research, a two-stage M2D approach is considered for the ECS. The two-stage approach involves a collision target selection algorithm and an active stiffness controller algorithm for the AV's crumple zones. The purpose of the collision target selection algorithm is to select the path-dependent on the selected setting (based on philosophical views or social actions). The active crumple zone algorithm's purpose is to evaluate if

the collision scenario can be improved by altering the vehicles structural properties. The stiffness controller for the AV crumple zones form the basis of a UK and International patent, see Appendix 1.0. The required technology behind the ECS and the M2D approach will be detailed (e.g. autonomous vehicle sensors, estimation of mass and prediction of impact collision velocity), along with details of the two-stage M2D approach. Throughout the development of this research, various assumptions are made; with a full list being presented in Appendix 2.0.

3.2 PROBLEM STATEMENT

The compelling autonomous vehicle (AV) collision ethical issue has been detailed in Chapter 2, i.e. selecting a collision outcome. To address this issue, the research documented in this thesis is focussed on addressing the ethical dilemma via the development of a framework which hinges on an ethical collision system (ECS). Initially, within the ECS, collision target selection algorithms will be explored. The development of the ECS for the collision target selection algorithms will involve a model-to-decision (M2D) approach where lumped parameter models (LMPs) of the collision scenarios are developed. Using the M2D approach, various decision algorithms can be tested based on philosophical views and social actions, known as the ethical decision maker (EDM). A further investigation is undertaken into the potential use of active crumple zones (using an active LPM) to reduce the severity of a given collision (further details of this are given in Section 4.4, Chapter 4), known as the active collision system (ACS). The two-stage proposed solution is detailed in Section 3.3.4, where initial details of the collision target algorithm development and active crumple zone algorithm are given.

3.2.1 SCENARIOS TO BE CONSIDERED

To demonstrate and evaluate the benefits of the ECS approach, two scenarios are investigated. The two scenarios are inspired by the work presented in (Bonnefon, Shariff and Rahwan, 2015) and (Bonnefon, Shariff and Rahwan, 2016). In all the scenarios considered, it is assumed that all collision mitigation methods have been exploited and

a collision between two possible outcomes is certain. The collision scenarios considered in this work are:

- AV to pedestrian(s)/wall
- AV to AV/AV

The action of the EDM is for the AV to either continue along its natural path or to swerve into an alternative target. For example, the AV could be programmed to minimise injuries or/and fatalities and may need to swerve to do so. In all scenarios involving occupants and pedestrians, it is assumed that the relationship between all of the potential targets is neutral, i.e. there is no family relationship. It is further assumed that all occupants (in this Section, only one occupant is considered on-board the AV, but this is altered in Chapters 7 and 8) and pedestrians involved represent equal value to society. In the development of the EDM for the AV to pedestrian(s)/wall, the scenarios are limited to cases where an AV should decide between swerving to avoid 1 or 10 pedestrians and to collide full-frontal into a solid immoveable rigid wall, as illustrated in Figure 3-1 (left, where 1 pedestrian is illustrated). Alternatively, there is the case where a decision is taken to swerve to avoid a solid immovable rigid wall (IRW) and to collide into 1 or 10 pedestrians, as illustrated in Figure 3-1 (right, where 1 pedestrian is illustrated). The collision scenario illustrated in Figure 3-2 involves multiple AVs. In such scenarios, one AV takes the lead in the ethical decisions, this AV is known as the host, i.e. the AV that leads in taking action. It is the author's belief that only one AV should take the 'lead' in the ethical decision-making process, however, all the AVs will have the ability to communicate information and influence the decision-making process. The scenario of an AV to AV/AV follows similar ethical decision logic, in that the host AV has to make a decision between swerving to avoid a given AV in its path or to collide with another AV, see Figure 3-2.

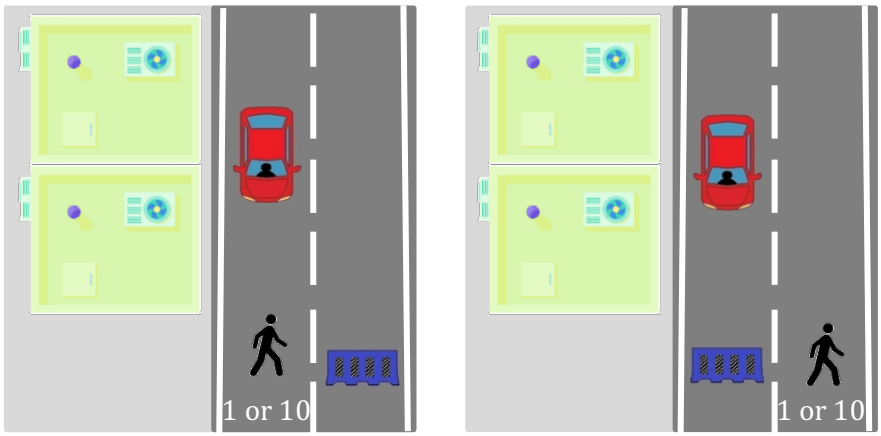

Figure 3-1: *Autonomous Vehicle Making a Decision Between Swerving to Avoid 1 or 10 Pedestrians and to Collide into a Immoveable Rigid Wall (Left) and Autonomous Vehicle Making a Decision Between Swerving to Avoid a Immoveable Rigid Wall and to Collide with 1 or 10 Pedestrians (Right)*

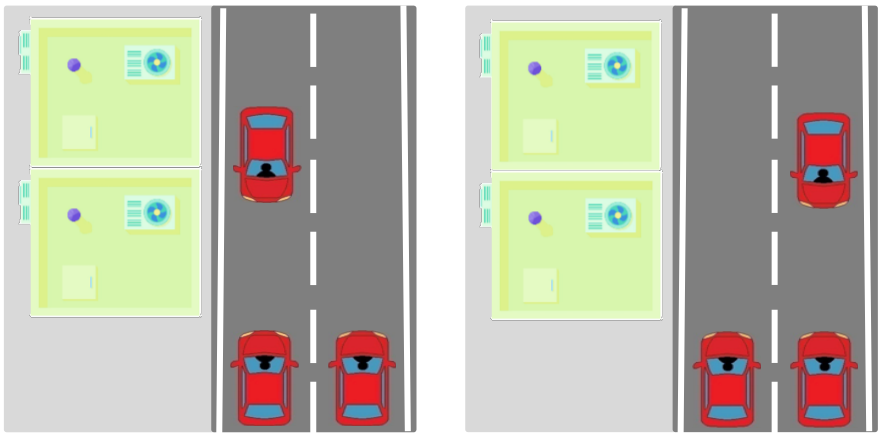

Figure 3-2: *Illustrating the Host Autonomous Vehicle (Upper Autonomous Vehicle, Left and Right) Making a Decision Between Swerving to Avoid a Given Autonomous Vehicle in the Path and to Collide Head-on with another Autonomous Vehicle (Left and Right)*

3.2.2 THE APPROACH

The approach is initially detailed in this Section, with further information provided in this Chapter, and then the approach is developed in Chapters 4 to 8. The approach to address the problem in this Thesis is as follows:

1. Develop a framework for the proposed ECS that contains a M2D approach, where the model consists of mathematical collision models and the decision consists of an EDM.
2. Investigate vehicle collision safety for a single-vehicle collision into an IRW using a finite element (FE) model. The FE model used will be reverse engineered based on an actual vehicle. Using the FE vehicle model, the key features of peak deformation, peak acceleration and collision energy will be captured.
3. Investigate occupant collision safety for a single-vehicle collision into an IRW using a sled model. The acceleration versus time data from the FE vehicle model will be used as the input to the sled model. From the sled model outputs, the key features of peak head and peak chest acceleration should be captured.
4. Investigate the physics of vehicle-to-vehicle collisions, the possibility of using active collision structures to reduce the injury severity of collisions (single-vehicle collision into an IRW and vehicle-to-vehicle) and the vulnerable road users of pedestrians.
5. Develop linear and nonlinear nodal/modal lumped parameter models (LPMs) of the collision scenarios of interest (vehicle into IRW and vehicle-to-vehicle) that accurately capture the vehicle key features of peak deformation, peak head and peak chest acceleration. Tuning methods for the linear and nonlinear LPMs will need to be developed. Once the models are simulated and compared to the FE data, verification of the models should be undertaken.
6. Using the developed LPM that best captures the key features of the vehicles for the one and two-vehicle collision cases, develop surfaces/look-up tables for ranges of collision velocities and vehicle masses. In the case of a two-vehicle collision, one vehicle remains at the nominal mass value. Develop a method for interpolation between pre-determined points of the look-up tables using ideas borrowed from fuzzy logic. These look-up tables form the basis of the EDM, thus

using pre-determined collision outcomes to allow the initial collision scenario to be evaluated and then the injury severity of the predetermined collision outcomes to be estimated for the occupant(s) within the AV.

7. Develop an EDM utilising injury severity levels (occupant(s) and pedestrian(s)) that allows the philosophical actions (Kant and Bentham) and social actions (altruism and selfishness) to be developed into collision target algorithms. The effects of each EDM algorithm (philosophical and social actions) should be tested, with the results documented and suggestions of how a user's preference would influence the outcome. Example results should be given, along with a quantification/verification study undertaken that investigates variables of the model, e.g. AV mass and velocity.
8. Using the developed mathematical models for the one and two-vehicle collision cases, vary the model stiffness value of the vehicle crumple zones from the nominal stiffness by an appropriate scaling factor. Then capture the key features for the one and two vehicle cases and develop surfaces/look-up tables for the changes in stiffness value. These look-up tables form the basis of the stiffness controller part of the EDM, allowing the effect of changes to the structural stiffness to be determined, i.e. vehicle peak deformation and occupant peak head and chest acceleration. This allows decisions to be made to improve (de-risk) the collision scenarios. Evaluate the benefits of the stiffness controller and the effect this has on the injury severity levels of the occupants.

3.3 PROPOSED FRAMEWORK OF ACTIVE COLLISION SYSTEM

This Section details the areas that are important to the development of the ECS. In the case of an AV entering an imminent collision, the proposed automatically controlled response takes motivation from nature (detailed in Section 3.3.1). Details of a nature-inspired approach are given, with this continually monitoring its surroundings and taking appropriate action when required, like many control systems found in the natural

world. Details of the M2D approach are then given (detailed in Section 3.3.2), that require a level of technology (detailed in Section 3.3.3) to develop a two-stage approach to form the operation (detailed in Section 3.3.4), i.e.

- Collision target selection algorithm
- Active crumple zones algorithm

3.3.1 PROPOSED NATURE INSPIRED APPROACH OF ACTIVE COLLISION SYSTEM

The envisaged solution for future autonomous vehicles (AVs) is that they will have the ability to exhibit an automatically controlled response upon entering a collision scenario when required. Such a response may be likened to the attacking/defensive response phenomena which is commonly found in the natural world. In the context of AVs, the notion of a natural attacking phenomenon may not be so immediately analogously obvious, but it is interesting to record here how snakes have evolved with their internal self-protection, i.e. analogous to a vehicle's occupant restraints. Snakes in general, see (Penning, Sawvel and Moon, 2016), have an in-built ability within their body structure to withstand accelerations up to $279 m/s^2$ and velocities up to $3.53 m/s$ over short distances $0.086 - 0.270 m$ and for short time durations between $48 - 84 ms$. An illustration of a snake in attacking mode is given in Figure 3-3(a). Examples of natural defensive approaches include the self-preserving properties of trees, whereby they can automatically flex and change their shapes in response to dynamic loads, e.g. to counteract effects of wind and adapt to the variation in humidity levels, see (James, Haritos and Ades, 2006) and Figure 3-3(b). Living creatures such as hedgehogs and woodlouse change their external features when threatened, see Figures 3-3(c) and 3-3(d). In both cases, when threatened the creatures roll up into a ball. In the case of the woodlouse, a hard shell is formed in self-protection and with the hedgehog, a ball with external spikes is formed to deter predators. This inspiration from nature is also analogous with the flexing of muscles of a human being prior to exerting effort to oppose an external force.

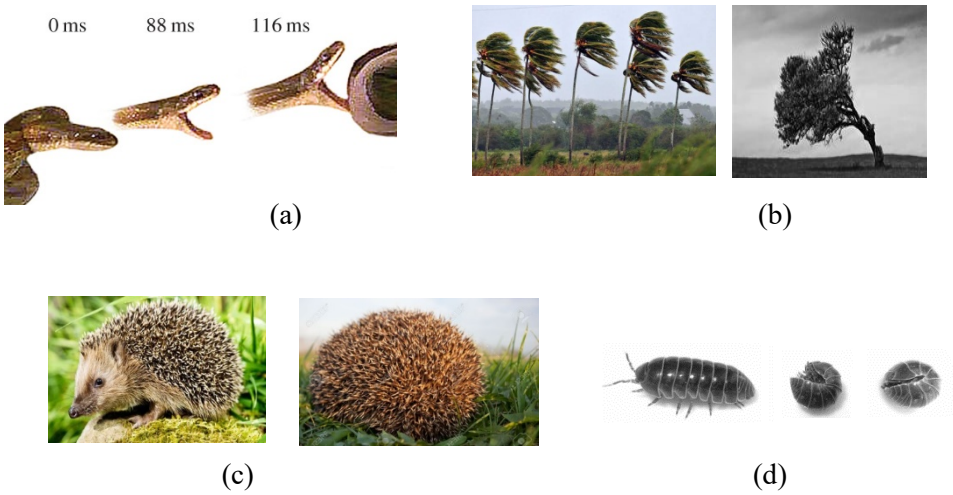

Figure 3-3: *Natural Response Phenomena Inspired by Nature for Potential Design of Autonomous Vehicles*

3.3.2 MODEL-TO-DECISION APPROACH FOR ACTIVE COLLISION SYSTEM

Based on the nature inspired approach, the M2D approach is to be developed for the ECS as a possible solution for the AV collision ethical dilemma, as detailed in Chapter 2. The application of M2D in the ethics domain is known as machine ethics (also known as computation ethics), with this being concerned with the moral behaviour of artificially intelligent beings. In (Bonnefon, Shariff and Rahwan, 2015), (Goodall, 2014) and (Goodall, 2016), the authors suggest that methods developed within experimental ethics can be used to investigate judgements concerning ethical dilemmas applicable to AVs. It is generally agreed that an action is ethically moral if the outcome of an action can be quantified and that it successfully maximises or minimises some form of measurable cost function, see (Goodall 2014). In (Goodall, 2014), the author suggests that this approach could be applied to AVs, where the utility is defined as the AV safety, or even the inverse of damage costs, with intensity, duration and probability estimated. Various machine ethic software tools have been developed in other domains that guide scenarios that require ethics. In (Anderson, Anderson and Armen, 2004) the developed software, known as 'Jeremey', measures the state of utility of any outcome by using the product of the outcomes utility intensity, duration and probability – these being estimated by the

user. The creators of Jeremey then developed a duty-based ethical theory, see (Anderson, Anderson and Armen, 2005), with this work being influenced by (Ross, 1930) and (Rawls, 1999). In (Anderson, Anderson and Armen, 2006), the authors later developed a programme named 'MedEthEx'; this being a software tool used in medical ethics that uses machine learning to determine if a given scenario is moral or immoral. This decision is based on ethical principles, with expert knowledge being input into the software to make these assessments. The output is a decision as to whether an action is morally right or wrong, and the software also indicates the ethical theory used and how these were important in making the decision. In (Mclaren, 2006), the author developed an ethical decision-making procedure named 'Truth-Teller'. The software effectively decides whether or not to tell the truth based on two input case studies. The software has the capability to identify the similarities and differences between the two cases, and then provides a list of reasons for and against telling the truth in each of the two case studies. Such a method is known as casuistic reasoning, where the reasoning is used to research a conclusion of such a problem and is achieved by extracting or extending theoretical rules from scenarios and then applying these rules to new scenarios. More recently, in (Reed and Jones, 2013), the U.S. Army funded research into the development of an automated ethical decision-making software that attempts to determine the morality of two competing actions in a combat environment. The developed software is known as the 'Metric of Evil', and it attempts to resemble human reasoning about morality and evil, thereby removing the human input from the decision-making process. In effect, the software evaluates and sums the evil of each consequence of an action. The software factors in low and high estimates of evil, along with a confidence interval. It should be noted that the software's consequences are adjusted with weighted parameters by a panel of experts for the output to match expert judgment or that expected.

The M2D approach being developed in this research is used to provide the AV an automated response when collisions involving ethical decisions, like the approaches involving nature that are described above. The M2D approach involves the use of a logic model (in the form of a mathematical model) of the collision scenarios with a decision-making process/algorithm, see Figure 3-4. The logic model is used to predetermine quantifiable information regarding a given collision scenario, i.e. the level of injury severity (low, low-medium, medium, medium-high and high). For such an approach, estimates/predictors of the vehicle mass and collision velocity are needed for the mathematical model. The information from the logical model can then be used in the decision making process to give an outcome, i.e. to steer the AV into a collision target.

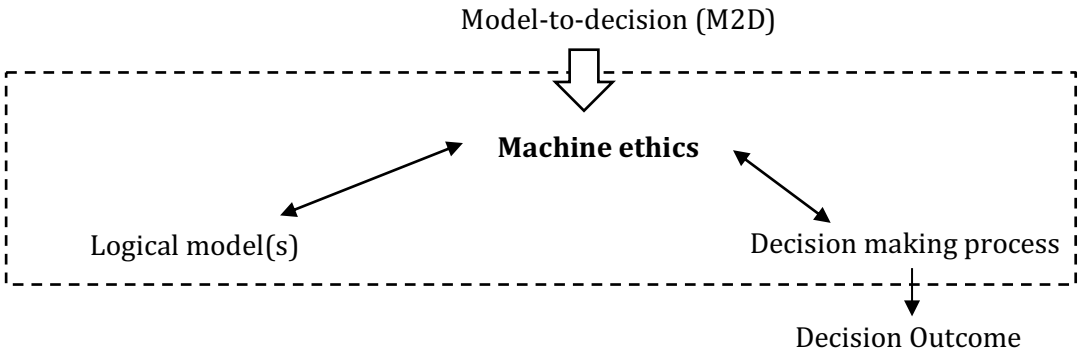

Figure 3-4: *Model-to-Decision Approach*

3.3.3 REQUIRED TECHNOLOGY

The overview of the realisation of the ECS for a single AV is shown in Figure 3-5. The ECS approach assumes that AVs have full autonomy, i.e. SAE level 5 (see Chapter 2, Section 2.2, Table 2-1). Each AV is equipped with autonomous features such as sensors, on-board V2V, vehicle to infrastructure (V2I) or in general vehicle to anything (V2X), communication technology and embedded microcontrollers as part of the on-board advanced driver assisted systems (ADAS), with this providing on-board active safety systems (ASSs), which also consists of the M2D approach. The M2D approach has the ability to select the collision target and control the stiffness of the crumple zones. The on-board microprocessor monitors information from the object detection sensors and the object recognition camera, in a manner which is known in ADAS systems, see for example (Katahira, Shibata and Monji, 2007). This information is then used in the M2D approach. In terms of the sensors, Figure 3-5, shows a front object detection sensor, a rear object detection sensor and a side object detection sensor. The number and position of the object detection sensors may vary according to the specifics of the installation of the system. However for this work, only single rear, front and side sensors are shown. In such systems, the object detection sensors and object recognition camera are used to identify any other vehicles, street furniture, pedestrians etc. which are in the vicinity of the vehicle and to determine the likelihood of a collision with any identified features. In the case of a multiple AV collision, V2V communication between AVs occurs using a standard handshake protocol, where the vehicle of largest mass takes charge (i.e. becomes the master and the other vehicle(s) become the slave(s)). This involves the AVs in the vicinity being identified and once a connection is established, bi-directional communication begins to exchange information between the multiple AVs. Between the multiple AVs, information required for the M2D approach will be the estimated laden mass and predicated velocity values. Estimating the AVs velocity and laden mass values are non-trivial tasks, as discussed further below. Such V2V communication systems are

already available, see for example (Mologni et al., 2014) and (Chen, Chamadiya and Bueker, 2015). The communication must be secure and robust to prevent a cyber-attack and as such, this topic has been identified as an area for future research.

With consideration to the early operational days of the ECS, when vehicles in the vicinity of the host vehicle are not equipped with V2V communication, or a communication failure occurs, the processor uses the object recognition camera to determine characteristics of the vehicle and the system would operate in a fault tolerant mode. The object recognition camera and processor are configured to identify objects, such as the likely make and model of a human driver vehicle (HDV), see (Deshpande, Kutty and Mani, 2015). Furthermore, by using the object detection sensors (such as a camera), the processor is able to determine relative velocity of the neighbouring vehicle.

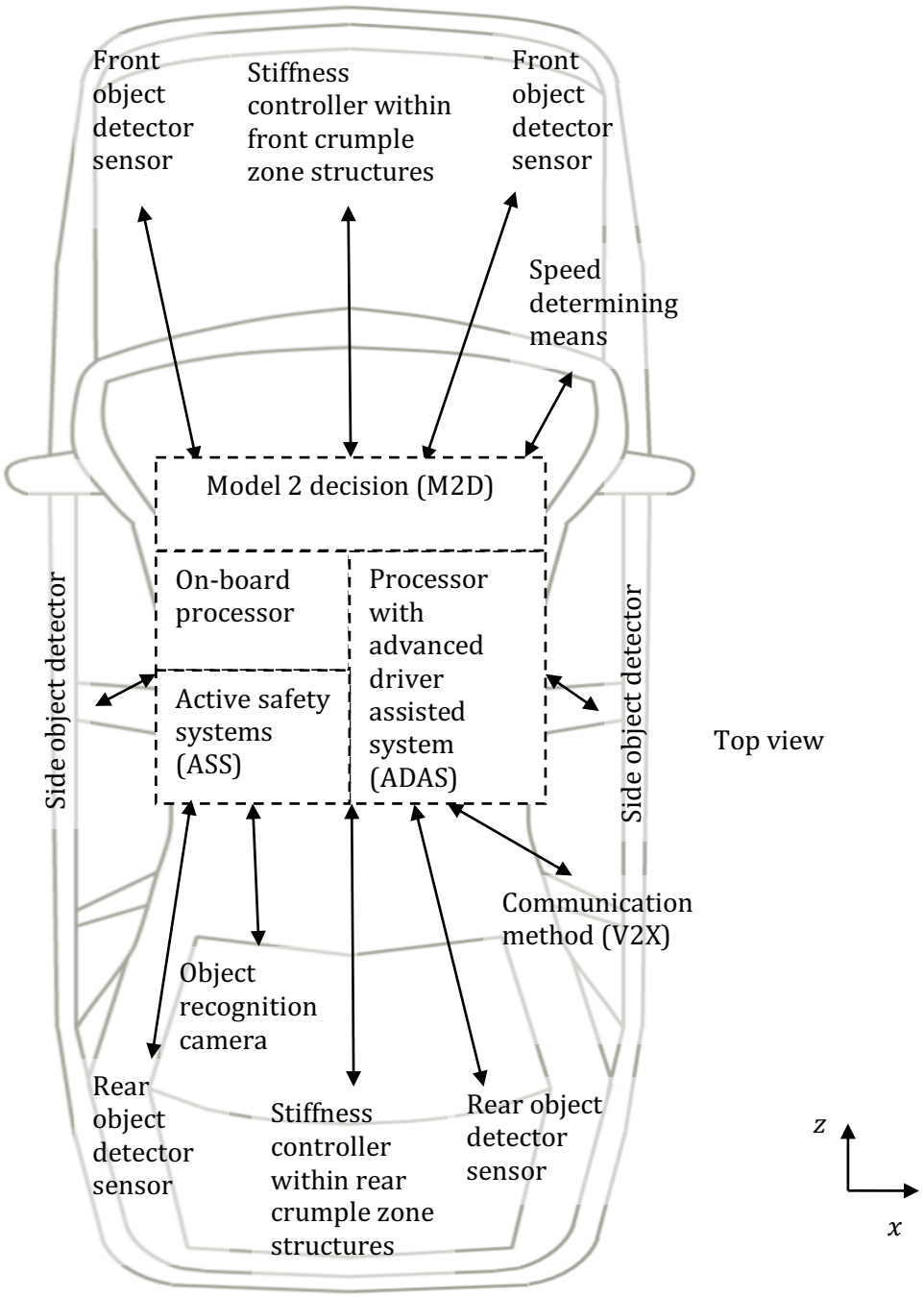

Figure 3-5: *Schematic Representation of Technology Required to Realise the Active Collision System*

Each vehicle is equipped with a first crash structure which is made of, at least in part, smart materials. The front and rear crash structures have attached thereon a stiffness controller which is configured to actively change the stiffness of the front/rear crumple zone structures, see Figure 3-5. The processor is therefore further configured to activate the stiffness controller such that the structure can be appropriately activated and is configured to apply a certain control signal, leading to an electrical current to achieve the desired stiffness properties.

It is conjectured that estimates of laden mass and longitudinal velocity will be available on-board the AV's control area network (CAN) bus of future AVs. Estimation of vehicle laden mass and longitudinal velocity are non-trivial tasks. Both quantities represent fundamental and important information for many of the on-board systems, particularly the control systems linked to ADAS. Online estimation of laden mass and longitudinal velocity possesses difficulties which have received significant interest from scientific research groups and automotive oriented research groups world-wide, see (Vahidi, Stefanopoulou, 2005), (Peng, 2005) and (Wragge-Morely et al., 2015) for laden mass and gradient estimation and the work of (Moaveni, Abad and Nasiri, 2015) for longitudinal velocity estimation during the braking process. Once estimates of the individual AV velocities have been obtained, the collision velocity can be readily determined. In the case of vehicle laden mass estimation, it is found that the problem is intrinsically linked to road gradient and the two-time varying quantities interact with each other in the estimation process. Their effects may be distinguished due to considerations of time-scale whereby gradient can be expected to change more frequently over a shorter time-scale than laden mass. However, laden mass may change suddenly due to passengers boarding and alighting. In (Vahidi, Stefanopoulou. 2005), a scheme employing recursive least squares with forgetting factors is utilised. Whereas, in the more recent work cited in (Wragge-Morely et al., 2015), use is made of a novel

data rejection method whereby a Kalman filter (KF) management system is implemented to discard corrupted data. It is reported in (Wragge-Morely et al., 2015) that the corrupted data is typically characterised by erroneous impulse-like fluctuations and periods of prolonged steady state. In the case of longitudinal velocity, see for example (Moaveni, Abad and Nasiri, 2015), use is made of an unknown input KF with the rotational wheel velocities being measured and an estimate of longitudinal velocity is based on the difference between the rotational velocities of the powered wheels and the free driven wheels, the former velocity being greater that than the latter with the difference being due to the slip. Errors in estimating/predicting the vehicle laden mass and/or vehicle velocity need to be accounted for, thus a quantification/vertification analysis is undertaken in Chapter 7 for the ethical M2D approach being developed.

The above requirements are not considered to be unrealistic for a future fleet of AVs, and the existence and applicability of such technology is one of the main underlying assumptions.

3.3.4 OPERATION

A schematic overview of the proposed ECS is given in Figure 3-6, indicating the primary, secondary and tertiary decision stages of a collision. The ECS to be developed will be made up of Phases 1, 2, 3 and 4 only. Post collision scenarios are beyond the scope of the study, but would represent an opportunity for further work.

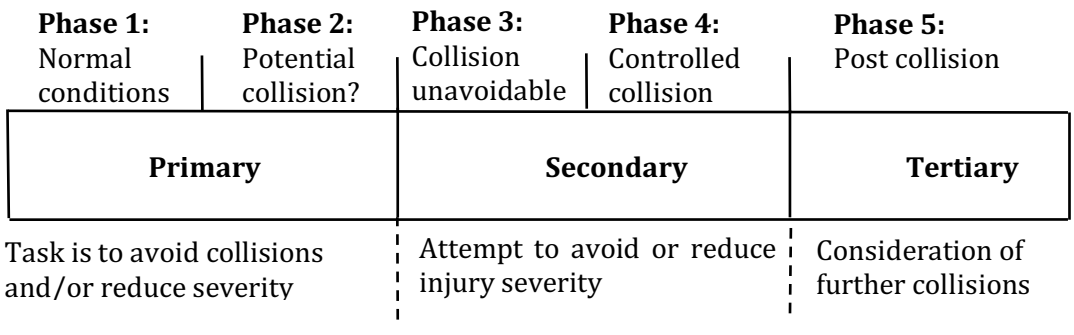

Figure 3-6: *Schematic of ECS, Showing Primary, Secondary and Tertiary Stages*

In a full realisation, Phase 1 would involve continual data harvesting of the AV's longitudinal velocity and laden mass, the number and location of occupant(s) on-board the AV and pedestrian(s), with details of their properties, e.g. age, fragility, mass and sex, as well as monitoring the environment surrounding the AV's dynamic motion trajectory and scanning for specific objects. In this work, the details of the occupant properties are not considered, except the absolute number of occupants. For simplicity, the utility of each occupant/pedestrian in this work is assumed to be equal. A more detailed occupant analysis is considered as further work. Phase 2 involves an AV entering a potential collision zone(s), i.e. in the vicinity of other AVs, object(s) or pedestrian(s). Whilst the AV is in motion, a risk assessment is automatically carried out and on-board features such as active steering, i.e. collision avoidance, full emergency braking and combinations of these are deployed. Phase 3 assumes that all active collision avoidance systems (e.g. full emergency braking and active steering) have been deployed and an imminent collision is unavoidable, and so the AV prepares to take appropriate action. How this process is carried out is not detailed in this work. Rather, it is assumed that an imminent full-frontal collision is unavoidable and the AV is already aligned either with an IRW, another AV or a pedestrian group of one or ten. Phase 3 will involve the AV determining in real-time the collision target, thus whether the AV collides into a pedestrian, a group of ten pedestrians, an IRW or another AV. Phase 3 also considers the active control of the crumple zones to minimise the severity of the collision outcome. This Phase involves the use of a M2D approach that is given in more detail in Section 3.3.2, 3.3.4.1 and 3.3.4.2. The 'planning' of the collision in Phases 1- 3 is realised in Phase 4, i.e. this will involve the actual collision scenario. In this work, it will be assumed that a collision is unavoidable (Phase 3), hence Phases 1 and 2 will not be the focus of this work. Focus of this work will be on Phase 3 and how the M2D approach is programmed to give a controlled collision (Phase 4).

Phase 5 involves considerations which have been highlighted for further research. These are triggered by the primary collision event to consider further secondary and tertiary collision events. It is feasible, building on from the assessment of the primary collision to predict the dynamic motion of the combined structures and the known trajectories of the surrounding secondary and tertiary groups of AVs. As a potential multiple AV collision widens to encompass secondary and tertiary collisions, the scope for introducing further safety and ethical actions becomes apparent and is noted as a worthy area of further work.

3.3.4.1 COLLISION TARGET SELECTION ALGORITHM

The EDM is designed for AVs to automatically determine the target in the occurrence of an imminent collision event with the targets detailed in Section 3.2.1, i.e. with either a pedestrian or group of pedestrians, an IRW or another AV, or choosing a target between multiple AVs. As discussed above, the operation of the decision making process involves the use of a M2D approach. The primary stage of the M2D approach involves the use of LPMs in conjunction with an EDM to determine the collision target, see Figure 3-7. The EDM collision target system for the single and two-AV cases is further developed in Chapters 7 and 8, respectively.

A FE model is used to tune LPMs that are used, developed and applied in this research. LPMs have been used to determine the severity of vehicle accidents since the early 1970s (Kamal, 1970). More detailed and computer processing intensive FE models were introduced in the early 1980s (Ni and Song, 1986). In this research, in Chapter 4, an FE model is used to capture corresponding output collision data, such as force versus deformation. This data is then used to develop and tune LPMs in Chapters 5 and 6 that closely represent AV collision phenomenon, e.g. an AV colliding into an IRW. The approach to developing the LPMs of AV crumple zone structures in this research will initially use ideas borrowed from previous authors, as detailed in Section 5.2.2, Chapter

5. LPMs offer low complexity (typically 1-2 degrees of freedom) compared to that of FE models (typically tens and tens of thousands of degrees of freedom), thus the computational time of LPMs is significantly lower. The LPM could potentially be used on-line before the collision in conjunction with the EDM, thus a low computational model is needed. However, the developed LPM must be capable of capturing the key features of an AV collision, e.g. peak deformation of the AVs crumple zone structure. The initially used ideas are on linear LPMs, where there is an abundance of literature on the topic. In contrast, there are rather fewer articles on nonlinear AV collision LPM; with no general approach being available. With the aim of developing a LPM to best capture the collision phenomenon of an AV, a nonlinear LPM is to be developed, as this may better capture the collision phenomenon. Thus, in Chapter 5, the single AV into an IRW linear and nonlinear LPMs are developed and in Chapter 6 the AV to AV linear and nonlinear LPMs are developed. Central to the approach is the ability of the AV to determine the predicted key features before the collision scenario, i.e. peak vehicle deformation, peak occupant head and chest accelerations. The developed LPMs are used to determine the key features and then the injury severity (e.g. risk of low injuries or risk of severe injuries) of a collision scenario, prior to the event. The severity of collision outcomes corresponds to the occupants within the AVs and the pedestrian(s), where the vehicle properties are an influencing factor, e.g. AV mass, velocity and crumple zone stiffness (detailed in Chapter 3).

In conjunction with the LPM, it is envisaged that the EDM could work on-board in future AVs in real-time, by having pre-determined values in look-up tables using fuzzy logic to interpolate between points (however the LPMs could be used online in real-time). The use of look-up tables is proposed to store collision outputs (i.e. peak deformation, peak occupant head and peak chest accelerations) corresponding to a range of collision velocities and laden mass values. Thus, the look-up tables can be interpolated to

determine the outputs that correspond the estimated values of vehicle laden mass and predicted collision velocity. The injury severities are then used within the EDM and a decision is made regarding the collision outcome/target/path. The collision outcome will depend on the chosen algorithm within the EDM. The ethical algorithms of interest in this research will be that of philosophical actions (as detailed in Section 2.3.2) and social actions (as discussed in Section 2.4). The two social actions of altruism and selfish are investigated as potential approaches for an AV, along with the deontological and utilitarian approaches (philosophical actions). Spite is briefly considered for completeness, but it is not considered as an appropriate means of programming an AV from a moral and ethical viewpoint.

In further work, the LPMs and the developed look-up tables can be extended to include multiple collision scenarios, hence vehicle orientation for offset collisions as well as environmental conditions. In a practical realisation of the approach, the look-up tables would be of a higher dimension than those described here, and developed in Chapters 7 and 8.

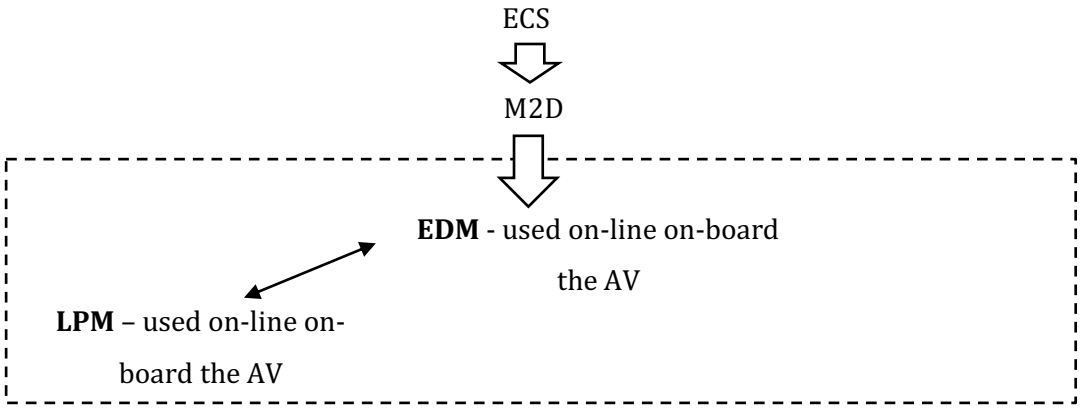

Figure 3-7: *Proposed Solution to the AV Ethics Problem via the use of a Model-to-Decision Approach for On-board a Future AV*

3.3.4.2 ACTIVE CRUMPLE ZONES ALGORITHM

The secondary stage of the M2D approach introduces the idea of a stiffness controller for on-board future AVs front crumple zone structures, known as the ECS. It is conjectured that adjustment of the vehicle crumple zone stiffness values may be possible with the future developments in smart materials and structures. Such a development would allow an ethical approach to be developed to enable those involved in a collision to have a better chance of survival and would potentially reduce the risk of injury to all involved in a collision, with more detail given in Section 4.4, Chapter 4. The ECS is designed for AVs to improve the injury severity outcome of an imminent collision event with the targets detailed in Section 3.2.1, i.e. with either a pedestrian or group of pedestrians, an IRW or another AV, or choosing a target between multiple AVs. The primary stage of the ECS approach involves the use of a LPMs in conjunction with an EDM to determine the collision severity, and then the LPMs to improve the injury severity, see Figure 3-8. If a decision is taken to collide into an immoveable rigid wall or another AV, a decision is then taken whether to adjust the stiffness of the vehicle crumple zones to reduce the severity of the collision. This is achieved by active adjustment of an AV's frontal structural stiffness values before the imminent collision. In the single vehicle case of a collision into an immoveable rigid wall, a decision by the EDM stiffness controller may be taken to stiffen and as a result reduce deformation, with an increase in occupant acceleration levels being experienced. Alternatively, a decision may be taken to soften the structure to utilise potential spare deformation capacity, leading to a reduced acceleration experienced by the occupants; this relationship is detailed in Section 4.2.3, Chapter 4. The EDM stiffness controller system for the single and two-AV cases is further developed in Chapters 7 and 8, respectively.

In the case of a two AV collision, it will be assumed all AVs have the same structural crumple zone stiffness. The stiffness controller within the EDM will assess whether

there is scope to reduce the overall severity of the collision, this relationship is detailed in Section 4.3.2, Chapter 4. The approach in this stage builds on the above, and uses the LPM to develop an active LPM, see Figure 3-8. Thus allowing for the effects of stiffening/softening of the crumple zones to be explored. A developed ACS will involve the use of pre-determined effects from the active LPM (i.e. deformation of crumple zones and occupant accelerations) for stiffening/softening the crumple zones over a range of AV collision mass and velocity values (these will be captured off-line). The pre-determined effects will be stored in 3-dimensional (3D) look-up tables on-board the AV that can be interpolated in real-time by an interpolation method, i.e. Fuzzy logic. In the case of a pre-empted collision, the 3D look-up tables can be used to pre-determine the severity of the event, in the case of a pre-determined severe collision. The ACS is then used in an attempt to reduce the severity of the collision through stiffening/softening of the crumple zones. In the context of AVs, the altruistic action is very much key to the motivation for an EDM and a structural stiffness controller

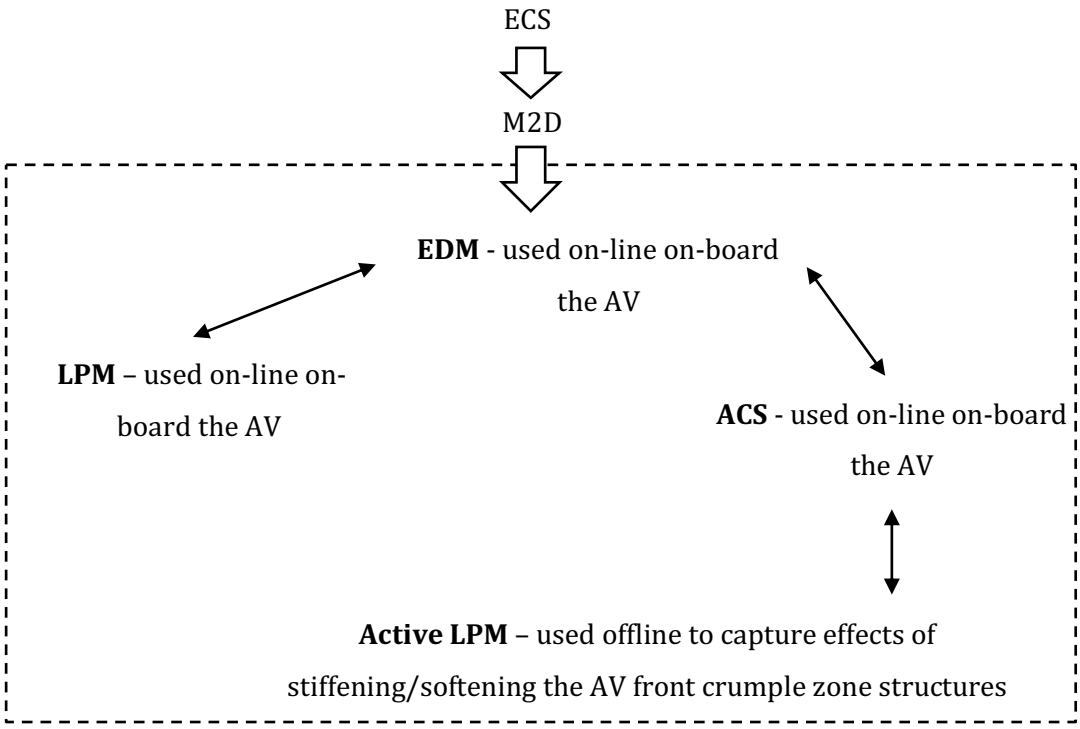

Figure 3-8: *Proposed Solution to the AV Ethics Problem via the use of a Model-to-Decision Approach including a Structural Stiffness Controller for On-board a Future AV*

3.4 SUMMARY

This Chapter has now set in place the main focus on the research. The problem statement has been outlined, with the scenarios detailed that are to be investigated in this research. In the development of the approach, the set of collision targets is limited to another AV, a single pedestrian, a group of ten pedestrians or an immovable rigid wall (IRW). Details of the proposed approach and required technology have been given, known as the ethical collision system (ECS) which uses a model-to-decision (M2D) approach. The ECS to be developed in this research consists of two stages, the collision target selection algorithm and the active crumple zone algorithm. The first algorithm selects the collision target based on the selected setting (philosophical or social actions), and the second algorithm involves the use of a stiffness controller in an attempt to reduce the severity of the collision, i.e. injury severity of the occupant(s).

4. BACKGROUND TO VEHICLE COLLISION SAFETY

4.1 INTRODUCTION

This Chapter introduces the background to vehicle collision safety that is needed for the development of the ethical collision system (ECS) detailed in Chapter 3. Based on this background into collision safety, simplified models are then developed in Chapters 5 and 6 that capture the key collision features. An initial background into single-vehicle collision safety is presented, with consideration being given to finite element (FE) collision modelling. Further considerations are given to the FE modelling, in particular: crashworthiness testing, the conservation of momentum and energy, collision forces, structural stiffness and occupant sled modelling. To capture the required data which define the key features of a full-frontal vehicle collision, FE simulation data from a Toyota Yaris Sedan (TYS) 2010 vehicle is used. The features of interest from the FE model are specifically: peak deformation (this forming a key feature), peak acceleration and collision energy (the latter is used as a means of model verification). As introduced above, these features are used in the development of a mathematical collision model in Chapter 5. A further study is undertaken into the occupant properties, and two further key features of peak head and peak chest accelerations are of interest, i.e. three key features in total. These two latter features are obtained by making use of the acceleration versus time data from the TYS 2010 FE simulation as an input to a sled model containing an anthropometric test device (ATD), i.e. an instrumented collision test dummy. Building on the single-vehicle collision safety, two-vehicle full-frontal head-

on collision safety is considered. For this, FE collision modelling is not used as this was determined to be problematic, with this giving unreliable results. As in the single-vehicle collision case, the conservation of momentum and energy, collision forces and structural stiffnesses are considered for the two-vehicle collision. Further to this, a two-vehicle full-frontal mathematical model is developed in Chapter 6, with the same key features of interest, i.e. peak deformation, peak head acceleration and peak chest acceleration. The current development in active collision structures is explained, with the aim of these devices to reduce injuries to the occupants contained within a vehicle when facing a collision with another vehicle or/and an immovable rigid wall (IRW). In the development of the ECS, cases involving pedestrian incidents are considered and therefore a review into pedestrian vulnerability is undertaken in this Chapter.

4.2 BACKGROUND INTO SINGLE VEHICLE COLLISION SAFETY

In this Section, the details of a finite element (FE) collision simulation of a single-vehicle into an immovable rigid wall (IRW) based on testing legislation used for this research is introduced. The input to the FE collision simulation is derived from the initial condition due to the collision impact velocity and vehicle laden mass and the outputs are deformation versus time, acceleration versus time and collision deformation energy. Note that displacement is interpreted as deformation of the crumple zone is this research.

The FE collision model is used as a surrogate for an actual vehicle collision. In the absence of an actual vehicle collision, the FE model goes some way to explain the physical phenomena, i.e. the conservation of momentum and energy, the coefficient of restitution, the collision forces and the structural stiffness. Based on the FE collision simulation output data of acceleration versus time, an occupant sled model is used to further explore the occupant(s) collision injury properties. The potential safety issues that are subjected by the occupant(s) on-board vehicles are then briefly covered.

4.2.1 FINITE ELEMENT SET-UP BASED ON CRASHWORTHINESS TEST

As stated in Chapter 1.0, an FE model is used for this research. The FE model was developed through the process of reverse engineering at the National Crash Analysis Centre (NCAC), George Washington University (GWU), see (Marzougui et al., 2012). The FE model is based on the 2010 Toyota Yaris Sedan (TYS).

The process of reserve engineering involved disassembling the TYS vehicle part by part, detailing the geometry, gauge and material type for each part and undertaking tensile tests to capture the material characteristics, i.e. stress and strain values. The determined properties from the TYS were modelled and analysed using FE to ensure the modelled parts matched up well with the actual vehicle's parts. The FE model also included features such as fully functioning steering and suspension. In Figure 4-1, the 2010 TYS FE model is illustrated and compared to the actual TYS vehicle. The 2010 TYS FE model is available for research as an open-access source from the Centre for Collision Safety and Analysis (CCSA) website, see (Centre for Collision Safety and Analysis, 2017). It should be noted that the purpose of this section is not to develop the FE model, but rather to gain an understanding of the cause and effect properties of a full-frontal collision, i.e. input (cause) and output (effect) properties. The computation and analysis of the FE model were undertaken using the proprietary LS-DYNA explicit computer solver. The 2010 TYS FE model will be used as the nominal benchmark vehicle collision model in this work. The FE collision model is effectively taken as a surrogate for the actual vehicle collision system as this simulation provides the closest match to an actual realistic collision, see Table 4-1 Section 4.2.3.

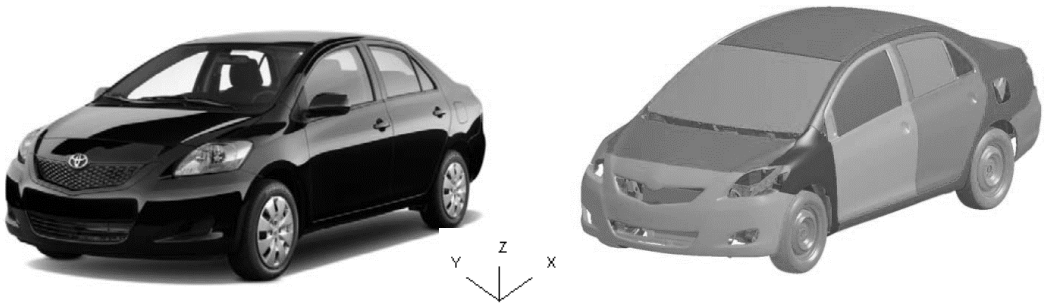

Figure 4-1: *Actual and Finite Element Analysis Model of a 2010 Toyota Yaris Sedan (Marzougui et al., 2012)*

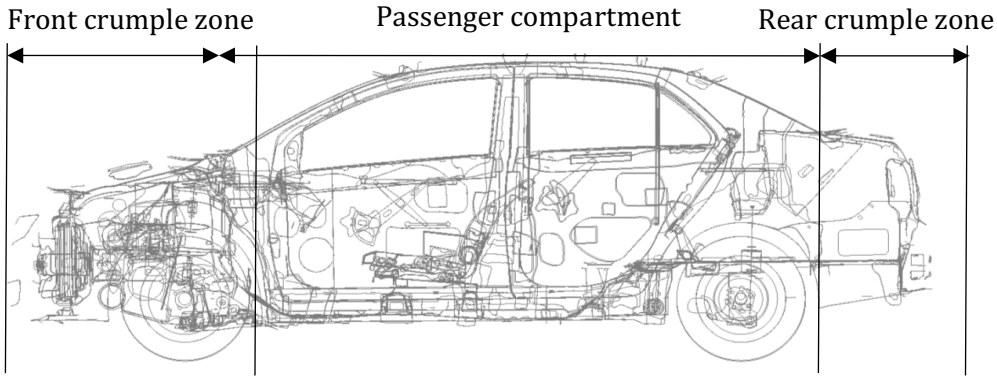

Figure 4-2: *Front and Rear Crumple Zones and Passenger Compartment Forming the Vehicle Body Structure (Marzougui et al., 2012)*

A typical vehicle body structure (VBS) is effectively divided into three zones; the passenger compartment and the front and rear the crumple zones. The three zones are illustrated in Figure 4-2, where a cross-section view of the TYS FE model is used. Crumple zones were first detailed in a Patent (Number 854157) in 1952 by Mercedes-Benz, see (Eckermann, 2001). At that time, crumple zones presented a radical change in the safety design philosophy of vehicles as it went against the concept of a safe VBS needing to be rigid to protect occupants from injuries and fatality. The Patent by Mercedes-Benz introduced the notion of crumple zones being designed to fail/buckle at a pre-determined load or force. In the event of a collision, the design objective of the crumple zones is to absorb the collision kinetic energy through 'designed-in' passively controlled failure/buckling, see (Bhuyan and Ganilova, 2012) and (Alghamdi, 2001).

Consequently, by design, the collision time duration of a buckling crumple zone can be increased (as opposed to that of a rigid structure) and the acceleration/decelerations experienced by the occupant(s) on-board the vehicle are reduced (O'Neill, 2009). The absorption of the collision energy through buckling must take place within the design deformation length of the crumple zone, i.e. avoiding intrusion into the passenger compartment. The passenger compartment is typically constructed with materials exhibiting high stiffness, e.g. high carbon steel (Keeler and Kimchi, 2015), as the passenger compartment is designed to remain rigid during a collision. Intrusion into the passenger compartment is undesirable; therefore, a stiff/rigid structure is designed to resist intrusion whilst considering other design factors, e.g. vehicle mass, noise and vibration. In the case of full-frontal impact tests, as may be expected, it was determined in (Thomas, Charles and Fay, 1995) that intrusion into the passenger compartment increases the risk of lower limb injury. Increased vulnerability of the occupant(s) was found to be due to the foot pedals located in the driver's footwell increasing the risk of injury by some 54% when there is $0.02m$ intrusion into the passenger compartment. Further improvements to vehicle safety have also come about through the introduction of restraint systems within the passenger compartment, e.g. airbags and seat belts are used to minimise the acceleration/deceleration experienced by the occupants through increasing the occupant's impact time duration, see (King, 2017) and (Zaseck, 2017).

In the automotive industry, safety is governed by the crashworthiness performance of a given vehicle. Crashworthiness provides a measure of the ability of a VBS to protect its occupants from serious injuries and fatality during a collision with another vehicle or an object. The introduction of crashworthiness testing has been a success, with a reduction in the number of collision-related fatalities, see (Dischinger et al., 2013).

In Europe, the crashworthiness testing legislation for which vehicle manufactures must comply with, is known as the European New Car Assessment Programme (Euro NCAP), see (Van Ratingen et al, 2016) for a historical overview of the testing programme. Established in 1997, the Euro NCAP comprises specific tests to evaluate the performance of the VBS. In these tests, the VBS is subjected to the following: partial frontal impact, full-width frontal impact, a barrier to vehicle side-impact and pole to vehicle side impact. The crashworthiness of the VBS performance is assessed, where a five-star rating is the highest. The United States of America (USA) also have crashworthiness tests overseen by the National Highway Traffic Safety Administration (NHTSA) authority. Tests in the USA are referred to as the United States New Car Assessment Programme (US NCAP). The tests are very similar to those of the Euro NCAP, although do not include a pole to vehicle side impact test and have an addition of a roof structure test to evaluate the effect of a vehicle roll-over.

Of interest to this research is the full-width frontal impact test. For this test, the Euro NCAP involves the vehicle being tested at $31mph$ ($13.8582m/s$) into an IRW (Euro NCAP, 2017a), whereas the corresponding US NCAP involves the vehicle being tested/driven at $35mph$ ($15.6464m/s$) into an IRW (US NCAP, 2017) as illustrated in Figure 4-3 for the 2010 TYS FE model. Using the TYS FE model which is illustrated in Figure 4-4, a simulation was set-up based on the US NCAP crashworthiness test, with a FE mesh (i.e. mathematical model) applied to the structure consisting of elements (typically around one million elements). The nominal test mass, denoted m_a of the TYS vehicle, is $1247kg$ and the velocity, denoted v_a is applied in the longitudinal-coordinate, i.e. $15.6464m/s$. The FE model contains two virtual accelerometers of interest within this study. These are located at the left and right rear seat positions, and these capture the acceleration experienced by the occupant(s) upon impact with the IRW, see Figure

4-4. The simulation set-up of the TYS FE model detailed in this Sub-Section is used throughout this research.

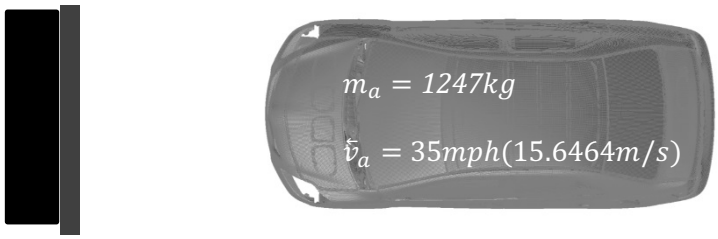

Figure 4-3: *Pre-Impact Conditions of One Colliding Body into an Immovable Rigid Wall, as with the case of the United States New Car Assessment Programme Full Frontal Test (Marzougui et al., 2012)*

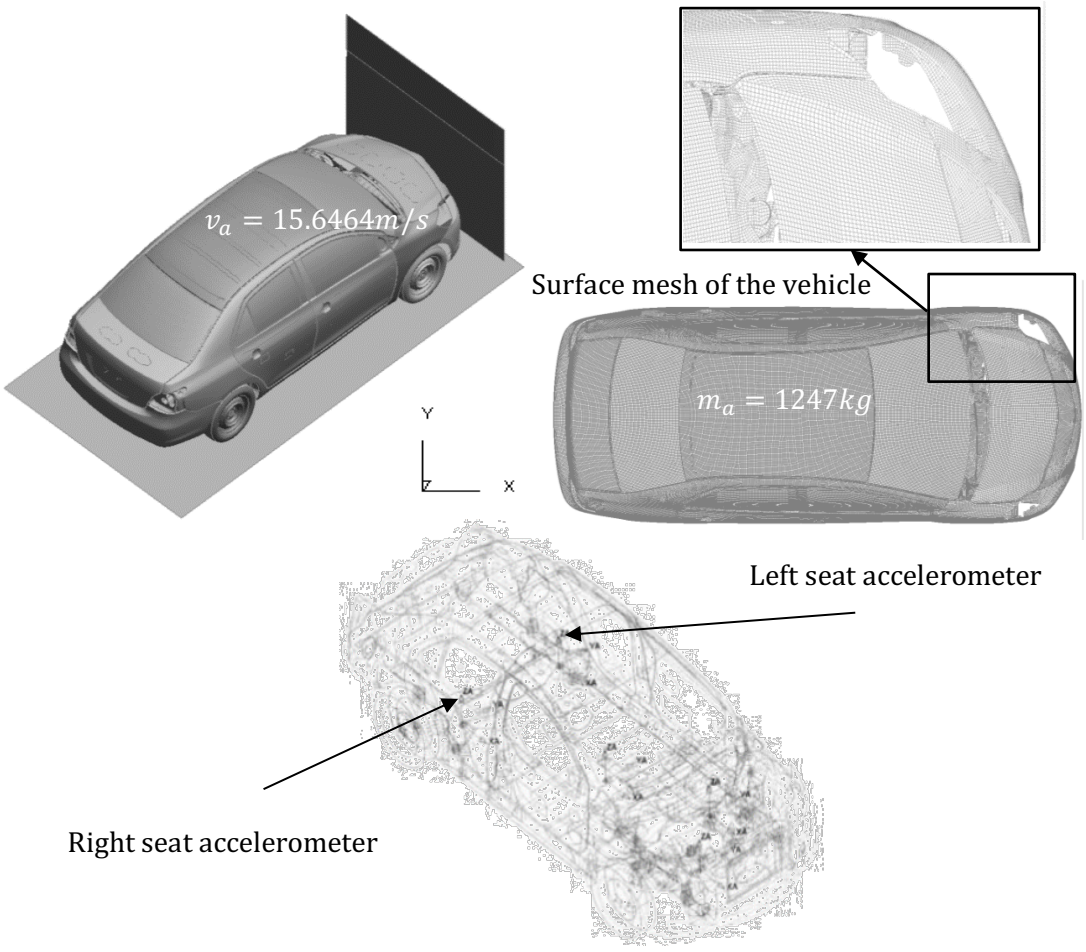

Figure 4-4: *Typical Finite Element Analysis Set-Up of a Single Vehicle Full Frontal Collision into an Immovable Rigid Wall and Accelerometer Positions of Interest, as Developed by (Marzougui, et al., 2012)*

4.2.2 CONSERVATION OF MOMENTUM AND ENERGY

Consider the full-frontal impact test, as illustrated in Figure 4-4. For the collision, Vehicle a, of mass, denoted m_a, is driven into an IRW with an impact collision velocity, denoted v_a. Newton's Second Law states that a force, denoted f_a acting on an object, here Vehicle a, is proportional to the time rate of change of its linear momentum (velocity). The momentum is the product of mass and velocity, i.e. $m_a v_a$, so that the force expressed as a function of time may be alternatively expressed by:

$$f_a(t) = m_a \frac{dv_a(t)}{dt} = m_a \frac{d^2x_a(t)}{dt^2} \tag{4-1}$$

where x_a denotes the deformation of the crumple zone of Vehicle a. The force and momentum are vector quantities and the resultant force is found by vector addition from all the forces present. As the vehicle collides with the IRW, the velocity v_a will decay from its initial impact value, this being due to the frontal vehicle crumple zones buckling and thus absorbing the collision energy. Considering Equation (4-1), if the vehicle mass increases (e.g. additional passenger(s) and luggage) between two collisions, but with the same impact velocity, the vehicle deceleration will decrease. Likewise, with increased impact velocity, but with the same vehicle mass, the vehicle deceleration will increase. The original equipment manufacturer (OEM) designs the frontal crumple zones to satisfy the Euro/US NCAP frontal collision tests. Hence, the VBS is designed to absorb a pre-determined amount of collision energy based on known properties, including vehicle laden mass m_a and initial collision impact velocity v_a. It is known that to satisfy the crashworthiness tests, OEMs are required to design the frontal crumple zones to absorb a designed maximum collision deformation energy, denoted ΔE_{a_D}, where the subscript D denotes design and is given by:

$$\Delta E_{a_D} = \frac{m_{a_D} {v_{a_D}}^2}{2} \tag{4-2}$$

where, for a given vehicle, denoted Vehicle a, ΔE_{a_D} is the design maximum collision energy, m_{a_D} is the design vehicle test collision mass and v_{a_D} is the design vehicle test impact collision velocity (the quantity ΔE_a with respect to Vehicle a denotes the deformation energy that is absorbed in a collision – as will become clear in the sequel). Equation (4-2) is later used in Section 4.2.3 to verify the TYS FE model together with the mathematical models that are developed for a single-vehicle collision in Chapter 5, i.e. linear and nonlinear single-vehicle collision static/dynamic models. It is interesting to note that the US NCAP crashworthiness full-frontal impact test involves a greater amount of collision deformation energy to be absorbed by the vehicles crumple zones than the Euro NCAP test. This is due to the higher design vehicle test impact collision velocity.

4.2.3 COLLISION FORCES AND STRUCTURAL STIFFNESS

In this Section, consideration is given to the 2010 TYS FE model with the vehicle in a full-frontal collision into an IRW. The vehicle model is set-up with the conditions as detailed in Section 4.2.1, see Figure 4-4. It can be observed in Figure 4-5 that the actual vehicle's frontal collision structure deformation is very similar to that of the vehicle's FE simulation model frontal crumple zone.

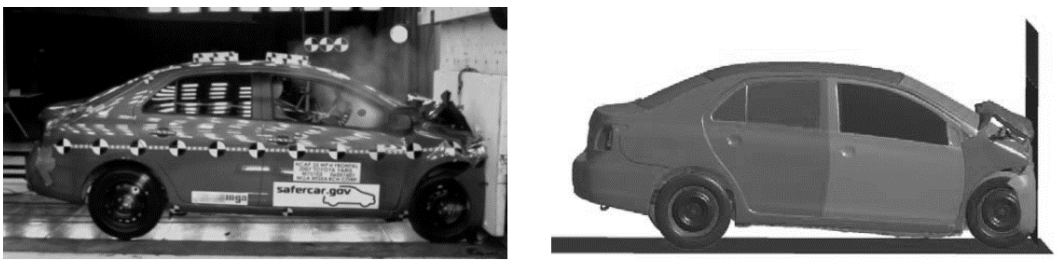

Figure 4-5: *Comparison of 2010 Toyota Yaris Front Collision Structure Deformation to the Finite Element Analysis Vehicle Model, see (Marzougui et al., 2012)*

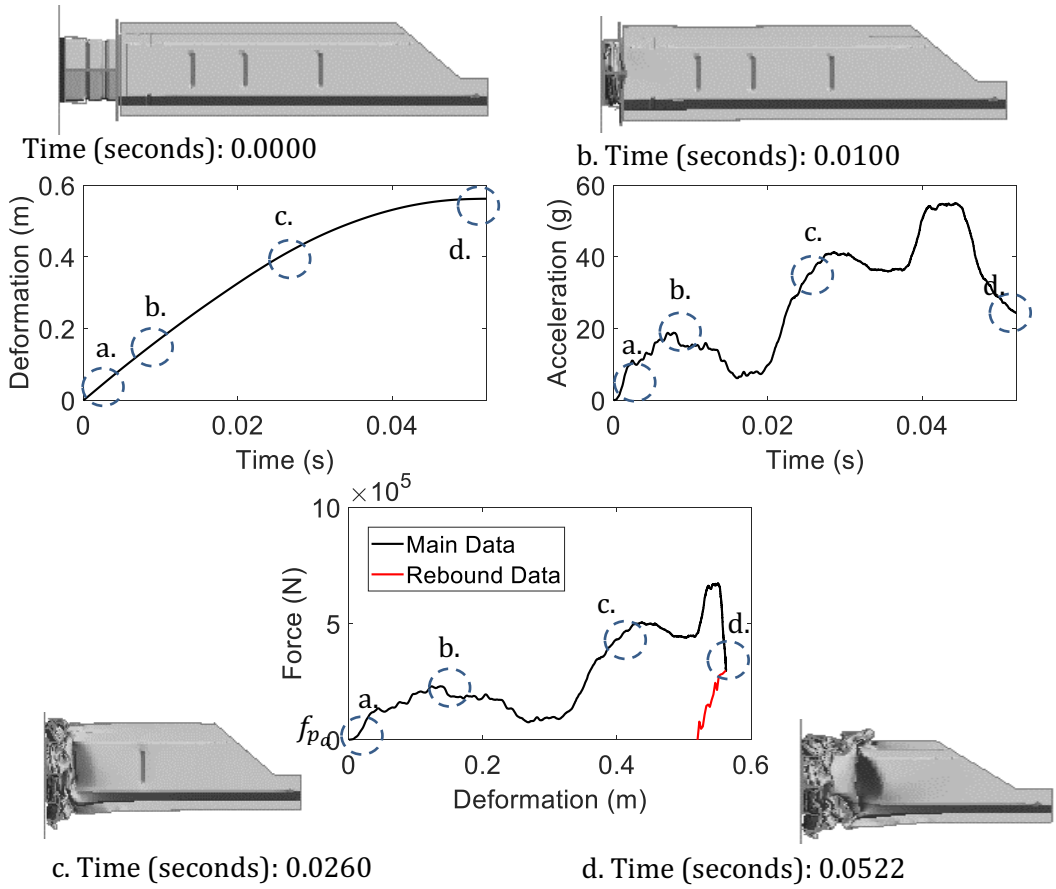

Figure 4-6: *Illustrating Buckling of a Crumple Zone due to Compressive Axial Force, with the Corresponding Toyota Yaris Sedan Finite Element Analysis Model (Marzougui et al., 2012)*

In the event of a full-frontal Euro/US NCAP impact test (as detailed in Section 4.2.1), when the vehicle strikes the IRW, a force, denoted f_a, is applied based on the design test mass, denoted m_{a_D} and the acceleration, denoted a_a. As a result, an equal and opposite force is created as the crumple zones resist failure/buckling, which is denoted f_{a_s}, such that $f_a = -f_{a_s}$. An arbitrary illustration of a vehicle's frontal crumple zone is presented in Figure 4-6 (upper-left). If the force f_a acting on the crumple zone exceeds the failure/buckling point force, denoted f_{p_a}, i.e. $\frac{f_a}{f_{p_a}} > 1$, then axial deformation of the crumple zone commences. In theory, the pre-determined failure point of a vehicle crumple zone, denoted f_{p_a}, may be determined using Euler's buckling formula see (Goriely, Vandiver and Destrade, 2008).

The force versus deformation output data is extracted from the left seat virtual accelerometer, noting that there was only a slight difference between the left and right accelerometer outputs, which was similarly reported in (Marzougui et al., 2012). The acceleration versus time plot in Figure 4-6 (upper-right) displays the filtered outputs from the TYS FE simulation of the full-frontal single-vehicle collision event. The time duration up to the point of the peak deformation is required to be considered, as is commonly adopted, see (Du Bois et al., 2004). In this case, a time period of 0.0522 seconds ($52.22ms$) is observed (upper-left plot in Figure 4-6) and this would also correspond to zero velocity (the plot of velocity is not given). The force acting on the vehicle crumple zones is determined by taking the product of the vehicle laden mass and the acceleration output values (upper-right plot in Figure 4-6), where g denotes the gravitational constant, taken here to be $9.81m/s^2$. The plot of force versus deformation presented in Figure 4-6, (lower-centre plot), provides an illustration of the energy absorption in the collision. The area under the curve corresponds to the collision energy absorbed by the vehicle crumple zone sections. These sections include the bumper, the crush cans and longitudinal members. The collision energy can be determined for such a collision by integrating the area under the curve, noting that the deformation commences between the initial value, denoted δ_{a_i} to a final arbitrary value, denoted δ_{a_f}. This is expressed as follows, (Serway and Jewett, 2012):

$$\Delta E_{a_A} = \int_{\delta_{a_i}}^{\delta_{a_f}} f_{\mathrm{a}}\, d\delta_a \tag{4-4}$$

where the subscript A denotes actual (i.e. as opposed to design) and δ_a denotes the deformation. Substituting Hooke's law, i.e. $f_a = -k_a\delta_a$ into Equation (4-4), where k_a is the average crumple zone stiffness value, the following expression may be stated:

$$\Delta E_{a_A} = \int_{\delta_{a_i}}^{\delta_{a_f}} (-k_a \delta_a)\, d\delta_a \tag{4-5}$$

Integrating yields:

$$\Delta E_{a_A} = \left| -\frac{1}{2} k_a \delta^2 \right|_{\delta_{a_i}}^{\delta_{a_f}} \tag{4-6}$$

giving:

$$\Delta E_{a_A} = \left| \frac{1}{2} k_a \delta_{a_f}^2 - \frac{1}{2} k_a \delta_{a_i}^2 \right| \tag{4-7}$$

The above expression is, in fact, the work done by deforming the frontal crumple zones, from an initial value δ_{a_i} to a final deformation value δ_{a_f}. It is therefore expected that the value for collision energy in Equation (4-7) from the FE force versus deformation data closely matches the value given in Equation (4-2), i.e. the collision energy, ΔE_{a}. However, it is known that not all the kinetic energy given by Equation (4-2) will be converted into collision energy absorbed by the crumple zone, hence that given by Equation (4-7), see (Kuwabara and Goro, 1987). In practice, collisions into an IRW will involve both inelastic deformation and an element of elastic rebound. An element of elastic rebound is highlighted in Figure 4-6 (referred to as rebound data in the legend) of the FE simulation, with the rebound energy causing the vehicle crumple zone structure to restore slightly. The restoring phenomenon of the vehicle crumple zone is explained by the coefficient of restitution. In (Zaikin, Korablin, Dyulger and Barnenkov, 2017), it is stated that many attempts have been made to determine a value for the coefficient of restitution, but they do not always give acceptable results. Consequently, in this research, a detailed study into the coefficient of restitution is not undertaken.

Considering the TYS FE simulation model force versus deformation output given in Figure 4-6, the area depicted by the 'rebound data' line illustrates the presence of restitution, and an approximate value for the coefficient of restitution is later determined in this Section.

As well as absorbing the collision energy, the crumple zones are designed to minimise the acceleration g-forces experienced by the occupant(s) on-board the vehicle by increasing the time duration of the collision through passive buckling. Figure 4-6 illustrates the corresponding acceleration (filtered) versus time, this data is utilised in Section 4.2.4, where the occupant properties are further considered with the occupant 'sled' model in Section 4.2.4. To minimise the acceleration g-force experienced by the occupant(s) on-board the vehicle, passive buckling of the crumple zone is implemented via a designed pre-weakening during manufacture. Pre-weakening is realised via various forms of shaped slots, which include designs such as: bird beaks (corner notches), corner holes and surface beads, as illustrated in Figure 4-6. These features aid symmetric axial buckling, whilst avoiding bending during the collapse, see (Kumar, 2008). The corresponding failure/buckling trend of the crumple zone is illustrated in Figure 4-6, where the upper-left time instant capture is at zero time (a), the upper-right time instant capture is at 0.0100 seconds (b) with this involving the full deformation of the crush can, the lower-left time instant capture is at 0.0260 seconds (c) with this involving the failure/buckling of the longitudinal member and the lower-right time instant capture is at 0.0522 seconds (d), with this involving the end of the failure/buckling. The four captured time instants (i.e. a, b, c and d) are approximately mapped out on the graph of force versus deformation by making use of dashed circles.

The amount of deformation will depend on the structural stiffness, denoted k_a, of the crumple zone. The structural stiffness is effectively given by the gradient or the trend of

the force versus deformation plot in Figure 4-6. This can be described by the linear form of Hooke's law, i.e. $f_a = k_a \delta_a$. As $f_{a_s} = m_a \frac{dv_a(t)}{dt}$ (see Equation 4-1, i.e. the conservation of momentum). The vehicle laden mass and initial impact velocity will influence the vehicle deformation and the corresponding accelerations experienced by the occupant(s) on-board the vehicle. With reference to the Euro NCAP website, see (Euro NCAP, 2017), it is stated that the introduction of crashworthiness testing has resulted in the stiffer design of the VBS. Consequently, the passenger compartment is less prone to collapse (i.e. resists intrusion). Increased stiffness values of the vehicle crumple zone structures have led to higher passenger compartment decelerations. This relationship is demonstrated in (Hollowell et al., 1998), where two-vehicles, the 1996 Ford Taurus and a 1995 Ford Ranger Pickup truck, both of similar masses (i.e. $1750kg$), are subjected to the US NCAP full-frontal IRW test. The crumple zone stiffness is significantly higher for the Ranger than the Taurus. In the case of a collision, the occupants within the Ranger experience higher accelerations, which would lead to an increase in the risk of severe injuries, especially in the head and chest regions of the more vulnerable, younger, slightly built or elderly occupants, see (Ekambaram and Frampton, 2016). However, as expected, the deformation of the Ford Ranger Pickup truck is significantly lower than that of the Ford Taurus. This highlights that the US/Euro NCAP full-frontal impact tests and the design of the crumple zones poses a compromise between lower leg (excessive intrusion into the passenger compartment) and head and chest injuries (high acceleration rates).

Corresponding to the TYS FE simulation outputs (these based on a simulation of the US NCAP full frontal impact test) illustrated in Figure 4-6, key features from the data have been extracted and documented in Table 4-1. One of the key features is the peak deformation output, i.e. at the point before rebound on the force versus deformation plot. The designed deformation length, denoted δ_{a_D}, is also given in Table 4-1, with this

being the length of the crumple zone area (above this value would result in deformation into the passenger cell). Note that the peak deformation from the FE simulation of the Euro NCAP testing is lower than the design deformation length (i.e. by $0.02725m$), therefore no risk is presented to the occupant(s) within the vehicle through deformation into the passenger cell, see Figure 4-7. Of interest, in Table 4-1 is the peak acceleration and the resulting collision energy (with consideration of the rebound data). The latter is mainly used as a means of verifying the FE model, considering laws of conservation of momentum and energy, as detailed in Section 4.2.2. From the data detailed in Table 4-1, it can be confirmed that the TYS FE vehicle model data matches the actual vehicle post-test deformation (i.e. rebound) and peak deformation data sufficiently closely (Marzougui et al., 2012). It is also clear that the peak acceleration of the actual TYS vehicle matches the FE model closely (the peak acceleration for the actual vehicle was directly obtained from an acceleration versus time graphical output). The actual vehicle collision force versus deformation data and collision duration data values were not attainable, thus the collision deformation energy could not be determined. However, based on Equation (4-2), the pre-collision kinetic energy is determined to be 153 kJ, and this does closely match the collision energy (main data) value of 149 kJ. The difference in the two values (i.e. 153 kJ and 149 kJ) is likely to be due to factors such as energy being absorbed by the tyres, sound and vibration. In Figure 4-6, the area depicted by the falling dotted line (i.e. the rebound data) was determined to amount to some $7kJ$ of the collision energy, thus 142 kJ of the collision energy would account for the energy absorbed by the crumple zones of the vehicle with $7kJ$ of the collision energy being restored, see Table 4-1. The difference between the two collision deformation energy values (i.e. 149 kJ and 142 kJ) is probably explained by the restitution, where a difference of 4.9% is present. In this research, it will be assumed that the coefficient of restitution is fixed for a given vehicle crumple zone, i.e. increases or changes to the collision laden mass or velocity would not change the value. Based on the data presented

in Table 4-1, the FE model is taken to be an adequate surrogate for the actual vehicle. The data values presented in Table 4-1 become the defining key features when developing the one-vehicle collision models involving an IRW in Chapter 5 and the two-vehicle collision models that are developed in Chapter 6.

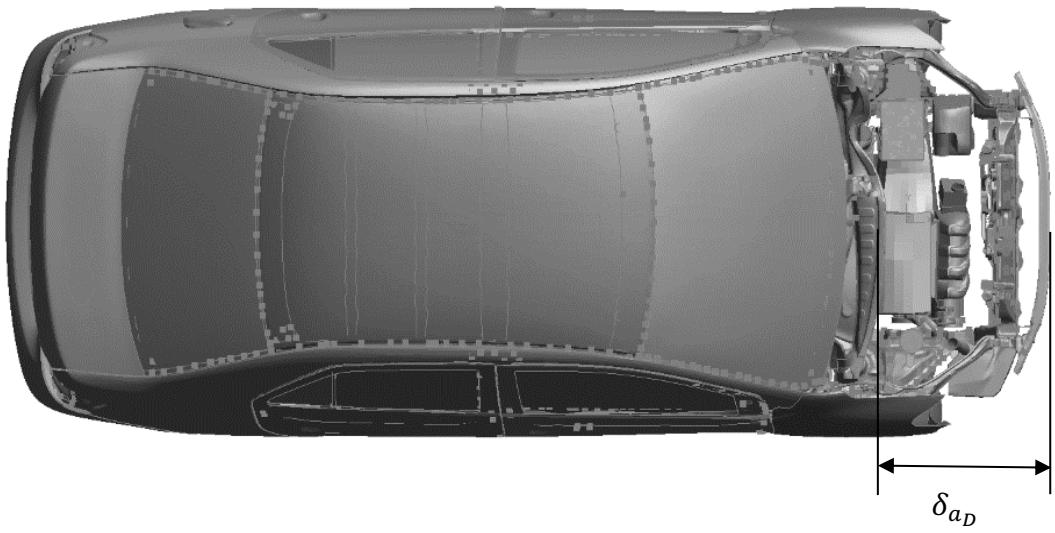

Figure 4-7: *Illustrating the Designed Deformation Length of the 2010 Toyota Yaris Sedan Finite Element Model (Marzougui et al., 2012)*

Table 4-1: *Typical Frontal Collision Output Results for Actual Data and Finite Element Model (Marzougui et al., 2012)*

	Actual Vehicle	**FE Model**
Mass $[kg]$	1271	1247
Impact Velocity $[m/s]$	15.6464	15.6464
Post-Test Deformation $[m]$	0.5170	0.5201
Peak Deformation $[m]$	0.5620	0.5625
Designed deformation length [m]	---	0.5900
Peak Acceleration $[g]$	~ 52.00	55.04
Collision energy – Main Data [kJ]	---	149.1
Collision energy – Rebound Data [kJ]	---	7.560
Collision Energy [kJ]	---	141.5
Collision Duration $[s]$	---	0.0522

4.2.4 OCCUPANT SLED MODEL

To investigate occupant injuries, the automotive industry uses physical cabin sub-models to assess and tune the vehicle restraint systems, e.g. seat belts, as illustrated in Figure 4-8. In this research, a well-developed physical cabin sub-model is used to gain typical occupant head and chest acceleration versus time output data, with the peak values of head and chest acceleration being of primary interest. The cabin sub-model used in this research includes the vehicle interior, containing vehicle trim, seat, steering wheel and seatbelt to replicate the occupant environment. The sled model can be used to adjust the restraint systems, including seatbelt pre-tensioner timings, load limiter levels and airbag inflation. The sled model contains anthropometric test devices (ATDs), i.e. crash dummies that are contained within the sled model in a typical seating position including a seat belt. In this research, a 50 percentile male is placed in a seating position representing a typical UK driver with an airbag. The mass of the ATD 50% is approximately $78kg$ and with a height of $1.75m$. The sled model can be used to investigate occupant injuries due to inertia forces and occupant contact with the dashboard and steering wheel (with the aim of avoiding/mitigating such contact). The sled and ATD model have been created by Arup, and together are known as the Arup Generic Sled Model. As with the TYS vehicle model, the ATD model is available for research via an open-access source and accessible from the Livermore Software Technology Corporation (LSTC), see (LSTC, 2017). The content displayed in Figure 4-8 has been obtained from the sled model simulation when subject to the acceleration versus time data presented in Figure 4-6. The left plot shows the occupant and sled prior to the collision and the plots to the right show the occupant position on impact. The upper illustrations show the plan/side view of the occupant and the lower illustrations show the side view depicting the windscreen (left) and airbag deployment (right). It should be noted that a detailed study into occupant safety is worthy of a research project

in its own right and it would be necessary to consider a more detailed occupant analysis, as undertaken in (Bastien, 2014) and (Ekambaram, 2016).

Using the cabin sub-model with the 50% ATD model, the acceleration versus time output data (illustrated in Figure 4-6 from the TYS FE simulation) is applied as an input to the sled model, with the responses given in Figure 4-9 for the ATDs head (left-plot) and chest (right-plot) accelerations. Access to actual sled model data was not obtainable, therefore the sled model results are taken as a surrogate for the actual vehicle collision containing an ATD. The peak values of the responses are taken as the corresponding g-forces experienced by the occupants' head and chest. The peak values of the sled test model are given in Table 4-2. Based on these, the severity of a given collision scenario may be quantified by considering the accelerations experienced to the occupants' head and/or chest. In (Stapp, 1970) and (Kun, Haibin and Yang, 2016), based on collision testing methods (i.e. U.S. NCAP), the maximum/peak acceleration of an occupant's head should not exceed $80g$ for more than $3ms$, see Table 4-2. It is considered that a higher value could cause a high risk of injuries to the face and weaker parts of the human skull. It is assumed that such values are experienced upon the occupants' head striking the vehicle structure or steering wheel (Ekambaram, 2016). The US Federal Motor Vehicle Safety Standard (FMVSS), namely the 208 Standard, implies a frontal impact test limit of $60g$ for occupant peak chest acceleration (Prasad, 2015), see Table 4-2. Interestingly, the peak head acceleration and peak chest acceleration are within the testing limits, see Table 4-2.

Acceleration versus time output data from the Toyota Yaris Sedan FEA simulation applied to the sled model

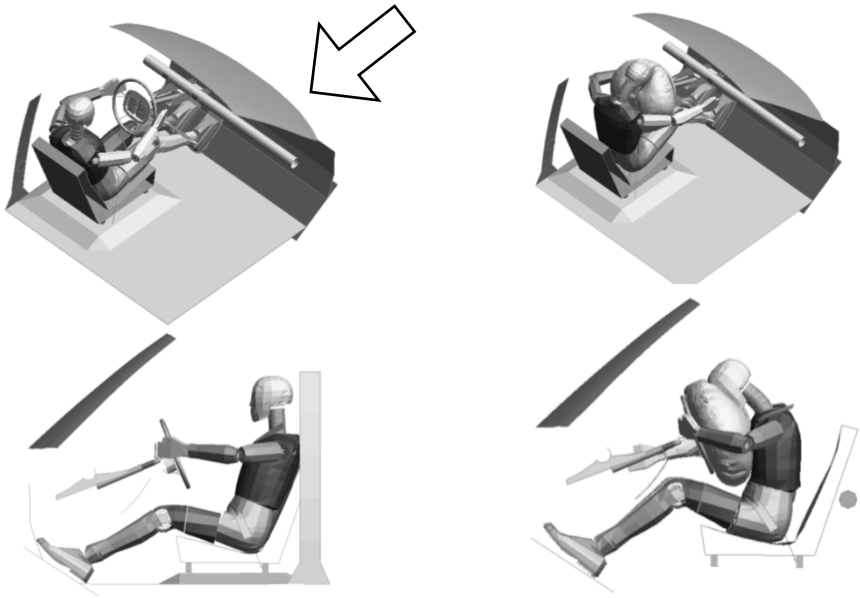

Figure 4-8: *Illustrations of Occupant Simulation Run-Time, Occupant Location with Occupant Hitting an Airbag*

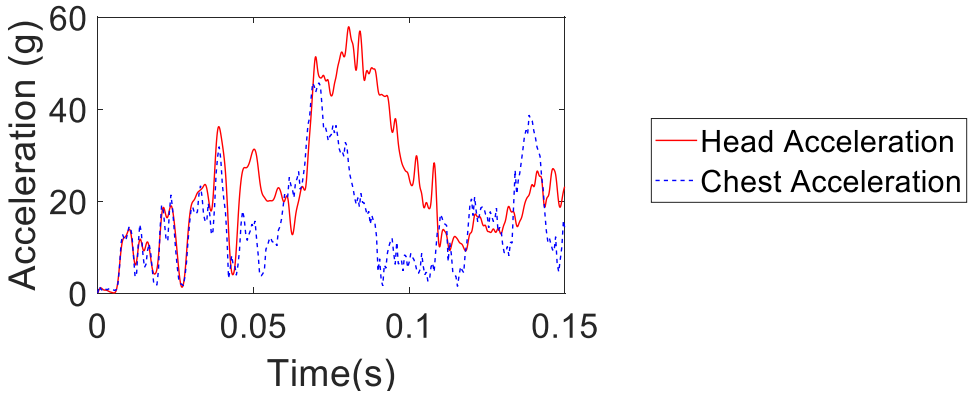

Figure 4-9: *Occupant Head and Chest Data Obtained from Sled Model*

Table 4-2: *Comparison of Actual Test and Sled Model Test Occupant Properties*

	Sled Model	**Testing Limits**
Peak Head Acceleration [g]	57.95	80
Peak Chest Acceleration [g]	45.74	60

4.3 BACKGROUND INTO MULTIPLE VEHICLE COLLISION SAFETY

The background into multiple vehicle collision safety relevant to this research for the ECS is presented in this Section, with attention being given to two-vehicle full-frontal head-on collisions. In this Section, unlike in Section 4.2, a FE collision simulation is not used to explain the physical phenomena around multiple vehicle collisions. Following initial studies into multiple FE collision simulations (structural and occupant), it was found that the results proved to be inadequate, e.g. after filtering the acceleration versus time collision data from a two-vehicle full-frontal collision, the forces were found to be not equal and opposite. (Hence the FE model was not taken further.) However, based on the findings using the developed lumped parameter models (LPMs), see Chapters 5, the one-vehicle models were readily extendable to the two-vehicle case. It is also noted that the basic physics of multiple vehicle collisions, i.e. conservation of momentum and energy, collision forces and structural stiffness is readily scalable to the multiple vehicle cases. It is also assumed that the coefficient of restitution value determined in Section 4.2.4 (i.e. 4.9%) is adequate in explaining the phenomena in multiple vehicle collisions of varying masses and velocities. Note, therefore, that the FE models are not used in this Section to further explain the collision phenomenon of two-vehicle collisions.

4.3.1 CONSERVATION OF MOMENTUM AND ENERGY

Considering a two-vehicle full-frontal head-on collision, the pre- and post-impact conditions are illustrated in Figure 4-10 (Upper) and 4-10 (Lower), respectively. It is well known from Newtonian dynamics that when two bodies collide the resulting momentum of the combined body is given by the momenta of the two bodies prior to the collision, i.e. the momentum of the two moving bodies is conserved within the single combined moving body. This may be expressed as follows:

$$m_a\overrightarrow{v_a} + m_b\overleftarrow{v_b} = m_{a+b}\overrightarrow{v_f} \qquad (4\text{-}8)$$

where m_a and m_b denote the masses of two colliding AVs, namely Vehicles a and b, $\overrightarrow{v_a}$ and $\overleftarrow{v_b}$ denote the velocities of the two-vehicle masses and $\overrightarrow{v_f}$ denotes the final velocity of the combined vehicle mass, denoted m_{a+b}, where $m_{a+b} = m_a + m_b$.

The arbitrary illustrative example given by Equation (4-8) and shown in Figure 4-10 indicates that the momentum $m_a\overrightarrow{v_a}$ is greater than $m_b\overleftarrow{v_b}$ and, noting the opposing motions of the two moving bodies, it is clear that $m_{a+b}\overrightarrow{v_f}$ has the same sign as $m_a\overrightarrow{v_a}$, hence the same direction of travel for the combined body. Rearranging Equation (4-8), the final velocity of the combined mass can be expressed as follows:

$$\overrightarrow{v_f} = \frac{m_a\overrightarrow{v_a} + m_b\overleftarrow{v_b}}{m_{a+b}} \tag{4-9}$$

The principle of conservation of energy states that the kinetic energy pre- and post-collision must be identical. This may be expressed as follows:

$$\underbrace{\frac{1}{2}m_a\overrightarrow{v_a^2} + \frac{1}{2}m_b\overleftarrow{v_b^2}}_{\text{Pre-collision}} = \underbrace{\frac{1}{2}m_{a+b}\overrightarrow{v_f^2} + \Delta E_{a+b}}_{\text{Post-collision}} \tag{4-10}$$

where ΔE_{a+b} denotes the collision deformation energy. Thus, it is possible from Equation (4-10) to deduce and pre-determine the ΔE_{a+b} from a two AV collision scenario.

Pre-collision:

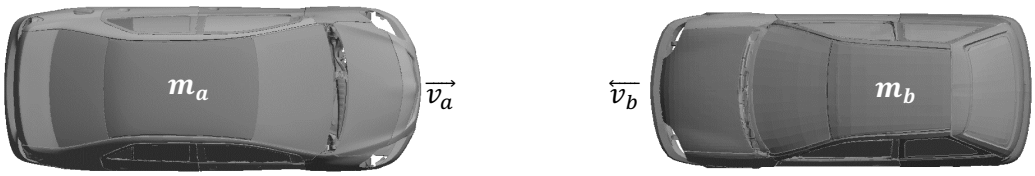

Post-collision:

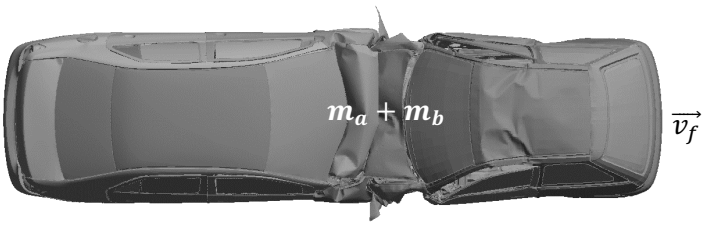

Figure 4-10: *Illustrating Pre- and Post-Impact Conditions of Two Colliding Bodies (This Arbitrary Example is used for Illustrative Purposes Only)*

4.3.2 COLLISION FORCES AND STRUCTURAL STIFFNESS

In the event of a full-frontal two-vehicle impact collision, when the AVs collide, equal and opposite forces are applied to the two vehicles collision structures, with the following being given for Vehicle a:

$$f_a = m_a a_a = m_a \frac{d^2 x_a(t)}{dt^2} \tag{4-11}$$

and for Vehicle b:

$$-f_b = -(m_b a_b) = -\left(m_b \frac{d^2 x_b(t)}{dt^2}\right) \tag{4-12}$$

where a_a and a_b are the two vehicles accelerations and f_a and f_b are the two-vehicle opposing forces, respectively. As with the single vehicle case detailed in Section 4.2, the amount of deformation to each of the vehicles' collision structures will depend on the structural stiffness, vehicle mass and initial impact velocity. Considering Hooke's law, i.e. $F_a = k_a x_a$ for Vehicle a and $-F_b = -(k_b x_b)$ for Vehicle b, where k_a and k_b, denote,

respectively the structural stiffness values of the two vehicles and x_a and x_b, denote, respectively the two vehicles' deformations, assuming the vehicles have identical structural stiffness, the result of a two-vehicle full-frontal collision would result in equal deformation, see Figure 4-11. Consequently, both vehicles would result in an equal distribution of the collision energy, as detailed by Equation 4-10 and illustrated in Figure 4-11. In the case of the mass of one of the vehicles increasing (due to passenger numbers and luggage) and assuming the two colliding vehicles have identical collision structures (i.e. stiffness and geometry), this would result in a lower acceleration experienced by that vehicle and a higher acceleration experienced by the other vehicle.

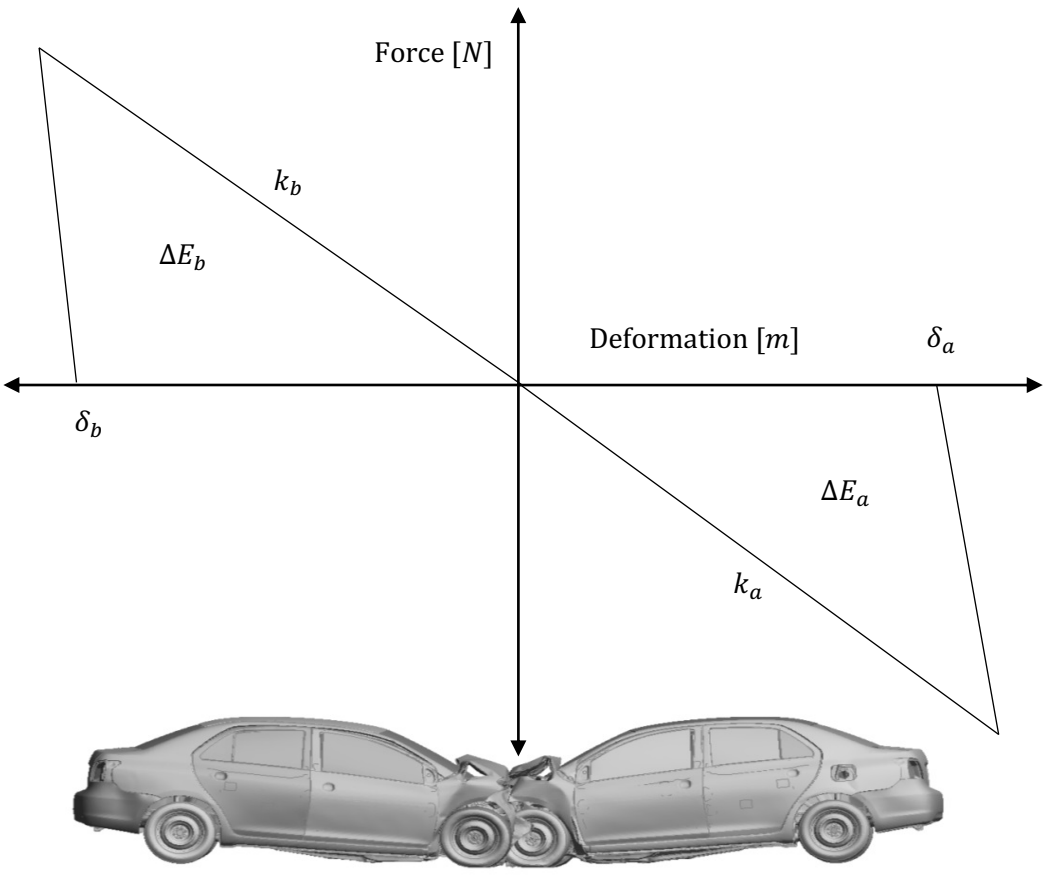

Figure 4-11: *Illustrating the Graphical Collision Output Responses from a Two Vehicle Full Frontal Head-on Collision with Equal vehicle Mass and Structural Stiffness (Note that the areas under the curve ΔE_a and ΔE_b are equal)*

4.4 ACTIVE COLLISION STRUCTURES

The potential benefit of an active structural controller for the vehicle crumple zones is introduced to reduce injuries to the occupants contained within the vehicle(s). The effect of altering the crumple zone properties allows reduced/increased deformation. Such changes have the accompanying effect of reducing/increasing the acceleration/deceleration experienced by the vehicle occupants. The current literature of active collision structures will be detailed, however, an interesting common fact among these early proposals is that none have yet been practically realised on a production vehicle.

Early proposals date back to the 1970s, with one appealing approach proposed in 1973 by Appel and Tomas, where the authors proposed a 'soft nose' on vehicles. The motivation for this early work was to decrease the level of deformation experienced by lighter vehicles when colliding with heavier vehicles. The soft nose concept could effectively be realised nowadays as a tuneable shock absorber in the longitudinal axis. It is interesting to note that it was not until 1994 that Clark, see (1994), proposed an embedded airbag system within the bumper. However, the main motivation here was to reduce damage to the vehicle. Combining this concept with the soft nose could conceivably lead to the use of pre-pressurised airbag systems within the bumpers. In 1999, Witteman proposed a new front-end crashworthiness structure which involved a system of integrated cables and pulleys, with brakes applied to sliding guides, where the aim was to transfer the load from one longitudinal member to another in an asymmetrical collision. It was claimed that the energy absorption was similar for almost all types of frontal collision, see Figure 4-12 (a), (Witteman, 1999), (Witteman and Kriens, 2001) and (Witteman, 2005). In 2001, Honda patented a new method which was developed to control the rigidity of the longitudinal members, thereby changing the deformation of the front-end structure. In this concept, it was conjectured that external

forces would be sensed to activate local devices attached to the two longitudinal members, see Figure 4-12 (b), (Honda Motor, Co, 2001). The means of adjusting the rigidity via actuation is proposed by using smart materials such as magnetostriction element or piezoelectric. Smart materials have the ability to possess functions such as sensing, actuating and controlling. These functions can be used in a structure where there is a need to react under the influence of the environment, i.e. an induced force (Gupta and Srivastava, 2010). There are high-value military applications of smart materials, for example, wearable bulletproof armour which employs woven piezoelectric devices to provide rapid mechanical response changes to prevent intrusion of high-speed bullets (Schuster, Fels and Akzo Nobel, 1998). Other high-value engineering examples of applications where smart materials are already being deployed include rotor blades of high-speed turbines used within the aerospace industry (Hartl and Lagoudas, 2007) and renewable wind energy generation in the power industry (Barlas, Vab Kuik, 2010). In 2002, Jawad proposed an extendable hydraulic bumper system to effectively increase the deformation length of the vehicle. It was also proposed that stiffening or softening could be implemented depending on the severity of the collision, see (Jawad, 2002). In 2004, Honda Motor Co., filed a further patent in which piezoelectric actuation devices were proposed and this built on the initial concept that was patented in 2001, see (Honda Motor Co, 2004). It was claimed that use of the piezoelectric devices could control buckling, hence deformation, of the longitudinal members. The authors, (Ostrowski, Griskevicius and Holnicki-Szulc, 2005) proposed an adaptive system using controlled pyrotechnic detachable connectors that were attached to the two longitudinal members. The approach was prompted by the fact that the severity of frontal impacts become exacerbated when there is a partial offset, with the idea being to balance the loading across the two members. An illustration of the detachable connectors is shown in Figure 4-12 (c). In 2007, Elmarakbi and Zu, built on the proposal of Jawad from 2002 to similarly propose an extendable bumper system,

but it accommodated for offset collisions and was designed with controlled stiffening and softening of the front-end longitudinal structures, see Figure 4-12 (d) and (Elmarakbi and Zu, 2007). In 2016, in (Graczykowski, 2016), the author proposed adaptive inflatable structures to use for impact absorption. The system developed in simulation involved inflatable structures equipped with controllable valves that served for internal pressure control. It is thought such an approach could potentially be applied to the vehicle collision structure to control the deformation rate. In 2014, prompted by the patent proposed by the Honda Motor Co., the author filed a UK patent for an active buckling control system and subsequently, an International patent has been granted in the USA, 2017. Further details of the patent are given in Appendix 2.0.

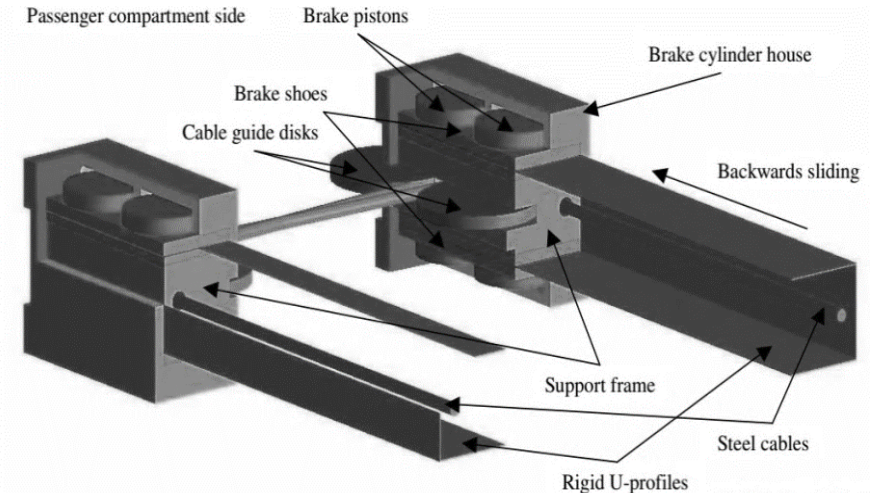

(a)

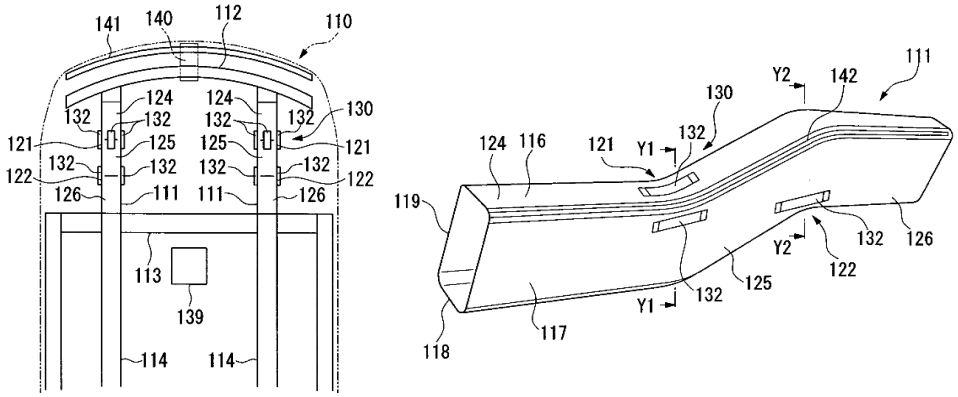

(b)

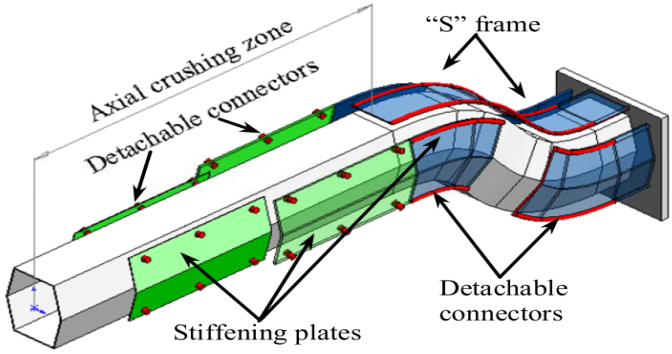

(c)

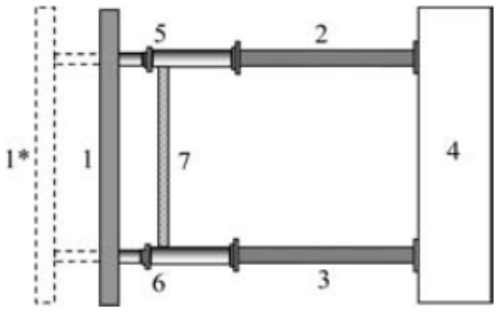

1) Bumper
1*) Bumper in extendable position
2) Right longitudinal member
3) Left longitudinal member
4) Body of the vehicle
5) Right hydraulic cylinder
6) Left hydraulic cylinder
7) Cross member

(d)

Figure 4-12: *Previously Proposed Active Crumple Zone Structures and Systems*

4.5 VULNERABLE ROAD USER CONSIDERATIONS

Vulnerable road user (VRU) is the general term used to describe pedestrians, cyclists, motorists and horse riders. Pedestrian fatalities account for approximately 14 percent of road fatalities across Europe, with children and the elderly being at a significantly higher risk, see (Euro NCAP, 2017b). Early considerations for the design of vehicles to consider VRUs include Rolls-Royce re-designing their bonnet mascot, the spirit of ecstasy, with this retracting into the bonnet upon impact. More recently, Jaguar and Mercedes have removed their protruding mascots to meet the new strict testing and legislation criteria for improved pedestrian impacts, see (Dokoupil, 2008).

Pedestrian testing was introduced to the Euro NCAP upon it being founded in 1997 (Hobbs and McDonough 1998). ATDs are used for the testing of pedestrian-vehicle collision performance. The test involves a vehicle being driven at $40 km/h$ into the ATD, specifically the velocity at which most pedestrian incidents occur, commonly within cities. The tests involve investigating head impact, upper leg impact and lower leg impact. The testing procedure strongly promotes the use of energy-absorbing structures and more forgiving geometry that mitigates injuries (Li, Yang and Simms, 2017) and (Crandall, Bhalla and Madeley, 2002). More recently, devices such as pop-up hoods triggered by pyrotechnic devices have been used to raise the bonnet away from the engine (such as the Jaguar XK). Similar to the airbags that are used within the passenger compartment to minimise accelerations experienced by the occupants in the event of a collision, airbags have also been fitted under the bonnet and are deployed to protect the pedestrian's head from stiff structures, such as the base of the windscreen and the A-pillar (such as the Jaguar XJ and Volvo V40).

4.5.1 PEDESTRIANS AND THEIR SURVIVABILITY

To prepare for the development of the ECS in Chapter 7 for the single-vehicle collision scenario into a pedestrian, the injury severity and fatality risk in typical pedestrian-vehicle incidents need to be studied.

In the event of a pedestrian being struck by an AV, the severity of injuries and the probability of survival depends on the following factors:

- Age of the pedestrian, see (Henary, Ivarsson and Crandall, 2006), (Peng and Bongard, 1999) and (Sze and Wong, 2007).
- Vehicle type, see (Ballesteros, Dischinger and Langenberg, 2014), (Desapriya et al., 2010) and (Lefler and Gabler, 2004).
- Collision impact velocity, see (Richards, 2010) and (Rosén and Sander, 2009).

In this work, it is assumed that future passenger vehicles will be driverless AVs, with the same size/type structurally and designed such that the variation of influence the AV has on pedestrian-vehicle collision survivability is minimal. This aligns with the findings in (Mizuni and Kajser, 1999), where it is concluded that it is the structure that affects the pedestrian-vehicle injury severity. These factors are particularly important when considering the interests of improved road safety combined with the effect of AV laden mass on peak deformation and occupant peak chest and head accelerations.

In (Gustafsson and Thulin, 2003), the authors demonstrated that increased risk of fatality to a pedestrian occurs between the ages of 45 and 64. Similarly, in (Kröyer, 2015), the authors indicated that the risk might start to increase between the ages of 40 to 45. Younger age groups (less than 20 years of age) are also at higher risk of severe injuries, see (Pitt et al, 1990). It is therefore observed that the relationship between age and severe injuries is an inverted U-shaped function, as noted in (Kröyer, 2015).

The collision impact velocity has a significant effect on the force of the impact; this being the most direct variable to determine injury severity, see (Pitt et al, 1990). Studies by various authors have demonstrated that the risk of severe injuries and the risk of fatality are dependent on the vehicle-pedestrian impact velocity, see (Tefft, 2011), (Roudsari et al., 2004), (Fredriksson, Rosén and Kullgren, 2010), (Davis, 2001) and (Rosén and Sander, 2009). It is noted that the author's findings vary, i.e. the resultant fatality risk values. It is stated in (Kröyer, Jonsson and Várhelyi, 2014) that a $10km/h$ increase in collision impact velocity of a vehicle into a pedestrian will result in a doubling of the fatality risk at city velocities. In (Richards, et al., 2010), the authors show that human driver vehicles (HDVs) travelling at higher velocities are more likely to be involved in serious pedestrian accidents than those travelling at lower velocities. In (Kröyer, 2015), the author showed that when the mean velocity was below $39km/h$ (i.e. $10.8333m/s$ or $24.2335mph$), fatal accidents were rare, with only 1 out of 19 accidents being fatal. The fatal accident is that of an 86-year-old who was struck by a heavy truck. In (Leaf and Preusser, 1999), around 10% of fatal accidents occurred at velocities equal or below $40km/h$ (i.e. $11.1111m/s$ or $24.8548mph$). A similar study was undertaken in (Kröyer, 2015), where a value of 5.8% was determined. In (Tefft, 2013), data from the United States of America (USA) was presented. It was determined that 31.7% of severe injuries occurred at vehicle collision impact velocities below $32km/h$ (i.e. $8.8889m/s$ or $19.8839mph$). Similarly, data from the UK, see (Ashton, 1980), states that 32.7% of severe vehicle collision injuries occur at velocities below $30km/h$ (i.e. $8.3333m/s$ or $18.6411mph$). Although the data for the UK and USA were published at different times, 2013 and 1980, respectively, the values are very similar. However, the data suggests that for severe injuries to be avoided, $30km/h$ may not be a low enough impact velocity. It is expected in the case of the UK, that vehicle design has now improved so the percentage of severe injuries published in 1980 (Ashton, 1980) for impact velocities of $30km/h$ is currently likely to be too high. The paper by Cuerden, Richards and Hill, see

(Cuerden, Richards and Hill, 2006) reports on an on-going project known as 'On the Spot' (OTS) accident data collection, which started in 2000. The OTS project collected data from 500 road accidents per year and worked closely with both the Nottinghamshire and Thames Valley Police Forces. Of the 3000 road incidents investigated, 108 involved pedestrians and road vehicles. The purpose of the publication was to examine the causes of the pedestrian injury severity using the UK Governments accepted descriptions of slight, severe and fatal, see (Department of Transport, 2017). Whilst the data set is small, the findings are in broad agreement with an earlier study carried out in 1979 by Ashton and MacKay, see (Ashton and MacKay, 1979), whose work was used to promote the 'Think! Road Safety' campaign for the Department of Transport. The slight differences (suggesting improvements) in the findings go some way to demonstrate that current vehicles designed to satisfy the pedestrian sub-system impact tests as part of the Euro NCAP are now more pedestrian-friendly than the vehicles in the fleet of the past. Placing the findings of the paper in the context of the research being carried out here, the main results are summarised in Table 4-3, which highlights the percentage of injuries arising over a range of impact velocities. Of the 108 incidents, 70% of the injuries were to the head, and 90% of the fatalities having injuries to the head. In most cases, it was the A-pillar where the collision impact took place. Most of the slight injuries were to the lower leg and knee due to a collision impact with the front bumper. Some 85% of the incidents with pedestrians occurred at impact velocities lower than $50kph$ (i.e. $13.8889m/s$ or $31.0686mph$) where there is a lower probability of fatality. However, it is interesting to note that most of the pedestrians are hit on the side walking across the path of the vehicle and are typically struck by the front of the moving vehicle.

Figure 4-13 illustrates the relationship between mean travelling velocity of a vehicle and the collision impact velocity involving a 40-year-old pedestrian versus percentage

possibility of fatality, see (Kröyer, 2015) and (Rosén and Sander, 2009). The difference in these curve profiles is since a driver typically brakes to reduce the impact velocity before the actual collision event. Of interest, in this study is the impact velocity versus percentage possibility of fatality. It is also worth highlighting that the curve in Figure 4-13 closely matches the data presented in Table 4-3. For example, in Table 4-3, an impact velocity of 50 – $60 km/h$ (i.e. $31.0686 mph$ –$37.2623 mph$) gives a fatal injury percentage of 11%which closely matches the $60 km/h$ value given in Figure 4-13.

Table 4-3: *Highlighting Severity of Pedestrian Injury and Corresponding Impact Velocity (Cuerden, Richards and Hill, 2006)*

Impact Velocity [km/h]	Slight Injury (%)	Severe Injury (%)	Fatal Injury (%)
0 – 10 ($6.2137 mph$)	100	-	-
10 ($6.2137 mph$) – 20 ($12.4274 mph$)	60	40	-
20 ($12.4274 mph$) – 30 ($18.6411 mph$)	67	33	-
30 ($18.6411 mph$) – 40 ($24.8548 mph$)	53	43	4
40 ($24.8548 mph$) – 50 ($31.0686 mph$)	22	65	13
50 ($31.0686 mph$) – 60 ($37.2623 mph$)	-	89	11
60+ ($37.2623 mph$)	-	50	50

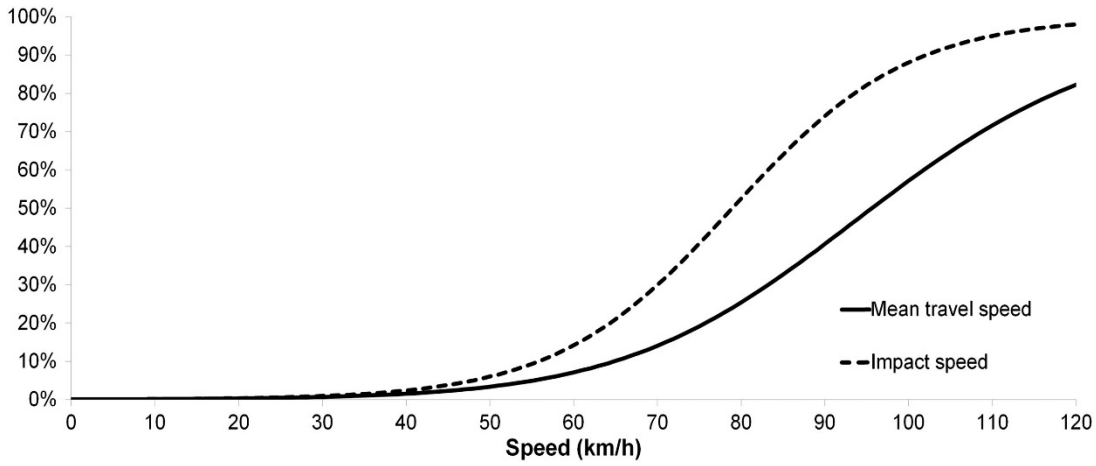

Figure 4-13: *Fatality Risk Curve Based on Impact Velocities, see (Rosén and Sander, 2009) and Fatality Risk Curve Based on Mean Travelling Velocity for a 40-year-old victim, see (Kröyer, 2015)*

REMARK 4-1

It is the view of the author that vehicle-pedestrian collision safety is a non-trivial task. From understanding the literature review into pedestrian safety, there are limitations to the studies. as they are heavily reliant on the precision and accuracy of the accident reports. A further study exploring the variations of vehicle-pedestrian collisions is needed. This could be conducted by combining an FE vehicle simulation with an ATD and is an identified area for further work.

¤

4.6 SUMMARY

This Chapter has introduced the background into vehicle collision safety. Finite element (FE) has been used to gain a further insight into the collision properties of a Toyota Yaris Sedan (TYS) 2010 vehicle. FE models are initially used to obtain deformation versus time, acceleration versus time and force versus deformation, hence extracting collision deformation energy. The acceleration versus time data is used in conjunction with a sled model to extract the peak occupant head and chest g-force values. The peak occupant head and chest g-forces, along with peak deformation form the three key features that are used in the ethical collision system (ECS) that is to be developed in Chapter 7. The focus was then given to a two-vehicle full-frontal collision scenario, however with an FE model not used. Instead, the conservation of momentum and energy, collision forces and structural stiffness are considered. As with the one-vehicle collision into an immovable rigid wall, the same three key features (i.e. peak deformation, peak chest acceleration and peak head acceleration) are of interest. A possible solution to improving collision scenarios is introduced through the use of active collision structures. However, to date, none have been realised and the potential of this will be explored in this research. A review of studies on pedestrian vulnerability has then been considered with varying levels of severity, with these to be further developed when used within the ECS.

5. SYSTEMS MODELLING OF A VEHICLE COLLISION: IMMOVABLE RIGID WALL

5.1 INTRODUCTION

This Chapter is focused on the development of a linear single lumped parameter model (LPM) to present the phenomenon of a full-frontal collision into an immovable rigid wall (IRW). An initial literature review into previous work undertaken on linear LPMs is undertaken. Chapter 4 established values for the five key features (i.e. three structural properties and two occupant properties), a linear single 2nd order LPM is initially developed to capture the five key features. The purpose of the model is to replicate collision data extracted from the finite element (FE) simulation, which is taken here as a realistic surrogate for the actual system. The linear single LPM stiffness element is tuned based on the FE Toyota Yaris Sedan (TYS) 2010 vehicle force versus deformation collision data using the method of linear least squares. The linear single LPM is then simulated and the outputs from the model (i.e. the five key features) are then compared to the FE collision data. The single LPM is simulated up to the first quarter cycle since this relates to the maximum/peak deformation of the full-frontal collision scenario. To determine if there is a departure from linearity, initially a piecewise linear modelling approach is considered. A literature review of nonlinear collision models is then undertaken, with a focus on previous applications of novel bilinear modelling and control. Novel static and dynamic bilinear collision models are then developed, along with tuning methods, with the aim being to capture the five key features more accurately. The bilinear single LPM is then simulated up to the first quarter cycle and

the outputs from the model (i.e. the five key features) are then compared to the FE collision data. To conclude the Chapter, model verification is undertaken whereby the developed bilinear single-vehicle LPM is simulated over a range of mass and velocity values to ensure that the physics of the model behaves as expected.

5.2 LINEAR NODAL LUMPED PARAMETER MODEL

In this Section, preliminary dynamic model considerations are given for a linear LPM. This consists of mass and stiffness coefficients, with damping assumed to be zero. Damping is assumed to be zero in this research, for simplicity as only the first quarter cycle of the dynamic system response needs to be considered; this corresponding to the maximum deformation/displacement of the vehicle crumple zone. A literature review into LPMs is undertaken in Section 5.2.2, with this forming the background to the modelling and simulation work undertaken in this Chapter, thus a linear single LPM is initially developed in Section 5.2.3. Making use of the TYS FE force versus deformation data, detailed in Chapter 4, a least squares parameter estimation process is applied to capture a constant linear stiffness value for the LPM. A simulation is then set up in MATLAB and Simulink using the linear single LPM, using the stiffness value captured from the linear least squares and the known TYS vehicle mass. Based on the TYS FE simulation in Chapter 4 (see Sections 4.2.3 and 4.2.4), the following key structural properties are of interest when considering the level of injury severity:

- Peak deformation
- Peak acceleration
- Collision energy

Based on the peak acceleration of the vehicle and the occupant FE simulation documented in Chapter 4, the following occupant properties are deemed to be of interest:

- Peak head acceleration
- Peak chest acceleration

The TYS FE simulation properties detailed above provide the defining benchmark when developing the LPM.

5.2.1 PRELIMINARY DYNAMIC MODELLING CONSIDERATIONS

The modelling work to be undertaken makes use of an LPM consisting only of mass and stiffness values, i.e. a second-order linear differential equation. As mentioned above, modelling of the damping for the LPM is considered unnecessary in this work and is therefore ignored. It is, however, known that damping exists within almost all mechanical structures as a means of dissipating energy, with a typical damping-to-stiffness ratio being of the order between 0.01:1 and 0.001:1, see (Gawronski, 2004). In (Gawronski, 2004), it is argued that damping within structures is difficult to define and at best is only roughly approximated. Therefore, for convenience and consistency throughout this thesis, the mechanical damping is assumed to be negligible and is therefore ignored within the developed models. This is justified since only the first quarter cycle of the dynamic response is considered.

In theory, applying an impulse as an input to an undamped LMP (such as that developed in Section 5.2.3) produces a sinusoidal displacement with constant amplitude, as is illustrated in Figure 5-1. When discussing the TYS FE model in Chapter 4, the time duration up to the peak deformation is of interest (which corresponds to the point where the velocity becomes zero). When considering the sinusoidal response in Figure 5-1, the only portion of interest is the first quarter cycle. In terms of the collision modelling, the peak of the first quarter cycle represents the peak structural deformation and the time duration to reach this peak provides information on the force from which the collision energy may be derived (related to the area under the first quarter cycle). The modelling study aims to develop an LPM that is capable of capturing the five key features of sufficient accuracy, whilst bearing in mind that mathematical/numerical models are approximations.

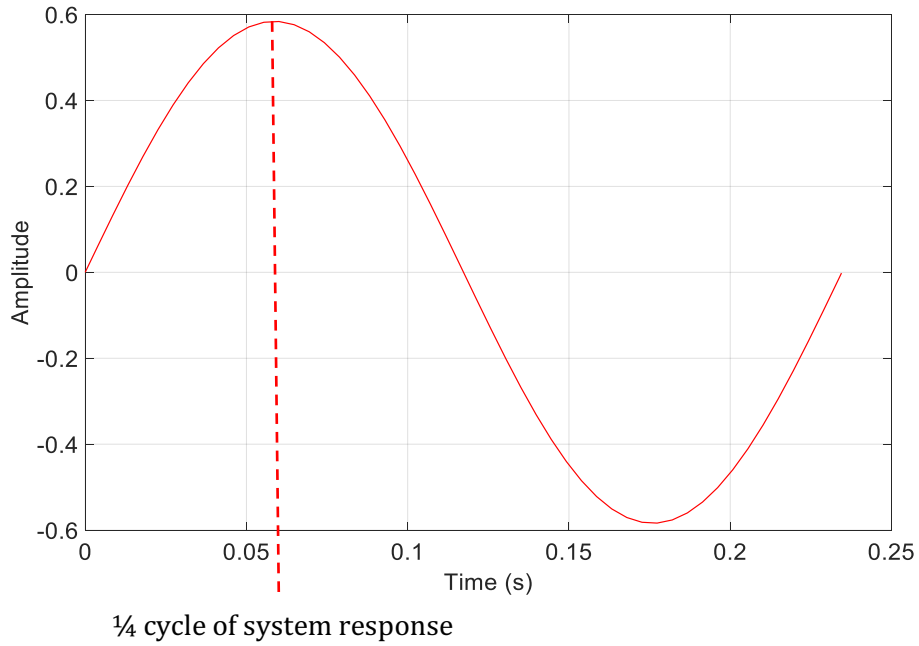

Figure 5-1: *Undamped System Response with the First Quarter Cycle Highlighted*

5.2.2 BACKGROUND INTO LINEAR ONE LUMPED PARAMETER MODELLING

One of the early implementations of an LPM was detailed in (Kamal, 1970), when an LPM was used to simulate a full-frontal vehicle collision into an immovable rigid wall (IRW). The LPM contained three degrees of freedom (DOF) and consisted of three masses and eight springs, and was used for collisions between 0 and 30mph (13.4112m/s). The approach was accepted by engineers due to the accuracy of the results obtained as well as the simplicity of implementation. Improvements to the LPM approach were introduced in 1986 by Ni and Song, see (Ni and Song, 1986), through the combined use of LPMs and FE. In 1988, actual vehicle accident data was used to determine the coefficients for the spring and mass elements of the LPM as well as the time duration of an accident, see (Magee, 1988). The LPM stiffness (i.e. force versus deformation characteristic) is tuned based on the accident data to best match the peak acceleration and the accident timing. In (Bennett, Lust and Wang, 1991), an LPM was developed to investigate the vehicle collision dynamics and the corresponding occupant response. In (Gandhi and Hu, 1995), LPMs were developed to accurately capture the

collision characteristics of a vehicle when driven into an IRW, with use being made of system identification methods to determine the LPM coefficients. The aim and motivation for the research was prompted by the desire to reduce the amount of physical testing, with this being both time consuming and expensive. Further to this, (Cheva, et al., 1996) in a similar study to that undertaken by Magee in 1988, FE data was used to determine the characteristics of the spring stiffness coefficient of the LPM. The LPM was simulated and the acceleration versus time characteristic was compared to that obtained from the FE data with good agreement observed. However, the study undertaken by Cheva et al. does not detail how to use FE data to determine the LPM spring coefficients. In (Kim and Arora, 2003), a linear LPM was used to simulate vehicle collisions; the approach they adopted was largely theoretical. In 2008, (Deb and Srinivas, 2008) investigated the comparison between LPMs and FE data for vehicle side impacts. The latter study involved investigating the absorbed collision deformation energy in side-impact collisions when a moving barrier collided with a stationary vehicle. The spring elements used for the LPMs were elastoplastic, with the spring stiffness elements being determined from the FE simulation data using the Ls-Dyna software, as is used here in Chapter 4. Recent research with similar approaches to modelling vehicle collisions and tuning the parameters have been undertaken, see (Pawlus, Karimi and Robbersmyr, 2014), (Lim, 2015) and (Lim, 2017).

The approach adopted in this research is initially based on the ideas borrowed from the above authors to model a crumple zone using one linear LPM. This is then tuned to best capture the structural stiffness properties of the FE output data in an attempt to match the TYS FE full-frontal vehicle collision data, as detailed in Sections 4.2.3 and 4.2.4, Chapter 4.

5.2.3 ESTIMATION OF STIFFNESS VALUE, SIMULATION AND RESULTS

The following 2nd order differential equation is used as a representation of a single Vehicle, denoted Vehicle a, colliding into an IRW:

$$m_a \frac{d^2 x_a(t)}{dt^2} + k_a x_a(t) = f_a(t) \tag{5-1}$$

where m_a denotes the vehicle laden mass, k_a denotes the average structural stiffness value, f_a denotes the applied force to the IRW and x_a denotes the structural deformation of the vehicle crumple zone. The derivation of Equation (5-1) is given in Appendix 3.0. The coefficient for the spring stiffness constant $k_a$in Equation (5-1) needs to be tuned, such that the simulation of the LPM adequately replicates the FE simulation data; namely the five key features corresponding to a full-frontal vehicle collision as in Section 4.2.3, Chapter 4. This will determine the ability of the model to satisfactorily reproduce the key vehicle structural features (peak deformation, peak acceleration and collision energy) and the key vehicle occupant features (peak head and chest accelerations) to adequate levels of accuracy. A structural stiffness k_a value for Equation (5-1) will be determined using a linear least squares regression model. This will make use of the baseline TYS FE data captured based on the US NCAP test, i.e. a nominal mass of $1247kg$ and a velocity of $35mph$ ($15.6464m/s$). A linear regression single-section (straight-line) model of the force versus deformation plot, corresponding to a vehicle, denoted Vehicle a, is given by the equation of the following affine/linear form:

$$f_a = f_{p_a} + k_a \delta_a \tag{5-2}$$

where f_{p_a} denotes, respectively for Vehicle a, the crumple zone failure point (or buckling point) and δ_a denotes the progressive deformation of the vehicle's frontal longitudinal crumple zone. To estimate the failure point and the average stiffness value, a linear least

squares (LLS) approach is applied to the force versus deformation data, which effectively determines the 'best' fit to the observed data in the sense of minimising the sum of squares of the 'vertical' deviations from each point from a straight-line segment, i.e. if a data point lies on the fitted line, then the vertical deviation is zero. The LLS general form is given by (Hsia, 1977):

$$\hat{\theta}_a = [\Phi_a^T \Phi_a]^{-1} \Phi_a^T x_a \tag{5-3}$$

where $\hat{\theta}_a$is the estimated parameter vector, hence $\hat{\theta}_a = \begin{bmatrix} f_{p_a} \\ k_a \end{bmatrix}$ and Φ_a is the observation matrix consisting of simulated values of the inputs (force, due to the initial collision velocity) and the simulated values of the outputs (progressive deformation denoted x_a) which are the deformation values extracted from the TYS FE simulation data, as illustrated in Figure 4-6, Chapter 4.

In Figure 5-2, the result of applying the LLS approach is illustrated, where the single straight-line illustrates the fit to the TYS FE model force versus deformation data. The determined values for the failure point f_{p_a} and structural stiffness k_a can be found in Table 5-1. As a measure of the effectiveness of the estimated model obtained via application of the LLS approach to the FE collision data, integration is used to find the area under the force versus deformation plot (collision energy). The area under the force versus deformation plot for the single straight-line model fit is normalised to unity. For ease of comparison, see Row 1 of Table 5-1. Further estimated models are to be compared to the LLS model (in terms of errors in capturing the collision energy). Recall that the FE data is considered as a surrogate model so the use of the term 'error' is really interpreted here as a 'deviation'.

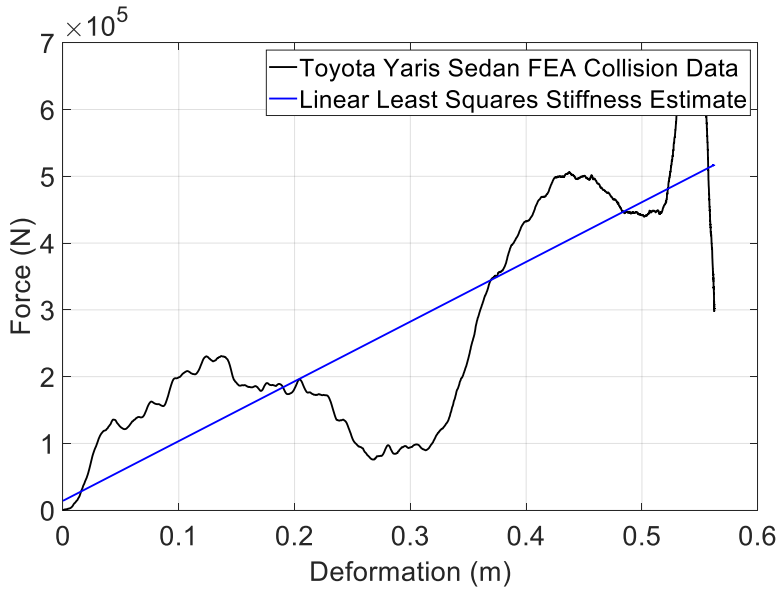

Figure 5-2: *Single Straight-Line Approximation using Linear Least Squares*

Table 5-1: *Normalised Area Under the Graph (Energy) for the Single Section Model*

Segment	**Estimate of stiffness k_a $[kN/m]$**	**Estimate of failure point f_{p_a} $[kN]$**	**Area under the graph – Energy $[kJ]$**	**Normalise to unity**
Single	894.3	1.410	149.2	1.000

The determined crumple zone failure point f_{p_a} and average structural stiffness value k_a, as well as the known nominal mass m_a of $1247kg$ and collision velocity v_a of $35mph$ $(15.6464m/s)$ are now used within a simulation of Equation (5-1). To set-up the MATLAB/Simulink simulation, Equation (5-1) is normalised by dividing through by the vehicle laden mass value, m_a to give:

$$\frac{d^2x_a(t)}{dt^2} + \frac{k_a}{m_a}x_a(t) = \frac{f_a(t)}{m_a} = a_a(t) \tag{5-4}$$

where $\frac{k_a}{m_a}$ is a normalised constant stiffness coefficient (or stiffness to mass ratio), also known as the square of the natural frequency $\omega_{n_a}^2$, or, as often termed in mechanical engineering literature, the smallest positive eigenvalue, see (Wilkinson, 1965). The

initial condition of the simulation model is applied internally via the impact collision velocity, as opposed to an external input as in Equation (5-4), hence the following is given:

$$\frac{d^2x_a(t)}{dt^2} + \frac{k_a}{m_a}x_a(t) = 0 \tag{5-5}$$

Transforming Equation (5-5) from the time-domain to the frequency domain via the Laplace transform gives:

$$\left(s^2 + \frac{k_a}{m_a}\right)X_a(s) = 0 \tag{5-6}$$

which may be configured in MATLAB/Simulink for simulation, as illustrated in Figure 5-3. The model parameters of stiffness, labelled k_a, (i.e. k_a) and failure point, labelled f_p_a, (i.e. f_{p_a}) are used directly within the simulation model. The corresponding offset acceleration is defined by the offset force, labelled f_p_a, i.e. f_{p_a}, divided by the vehicle laden mass, labelled m_a, i.e. m_a. Note that the acceleration is divided throughout by the gravitational constant to convert the results into g-force, taken here to be $9.81m/s^2$. The head and chest peak acceleration values are determined by multiplying the output acceleration by the respective gains, labelled a_h_a (i.e. a_{h_a}) for the head acceleration, and labelled a_c_a (i.e. a_{c_a}) for the chest acceleration, see Figure 5-3. Comparing the FE vehicle peak acceleration to that of the occupant peak chest and head accelerations from the sled model, the scaling factors for the chest and head are determined to be 0.831 and 1.053, respectively. This is undertaken to approximate the occupant peak head and chest accelerations/decelerations and the corresponding vehicle peak acceleration. The collision impact velocity is applied as an initial condition at the left-hand integrator in Figure 5-3. The simulation is set-up in MATLAB/Simulink such that the unforced free

dynamic response of the linear LPM captures the time-period up to the maximum/peak deformation, corresponding to the first quarter cycle, as stated earlier discussed in more detail in Section 5.2.1. Thus, the corresponding output data captured corresponds to this time period, i.e. velocity versus time, acceleration versus time, force versus deformation, head acceleration versus time and chest acceleration versus time. Note that the coefficient of restitution is not considered in the single LPM simulation model, i.e. the rebound is not modelled and simulated (only up to the peak deformation is considered).

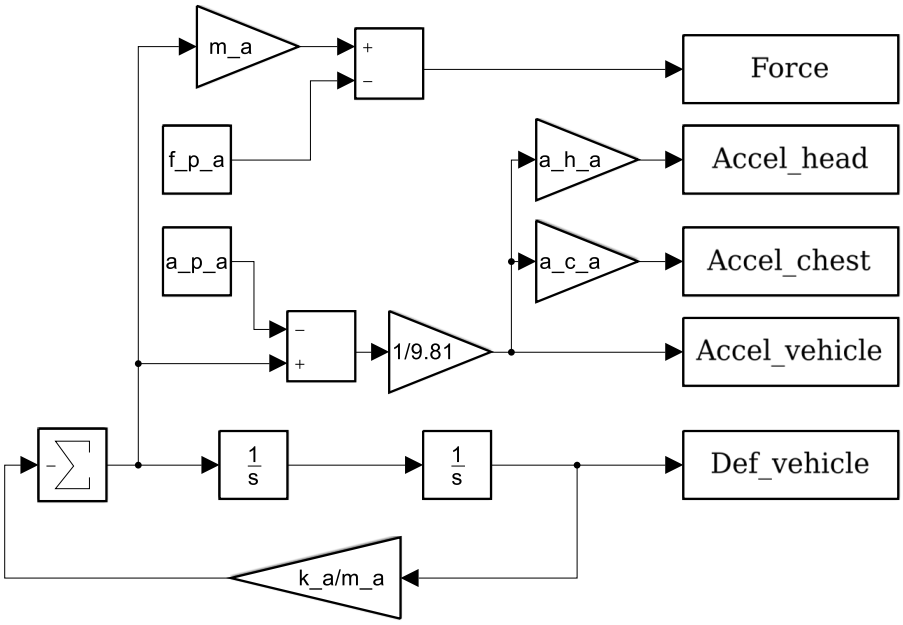

Figure 5-3: *Simulink Realisation in Phase Variable Form of a One Degree of Freedom Model (Note that underscore indicates variable subscript)*

The results of the linear single LPM output and the FE simulation data are compared in the sub-plots of Figure 5-4. These correspond to deformation versus time (upper-left hand sub-plot), acceleration versus time (upper-right hand sub-plot) and force versus deformation (lower-left hand sub-plot). The corresponding occupant accelerations are given for head acceleration versus time (left-plot) and chest acceleration versus time (right-plot) in Figure 5-5. The results relating to the key properties are summarised in Table 5-2, with these corresponding to the sub-plot structural properties and the sub-plot occupant properties, respectively. Note that the occupant acceleration plots in Figure 5-5 are simulated to 0.1 seconds, i.e. beyond that of the time period of the vehicle (structural) peak deformation. The additional time period of the occupant acceleration versus time outputs is due to the slight delay in the deployment of the vehicle's air bag and seat belt. It is worth noting that from the FE data (sled model) the time periods for reaching the peak head and chest accelerations are 0.0806 seconds and 0.0690 seconds, respectively. In the case of the simulated LPM model, the peak head and peak chest acceleration take place at 0.0590 seconds. The last column in Tables 5-2 gives the magnitude of the discrepancy expressed as a per unit value between the FE simulation output and the simulated LPM output obtained from:

$$Discrepancy = \left|\frac{FE\ Data - \ LPM\ Data}{FE\ Data}\right| \tag{5-7}$$

Expressed as a magnitude, the largest discrepancy is found to be for the structural peak acceleration, with a value of 0.2231. As expected, the peak chest and head acceleration values also have the same discrepancy. The single LPM peak deformation closely matches that of the FE data, however with a discrepancy value of 0.1303 for the collision duration. The discrepancy in the collision energy value for the single LPM has a value of 0.0791. Based on the conservation of energy principle (see Equation (4-2), Chapter 4), the LPM produces a value above that expected.

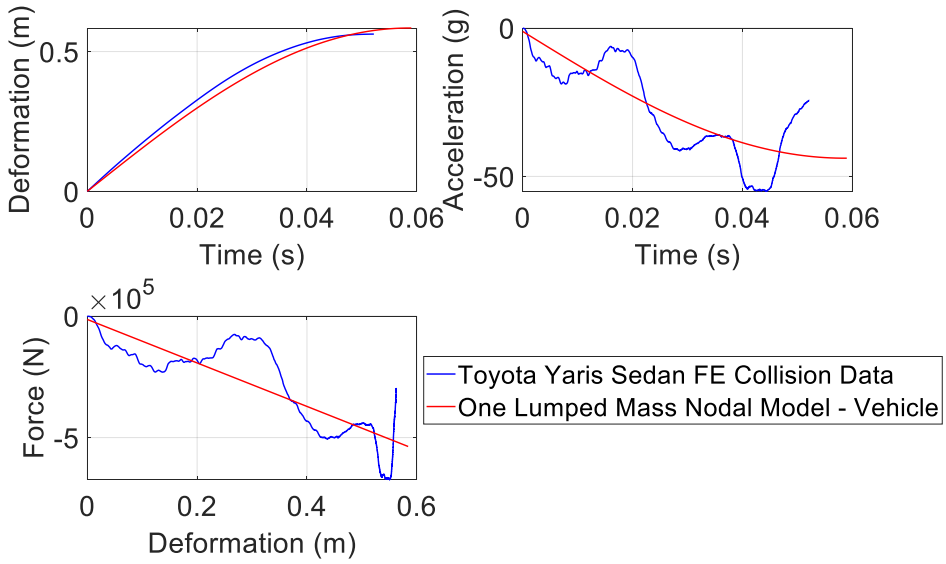

Figure 5-4: *Comparison of the Structural Properties of the FE Model to the One Lumped Parameter Model for Deformation Versus Time (top-left hand sub-plot), Acceleration versus Time (top-right hand sub-plot) and Force versus Deformation (bottom-left hand sub-plot)*

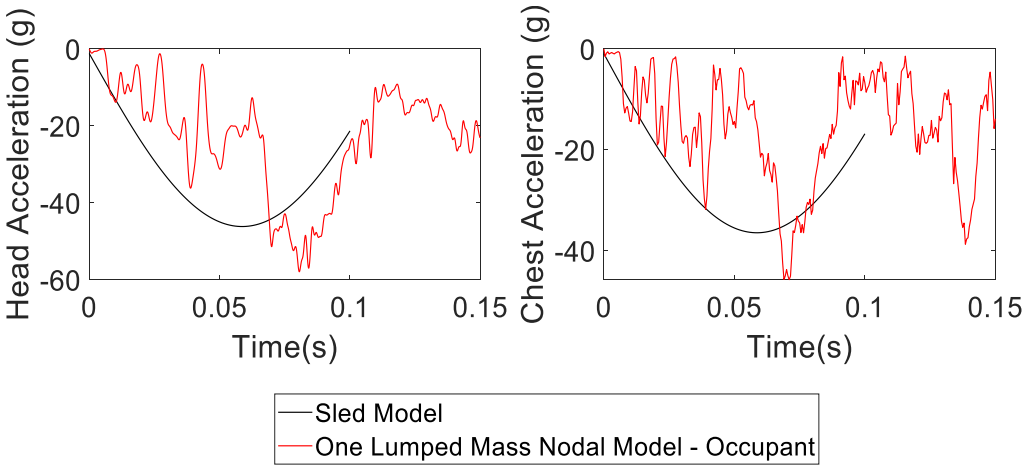

Figure 5-5: *Comparison of the Occupant Properties of the FE Model to the One Lumped Parameter Model for Head Acceleration versus time (left-hand plot) and Chest Acceleration versus Time (right-hand plot)*

Table 5-2: *Comparison of Structural and Occupant Properties of the FE Model to the One Lumped Parameter Model*

	FE Model	**One Lumped Mass Model**	**Discrepancy [-/+]**
Peak Deformation $[m]$	0.5625	0.5842	0.0386
Peak Acceleration $[g]$	55.04	43.86	0.2031
Collision energy [kJ]	149.1	160.9	0.0791
Collision Duration $[s]$	0.0522	0.0590	0.1303
Peak Head Acceleration [g]	57.95	46.19	0.2031
Peak Chest Acceleration [g]	45.74	36.45	0.2031

A further investigation carried out was is to remove the failure point f_{p_a} determined from the LLS process, along with the corresponding acceleration offset, i.e. a_{p_a}. The results of the linear LPM without the failure point are plotted in Figure 5-6, where these are again compared to the FE data. As before, these correspond to deformation versus time (upper-left hand sub-plot), acceleration versus time (upper-right hand sub-plot) and force versus deformation (lower-left hand sub-plot). The corresponding occupant accelerations are given for head acceleration versus time (left-plot) and chest acceleration versus time (right-plot), see Figure 5-7.

The results relating to the five key properties are summarised in Table 5-3 which correspond to the sub-plot structural properties and the sub-plot occupant properties. The last column in Tables 5-3 gives the discrepancies expressed as a per unit value between the FE simulation output and the LPM simulation output obtained from using Equation (5-7). It should be noted that removing the failure point f_{p_a} does not give as good a fit with the peak acceleration, with the discrepancy increasing slightly from 0.2031 to 0.2240. However, the collision energy discrepancy has been reduced to a value of 0.0235, such that in terms of the conversation of energy principle (see Equation (4-2), Chapter 4) a result is now produced which is considered to be more adequate and acceptable.

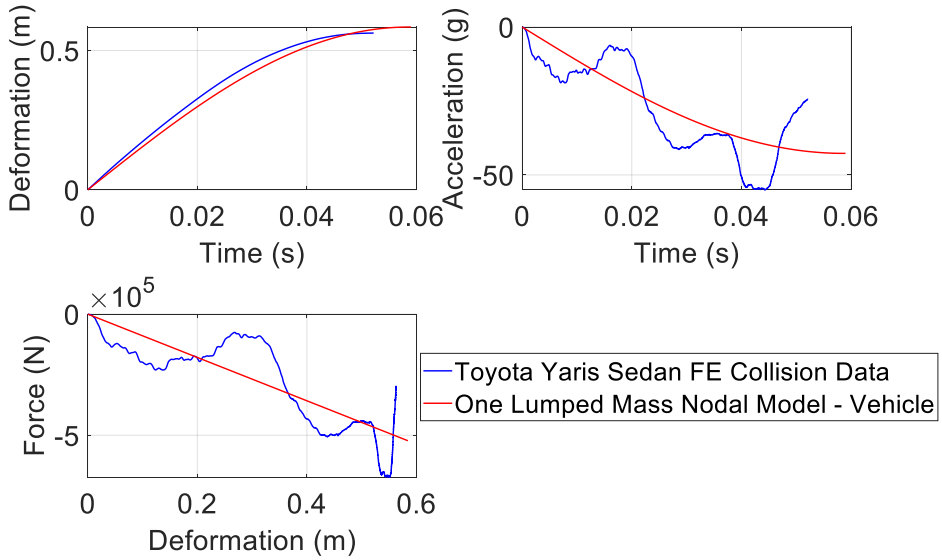

Figure 5-6: *Comparison of the Structural Properties of the Finite Element Model to the One Lumped Parameter Linear Model for Deformation Versus Time (top-left hand sub-plot), Acceleration versus Time (top-right hand sub-plot) and Force versus Deformation (bottom-left hand sub-plot)*

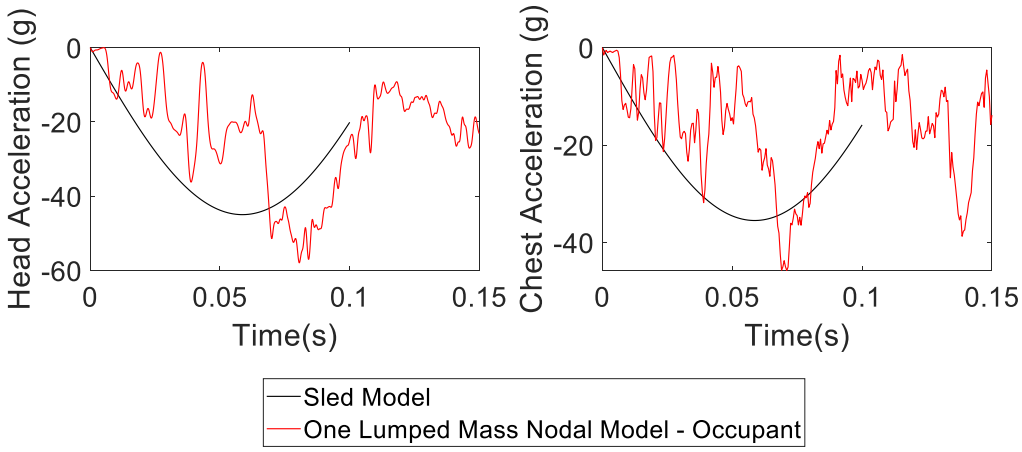

Figure 5-7: *Comparison of the Occupant Properties of the Finite Element Model to the One Lumped Parameter Linear Model for Head Acceleration versus time (left hand plot) and Chest Acceleration versus Time (right hand plot)*

Table 5-3: *Comparison of Structural and Occupant Properties of the Finite Element Model to the One Lumped Parameter Linear Model*

	FE Model	**One Lumped Mass Model**	**Discrepancy [−/+]**
Peak Deformation [m]	0.5625	0.5842	0.0386
Peak Acceleration [g]	55.04	42.71	0.2240
Collision Energy – Main Data [kJ]	149.1	152.6	0.0235
Collision Duration [s]	0.0522	0.0590	0.1303
Head Resultant Peak Acceleration [g]	57.95	44.98	0.2240
Chest Resultant Peak Acceleration [g]	45.74	35.50	0.2240

5.3 BILINEAR NODAL LUMPED PARAMETER MODEL

Building on Section 5.2, the aim in this Section is to develop a collision model that captures the five key features from the TYS FE data more accurately, with piecewise linear and nonlinear models being explored. A two-section piecewise linear static model is initially considered to identify if there is a departure from linearity. Static and dynamic nonlinear models are then developed, with the focus being towards exploring a bilinear model. A literature review into previous applications of bilinear systems modelling and control is given. The static and dynamic bilinear models with their tuning methods are then developed. A quantification/verification analysis is then undertaken whereby the developed bilinear one LPM is simulated over a range of mass and velocity values.

5.3.1 DEVELOPMENT OF PIECEWISE LINEAR ONE NODAL LPM

The initial motivation of the nodal piecewise linear vehicle model developed in this work was inspired by the earlier work discussed in the publication by Elmarkbi and Zu, namely (Elmarabi and Zu, 2004) and (Munyazikwiye, Karimi and Robbersmyr, 2013). Figure 5-8 illustrates a two-section piecewise linear model of the force versus deformation plot, where:

$$f_{p_{a_2}} = f_{p_{a_1}} + k_{a_{s_1}} \delta_{a_1} = f_{p_{a_2}} \tag{5-8}$$

and

$$f_{a_{3_{+/-}}} = f_{p_{a_1}} + k_{a_{s_1}}\delta_{a_1} \pm k_{a_{s_2}}\delta_{a_2} = f_{p_{a_2}} \pm k_{a_{s_2}}\delta_{a_2} \tag{5-9}$$

where $\delta_{a_2} = (\delta_a^* - \delta_{a_1})$, the failure points for the two sections are denoted $f_{p_{a_1}}$ and $f_{p_{a_2}}$, the final force value for the two-section piecewise linear model is denoted $f_{a_{3_{+/-}}}$, the structural stiffness values for the two-sections are denoted $k_{a_{s_1}}$ and $k_{a_{s_2}}$, the 'knee' point and maximum deformation of the two-section piecewise linear model are denoted by δ_{a_1} and δ_a^*, respectively.

In a similar manner to the estimation of the single straight-line model using the LLS procedure in Section 5.2.3, a least squares procedure is applied to estimate the two straight-line segments. The single straight-line fit to the data from Figure 5-2 is presented in the sub-plots of Figure 5-9 for visual comparison. The upper right-hand side plot illustrates a two-straight line segment approximation, with the knee point discontinuity, denoted δ_{a_1}, being found by a 'trial and error' procedure to provide a better fit. The knee point for the graphical outputs given in Figure 5-8 for dual section 1, dual section 2, dual section 3 are $0.2779m$, $0.2522m$ and $0.2972m$, respectively. The upper and lower left-hand plots illustrate two further two-straight line segment approximations. To allow comparison, the area under the force versus deformation (collision energy) for the single straight-line LPM has been normalised to unity for ease and convenience, as shown in Row 1 of Table 5-4. Row 2 of Table 5-4 corresponds to the upper left-hand plot, indicating that the two-section piecewise linear LPM gives a better fit o the FE collision data, i.e. a lower discrepancy. Row 3 and Row 4 correspond to the upper-right and lower-left plots, with the area approximating the collision energy. These arbitrary two-section LPMs give better fits, with the upper left-hand plot determined by

trial and error being found to provide a lower value in terms of the discrepancy metric, as highlighted in the results in Table 5-4. However, whilst both models indicate improvement in terms of the chosen error metric, it is also noted that there are discontinuities between the two straight-line segments.

The most important observation arising from the investigation of the two-section LPM is the fact that a departure from linearity is evident. This observation prompts the need for an alternative approach to deal with the potential nonlinear phenomenon that is present in the FE simulation data, which would suggest an increased stiffening as a function of progressive deformation. Based on this observation a bilinear model was considered to be a viable candidate for investigation, as introduced in Section 5.3.2.

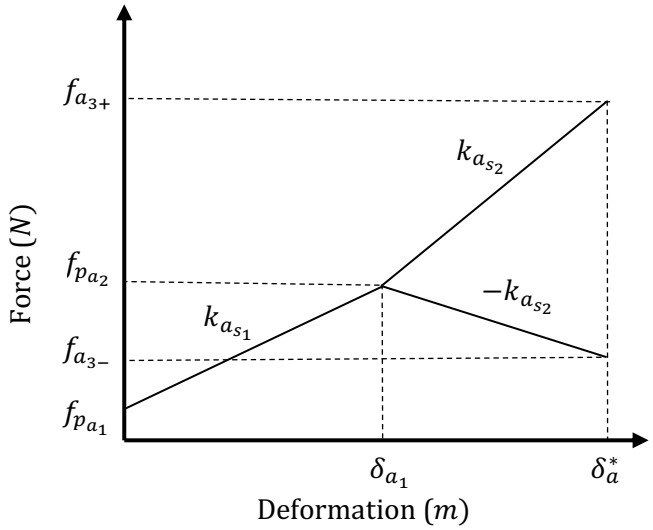

Figure 5-8: *Tuneable Two-Section Piecewise Linear Lumped Parameter Model*

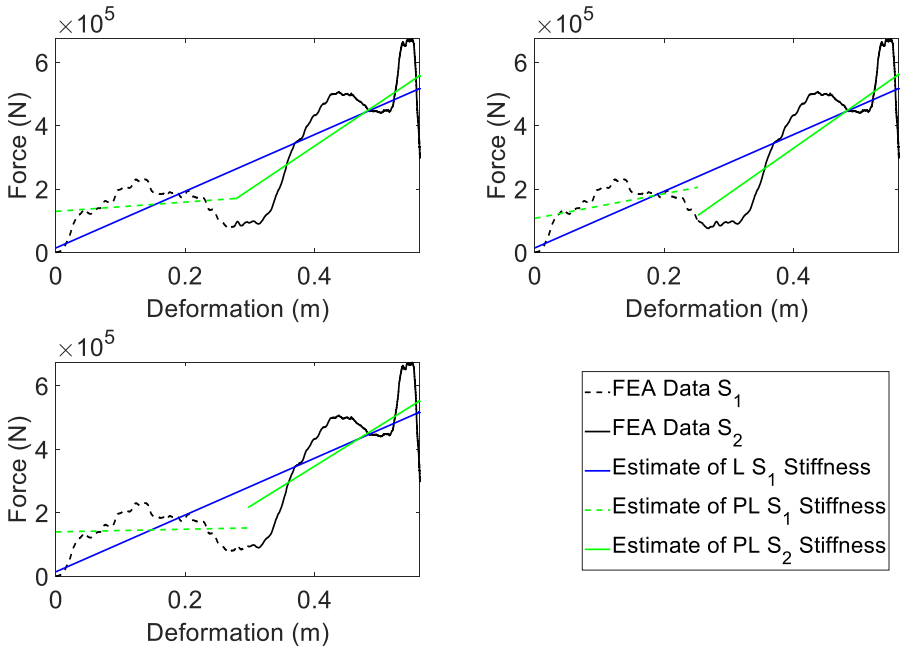

Figure 5-9: *Single and Dual Fitted Straight-Line Segments Fit using a Linear Least Squares Algorithm*

Table 5-4: *Normalised Area Under the Graph (Energy) for the Single and Dual Lumped Parameter Models*

Segments	Estimate of Stiffness $[kN/m]$	Estimate of Failure Point $[kN]$	Area under the graph – Energy [kJ]	Normalise to unity
Single Section	$k_a = 894.3$	$f_{p_a} = 14.10$	149.4	1.000
Dual Section 1	$k_{a_{s_1}} = 146.8$ $k_{a_{s_2}} = 1368$	$f_{p_{a_1}} = 129.4$	145.0	0.9706
Dual Section 2	$k_{a_{s_1}} = 387.7$ $k_{a_{s_2}=} = 1433$	$f_{p_{a_1}} = 107.6$	144.8	0.9689
Dual Section 3	$k_{a_{s_1}} = 41.88$ $k_{a_{s_2}} = 1267$	$f_{p_{a_1}} = 139.8$	145.4	0.9689

5.3.1.1 PIECEWISE LINEAR ONE NODAL LPM SIMULATION AND RESULTS

In Appendix 4.0, the coupled two-lumped mass-spring simulation model is detailed. It makes use of two stiffness values k_{a_1} and k_{a_2} derived from the static piecewise linear model detailed above. The initial condition in terms of the collision impact velocity,

denoted v_a is applied simultaneously to the two left-hand integrators in the two-linked lumped mass-spring models (i.e. same value applied to both).

As was similarly observed in (Munyazikwiye, Karimi and Robbersmyr, 2013), the task of reproducing the inputs and outputs in simulation led to unsatisfactory results. The distribution of the total mass, denoted m_a, of the vehicle between the two linked mass-spring models was not intuitive and the two mass values, m_{a_1} and m_{a_2} were required to be further tuned to match the FE simulation data. In the case of the two-lumped mass configuration, no sensible rationale could be found to determine a procedure to apportion the total mass value amongst m_{a_1} and m_{a_2} and led to an unsatisfactory and unresolved problem. The results corresponding to distribution ratios of 0.1:0.9 to 0.9:0.1 for m_{a_1}: m_{a_2} are given in Appendix 4.0. A ratio of 0.3:0.7 was found to give the better results, but this was still unsatisfactory, with the two nodal LPM giving larger discrepancy values than the one LPM model.

5.3.2 BACKGROUND INTO BILINEAR MODELLING

Linear models can often be over-simplistic and unable to adequately capture the dynamic behaviour and nonlinear phenomenon exhibited by some practical real-world systems. Such a nonlinear dynamic behaviour is, in this case, the force versus deformation collision characteristic of a vehicle's crumple zones. In the context of modelling the nonlinear nature of the spring stiffness element of a lumped parameter model to represent the collision phenomenon, there is a marked paucity of literature. However, it is noted that in 2007, researchers have assumed a cubic approximation, see for example (Elmarakbi and Zu, 2007). It is believed that such an approach leads to a potentially overs-specified model, rendering the approach appropriate for a specific case only (i.e. in terms of vehicle mass and collision velocity).

In this research, a class of nonlinear LPMs of interest is that of bilinear systems modelling approach. The area of bilinear systems modelling and control has received considerable attention from numerous researchers who have been based in the Control Theory and Applications Centre (CTAC), Coventry University, see for example (Burnham, 1991), (Dunoyer, 1996) and (Martineau et al, 2004). Applications of the bilinear phenomenon are found in areas of both the natural and man-made worlds, such as ecology, engineering, medicine and socioeconomics. For a comprehensive overview, see for example, (Mohler, 1973), (Bruni, Di Pillo and Koch, 1974), (Mohler and Kolodziej, 1980), (Burnham, 1991) and (Ekman, 2005). The bilinear approach permits a more generalised dynamic model to be developed, which in the specific application that is being considered in this research, allows the model outputs to be observed over a range of vehicle laden mass and collision velocity values.

Bilinear system models may be interpreted as a sub-class of the wider state-dependent system models. Bilinear system models include linear system models as a special sub-class, and they encompass continuous-time, discrete-time as well as quasi-static representations involving spatial variables, e.g. time constants and steady-state gain. Bilinear system models are characterised by an input dependent dynamic and steady-state behaviour. Consequently, by adopting a bilinear systems approach, it is possible to model complex nonlinearities within a relatively straightforward and easily understood mathematical framework. Thus, the bilinear systems modelling approach represents a natural first step when attempting to capture the observed nonlinearity (or a departure from linearity) that arises when dealing with practical systems exhibiting nonlinear behaviour, see (Burnham, 1991). Bilinear systems were originally defined in (Mohler, 1973) and were described as linear in both system state and control input when considered independently, with the bilinearity (or nonlinearity) arising from coupled terms involving products of the internal system state and control input.

In the case of the vehicle crumple zones considered in this research, the internal system state (or system output) is the longitudinal deformation and the input is the force derived from the initial conditions involving the vehicle laden mass and collision velocity. The original definition of a bilinear model stated by Mohler (1973) is mathematically different to a two-section piecewise linear approximation as discussed in Section 5.3.1, although it is noted that the term bilinear has been adopted by some researchers to describe such two-section piecewise linear models. In the work presented in this thesis, a bilinear model is defined in the sense of that originally introduced by Mohler. The static bilinear model possesses similar asymmetric features to the cubic approximation in (Elmarakbi and Zu, 2007). However, it is highlighted in the following Sections that the simplicity of the bilinear modelling becomes significant when compared to other nonlinear approximations, i.e. cubic. It is subsequently shown in Section 5.3.3 and 5.3.4 that the static and dynamic bilinear models are more appropriate for capturing the five key features, than the single-section linear static and linear dynamic LPMs and more intuitively applicable in concept than the two-section piecewise linear static and dynamic LPMs. The negative/positive bilinear static and bilinear LPM characteristics correspond to a progressive decrease/increase in the structural stiffness as the deformation of the vehicle crumple zone increases. It is understood that the decrease/increase in structural stiffness of the deformation is due to components within the frontal structure of a typical vehicle, including the TYS vehicle, e.g. bulkhead and combustion engine.

5.3.3 DEVELOPMENT OF A STATIC BILINEAR MODEL

A spatially dependent quasi-static bilinear model along with a tuning algorithm to capture the FE simulation output data of force versus deformation will be developed in this Section. In the case of the vehicle crumple zone considered here, the internal system state (or system output) is the longitudinal deformation and the input is the force derived from the initial conditions involving the vehicle laden mass and collision

velocity. In the context of this thesis, the system output is defined as the system state, i.e. the deformation. Attention is restricted here to a spatially dependent quasi-static bilinear model of the form:

$$f_a = f_{p_{a_1}} + k_{a_{s_1}}\delta_a \pm \eta_a \delta_a f_a \tag{5-10}$$

with reference to a single vehicle, denoted Vehicle a, δ_a denotes the progressive deformation of the vehicle crumple zone of Vehicle a. The constants $k_{a_{s_1}}$ and η_a denote the coefficients of the linear and bilinear terms, respectively, where $k_{a_{s_1}}$ is defined as the gradient of the first linear straight-line section of the two-section piecewise linear model and $f_{p_{a_1}}$ is the failure point of the first linear straight-line section of the two-section piecewise linear model, see Section 5.3.1. Note that the failure point f_{p_a} and stiffness value k_a from the linear nodal LPM could be used in Equation (5-10) instead of $f_{p_{a_1}}$and $k_{a_{s_1}}$. Exploiting the spatial nature of the modelling task, Equation (5-10) is rearranged into the following form:

$$f_a \pm \eta_a \delta_a f_a = f_{p_{a_1}} + k_{a_{s_1}}\delta_a \tag{5-11}$$

Recognising that f_a is common to both terms on the left-hand side of Equation (5-11), leads to:

$$(1 \pm \eta_a \delta_a) f_a = f_{p_{a_1}} + k_{a_{s_1}}\delta_a \tag{5-12}$$

From Equation (5-12), it follows that the force f_a may be represented as the ratio of two affine linear functions of deformation, yielding an overall bilinear function, given by:

$$f_a = \frac{f_{p_{a_1}} + k_{a_{s_1}}\delta_a}{(1 \pm \eta_a \delta_a)} \tag{5-13}$$

where a conceptual visualisation of the approach is illustrated in Figure 5-10.

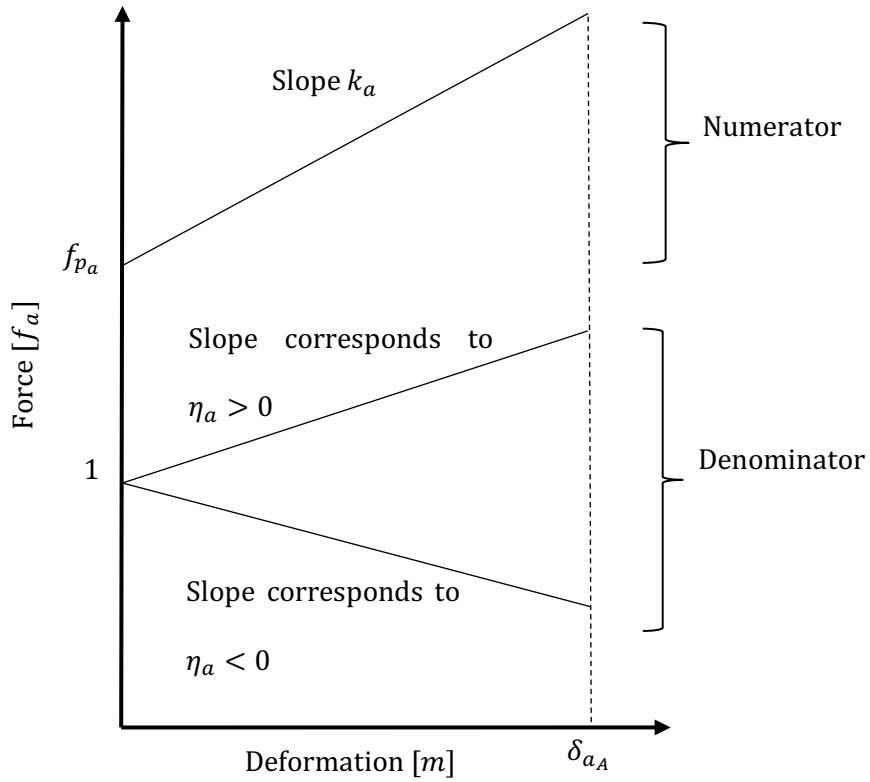

Figure 5-10: *Pictorial Representation of the Construction of a Spatial Bilinear Function*

The bilinear function, given by Equation (5-13) and represented in Figure 5-10, is evaluated for every point along the spatial deformation axis, i.e. from $\delta_a = 0$ to δ_{a_A}, where δ_{a_A} denotes the actual peak deformation. When plotting force versus deformation, the characteristic may be representative of a positive bilinearity when $\eta_a > 0$, or a negative bilinearity when $\eta_a < 0$, even though deformation is the dependent variable with force being independent. Note that when the bilinear coefficient η_a is equal to zero, the system is linear, as shown in Figure 5-11, which also shows typical bilinear characteristics for the cases when $\eta_a < 0$ and $\eta_a > 0$. The positive bilinear characteristic case corresponds to a progressive increase in the structural stiffness as the deformation of the vehicle crumple zone increases.

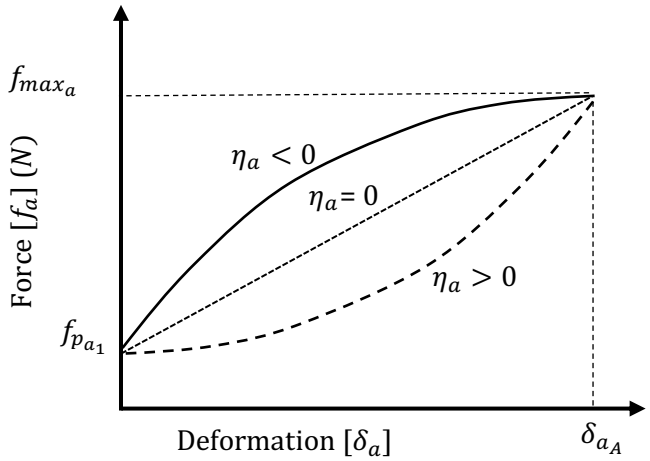

Figure 5-11: *Conceptual Illustration of Typical Bilinear Characteristics with an Offset for the Cases where $\eta_a < 0$, $\eta_a = 0$ and $\eta_a > 0$, i.e. Bilinearity is Negative, Zero and Positive, Respectively*

5.3.3.1 ESTIMATING STATIC BILINEAR MODEL VALUES AND RESULTS

Based on Equation (5-13), a guided search approach based on the bisection principle is set-up in an iterative manner. It is used to obtain the parameter value of α_a (i.e. $\gamma_a = \alpha_a k_a$ or $\gamma_a = \alpha_a k_{a_{s_1}}$) which results in the 'best' capture the key features from the TYS FE simulation (structural and occupant properties, as detailed in Sections 4.2.3 and 4.2.4, Chapter 4). Hence, for the nominal condition, i.e. vehicle mass value of $1247kg$ and collision velocity of 15.6464 m/s, ($35mph$). The procedure for obtaining a spatial bilinear model from the FE force versus deformation data is presented in Algorithm 5-1. The algorithm requires the maximum/peak deformation, denoted δ_{a_A} and the maximum force, denoted f_{max_a}. Note that given the configuration of the static model and the tuning algorithm, the maximum deformation and force are automatically captured. Therefore, the parameter value of α_a is tuned such that the required collision energy is captured. Also required for the algorithm are the failure point, denoted f_{p_a}, and the average stiffness value from section 1 of the piecewise linear model, denoted $k_{a_{s_1}}$ (or use k_a), see Section 5.3.1. Note that the stiffness value from the linear nodal lumped parameter model could instead be used, see Section 5.2.3. For Algorithm 5-2, a range of α_a values are simulated through Equation (5-13) that has initially been rearranged to make η_a the subject. Hence, a value for η_a is determined based on the known properties and with the force set to the maximum force value. Equation (5-13) is then simulated over $\delta_a = 0$ to δ_{a_A} in incremental steps. A value of α_a is then selected that gives the closest match to the required collision energy value. For the simulation, a value of $\alpha_a = 0.034$ was determined for the model with the failure point and $\alpha_a = 4.350$ for the model without the failure point. The graphical outputs obtained from Algorithm 5-1 are illustrated in Figures 5-12 and 5-13, where the plots correspond to simulations with and without the failure point, respectively The results obtained from Algorithm 5-1 are displayed in Figures 5-12 and 5-13 and presented in Table 5-5 for the spatial quasi-static bilinear model (with and without the failure point). The results obtained are compared

to the linear static model approximation and the 'best' dual section (piecewise linear) results found in Sections 5.2.3 and 5.3.1, respectively. Note that the interpretation of 'best' needs to be placed in context here because the model is actually unsatisfactory but nevertheless indicates that a better fit is possible. It is clear from the results in Table 5-1 and the graphical plots illustrated in Figures 5-12 and 5-13, that the bilinear model is the more favourable as it gives a 'better' fit to the data, i.e. peak deformation, peak force and collision energy. The two spatial quasi-static bilinear models (with and without the failure points) were both straightforward to tune to achieve the required collision energy. The results provide the justification to progress to the dynamic bilinear case.

Algorithm 5-1: *Determining the Coefficients of the Spatial Bilinear Model*

i. Obtain two-section piecewise linear model from least squares (see Section 5.3.1, Chapter 5)

ii. Determine f_{p_a}, f_{max_a} at δ_{a_A} and $k_{a_{s_1}}$

iii. Select a range of α_a values to simulate through the following equation to determine the value of η_a that gives the best fit (Step v.):

$$-\eta_a = \left(\left(\frac{\left(f_{p_a} + (\alpha_a \, \beta_a)\delta_{a_A} \right)}{f_{max_a}} \right) - 1 \right) / \delta_{a_A}$$

iv. Compute the function:

$$f_a = \frac{\left(f_{p_a} + (\alpha_a \, \beta_a)\delta_a \right)}{(1 - \eta_a \delta_a)}$$

over $\delta_a = 0$ to δ_{a_A} in incremental steps.

v. Select the α_a value that gives the closest match to the required collision energy value

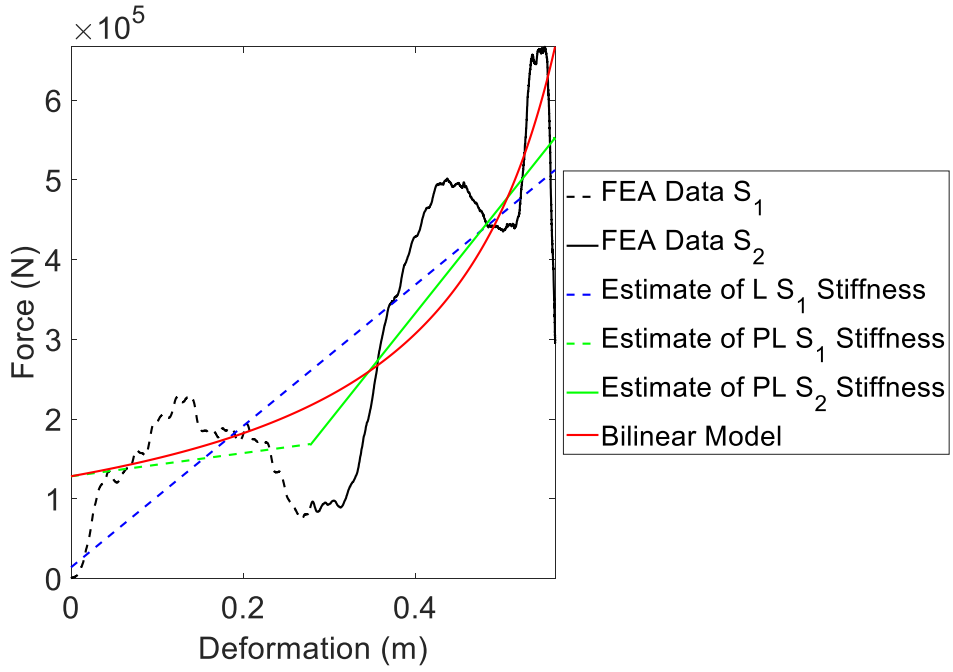

Figure 5-12: *Comparison of Single Straight-Line Section Static Linear, 'Best' Two Straight-Line Section Static Linear (Upper Left-Hand Sub-Plot of Figure 5-9) and Static Bilinear with Failure Point from Dual Section Model*

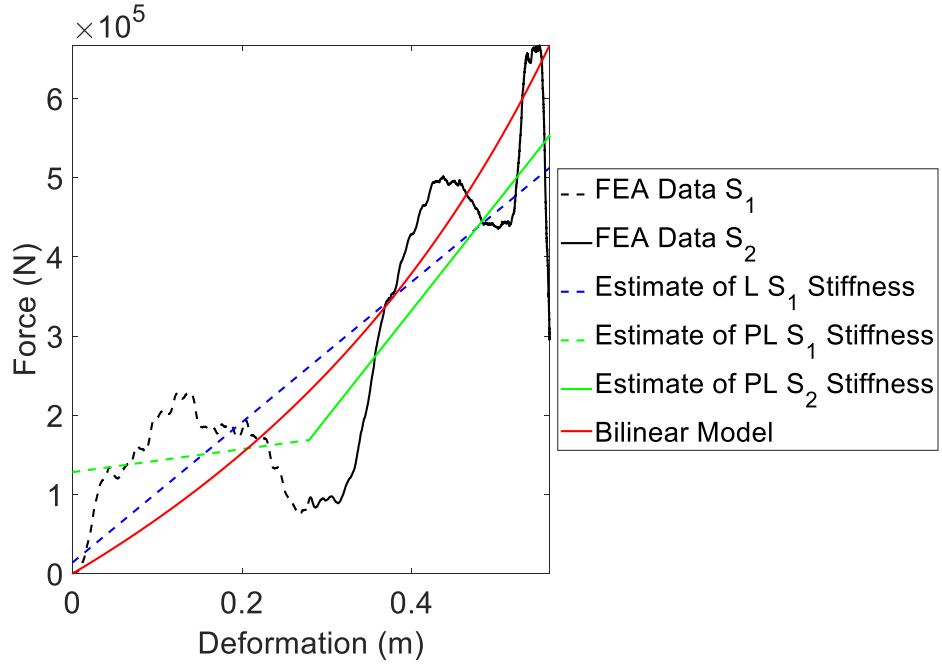

Figure 5-13: *Comparison of Single Straight-Line Section Static Linear, 'Best' Two Straight-Line Section Static Linear (Upper Left-Hand Sub-Plot of Figure 5-9) and Static Bilinear without Failure Point from Dual Section Model*

Table 5-5: *Normalised Area Under the Graph (Collision Energy) for the Static Single Section (Row 2 Table 5.4), Static Dual Section (Row 3 Table 5-4) and Spatial Quasi-Static Bilinear Models with (Row 4) and without (Row 5) the Failure Point*

Segments	Estimated/Used Stiffness [kN/m]	Estimate/Used Failure Point [kN]	Area under the graph – Energy [kJ]	Normalise to unity
Single Section	$k_a = 894.3$	$f_{p_a} = 14.10$	149.4	1.000
Dual Section 1	$k_{a_{s_1}} = 146.8$ $k_{a_{s_2}} = 1368$	$f_{p_{a_1}} = 129.4$	145.0	0.9706
Spatial Bilinear 1	$k_{a_{s_1}} = 146.8$	$f_{p_{a_1}} = 129.4$	149.4	1.000
Spatial Bilinear 2	$k_{a_{s_1}} = 146.8$	$f_{p_{a_1}} = 0$	149.4	1.000

5.3.4 DEVELOPMENT OF DYNAMIC BILINEAR MODEL

A one lumped-parameter bilinear dynamic nodal model along with a tuning algorithm to capture the five key features from the FE simulation will be developed in this Section. The bilinear dynamic model will then be simulated, with the key features of the model compared to the TYS FE simulation data captured in Chapter 4. A discussion into the benefits of the lumped parameter dynamic bilinear nodal model will conclude this Section, i.e. how does the bilinear dynamic model fit to the key features compared to the linear one-section dynamic model.

The formulation of the single lumped parameter dynamic bilinear nodal model builds on the linear static and dynamic models in Section 5.2, the bilinear systems modelling literature in Section 5.3.2 and the static bilinear model developed in Section 5.3.3. The state-dependent spring stiffness involving a bilinear function leads to the novel second-order dynamic bilinear system, represented by:

$$m_a\ddot{x}_a + k_a x_a \pm \eta_a f_a x_a = 0 \tag{5-14}$$

where the coefficient of the third term, i.e. η_a is obtained from a tuning process detailed in Section 5.3.4.1. The third term comprises the multiplicative bilinear product between the force f_a (derived as an internal force due to initial conditions based on the vehicle laden mass m_a and collision velocity v_a) and the deformation x_a (representing the system output) modelled here as an internal system state. The above result is now developed in a step by step manner by first considering the free-response from initial conditions of an arbitrary unforced (i.e. no external input) second-order bilinear representation of a mass-spring system, involving a single bilinear term which takes the form:

$$\ddot{x} + \beta x \pm \eta x u = 0 \tag{5-15}$$

where u and x denote the arbitrary system input (based on initial conditions) and system output, β denotes the coefficient of the linear part of the system and η denotes the coefficient of the bilinear product term involving the input and output (the output here being regarded as an internal system state). Rearranging Equation (5-15), noting that the output x is common to both the constant coefficient of the linear term and the input dependent coefficient of the bilinear term, leads to:

$$\ddot{x} + (\beta \pm \eta u)x = 0 \tag{5-16}$$

i.e. a system having an input dependent dynamic and steady state response. Now relate Equation (5-16) for the arbitrary system to the specific linear case of Equation (5-1), where it is known that the coefficient of the system output, i.e. x in the arbitrary system, corresponds to the spring stiffness value, denoted k_a. Note that in the absence of the bilinear term in Equation (5-16) of the above arbitrary system, the constant term $\frac{k_a}{m_a}$ in Equation (5-1) is equivalent to β in Equation (5-16). Thus the following is given:

$$m_a\ddot{x} + (k_a \pm \eta u)x = 0 \tag{5-17}$$

and dividing through by m_a leads to:

$$\ddot{x}_a + \left(\frac{k_a}{m_a} \pm \frac{\eta_a}{m_a}u_a\right)x_a = 0 \tag{5-18}$$

where $\frac{k_a}{m_a}$ is a normalised constant stiffness coefficient (or stiffness to mass ratio). The internal input u_a described in Equation (5-18), is equivalent to the internal input force f_a, generated from the vehicle laden mass and the collision velocity as an initial condition. Consequently, the input dependent bilinear model representation of the single vehicle collision system now becomes:

$$\ddot{x}_a + \left(\frac{\gamma_a}{m_a} \pm \frac{\eta_a f_a}{m_a}\right)x_a = 0 \tag{5-19}$$

where γ_a has been incorporated to become a tuneable factor of k_a (i.e. the linear approximation), where $\gamma_a = \alpha_a k_a$ (not that $k_{a_{s_1}}$ could be used instead). Full details of this are given in Section 5.3.4.1. Since the force derived from the initial collision velocity is given by $f_a = m_a\ddot{x}_a$, the following is now given:

$$\ddot{x}_a + \left(\frac{\gamma_a}{m_a} \pm \eta_a|\ddot{x}_a|\right)x_a = 0 \tag{5-20}$$

5.3.4.1 SIMULATION, OPTIMISING DYNAMIC BILINEAR MODEL VALUES AND RESULTS

Based on Equation (5-20), a guided search approach based on the bisection principle is set-up in an iterative manner. It is used to obtain the parameter values η_a and α_a (i.e. from $\gamma_a = \alpha_a k_a$) which 'best' capture the key features from the TYS FE simulation

(structural and occupant properties, as detailed in Sections 4.2.3 and 4.2.4, Chapter 4). Hence, for the nominal condition, i.e. vehicle mass value of $1247kg$ and collision velocity of 15.6464 m/s, ($35mph$). Note that the first section of the piecewise linear model in Section 5.3.1 (i.e. $k_{a_{s_1}}$) could be used instead of the linear stiffness term k_a in the search approach.

Converting Equation (5-20) from the time-domain to the Laplace domain gives the following:

$$s_a^2 + \left(\frac{\gamma_a}{m_a} + \eta_a|\ddot{x}_a|\right) X_a(s) = 0 \tag{5-21}$$

which may be configured for simulation in the familiar phase variable canonical form with the additional nonlinear multiplicative bilinear term, see Figure 5-14. Considering the linear Simulink block diagram realisation in Figure 5-3, Section 5.2.3, the bilinear Simulink block diagram in Figure 5-14 has the additional terms η_a (labelled n_a,) and γ_a (labelled y_a).

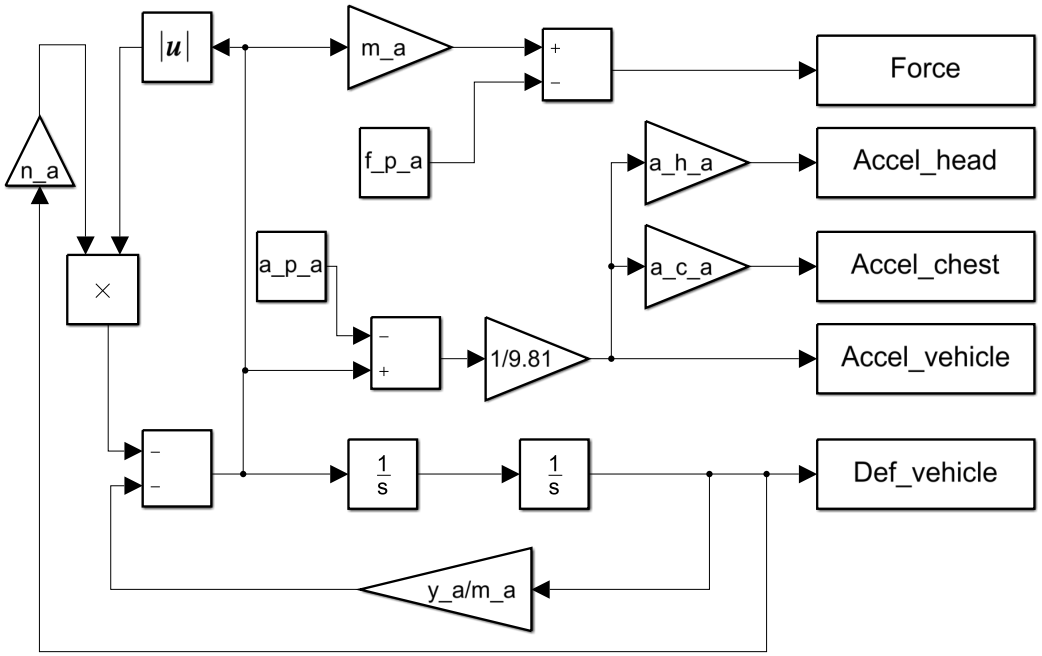

Figure 5-14: *Simulink Realisation in Phase Variable Form including Bilinear Function*

The process/algorithm used to determine the values of η_a and α_a that give the 'best' fit to the FE collision data (i.e. peak deformation, peak acceleration and collision energy) is given below, see Algorithm 5-2. For the process, ranges of β_a between 0.57:0.01:0.97 and α_a between 0.56: 0.01: 0.96 were determined to be effective. For the optimisation of the Euclidean metric (see Algorithm 5-2), the captured values from the bilinear Simulink block diagram model are firstly vector normalised, this is given by:

$$\hat{x} = \frac{|x - y|}{\sum(|x - y|)} \tag{5-22}$$

where x and y denote the bilinear model data and the FE collision data, respectively. The Euclidean metric is given by:

$$d = \sqrt{\hat{x}^2_{acceleration} + \hat{x}^2_{deformation} + \hat{x}^2_{energy}} \tag{5-23}$$

where d is the Euclidean distance metric, with the smallest value giving the 'best' result. Algorithm 5-2 was applied with the results illustrated on a three-dimensional graphical plot, see Figure 5-15. It was determined through the procedure obtained in Algorithm 5-2 that a failure point $f_{p_{a_1}}$ to give a better overall is when $f_{p_{a_1}} = 0$ (also more realistic). In Figure 5-15, the captured bilinear collision model results are represented by blue data points relating to the features of peak deformation, peak acceleration and collision energy. The green data point on Figure 5-15 represents the FE collision data, with the red data point highlighting the Euclidean metric, i.e. the shortest distance between the bilinear collision model and the FE collision data. Thus, the closest value to the FE collision data is selected for the continued use of the bilinear simulation model, with this forming as the baseline model, see Table 5-6.

Algorithm 5-2: *Guided Search Optimisation for Tuning β_a and α_a Values for the Bilinear One Lumped Mass Collision Model*

1. Obtain the following:
   - Vehicle laden mass, denoted m_a
   - Vehicle collision velocity, denoted v_a
   - Vehicle crumple zone stiffness of the linear model, denoted k_a
   - Vehicle crumple zone failure point of the linear model, denoted f_{p_a} and the corresponding offset of the acceleration, denoted a_{p_a} (defined by the force, denoted f_a divided by the vehicle laden mass m_a
   - The corresponding head and chest scalar factors to be multiplied by the output accelerations, denoted a_{h_a} and a_{c_a}
   - The corresponding head and chest scalar factors to be multiplied by the output accelerations, denoted a_{h_a} and a_{c_a}
2. Simulate the Simulink bilinear model for the ¼ cycle of the system response over the following ranges for α_a and η_a:

$$\alpha_a;\ 0.57{:}0.01{:}0.97$$
$$\eta_a;\ 0.56{:}\ 0.01{:}\ 0.96$$

3. Output the peak deformation, peak acceleration, collision energy, peak head acceleration, peak chest acceleration and simulation time
4. Vector normalise the Simulink bilinear model outputs (obtained in Step 3.) using:

$$\hat{x} = \frac{|x - y|}{\sum(|x - y|)}$$

where x and y denote the simulated bilinear model output data and the FE collision output data, respectively.

5. Apply the Euclidean metric:

$$d = \sqrt{\hat{x}^2_{acceleration} + \hat{x}^2_{deformation} + \hat{x}^2_{energy}}$$

where d is the Euclidean distance metric.

6. Select the smallest Euclidean distance metric d value
7. Re-run Steps 1 to 4 with $f_{p_a} = 0$ and $a_{p_a} = 0$ (determine if a better fit can be achieved)
8. Create a normalised bilinear stiffness function, given by: $\frac{\gamma_a}{m_a} + \eta_a|\ddot{x}_a|$ where $\gamma_a = \alpha_a k_a$)

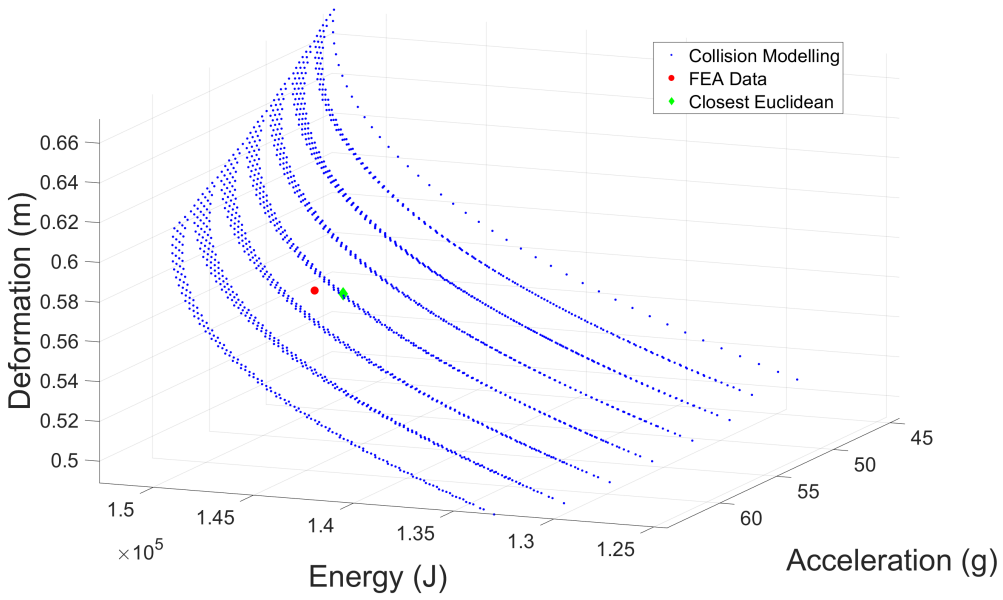

Figure 5-15: *Three-Dimensional Graphical Plot from the Guided Search Optimisation, with the Closest Euclidean Indicated*

Table 5-6: *Tuned Model Values of* η_a *and* α_a *from the Guided Search Optimisation*

Model	Tuned model values
Bilinear	$\eta_a = 0.77$
	$\alpha_a = 0.75$

Simulating the block diagram representation of the bilinear collision model in Figure 5-14 with the obtained tuned values in Table 5-6 and the known parameters give the graphical outputs plotted in Figure 5-16. These correspond to deformation versus time (upper-left hand sub-plot), acceleration versus time (upper-right-hand sub-plot) and force versus deformation (lower-left hand sub-plot). The corresponding occupant accelerations are given for head acceleration versus time (left-plot) and chest acceleration versus time (right-plot) in Figure 5-17. The results relating to the key properties are summarised in Table 5-7 which correspond to the sub-plot structural properties and the sub-plot occupant properties, respectively. As with the linear model, the occupant acceleration plots in Figure 5-17 are simulated to 0.1 seconds, i.e. beyond that of the time-period of the vehicle (structural) peak deformation, see Section 5.2.3 for full details. The last column in Table 5-7, gives the discrepancy expressed as a per-unit

value between the FE simulation output and the model output obtained, see Section 5.2.3. The one lumped mass bilinear model discrepancy values will be compared to the one lumped mass linear model discrepancy values given in Tables 5-2 for the structural properties and occupant accelerations. Expressed as a magnitude, the largest discrepancy is found to be for the collision energy, with a value of 0.0235 for the linear model. The peak acceleration discrepancy for the bilinear model is found to be 0.0093, compared to a value of 0.2031 for the linear model. As expected, the peak chest and head acceleration values also consist of the same discrepancy. The peak deformation output for the bilinear model matches very closely to the FE data with a discrepancy of 0.0012, with this given a closer match to the FE collision data than the linear model with a discrepancy value of 0.0386. The discrepancy of the bilinear model for the collision duration is given by 0.0345, compared to the linear model value of 0.1303. Overall the bilinear model matches the FE structural and occupant data more closely than the linear model, with the bilinear model performing much better at capturing the peak acceleration, and, thus the peak head and chest acceleration. Based on the results from the linear and bilinear collision modelling into an IRW, the bilinear model will be used for the ethical model-to-decision approach to be developed in Chapter 7.

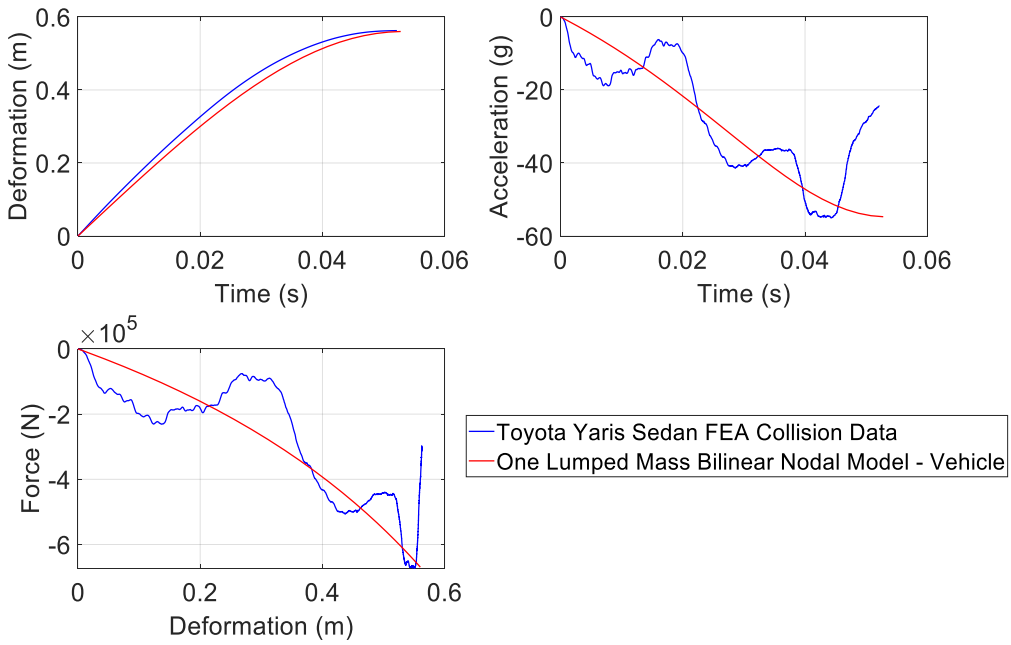

Figure 5-16: *Comparison of the Structural Properties of the Finite Element Model to the One Lumped Mass Bilinear Model for Deformation Versus Time (top-left hand sub-plot), Acceleration versus Time (top-right hand sub-plot) and Force versus Deformation (bottom-left hand sub-plot)*

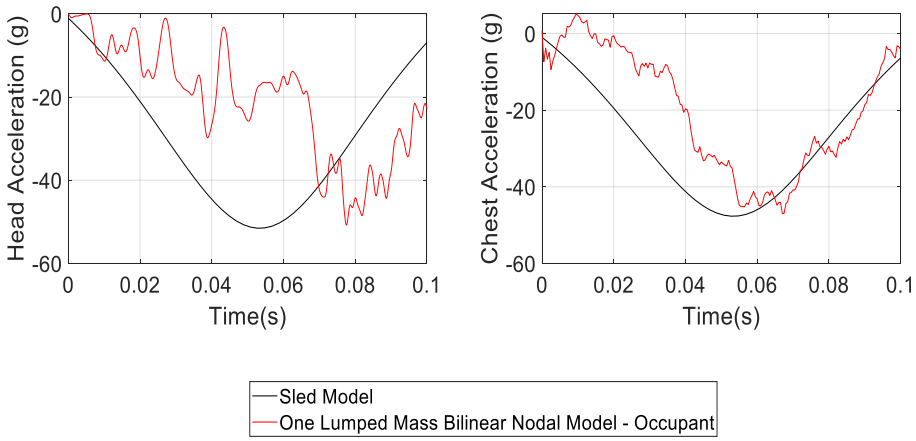

Figure 5-17: *Comparison of the Occupant Properties of the Finite Element Model to the One Lumped Mass Bilinear Model for Head Acceleration versus time (left hand plot) and Chest Acceleration versus Time (right hand plot)*

Table 5-7: *Comparison of the Key Properties (Structural and Occupant Properties) of the Finite Element Model to the One Lumped Mass Bilinear Model*

	FE Model	One Lumped Mass Bilinear Model	Discrepancy [-/+]
Peak Deformation [m]	0.5625	0.5632	0.0012
Peak Acceleration [g]	55.04	54.53	0.0093
Collision Energy – Main Data [kJ]	149.1	152.6	0.0235
Collision Duration [s]	0.0522	0.0540	0.0345
Head Resultant Peak Acceleration [g]	57.95	57.42	0.0093
Chest Resultant Peak Acceleration [g]	45.74	45.31	0.0093

5.3.4.2 VERTIFICATION OF DYNAMIC BILINEAR MODEL

The bilinear collision model with an IRW is simulated over a range of laden mass and collision velocity values. The initial outputs of interest are peak deformation, peak acceleration and collision energy. Initially the nominal laden mass ($1247kg$) is considered, with five velocities of $6.7060m/s$, $11.1760m/s$, $15.6464m/s$, $20.1168m/s$ and $24.5870m/s$ ($15mph$, $25mph$, $35mph$, $45mph$ and $55mph$) explored, see the sub-plots in Figure 5-18. Similarly, the sub-plots in Figure 5-18 correspond to a set of collision scenarios, where the nominal laden mass value (1.0 x $1247kg$) is increased by factors of 0.10 from 1.00 to 1.40, (i.e. 1.10 x $1247kg$), 1.20 (i.e. 1.20 x $1247kg$), 1.30 (i.e. 1.30 x $1247kg$) and 1.40 (i.e. 1.40 x $1247kg$). It is observed from the results presented in Figure 5-18, that as the vehicle laden mass increases with the bilinear stiffness function remaining unchanged, the stiffness to mass ratio decreases, resulting in larger deformation and lower acceleration. Considering Equation (4-2) in Chapter 4, the collision energy values are as expected, i.e. increasing as the collision velocity and the vehicle mass increases. Increasing the collision impact velocity leads to an increase in the deformation and acceleration. The determined effect of the vehicle mass and collision velocity comply with the Laws of Physics, as detailed in Sections 4.2.2 and 4.2.3, Chapter 4. These simulations generate three sets of data which provide the basis for the look-up tables, where the full sets of data can be found in Appendix 5.0.

The time required to reach the peak deformation is affected by the stiffness to mass ratio, as is visible in Figure 5-19. Increased values of the vehicle laden mass results in a lower natural frequency, hence increasing the time period required to reach the quarter cycle, corresponding to the peak deformation. Considering the linear case, the increased time required to reach the quarter cycle can be explained from the observation that $\omega_{n_a} = \sqrt{\frac{k_a}{m_a}} = 2\pi f$, where f denotes frequency. It is known that the periodic time for a full cycle is $T = \frac{1}{f}\ second$, hence the time required for a quarter cycle, which may be expressed as $0.25T$, becomes $0.5\frac{\pi}{\omega_{n_a}}\ second$.

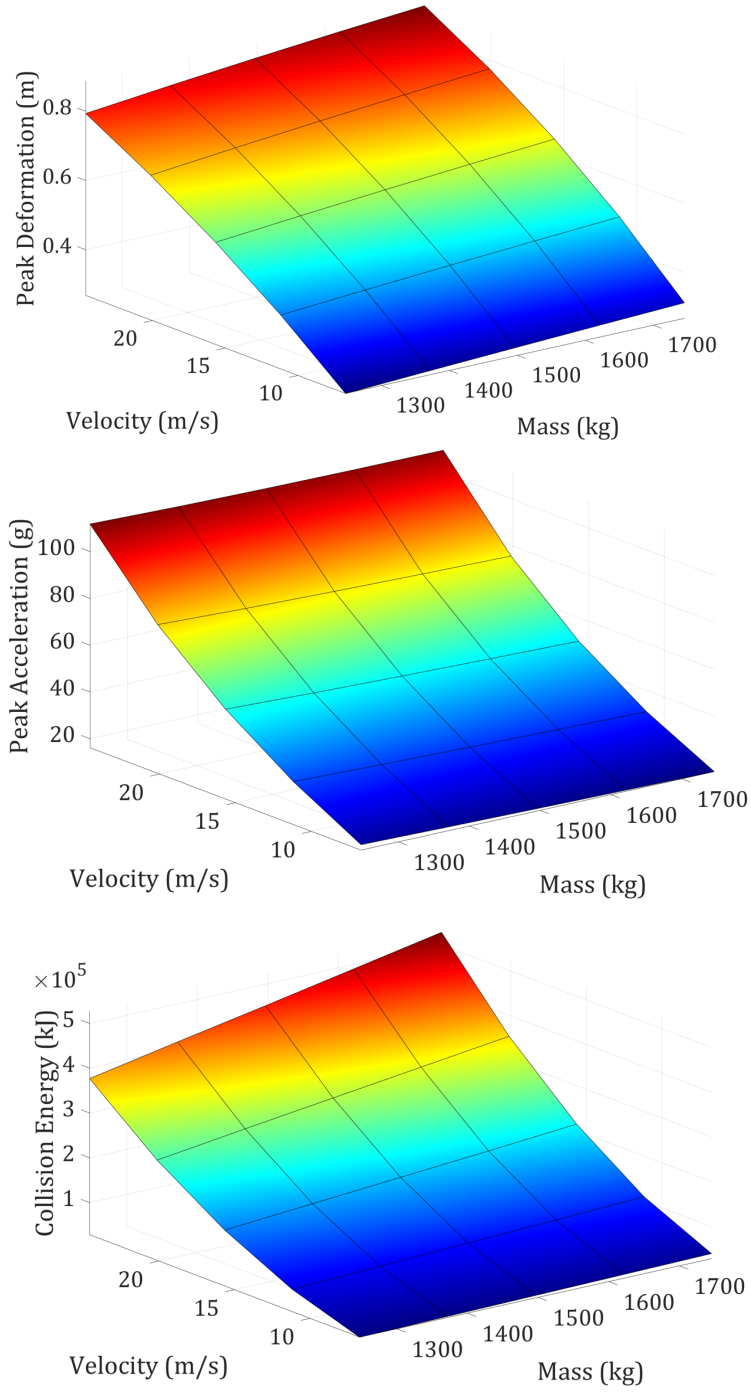

Figure 5-18: *Single Vehicle Collision Model: Peak Deformation (Top), Peak Acceleration (Middle) and Collision Energy (Bottom) as a Function of Laden Mass and Collision Velocity*

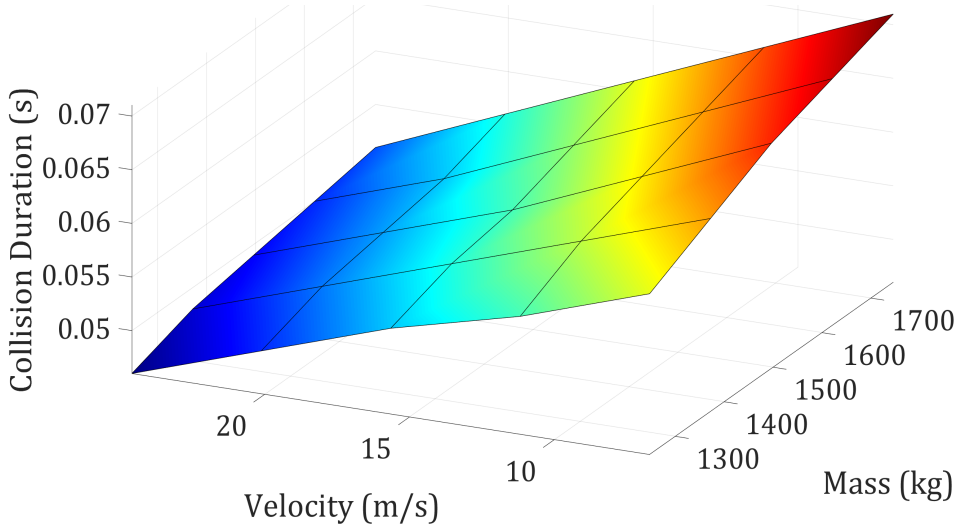

Figure 5-19: *Single Vehicle Model: Collision Duration*

5.4 SUMMARY

Building on the observations in Chapter 4, this Chapter has proposed a nonlinear single mass and spring model for a single-vehicle collision with an immovable rigid wall (IRW). The nonlinear structure adopted is bilinear which includes a product term between force, due to a free-response following an initial collision impact velocity, and deformation; these being the input and output quantities.

A quasi-static spatial bilinear model was initially developed as a means of identifying the coefficients of the dynamic bilinear mass-spring model. The approach commences with piecewise dual section linear model to obtain an initial value for the force versus deformation characteristic, thus representing an initial stiffness value. The advantage of the quasi-static spatial bilinear model is simplicity and transparency, noting that the two-lumped mass linear model (based on a dual piecewise linear model fit) developed is more cumbersome to tune than that of the proposed bilinear approach. Building on the quasi-static spatial model, a dynamic model has been developed which makes use of a simple point mass and nonlinear (bilinear) spring characteristic; the latter being obtained from the quasi-static spatial model. The model is tuned to match the baseline (i.e. m_a = 1247kg and v_a = 15.4646m/s) finite element (FE) simulation data for

capturing the peak deformation, peak acceleration (relating to the peak head and chest accelerations, i.e. *g*-forces). A single bilinear model having fixed parameter values, tuned around the nominal case is found to have a mean value of 0.0113 discrepancy when compared to the FE simulation data (considering peak deformation, peak acceleration and collision energy), with the maximum per unit discrepancy being 0.0235. This gives sufficient improvement when compared to the linear model, with this found to have a mean value of 0.1069 discrepancy and the maximum per unit discrepancy being 0.2031.

Note that FE simulation data is not considered to be precise, but is taken here to be the datum in the absence of real collision data. The performance of the developed bilinear model in terms of accuracy and overall generalisability for dealing with a single-vehicle collision is superior to the linear approaches considered. A verification study has been undertaken that demonstrates that the model complies with the Laws of Physics as detailed in Section 4.2.3, Chapter 4.

6. SYSTEM MODELLING FOR VEHICLE COLLISIONS: MULTIPLE VEHICLES

6.1 INTRODUCTION

This Chapter builds on the system modelling of a single-vehicle collision into an immovable rigid wall (IRW) presented in Chapter 5, where a finite element (FE) model was used as a surrogate to develop a single-vehicle lumped parameter model (LPM). Having developed the single-vehicle LPM, this then becomes the new surrogate for developing the two-vehicle collision model. This is considered justified since in Chapter 5, a single-vehicle LPM has been demonstrated to provide an adequate collision model. Consequently, such an approach is adopted within this Chapter for each vehicle within the two-vehicle full-frontal collision scenarios. As with the single-vehicle LPM, a two-vehicle collision model is developed to capture vehicle structural properties (i.e. peak deformation, peak acceleration and collision deformation energy) and the occupant properties (i.e. peak occupant head and chest acceleration *g*-forces). The initial conditions (collision velocity and vehicle mass) are initially set-up as in Chapter 5 to ensure that the two-vehicle mathematical model adequately captures the collision phenomenon. Hence, when the vehicle collision velocities and masses are the same, as used for the benchmark model in Chapter 5, the results for the two-vehicle collision should be identical. As a point of clarification, and building on the findings thus far, only a single mass per vehicle is considered from now onwards. The two-vehicle collision model needs to be generalisable such that the system properties can be changed, e.g. the mass, velocity and structural stiffness values. As in the single-vehicle collision model

case, initial attention for the two-vehicle collision model is given to the linear and bilinear nodal models. Due to the appealing properties of the modal model representations, with the eigenvalues being explicitly expressed as the stiffness to mass ratios, the equivalent linear and bilinear modal model representations are presented. To conclude the Chapter, model verification is undertaken whereby the developed bilinear two-vehicle LPM is simulated over a range of laden mass and collision velocity values to ensure that the physics of the model behaves as expected.

6.2 TWO VEHICLE FULL FRONTAL COLLISION MODEL

In this Section, the two-vehicle collision LPMs are developed. As when developing the single-vehicle collision LPM into the IRW, the same considerations are given here, hence mass and stiffness values are assumed with the damping being zero. Likewise, the two-vehicle LPM is simulated only for the first quarter cycle of the dynamic system response for each of the vehicles. A literature review into two-vehicle LPMs is undertaken in Section 6.2.1, with the nodal models (linear and bilinear) developed in Section 6.2.2. and the modal models (linear and bilinear) developed in Section 6.2.3. Simulations of the four models are then set up in MATLAB and Simulink using the stiffness values and tuning parameters captured in Chapter 5 for the linear and bilinear dynamic models. As in Chapter 5, based on the Toyota Yaris Sedan (TYS) finite element (FE) simulation in Chapter 4 (see Sections 4.2.3 and 4.2.4), the following key structural properties are of interest and are taken into consideration when assessing the level of injury severity:

- Peak deformation
- Peak acceleration
- Collision energy

Also, based on the peak acceleration of the vehicle (structural properties), and the occupant FE simulation documented in Chapter 4 (see Section 4.3.3), the following occupant properties are again deemed to be of interest:

- Peak head acceleration

- Peak chest acceleration

In Chapter 5, the effect of the offset failure point was explored, where zero offset was determined to give the more accurate results for the bilinear model. Therefore, the offset failure points for the two-vehicle LPM are also set to zero.

6.2.1 BACKGROUND INTO THE LINEAR ONE LUMPED PARAMETER MODELLING

Research into the two-vehicle full-frontal collision mathematical modelling is sparse. However, the following authors (Elmarakbi and Zu, 2004), (Elmarakbi and Zu, 2006) and (Munyazikwiye, Karimi and Robbersmyr, 2017) have published on this topic. In both of Elmarkbi and Zu's publications (2004 and 2006), the authors investigate the use of an extendable front crush structure for the vehicle to vehicle collisions. Offset and full-frontal collisions are investigated with a piecewise linear dynamic model. In (Munyazikwiye, Karimi and Robbersmyr, 2017), the authors use a genetic algorithm to tune a two-vehicle collision model based on actual collision data. Unfortunately, the model presented in the latter paper would appear to be too inflexible and rather simplistic, and does not readily lend itself for enabling variations in the model parameters to be explored; i.e. variations in individual vehicle laden masses, collision velocities and structural stiffness values.

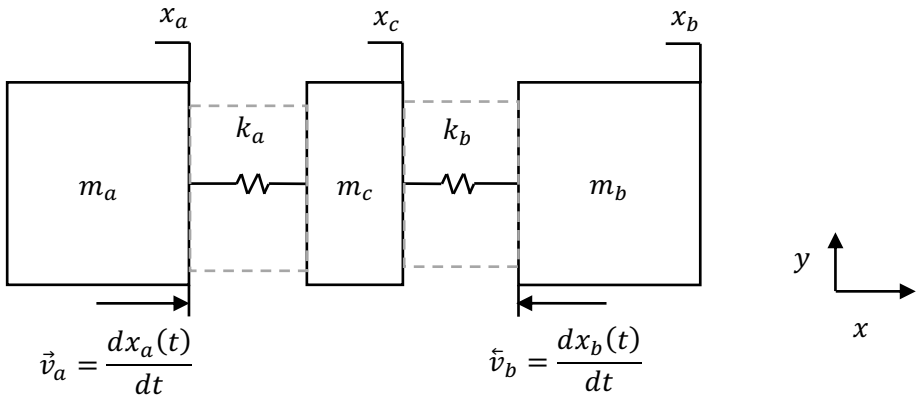

Figure 6-1: *Illustrating the Two Vehicle Full-Frontal Mass Spring Model*

6.2.2 LUMPED PARAMETER LINEAR AND BILINEAR NODAL MODEL

Consider the unforced two-vehicle collision system illustrated in Figure 6-1. This is represented in the familiar nodal coordinates second order matrix differential equation form:

$$M_n\ddot{x} + K_n x = 0 \tag{6-1}$$

where the matrix quantities M_n and K_n denote the mass and stiffness matrices, respectively, and the vector quantities denoted x and $\ddot{x}$, are given by:

$$\begin{bmatrix} m_a & 0 & 0 \\ 0 & m_c & 0 \\ 0 & 0 & m_b \end{bmatrix}\begin{bmatrix} \ddot{x}_a \\ \ddot{x}_c \\ \ddot{x}_b \end{bmatrix} + \begin{bmatrix} k_a & -k_a & 0 \\ -k_a & (k_a + k_b) & -k_b \\ 0 & -k_b & k_b \end{bmatrix}\begin{bmatrix} x_a \\ x_c \\ x_b \end{bmatrix} = 0 \tag{6-2}$$

Note that the subscript n denotes nodal representation. The derivation of Equation (6-1) is given in Appendix 6.0. Normalising (6-1) by diving through by the corresponding individual mass values, i.e. m_a, m_c and m_b gives:

$$\ddot{x} + \widetilde{K}_n x = 0 \tag{6-3}$$

where $\widetilde{K}_n$ is the normalised nodal stiffness to mass ratio matrix for the two-vehicle collision model and is given by:

$$\widetilde{K}_n = \begin{bmatrix} \frac{k_a}{m_a} & -\frac{k_a}{m_a} & 0 \\ -\frac{k_a}{m_c} & \frac{(k_a + k_b)}{m_c} & -\frac{k_b}{m_c} \\ 0 & -\frac{k_b}{m_b} & \frac{k_b}{m_b} \end{bmatrix} \tag{6-4}$$

which may be configured in MATLAB and Simulink for simulation, as is illustrated in Figure 6-2. The model parameters of the stiffness values for Vehicle a and Vehicle b are labelled k_a (i.e. k_a) and k_b (i.e. k_b), respectively. The model parameters of mass for Vehicle a and Vehicle b are labelled m_a (i.e. m_a) and m_b (i.e. m_b), respectively. Note that there is a central mass that connects Vehicle a and Vehicle b, labelled m_c (i.e. m_c). To determine the force that is necessarily common for each of the vehicles, the vehicles acceleration is multiplied by the corresponding mass. Note that for both vehicles, the acceleration is divided throughout by the gravitational constant to convert the results into g-force. As with the model developed in Chapter 5, the head and chest peak acceleration values are determined by multiplying the output acceleration by the respective gains, labelled a_h_a (i.e. a_{h_a}) for the head acceleration and labelled a_c_a (i.e. a_{c_a}) for the chest acceleration, see Figure 6-2. When comparing the vehicle peak acceleration to that of the occupant peak chest and head accelerations from the sled model, the scaling factors are used as discussed in Section 5.3.4.1, Chapter 5 (recall that the scaling factors to be used for the peak head acceleration and peak chest acceleration are given by 0.831 and 1.053, respectively).

This is undertaken to approximate the occupant peak head and chest accelerations/decelerations and the corresponding vehicle peak acceleration. The common collision impact velocity for Vehicle a and Vehicle b is realised via initial conditions applied to the upper and lower left-hand integrators, respectively, see Figure 6-2. The simulation is such that the unforced free dynamic response of the two-vehicle LPM captures the time-period up to the maximum deformation for each vehicle, corresponding to the first quarter cycle as stated earlier and discussed in more detail in Section 5.2.1, Chapter 5. Therefore, the corresponding output data captured for the two vehicles corresponds to this time period, i.e. velocity versus time, acceleration versus time, force versus deformation, head acceleration versus time and chest acceleration

versus time. Note that again, the coefficient of restitution is not considered here in the two-vehicle LPM simulation model. In other words the rebound is not modelled, i.e. only up to the peak deformation corresponding to the first quarter cycle is considered. In reality, of course, the restitution phenomenon will exist.

It is useful to consider the physical ramification of the two vehicle configuration of Figure 6-2 when both have the same mass values but differing stiffness values. It is 'clear' (or rather more intuitive) to imagine that since the forces on each vehicle are equal and opposite, that the displacements (in terms of deformation) will be different. Consequently, the net displacement of the combined two-vehicle system after the collision, see Figure 6-3, will be in the direction (sign) of the vehicle with the highest stiffness value. This fact is reinforced by the numerical example that is depicted in Figure 6-3, with the reader making reference to the Simulation diagram of Figure 6-2.

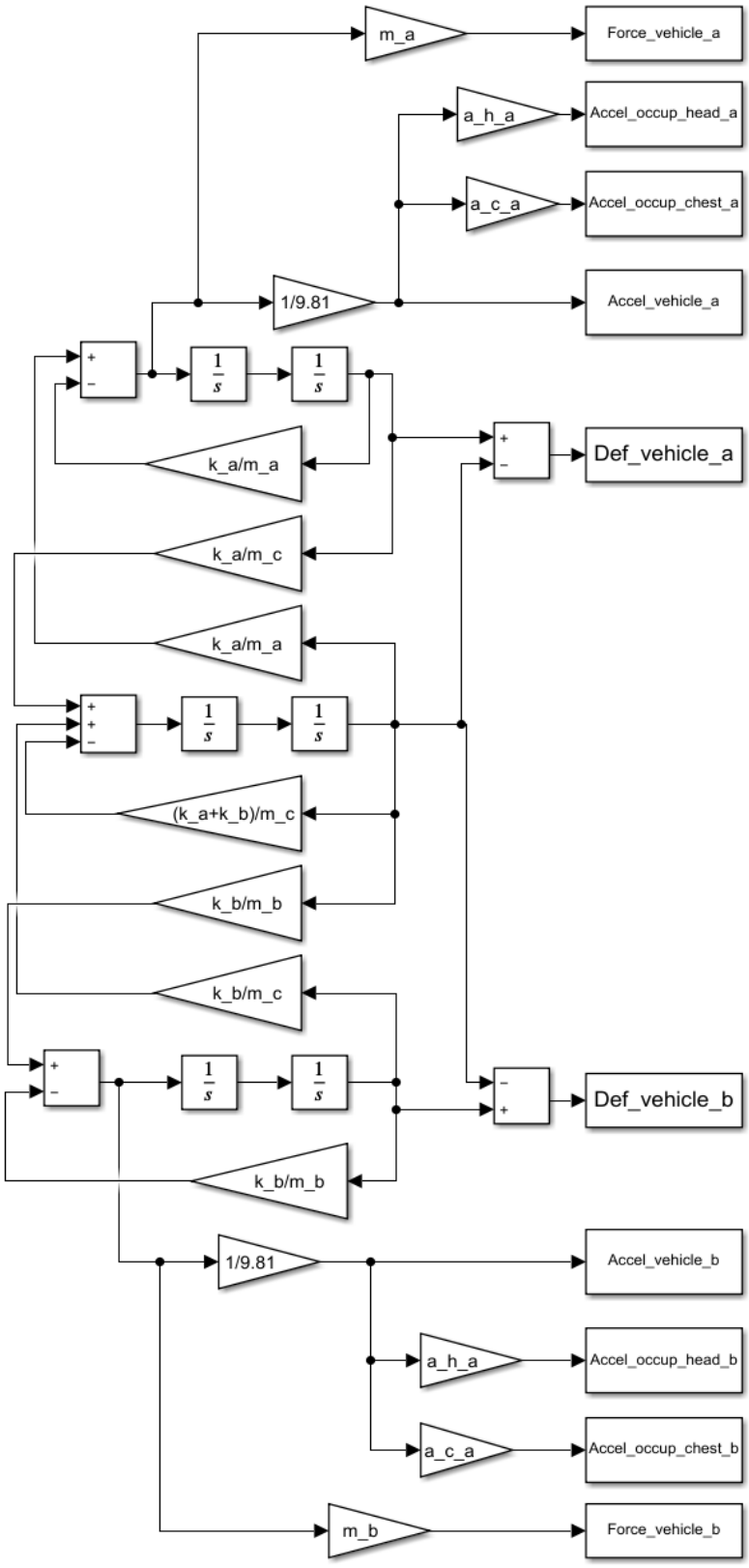

Figure 6-2: *Simulink Realisation in Phase Variable Form of Linear Nodal Model for a Two Vehicle Full Frontal Collision (Note that underscore indicates variable subscript)*

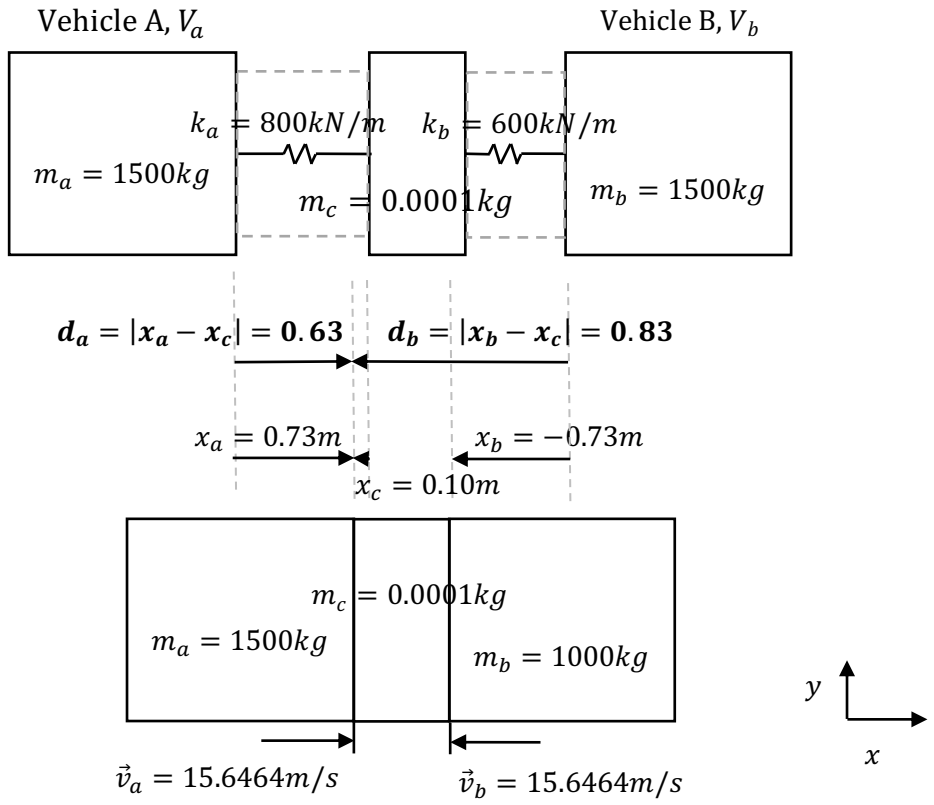

Figure 6-3 *Illustrating Resulting Displacements of Combined Two-Vehicle After the Collision*

Building on the linear two-vehicle full frontal collision model developed above, and the bilinear dynamic single vehicle model in Chapter 5, see Equation (5-20), the bilinear two-vehicle case is now developed. The linear two-vehicle full frontal stiffness matrix in Equation (6-4), denoted $\widetilde{K}_n$ is now given by for the bilinear case:

$$\widetilde{K}_n = \begin{bmatrix} \left(\frac{\gamma_a}{m_a} + \eta_a|\ddot{x}_a|\right) & -\frac{\gamma_a}{m_a} & 0 \\ -\frac{\gamma_a}{m_c} & \frac{(\gamma_a + \gamma_b)}{m_c} & -\frac{\gamma_b}{m_c} \\ 0 & -\frac{\gamma_b}{m_b} & \left(\frac{\gamma_b}{m_b} + \eta_b|\ddot{x}_b|\right) \end{bmatrix} \tag{6-5}$$

where η_a and η_b are the coefficients of the bilinear terms in the single mass models for Vehicle a and Vehicle b, respectively, γ_a and γ_b are tuneable factors of k_a and k_b (i.e.

the linear approximation), where $\gamma_a = \alpha_a k_a$ and $\gamma_b = \alpha_b k_b$. The unforced system described by Equation (6-5) may be realised as configured in MATLAB and Simulink for simulation, see Figure 6-3. Considering the linear Simulink block diagram realisation in Figure 6-2, the bilinear Simulink block diagram in Figure 6-3 has the additional terms η_a (labelled n_a,) and γ_a (labelled y_a) for Vehicle a and η_b (labelled n_b,) and γ_b (labelled y_b) for Vehicle b. Note that the same tuning factors used for the single LPM are used for the two vehicle model, i.e. $\eta_a = \eta_b = 0.77$ and $\alpha_a = \alpha_b = 0.75$ (see Section 5.3.4, Chapter 5).

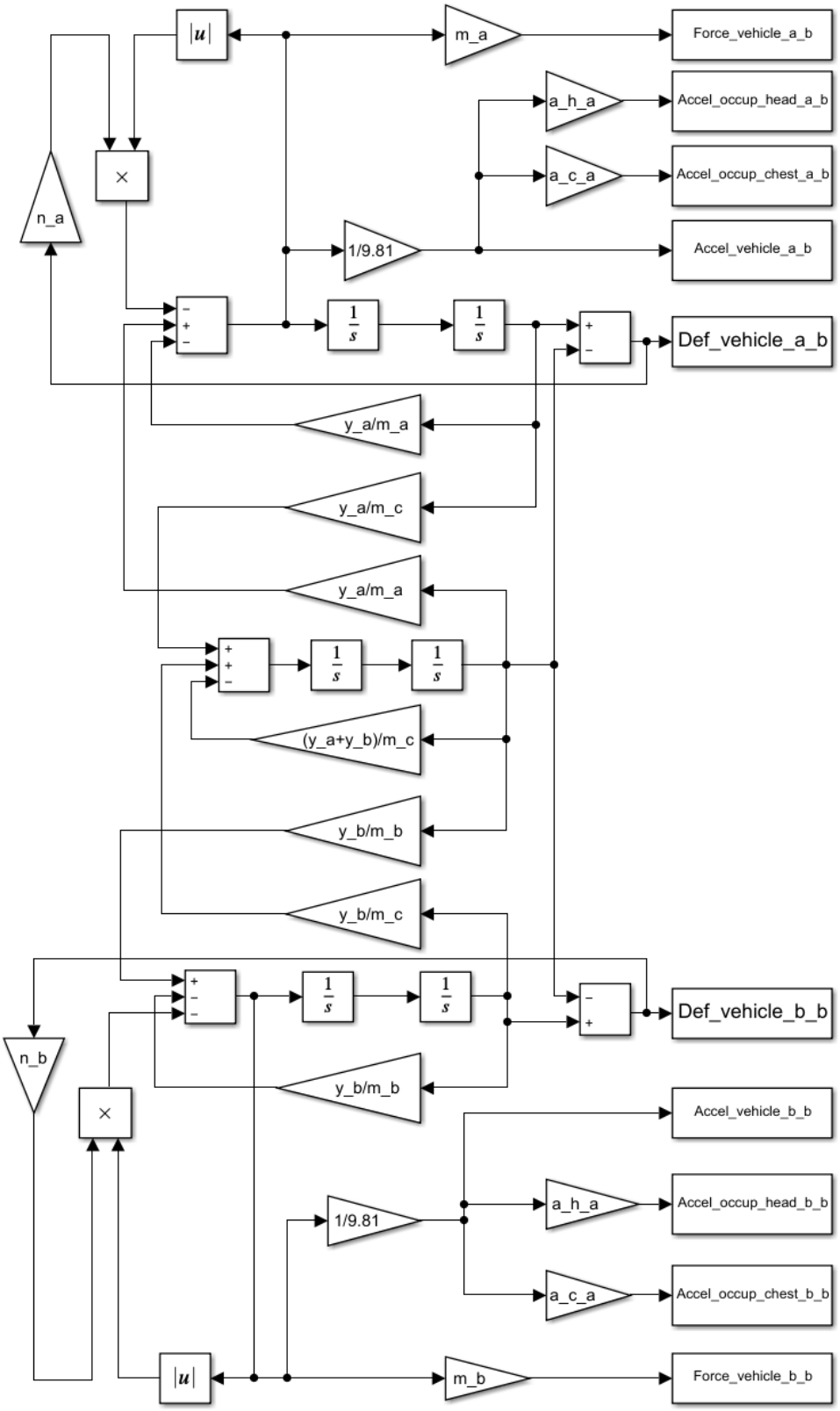

Figure 6-4: *Simulink Realisation in Phase Variable Form of Bilinear Nodal Model for a Two Vehicle Full Frontal Collision (Note that underscore indicates variable subscript)*

6.2.3 LUMPED PARAMETER LINEAR AND BILINEAR MODAL MODEL

The modal model representation commences with the nodal model representation and is centred around the linear transformation:

$$x = \Phi x_m \tag{6-6}$$

where x represents the nodal deformations, as defined in Equation (6-1), Φ is the modal matrix and x_m represents the deformations in the transformed modal coordinate system. Essentially the starting point is to obtain the eigenvalues from:

$$\det[M_n^{-1}K_n - \lambda I] = 0 \tag{6-7}$$

where M_n is the nodal mass matrix and K_n is the nodal stiffness matrix, respectively. The eigenvalues are positive quantities and correspond to the squared values of the natural frequencies of the system modes, i.e. the eigenvalues are $\omega_{n_a}^2$, $\omega_{n_c}^2$ and $\omega_{n_b}^2$. Of interest are the eigenvalues, $\omega_{n_a}^2$ and $\omega_{n_b}^2$, since these correspond directly to the stiffness to mass ratios, $\frac{k_a}{m_a}$ and $\frac{k_b}{m_b}$, of Vehicle a and Vehicle b, respectively.

It is instructive, having obtained an initial modal matrix Φ comprised of the eigenvectors stacked side-by-side, corresponding to the eigenvalues, to obtain the generalised modal mass matrix, being defined as the identity matrix. This is achieved by scaling the individual eigenvectors ϕ_i such that:

$$\phi_1 = p_1\phi_1^T M_n p_1 \phi_1 \qquad \text{i.e. } m_{11} = 1 \tag{6-8}$$

$$\phi_2 = p_2\phi_2^T M_n p_2 \phi_2 \qquad \text{i.e. } m_{22} = 1 \tag{6-9}$$

$$\phi_3 = p_3\phi_3^T M_n p_3 \phi_3 \qquad \text{i.e. } m_{33} = 1 \tag{6-10}$$

Since the p_i are scalar quantities, it follows that:

$$p_i^2 \phi_i^T M_n \phi_i \tag{6-11}$$

holds for all $i = 1, 2$ & 3. So that the p_i may be found from:

$$p_i = \sqrt{\phi_i^T M_n \phi_i} \tag{6-12}$$

for $i = 1, 2$ & 3, i.e.

$$p_i = \left(\phi_i^T M_n \phi_i\right)^{-\frac{1}{2}} \tag{6-13}$$

Thus, generating a new modal matrix $\widetilde{\Phi}$ given by:

$$\widetilde{\Phi} = [\tilde{\phi}_1 \quad \vdots \quad \tilde{\phi}_2 \quad \vdots \quad \tilde{\phi}_3] \tag{6-14}$$

where:

$$\tilde{\phi}_i = p_i \phi_i \tag{6-15}$$

so that:

$$\Phi^T M_n \Phi = M_m = I \tag{6-16}$$

Applying the new modal matrix to the nodal stiffness matrix will yield the generalised modal stiffness to mass ratio matrix. It actually does not change anything, for any scaling

of the eigenvectors has no effect on the invariant values or eigenvalues. It does however, allow the following to be expressed:

$$M_m\ddot{x}_m + K_m x_m = 0 \tag{6-17}$$

Re-defining the modal stiffness-to-mass ratio matrix in terms of the squared values of the natural frequencies, i.e.

$$\ddot{x}_m + \Omega^2 x_m = 0 \tag{6-18}$$

where:

$$\Omega^2 = \begin{bmatrix} \omega_{n_a}^2 & 0 & 0 \\ 0 & \omega_{n_c}^2 & 0 \\ 0 & 0 & \omega_{n_b}^2 \end{bmatrix} \text{ or } \begin{bmatrix} \frac{\gamma_a}{m_a} & 0 & 0 \\ 0 & \frac{\gamma_a+\gamma_b}{m_c} & 0 \\ 0 & 0 & \frac{\gamma_b}{m_b} \end{bmatrix} \tag{6-19}$$

Note that m_c is set to an arbitrary small value. Consequently, with the modal form being defined from the linear transformation:

$$x = \widetilde{\Phi} x_m \tag{6-20}$$

The uncoupled modal equations become:

$$\begin{bmatrix} 1 & 0 & 0 \\ 0 & 1 & 0 \\ 0 & 0 & 1 \end{bmatrix} \ddot{x}_m + \begin{bmatrix} \omega_{n_a}^2 & 0 & 0 \\ 0 & \omega_{n_c}^2 & 0 \\ 0 & 0 & \omega_{n_b}^2 \end{bmatrix} x_m = 0 \tag{6-21}$$

Defining the compact state-space form of the modal model:

$$\chi_{m_i} = \begin{bmatrix} x_m \\ \dot{x}_m \end{bmatrix} \tag{6-22}$$

so that:

$$\dot{\chi}_{m_i} = \begin{bmatrix} \dot{x}_m \\ \ddot{x}_m \end{bmatrix} \tag{6-23}$$

where χ_{m_i} is the initial form of the modal state-space, leading to:

$$\dot{\chi}_{m_i} = \begin{bmatrix} 0 & I \\ -\Omega^2 & 0 \end{bmatrix} \chi_{m_i} \tag{6-24}$$

Re-defining the state vector, gives:

$$\chi_{m_a} = \begin{bmatrix} x_{m_a} \\ \dot{x}_{m_a} \end{bmatrix} \tag{6-25}$$

$$\chi_{m_c} = \begin{bmatrix} x_{m_c} \\ \dot{x}_{m_c} \end{bmatrix} \tag{6-26}$$

$$\chi_{m_b} = \begin{bmatrix} x_{m_b} \\ \dot{x}_{m_b} \end{bmatrix} \tag{6-27}$$

so that a new state vector for the modal representation becomes:

$$\chi_m = \begin{bmatrix} \chi_{m_a} \\ \chi_{m_c} \\ \chi_{m_b} \end{bmatrix} \tag{6-28}$$

Thus, the uncoupled unforced modal state-space representation then becomes:

$$\dot{\chi}_m = A_m \chi_m \tag{6-29}$$

where the modal system matrix A_m comprises of three independent 2 x 2 block diagonal matrices, and is given by:

$$A_m = \begin{bmatrix} 0 & 1 & & & & \\ -\omega_{n_a}^2 & 0 & 0 & & 0 & \\ & & 0 & 1 & & \\ 0 & & -\omega_{n_c}^2 & 0 & 0 & \\ & & & & 0 & 1 \\ 0 & & 0 & & -\omega_{n_b}^2 & 0 \end{bmatrix} or\ A_m = \begin{bmatrix} A_{m_a} & 0 & 0 \\ 0 & A_{m_c} & 0 \\ 0 & 0 & A_{m_b} \end{bmatrix} \tag{6-30}$$

so that Equation (6-29) is now represented as:

$$\dot{\chi}_{m_a} = A_{m_a}\chi_{m_a} \tag{6-31}$$

$$\dot{\chi}_{m_c} = A_{m_c}\chi_{m_c} \tag{6-32}$$

$$\dot{\chi}_{m_b} = A_{m_b}\chi_{m_b} \tag{6-33}$$

which can now be realised as a Simulink diagram as three independent systems triggered by the initial conditions, given by:

$$\dot{x}_m(0) = \widetilde{\Phi}^{-1}\dot{x}(0) \tag{6-34}$$

where $\dot{x}(0)$ corresponds to the initial conditions, i.e. the longitudinal impact velocities $\dot{x}_a(0)$, $\dot{x}_b(0)$ and $\dot{x}_c(0)$, of Vehicle a, Vehicle b and the middle mass, respectively. The unforced system described by Equation (6-29) may be realised as configured in the MATLAB and Simulink diagram of Figure 6-5 for simulation. Considering the linear nodal Simulink block diagram realisation in Figures 6-1, Section 6.2.2, the modal Simulink block diagram in Figure 6-3 has the additional terms labelled omg_1 (i.e. ω_1) for Vehicle a, omg_2 (i.e. ω_2) for the middle mass and omg_3 (i.e. ω_3) for Vehicle b, phi1_1 (i.e. $\tilde{\phi}_{1_1}$), phi2_1 (i.e. $\tilde{\phi}_{2_1}$), phi3_1 (i.e. $\tilde{\phi}_{3_1}$) for Vehicle a, phi1_2 (i.e. $\tilde{\phi}_{1_2}$), phi2_2

(i.e. $\tilde{\phi}_{2_2}$), phi3_2 (i.e. $\tilde{\phi}_{3_2}$) for the middle mass and phi1_3 (i.e. $\tilde{\phi}_{1_3}$), phi2_3 (i.e. $\tilde{\phi}_{2_3}$) and phi3_3 (i.e. $\tilde{\phi}_{3_3}$) for Vehicle b. Using Equation (6-34), the initial conditions are applied to the upper, middle and lower left integrations in Figure 6-5.

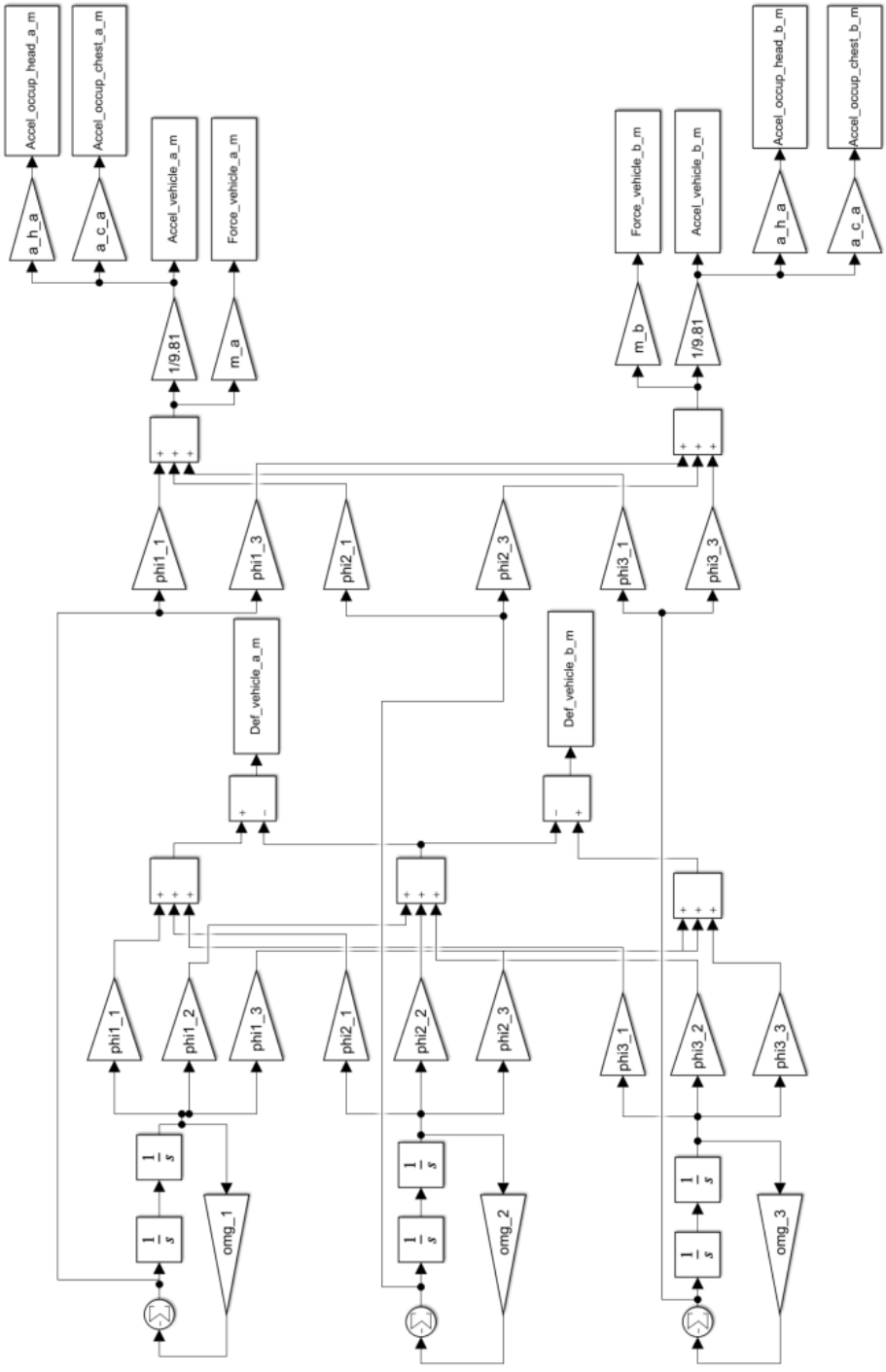

Figure 6-5: *Simulink Realisation in Phase Variable Form of Linear Modal Model for a Two Vehicle Full Frontal Collision (Note that underscore indicates variable subscript)*

Consider the bilinear case, given by:

$$\ddot{x}_m + \Omega^2 x_m + N x_m = 0 \tag{6-35}$$

where the matrix N comprises the multiplicative bilinear term:

$$N = \begin{bmatrix} \eta_a|\ddot{x}_a| & 0 & 0 \\ 0 & 0 & 0 \\ 0 & 0 & \eta_b|\ddot{x}_b| \end{bmatrix} \tag{6-36}$$

Defining $\tilde{\Omega}^2$ to be:

$$\tilde{\Omega}^2 = \Omega^2 + N \tag{6-37}$$

and recalling Equation (6-19) to determine Ω^2, the following is given:

$$\tilde{\Omega}^2 = \begin{bmatrix} \left(\frac{\gamma_a}{m_a} + \eta_a|\ddot{x}_a|\right) & 0 & 0 \\ 0 & \frac{\gamma_a + \gamma_b}{m_c} & 0 \\ 0 & 0 & \left(\frac{\gamma_b}{m_b} + \eta_b|\ddot{x}_b|\right) \end{bmatrix} \tag{6-38}$$

The unforced system described by Equation (6-38) may be realised as configured in the Simulink diagram of Figure 6-6 for simulation.

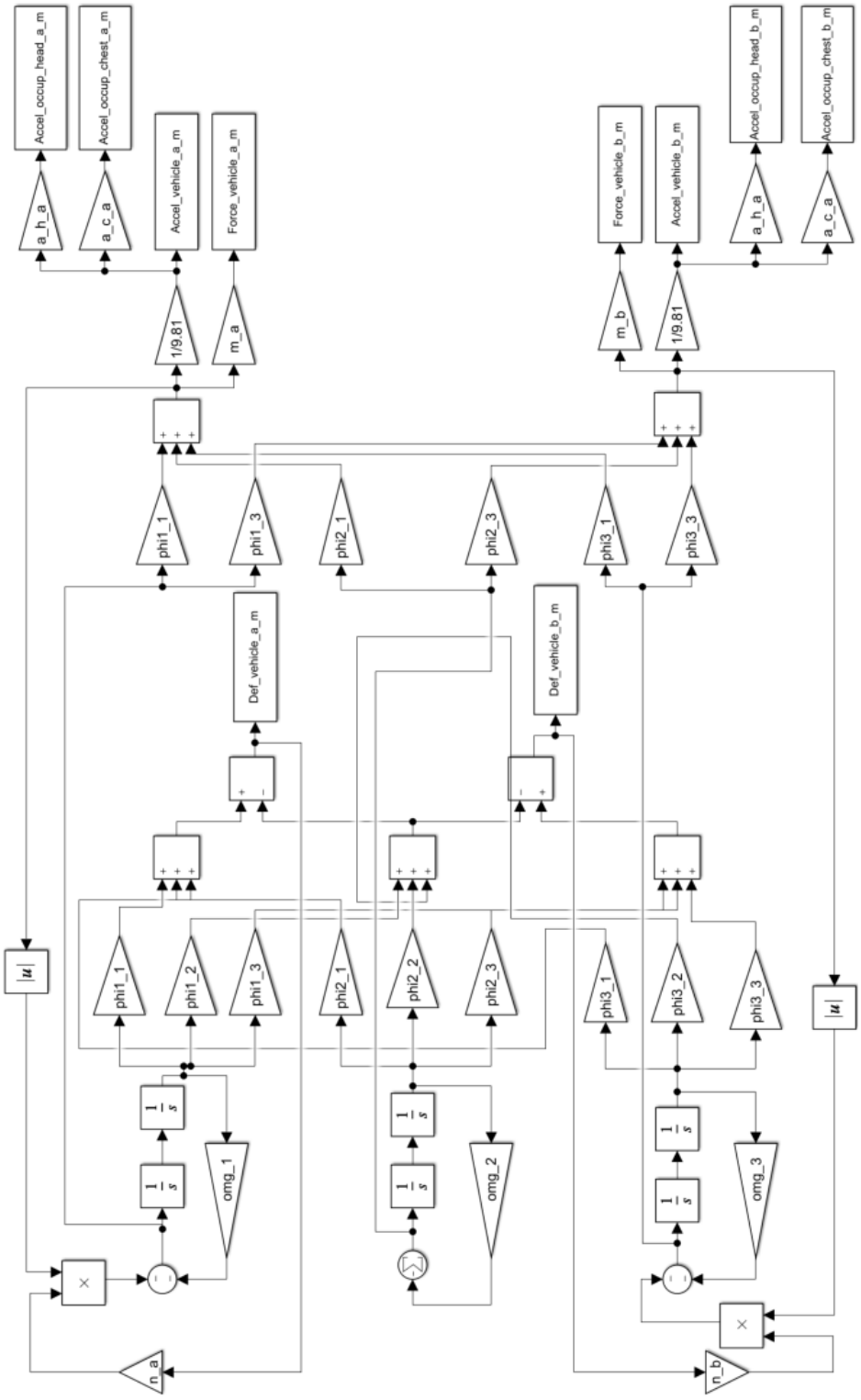

Figure 6-6: *Simulink Realisation in Phase Variable Form of Bilinear Modal Model for a Two Vehicle Full Frontal Collision (Note that underscore indicates variable subscript)*

6.2.4 SIMULATION AND RESULTS

Making use of the linear and bilinear one lumped mass (per vehicle), nodal model, in Section 6.2.2 and the linear and bilinear one lumped mass (per vehicle), modal model, in Section 6.2.4, simulations are performed. The AVs considered will have the same structural stiffness properties that are used in Chapter 5. The initial conditions (collision velocity and vehicle mass) are initially set-up as in Chapter 5 to ensure that the two-vehicle mathematical model adequately captures the collision phenomenon. Hence when the vehicle collision velocities and masses are the same, as used for the benchmark model in Chapter 5, the results for the two-vehicle collision should be identical.

The graphical output presented in Figures 6-7 and 6-9 corresponds to the key outputs of deformation versus time (upper left-hand plot), acceleration versus time (upper right-hand plot) and force versus deformation (lower left-hand plot) for the linear nodal/modal and bilinear nodal/modal models. The graphical outputs presented in Figures 6-8 and 6-10 correspond to the key outputs of chest acceleration versus time (left-hand plot) and head acceleration versus time (right-hand plot) for the linear nodal/modal and bilinear nodal/modal models. It can be observed that the outputs for the nodal and modal models are identical, as expected. Consequently, either the nodal or modal form could be used in combination with the linear or bilinear models. The key features from Figures 6-7 to 6-10 have been captured in Table 6-1, where it is identified that the captured outputs for each of the two-vehicles are identical to that of the single-vehicle collision model outputs in Chapter 5 (for both the linear and nonlinear model).

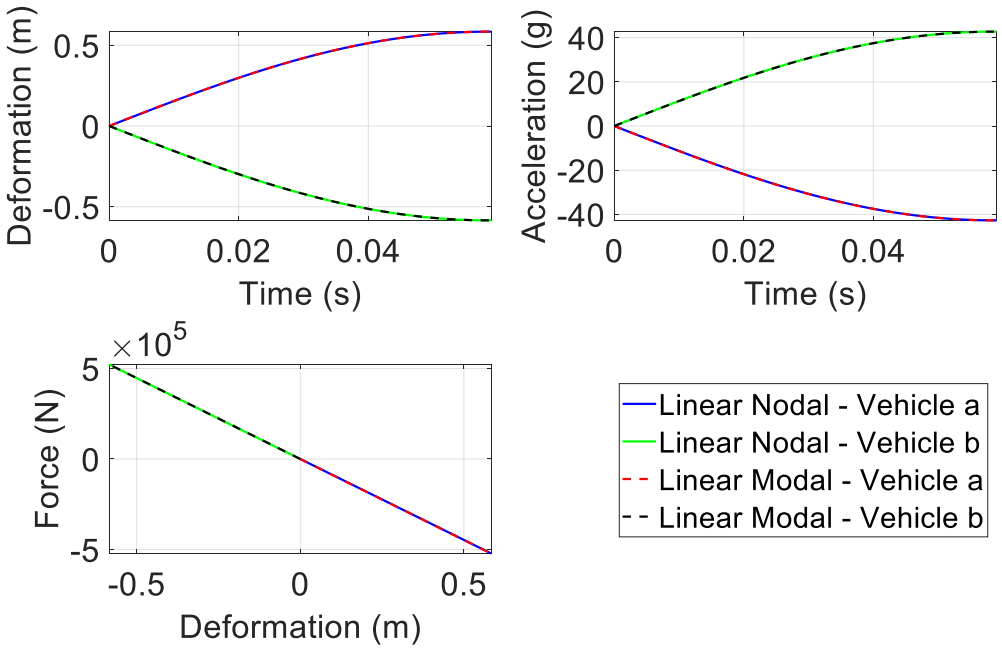

Figure 6-7: *Two Vehicle Lumped Mass Linear Nodal and Modal Model Simulation Results for Deformation Versus Time (top-left hand sub-plot), Acceleration versus Time (top-right hand sub-plot) and Force versus Deformation (bottom-left hand sub-plot)*

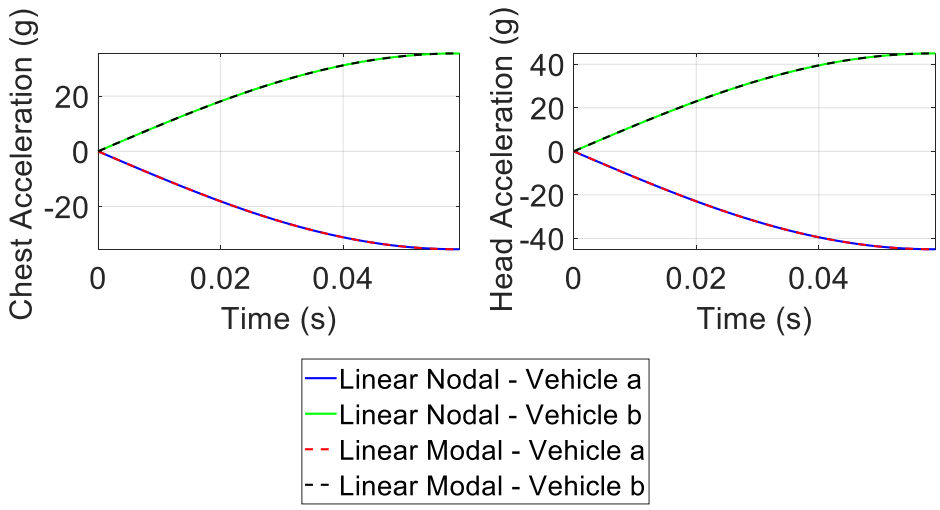

Figure 6-8: *Two Vehicle Lumped Mass Linear Nodal and Modal Model Simulation for Chest Acceleration versus Time (left hand plot) and Head Acceleration versus Time (right hand plot)*

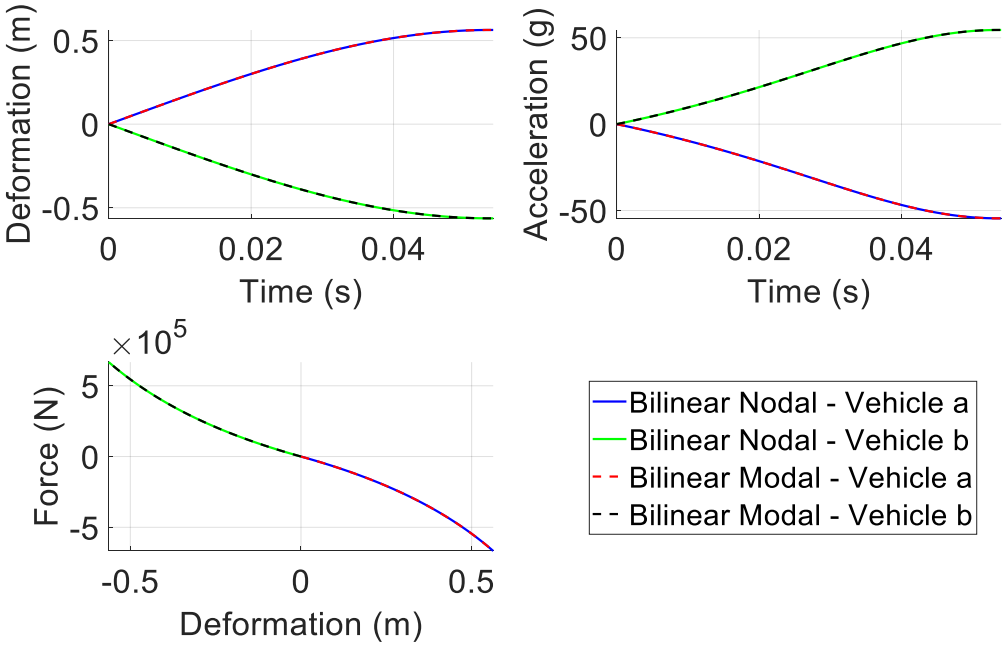

Figure 6-9: *Two Vehicle Lumped Mass Bilinear Nodal and Modal Model Simulation Results for Deformation Versus Time (top-left hand sub-plot), Acceleration versus Time (top-right hand sub-plot) and Force versus Deformation (bottom-left hand sub-plot)*

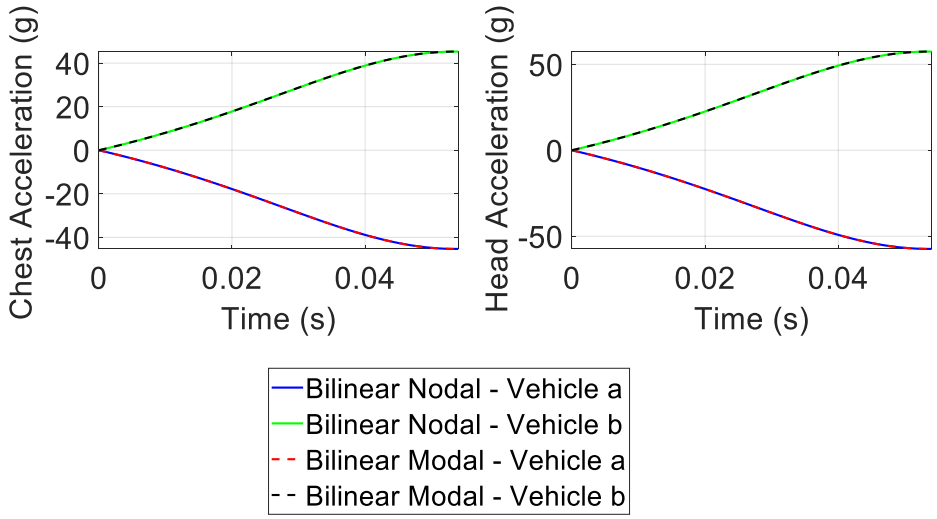

Figure 6-10: *Two Vehicle Lumped Mass Bilinear Nodal and Modal Model Simulation for Chest Acceleration versus Time (left hand plot) and Head Acceleration versus Time (right hand plot)*

Table 6-1: *Two Vehicle Lumped Mass Linear Nodal/Modal and Bilinear Nodal/Modal Simulation Results*

	Linear Nodal/Modal Models	**Bilinear Nodal/Modal Models**
Peak Deformation – Vehicle a [m]	0.5842	0.5632
Peak Deformation – Vehicle b [m]	0.5842	0.5632
Peak Acceleration – Vehicle a [g]	42.712	54.53
Peak Acceleration – Vehicle b [g]	42.712	54.53
Collision Energy – Main Data – Vehicle a [kJ]	152.6	152.6
Collision Energy – Main Data – Vehicle b [kJ]	152.6	152.6
Collision Duration – Vehicle a [s]	0.0590	0.0540
Collision Duration – Vehicle b [s]	0.0590	0.0540
Head Resultant Peak Acceleration – Vehicle a [g]	44.98	57.42
Head Resultant Peak Acceleration – Vehicle b [g]	44.98	57.42
Chest Resultant Peak Acceleration – Vehicle a [g]	35.50	45.31
Chest Resultant Peak Acceleration – Vehicle b [g]	35.50	45.31

6.2.5 VERFICATION OF BILINEAR MODEL

The developed two-vehicle bilinear nodal collision model in Equation (6-5) is simulated over a range of laden mass and collision velocity values. This is undertaken to verify the two-vehicle collision model, hence to ensure the model meets the Laws of Physics as detailed in Section 4.3, Chapter 4. Note that the equivalent bilinear modal model detailed in Section 6.2.3 could also be used. To generate the look-up tables for the verification, Vehicle a remains fixed at the nominal laden mass and velocity, i.e. vehicle laden mass value of $1247kg$, longitudinal impact velocity of 15.6464 m/s, ($35mph$) and the stiffness and bilinear coefficient terms that are detailed in Table 5-6, Chapter 5. The nominal laden mass of Vehicle b is increased by factors of 1.10 from 1.00 to 1.40, (i.e. 1.10 x $1247kg$), 1.20 (i.e. 1.20 x $1247kg$), 1.30 (i.e. 1.30 x $1247kg$) and 1.40 (i.e. 1.40 x $1247kg$), and five velocities of $6.7060m/s$, $11.1760m/s$, $15.6464m/s$, $20.1168m/s$ and $24.5870m/s$ ($15mph$, $25mph$, $35mph$, $45mph$ and $55mph$) are considered. By running

the collision simulations over the above ranges using the two-vehicle bilinear nodal model, the key features are extracted and look-up tables/surfaces are developed. The obtained three 5 x 5 look-up tables (surface plots), corresponding to peak deformation, peak acceleration and collision deformation energy may be found in Figure 6-11. The determined effect of the vehicle laden mass and collision velocity comply with the Laws of Physics as detailed in Sections 4.3, Chapter 4. The full sets of data which provide the basis for the three look-up tables can be found in Appendix 7.0.

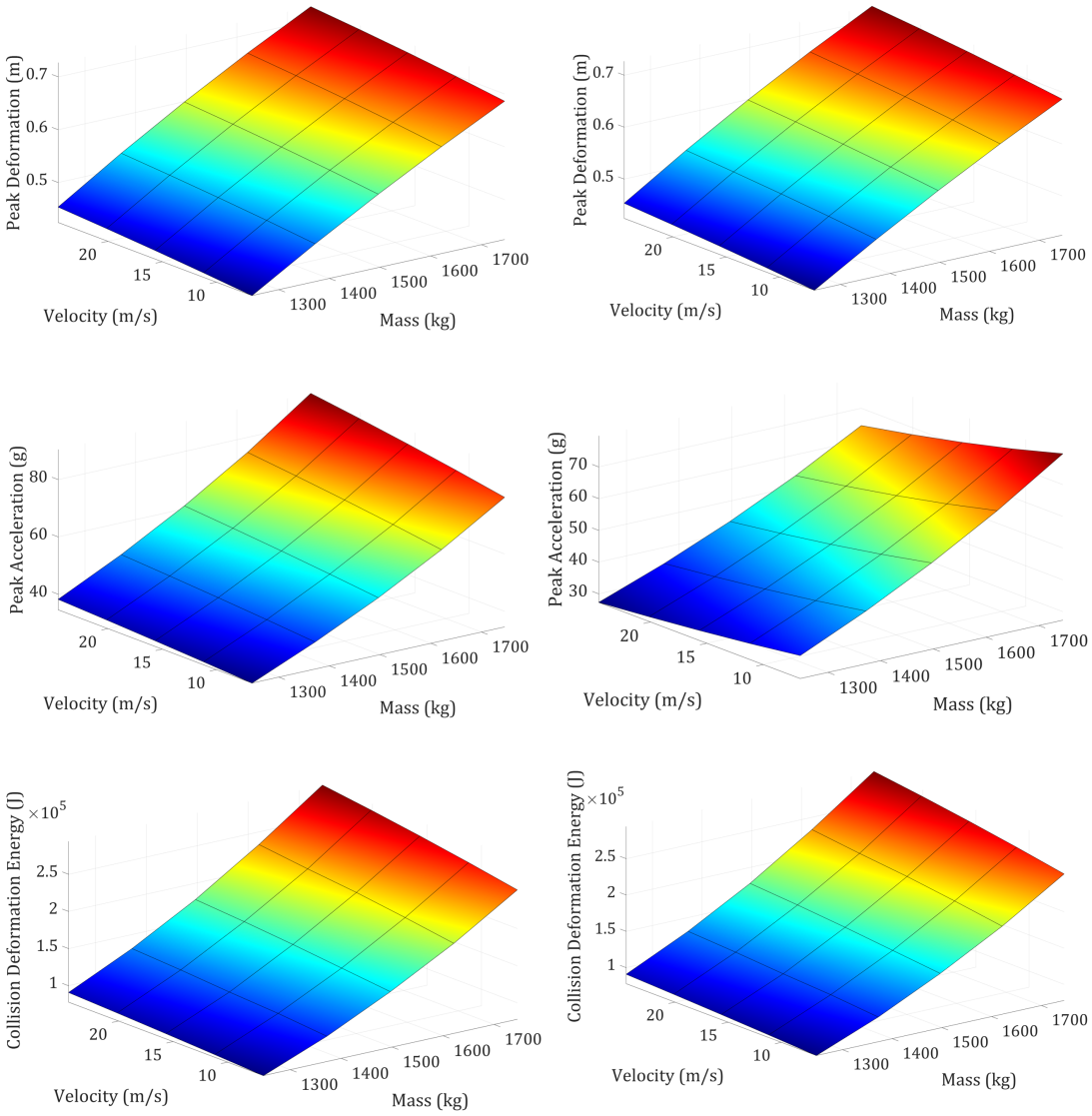

Figure 6-11: *Two Vehicle Collison Outputs where Vehicle A is illustrated on the Left and Vehicle B is illustrated on the Right for Peak Deformation (Top), Peak Acceleration (Middle) and Collision Deformation Energy (Bottom)*

6.3 SUMMARY

In this Chapter, two-vehicle full-frontal collision models have been developed. As in the single-vehicle collision case into an immovable rigid wall (IRW) in Chapter 5, linear and nonlinear (bilinear) models have been explored. Additionally, the mathematical representations of a two-vehicle collision was modelled in both nodal and modal form. The same tuning factors for the two-vehicle bilinear models have been used as for the linear and nonlinear single-vehicle models in Chapter 5, where the baseline model

values are initially used on both vehicles (each lumped mass). It was determined, as was expected, that both for the nodal/modal linear and nodal/modal bilinear models give rise to identical outcomes. Thus, this has demonstrated that the models are working as expected, with the bilinear model taken further. To verify the two-vehicle collision model, whilst keeping the properties of Vehicle a the same, the nominal laden mass of Vehicle b has been increased by factors of 1.10 from 1.00 to 1.40, (i.e. 1.10 x $1247kg$), 1.20 (i.e. 1.20 x $1247kg$), 1.30 (i.e. 1.30 x $1247kg$) and 1.40 (i.e. 1.40 x $1247kg$), and by five velocities of $6.7060m/s$, $11.1760m/s$, $15.6464m/s$, $20.1168m/s$ and $24.5870m/s$ ($15mph$, $25mph$, $35mph$, $45mph$ and $55mph$). It was determined that the effect of the vehicle mass and collision velocity comply with the Laws of Physics as detailed in Sections 4.3, Chapter 4.

The two-vehicle dynamic bilinear collision model is considered to be a main contributing feature to the novelty presented in this thesis. The two-vehicle dynamic bilinear model is exploited in Chapter 8, where multiple AV to AV collisions are investigated. The dynamic model is used within the active stiffness control strategy for altering the collision outcomes in terms of injury severity levels. The concept of injury severity levels and quantification of utility cost is further developed in Chapter 7 for the single AV case, and extended in Chapter 8 for the multiple AV collision case.

7. ETHICAL DECISION MAKER FOR A SINGLE AUTONOMOUS VEHICLE COLLISION

7.1 INTRODUCTION

This Chapter is focused on the development of the ethical decision-maker (EDM) for the case of a single autonomous vehicle (AV) collision into an immovable rigid wall (IRW) or into one or a group of pedestrians. Using the bilinear collision model developed in Chapter 5 and an approach using 3D surfaces (look-up tables) corresponding to the pre-determined passive collision outcomes, combined with interpolation using fuzzy logic, the following four Stages are detailed in this Chapter:

- Stage 1: pre-determine collision outcomes
- Stage 2: pre-determine collision injury severities
- Stage 3: activate stiffness controller
- Stage 4: collision target selection

Stage 1 involves the AV pre-determining the three key outcomes of a collision with an IRW, i.e. peak deformation, peak head acceleration and peak chest acceleration. Stage 2 uses the information from Stage 1, as well as the pre-determined outcome in terms of pedestrian impact velocity and applies collision injury severities to the four outcomes (for the AV and pedestrians). In Stage 3, the stiffness controller (when activated) is used to assess whether the AV collision severity into an IRW can be improved via softening/stiffening the collision structure. In Stage 4, with use being made of the injury severity levels, the four potential collision target selection algorithms based on

philosophical actions (deontological and utilitarian) and social actions (altruism and selfishness), which were introduced in Chapter 2, are evaluated. The four Stages involve the use of fuzzy logic for interpolation between the pre-determined collision outcomes (passive and active), along with a number of developed algorithms for the integrated operation of the four Stages. A function considering the utility cost of lives at risk is created to allow the results from the four algorithms to be compared, i.e. the most desirable ethical algorithm that gives rise to the lowest utility cost to society.

7.2 STAGES 1 AND 2: PREDETERMINING COLLISION SEVERITY

The initial scenario considered in this Chapter, as initially detailed in Section 3.2.1, Chapter 3, involves an autonomous vehicle (AV) containing 2 occupants making a decision between swerving to avoid 1 or 10 pedestrians and to collide into an immovable rigid wall (IRW) as well as the alternative scenario of an AV making a decision between swerving to avoid an IRW and to collide with 1 or 10 pedestrians.

As detailed in Chapter 5, the nonlinear (bilinear) vehicle collision model was found to adequately replicate the finite element (FE) simulation data corresponding to a single-vehicle collision into an IRW. In Section 5.3.4.2, three look-up tables were generated corresponding to the values of peak deformation, denoted δ_a, peak acceleration, denoted a_a, and collision deformation energy, denoted ΔE_a, over a range of values for AV laden mass and collision velocity. Recall that the subscript a relates to a Vehicle a.

As a short recap of the main points, five velocities of $6.7060 m/s$, $11.1760 m/s$, $15.6464 m/s$, $20.1168 m/s$ and $24.5870 m/s$ (corresponding to $15 mph$, $25 mph$, $35 mph$, $45 mph$ and $55 mph$, respectively) are considered, and the nominal laden mass value (1.0 x $1247 kg$) is incremented by factors of 0.10 from 1.00 to 1.40, (i.e. 1.10 x $1247 kg$), 1.20 (i.e. 1.20 x $1247 kg$), 1.30 (i.e. 1.30 x $1247 kg$) and 1.40 (i.e. 1.40 x $1247 kg$). Note that whilst the laden mass is increased above its nominal value, the structural stiffness,

modelled by the bilinear stiffness function remains unchanged. For the operation of fuzzy logic, the peak deformation (one of the three key collision outcomes) and peak acceleration look-up tables are used, with these forming the feature matrices. Note that the other two key collision outcomes (peak head acceleration, denoted a_{a_H}, and peak chest acceleration, denoted a_{a_C}) can be determined using the peak acceleration and the scaling factors, determined in Section 5.2.3, Chapter 5. The feature matrices are used in conjunction with fuzzy logic for interpolation between pre-computed values, with this forming Stage 1 of the ethical decision-maker (EDM), see Figure 7-1. Thus, based on estimates of the AV laden mass and predictions of the collision velocity, estimates of the collision outcomes (or properties) can be determined, i.e. peak deformation δ_a and peak acceleration a_a, with peak head acceleration a_{a_H} and peak chest acceleration a_{a_C} being derived using scaling factors. Note that the outcomes affecting collision injury severity are not considered in Stage 1, and that only AV collision velocity is required for Stage 2, see Figure 7-2. Note also that for Stage 1, the dynamic bilinear vehicle collision model could be used directly online, rather than using the three look-up tables and interpolating using fuzzy logic.

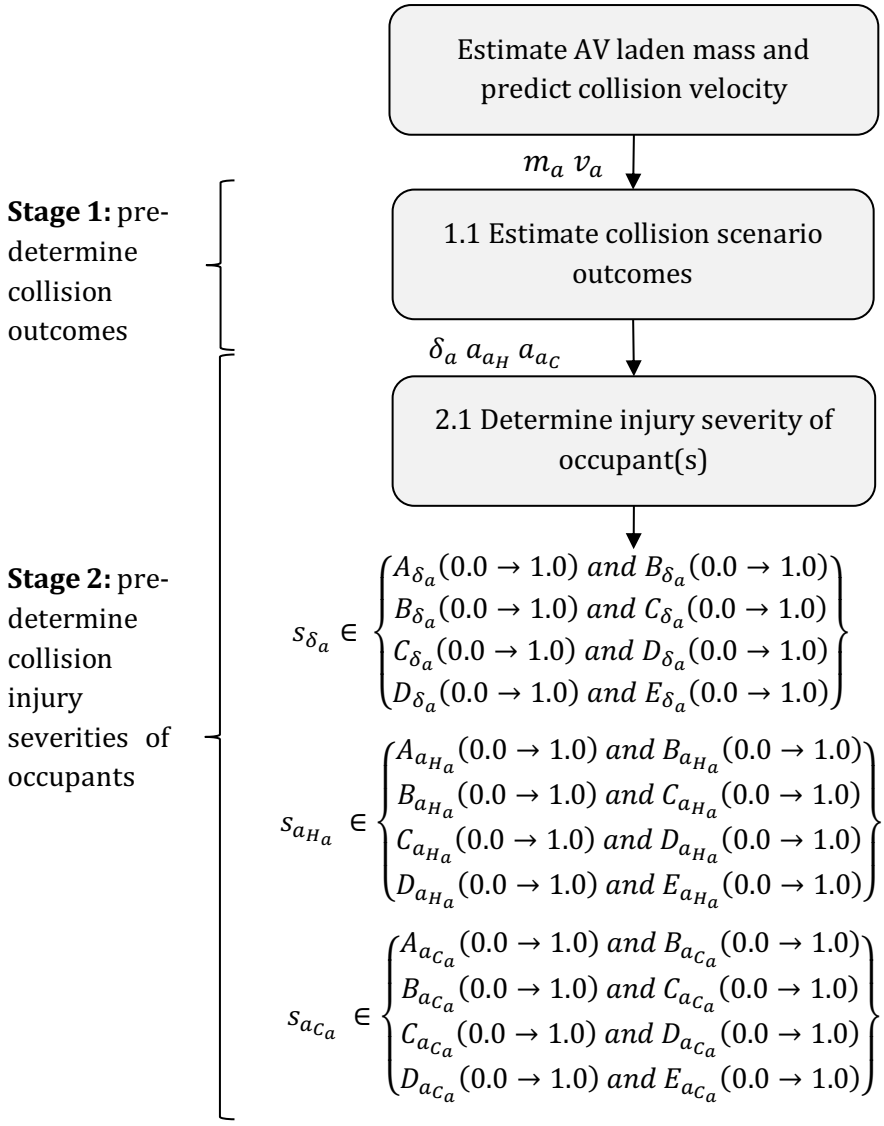

Figure 7-1: *Two Stage Approach for Pre-Determining the Collision Outcomes and Collision Injury Severities of Occupant(s)*

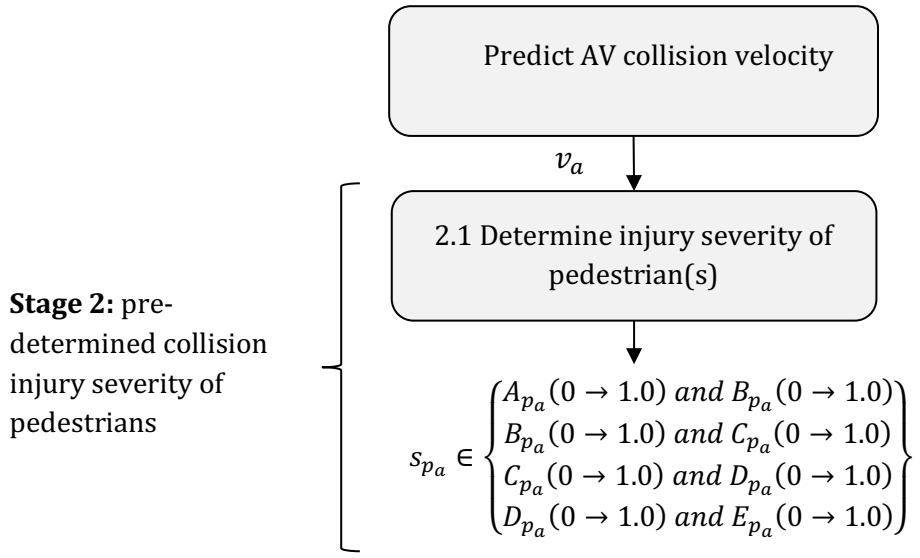

Figure 7-2: *Stage 2 for Pre-Determining the AV Collision Velocity and Collision Injury Severities of Pedestrian(s)*

Stage 2 involves determining the collision injury severity, denoted s, based on the collision outcomes. In (Department for Transport, 2017), the levels described as slight, less serious, moderately serious, very serious and fatal (killed) are used for the classification of injury severity using CRASH (collision recording and sharing system). The UK Government uses the descriptions of slight, severe and fatal, see (Department for Transport, 2017). In this work, the five levels of injury severity that align with CRASH are adopted. It is the author's view that the values of vehicle peak deformation, occupant peak chest acceleration, occupant peak head acceleration and pedestrian impact velocity provide a reasonable set of collision outcomes that may be arbitrarily assigned to the injury severity levels for the EDM in this work. Furthermore, it is the author's view, that whilst this is subjective, with the severity levels corresponding to fuzzy sets A, B, C, D and E (where fuzzy set A relates to the highest injury severity and E the lowest), there is much potential for further work. In the case of the adopted terminology, fuzzy set A could refer to fatal (or killed), C could refer to severe (or moderately/very serious) injuries and E could refer to slight injuries. The level of injury severity for each of the collision outcomes from Stage 1 will then be determined, with this forming Stage

2 of the EDM, see Figures 7-1 and 7-2 for the AV occupants and pedestrians, respectively. In other words, the four key outcomes from Stage 1 (peak deformation, peak head/chest acceleration and pedestrian impact velocity) form the inputs to Stage 2, with the outcomes from Stage 2 being the injury severity levels for the occupant(s) and pedestrian(s), associated with Vehicle a, where s_{δ_a} denotes the severity of the peak deformation, $s_{a_{H_a}}$ denotes the severity of the peak head acceleration, $s_{a_{C_a}}$ denotes the severity of the peak chest acceleration and s_{p_a} denotes the severity of the pedestrian(s) injury due to impact velocity, respectively.

The injury severities are determined based on a scale defined by fuzzy sets A to E, as discussed above (with the fuzzy sets A to E spanning the universe of discourse). The range of the levels of severity (lowest to highest) are detailed in Section 7.2.2, where, due to the nature of the fuzzy sets being identically triangular, an injury severity belongs to (i.e. $\in$) at most, two adjacent sets. For example, in terms of degrees of membership, the injury severity for peak deformation could be: $A_{\delta_a}(0.7)\ and\ B_{\delta_a}(0.3)$, where the fuzzy set A_{δ_a} relates to the highest injury severity for peak deformation.

7.2.1 STAGE 1: PRE-DETERMINING COLLISION PROPERTIES

The following provides an illustrative example for pre-determining the collision properties of peak deformation and peak acceleration for a full-frontal collision of a single AV into an IRW. Details of the fuzzy logic interpolation process that is used in conjunction with the look-up tables which determine the properties of peak deformation, peak head acceleration and peak chest acceleration will be described in the following Sections. Algorithm 7-1 details a typical fuzzy logic algorithm that is used in this Section.

Algorithm 7-1: *Fuzzy Logic Algorithm*

1. Define the linguistic variables and terms (initialisation)
2. Construct the membership functions (initialisation)
3. Construct the rule base (initialisation)
4. Convert crisp input data to fuzzy values using the membership functions (fuzzification)
5. Evaluate the rules in the rule base (inference)
6. Combine the results of each rule (inference)
7. Convert the output data to a set of non-fuzzy crisp values (defuzzification)

7.2.1.1 DEFINING THE RANGE OR UNIVERSE OF DISCOURSE

For a single AV, denoted Vehicle a, the matrix elements corresponding to the laden mass, denoted m_a, and collision velocity, denoted v_a, let the range of mass values for Vehicle a be:

$$m_{1.00} < m_a \leq m_{2.00} \tag{7-1}$$

and the collision velocity values for Vehicle a be:

$$v_{1.00} < v_a \leq v_{2.00} \tag{7-2}$$

in which $m_{1.00}$ and $m_{2.00}$ denote the upper and lower bounds of the laden mass values, thus defining the fuzzy universe of discourse, or range, for the laden mass values. Similarly, for the collision velocities, let $v_{1.00}$ and $v_{2.00}$ denote the upper and lower bounds, and again define the fuzzy universe of discourse, or range, for the collision velocity values of a single AV. The following arbitrary linguistic terms in Table 7-1 are used to describe the laden mass and collision velocity values for Vehicle a, where $m_{1.00}$ and $v_{1.50}$ denote the nominal design laden mass and collision velocity values based on

the United States New Car Assessment Programme (US NCAP), as detailed in Section 4.2.1, Chapter 4.

Table 7-1: Stage 1: *Fuzzy Sets of Laden Mass and Collision Velocity*

Laden mass [kg]		**Collision velocity [m/s]**	
$m_{2.00}$	Heavy (1.40*1247kg)	$v_{2.00}$	Fast (24.5872m/s)
$m_{1.75}$	Medium heavy (1.30*1247kg)	$v_{1.75}$	Medium fast (20.1168m/s)
$m_{1.50}$	Medium (1.20*1247kg)	$v_{1.50}$	Medium (15.6464m/s)
$m_{1.25}$	Medium light (1.10*1247kg)	$v_{1.25}$	Medium slow (11.1760m/s)
$m_{1.00}$	Light (1.00*1247kg)	$v_{1.00}$	Slow (6.7056m/s)

7.2.1.2 MEMBERSHIP FUNCTIONS

Membership functions are used in the fuzzification and defuzzification steps within a fuzzy logic based ethical decision-making process and control system. These are used to map the non-fuzzy input values, e.g. laden mass and collision velocity of an AV on to a universe of discourse described by fuzzy linguistic terms, whereby the linguistic terms are quantified according to their degrees of membership to the corresponding fuzzy sets. This is illustrated in Figure 7-3, where the linguistic terms corresponding to AV laden mass and collision velocity are each expressed on a universe of discourse. Use is made of triangular fuzzy sets located uniformly over each universe of discourse. A numerical value lying on the universe of discourse in this configuration may belong to either one or at most two adjacent membership functions, i.e. wholly a member of one set or partially a member of two adjacent sets. This follows the reasoning, according to Figure 7-3 and considering Table 7-1, that the laden mass of an AV might plausibly be considered as light and medium light at the same time, with different degrees of membership to each of the two adjacent fuzzy sets.

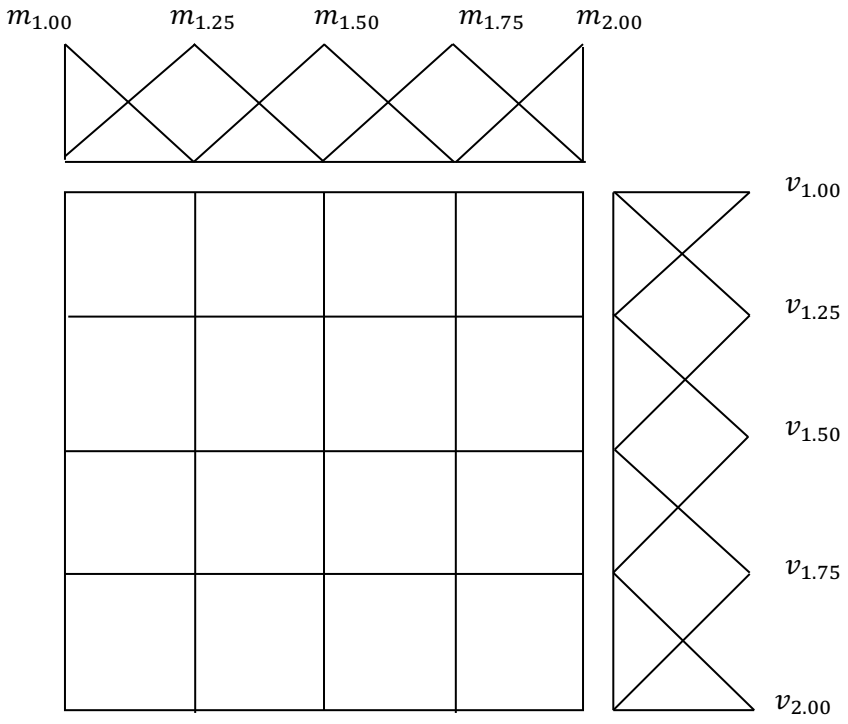

Figure 7-3: *Feature Matrix Formed by Expressing the Single Vehicle Laden Mass and Collision Velocity Values as Fuzzy Sets or Membership Functions each on its Universe of Discourse, with each Node Representing a Predetermined Value in a 5 x 5 Matrix Array*

Considering the passive case for an arbitrary single AV, denoted Vehicle a, in a collision with an IRW, the AV laden mass and collision velocity values considered across each universe of discourse will form a 5 x 5 x 3 tensor-matrix (i.e. a matrix whose elements are vectors). This is illustrated in Figure 7-3 which depicts a 5 x 5 surface, or array, where each element in the array represents a feature vector for peak deformation, peak head acceleration and peak chest acceleration values, denoted, respectively, δ_a, a_{a_H} and a_{a_C}. Therefore, for each element, denoted P_{ij}, in the 5 x 5 array, there is a corresponding quantity expressed as a 3 x 1 feature vector. Note that each vector contains crisp values. Consequently, with each element forming a vector, an alternative representation is a vector of matrices (or tensor), denoted $X_{P_{ij}}$, and is given by:

$$X_{P_{ij}} = \begin{bmatrix} R_{\delta_a} \\ R_{a_{H_a}} \\ R_{a_{C_a}} \end{bmatrix} \tag{7-3}$$

where a general rule base (or consequence matrix) within the vector of matrices is denoted R_C,where the general subscript C denotes peak deformation δ_a, peak head acceleration a_{a_H} and peak chest acceleration a_{a_C}. In general a matrix R_C describes a surface, see Figure 5-18, Chapter 5. Therefore, Equation (7-3) provides the information generated from Stage 1, i.e. to determine the collision outcomes, see Figure 7-1.

The rule base consequence matrices, or feature matrices, for peak deformation δ_a, peak head acceleration a_{a_H} and peak chest acceleration a_{a_C}, are, respectively, given by:

$$R_{\delta_a} = \begin{bmatrix} 0.2681 & 0.2801 & 0.2915 & 0.3024 & 0.3127 \\ 0.4242 & 0.4421 & 0.4589 & 0.4748 & 0.4900 \\ 0.5632 & 0.5853 & 0.6060 & 0.6254 & 0.6437 \\ 0.6860 & 0.7108 & 0.7340 & 0.7555 & 0.7756 \\ 0.7934 & 0.8198 & 0.8441 & 0.8666 & 0.8874 \end{bmatrix} \tag{7-4}$$

$$R_{a_{a_H}} = \begin{bmatrix} 19.50 & 18.75 & 18.09 & 17.51 & 16.99 \\ 36.37 & 35.18 & 34.15 & 33.24 & 32.45 \\ 57.42 & 55.92 & 54.66 & 53.58 & 52.64 \\ 88.96 & 82.42 & 81.22 & 80.22 & 79.42 \\ 117.7 & 116.7 & 116.0 & 115.7 & 115.5 \end{bmatrix} \tag{7-5}$$

$$R_{a_{a_C}} = \begin{bmatrix} 15.39 & 14.79 & 14.27 & 13.81 & 13.41 \\ 28.70 & 27.76 & 26.95 & 26.24 & 25.61 \\ 45.31 & 44.13 & 43.14 & 42.29 & 41.54 \\ 66.26 & 65.04 & 64.10 & 63.31 & 62.68 \\ 92.92 & 92.10 & 91.57 & 91.28 & 91.18 \end{bmatrix} \tag{7-6}$$

Figure 7-3 illustrates the five membership functions that are used to describe the universe of discourse for the AV laden mass and collision velocity values, where the triangular forms of the membership functions are used. Knowing that any point on the

universe of discourse (in the plausible range of values) can at most belong to two such overlapping adjacent functions, the degrees of membership to the two can be calculated by making use of the following relationships. For the AV laden mass, any two of the adjacent functions are denoted m_{a_l} and m_{a_h}, respectively, and for collision velocity are denoted v_{a_l} and v_{a_h}, respectively, where in each case the subscripts l and h correspond to the adjacent lower and higher membership functions. The degrees of membership to the pair-wise lower membership functions may be determined, from:

$$\mu_{m_{a_l}}(m_a) = \frac{p_{m_{a_h}} - m_a}{p_{m_{a_h}} - p_{m_{a_l}}} \tag{7-7}$$

and

$$\mu_{v_{a_l}}(v_a) = \frac{p_{v_{a_h}} - v_a}{p_{v_{a_h}} - p_{v_{a_l}}} \tag{7-8}$$

respectively, where $p_{m_{a_h}}$ and $p_{m_{a_l}}$ denote, respectively, the crisp values of laden mass and correspond to the peaks of the triangular fuzzy sets of the higher and lower adjacent membership functions. Similarly, $p_{v_{a_h}}$ and $p_{v_{a_l}}$ denote the crisp values of collision velocity and correspond to the peaks of the triangular fuzzy sets of the higher and lower adjacent membership functions, respectively. The degrees of membership to the adjacent pair-wise higher membership functions may then be determined, from:

$$\mu_{m_{a_h}}(m_a) = 1 - \mu_{m_{a_l}}(m_a) \tag{7-9}$$

and

$$\mu_{v_{a_h}}(v_a) = 1 - \mu_{v_{a_l}}(v_a) \tag{7-10}$$

respectively. To illustrate Stage 1, consider an AV with a laden mass $m_a = 1270kg$, travelling at a velocity $v_a = 11.6000m/s$ $(25.9485mph)$. These values lie within the

respective universes of discourse (ranges) for laden mass and collision velocity. In this illustrative example, the mass value of $1270kg$ lies within the fuzzy sets of $m_{1.00}$ and $m_{1.25}$ (i.e. $1247kg$ (lower) and 1.1*$1247kg$ (higher)). Consequently, the degrees of membership to the fuzzy sets $m_{1.00}$ and $m_{1.25}$ are determined to be 0.8156, from Equation (7-7) and 0.1844, from Equation (7-9), see Figure 7-4. The velocity value of $11.6000m/s$ lies within the fuzzy sets of $v_{1.00}$ and $v_{1.25}$ (i.e. $11.1760m/s$ and $13.4112m/s$), therefore, analogously, the degrees of membership to the fuzzy sets $v_{1.25}$ and $v_{1.50}$ are determined to be 0.8103 and 0.1897 from Equations (7-8) and (7-10), see Figure 7-4.

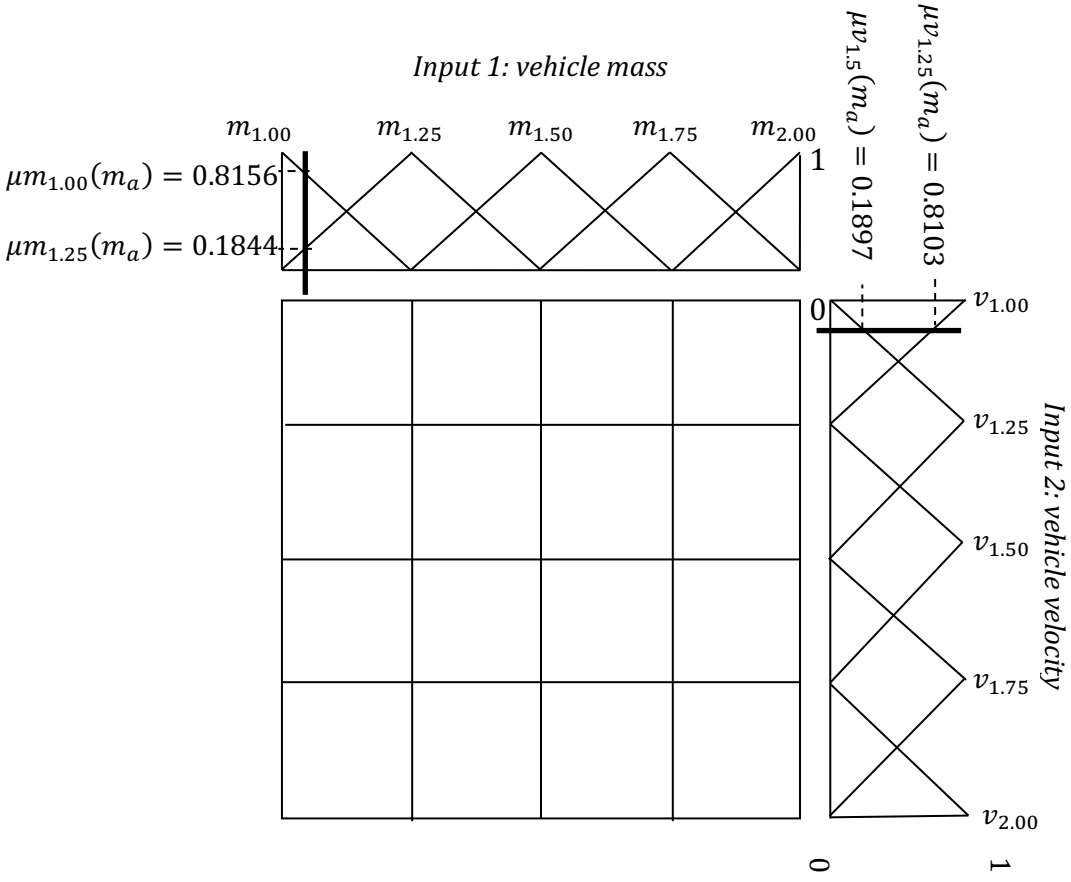

Figure 7-4: *Feature Matrix Formed by Expressing the Single Vehicle Laden Mass and Collision Velocity Values as Fuzzy Sets or Membership Functions on each Universe of Discourse for an Autonomous Vehicle*

7.2.1.3 FUZZY MEMBERSHIP AND INTERPRETATION OF FUZZY RULES

The degrees of membership to a general fuzzy set F of a variable x are denoted as $\mu F(x)$, so that in the single AV case, the vectors of degrees of membership of the variables m_a and v_a are denoted, respectively as, P_{m_a} and P_{v_a}, to the arbitrary fuzzy sets, $\{m_{1.00}, m_{1.25}, m_{1.50}, m_{1.75}, m_{2.00}\}$ and $\{v_{1.00}, v_{1.25}, v_{1.50}, v_{1.75}, v_{2.00}\}$ for laden mass and collision velocity, respectively. The vectors of degrees of membership, or vectors of firing strengths, P_{m_a} and P_{v_a}, are defined, respectively, by:

$$P_{m_a} = \begin{bmatrix} \mu m_{1.00}(m_a) \\ \mu m_{1.25}(m_a) \\ \mu m_{1.50}(m_a) \\ \mu m_{1.75}(m_a) \\ \mu m_{2.00}(m_a) \end{bmatrix} \triangleq \begin{bmatrix} P_{m_{a_{1.00}}} \\ P_{m_{a_{1.25}}} \\ P_{m_{a_{1.50}}} \\ P_{m_{a_{1.75}}} \\ P_{m_{a_{2.00}}} \end{bmatrix} \tag{7-11}$$

and

$$P_{v_a} = \begin{bmatrix} \mu v_{1.00}(v_a) \\ \mu v_{1.25}(v_a) \\ \mu v_{1.50}(v_a) \\ \mu v_{1.75}(v_a) \\ \mu v_{2.00}(v_a) \end{bmatrix} \triangleq \begin{bmatrix} P_{v_{a_{1.00}}} \\ P_{v_{a_{1.25}}} \\ P_{v_{a_{1.50}}} \\ P_{v_{a_{1.75}}} \\ P_{v_{a_{2.00}}} \end{bmatrix} \tag{7-12}$$

where the vector elements, denoted $P_{m_{a_i}}$ and $P_{v_{a_i}}$ (where i denotes the particular index 1.00, 1.25, 1.50, 1.75, 2.00), respectively, represent the degrees of membership to the fuzzy sets, denoted $\{m_{1.00}, m_{1.25}, m_{1.50}, m_{1.75}, m_{2.00}\}$ and $\{v_{1.00}, v_{1.25}, v_{1.50}, v_{1.75}, v_{2.00}\}$, corresponding to AV laden mass, m_a, and collision velocity, v_a, respectively.

Therefore, for the illustrative example, the vectors of firing strengths are readily shown to be given by:

$$P_{m_a} = \begin{bmatrix} 0.8156 \\ 0.1844 \\ 0 \\ 0 \\ 0 \end{bmatrix} \text{ and } P_{v_a} = \begin{bmatrix} 0.8103 \\ 0.1897 \\ 0 \\ 0 \\ 0 \end{bmatrix} \tag{7-13}$$

7.2.1.4 FUZZY SET OPERATIONS

Fuzzy set operations are performed to activate a set of fuzzy rules and the combination of individual rules is performed using fuzzy set operations. The two most commonly used operations are analogous to the Boolean OR and AND operations, relating to the fuzzy MAX and MIN operations (equivalently union and intersection). These lead to the following matrices, each being termed a matrix of firing strengths and given, by:

$$Max\{P_{m_a}, P_{v_a}\} = P_{m_a} \cup P_{v_a} \tag{7-14}$$

and

$$Min\{P_{m_a}, P_{v_a}\} = P_{m_a} \cap P_{v_a} \tag{7-15}$$

It is via the vectors comprising degrees of membership to the fuzzy sets that a matrix of firing strengths is computed. Due to the nature of the triangular fuzzy sets, the 5 x 5 matrices of firing strengths defined by Equations (7-14) and (7-15), will each comprise a 2 x 2 activation array. Each element, denoted $m_{P_{ij}}$, in the resulting activation array will be such that $m_{P_{ij}} \geq 0$, with all other elements in the resulting matrix of firing strengths necessarily being zero. The matrix of firing strengths is then superimposed over the 5 x 5 feature matrix with each element corresponding to a feature vector, see Equation (7-3). This results in a weighted activation of a set of consequences leading to a decision.

An initial estimate can be obtained from the fuzzy MAX operation to select the collision properties from the nearest pre-calculated point (corresponding to the largest (i.e. maximum) element in the 2 x 2 activation array). The fuzzy MAX operation allows for a low computational intensity fuzzification operation, i.e.

$$P_{m_a} \cup P_{v_a} \tag{7-16}$$

$$= \begin{bmatrix} Max\left\{P_{m_{a_{1.00}}} P_{v_{a_{1.00}}}\right\} & Max\left\{P_{m_{a_{1.00}}} P_{v_{a_{1.25}}}\right\} & Max\left\{P_{m_{a_{1.00}}} P_{v_{a_{1.50}}}\right\} & \cdots & Max\left\{P_{m_{a_{1.00}}} P_{v_{a_{2.00}}}\right\} \\ Max\left\{P_{m_{1.25}} P_{v_{a_{1.00}}}\right\} & Max\left\{P_{m_{1.25}} P_{v_{a_{1.25}}}\right\} & Max\left\{P_{m_{1.25}} P_{v_{a_{1.50}}}\right\} & \cdots & Max\left\{P_{m_{1.25}} P_{v_{a_{2.00}}}\right\} \\ Max\left\{P_{m_{a_{1.50}}} P_{v_{a_{1.00}}}\right\} & Max\left\{P_{m_{a_{1.50}}} P_{v_{a_{1.25}}}\right\} & Max\left\{P_{m_{a_{1.50}}} P_{v_{a_{1.50}}}\right\} & \cdots & Max\left\{P_{m_{a_{1.50}}} P_{v_{a_{2.00}}}\right\} \\ \vdots & \vdots & \vdots & \ddots & \vdots \\ Max\left\{P_{m_{a_{2.00}}} P_{v_{a_{1.00}}}\right\} & Max\left\{P_{m_{a_{2.00}}} P_{v_{a_{1.25}}}\right\} & Max\left\{P_{m_{a_{2.00}}} P_{v_{a_{1.50}}}\right\} & \cdots & Max\left\{P_{m_{a_{2.00}}} P_{v_{a_{2.00}}}\right\} \end{bmatrix}$$

The largest element (i.e. with maximum value) in the 2 x 2 activation array within the matrix of firing strengths is then simply selected. This will correspond to a single crisp pre-computed element in each of the three 5 x 5 rule base consequence matrices for δ_a, a_{a_H} and a_{a_C}.

Continuing with the illustrative example, it is implied that the AV laden mass is between light and medium light and the collision velocity is between slow and medium slow. The depictions in Figure 7-4 (solid lines) on each universe of discourse, indicate the degrees of membership. Using the above determined degrees of membership, the matrix of firing strengths using the fuzzy MAX operation becomes:

$$P_{m_a} \cup P_{v_a} = \begin{bmatrix} 0.8103 \\ 0.1897 \\ 0 \\ 0 \\ 0 \end{bmatrix} \begin{bmatrix} 0.8156 & 0.8103 & 0 & 0 & 0 \\ 0.8156 & 0.1897 & 0 & 0 & 0 \\ 0 & 0 & 0 & 0 & 0 \\ 0 & 0 & 0 & 0 & 0 \\ 0 & 0 & 0 & 0 & 0 \end{bmatrix} \tag{7-17}$$

$$\begin{bmatrix} 0.8156 & 0.1844 & 0 & 0 & 0 \end{bmatrix}$$

In this case, there are two elements within the activation array, or area of influence, that have joint highest value, namely the two elements of value 0.8156. The outcome would be to select the fuzzy rule corresponding to the highest firing strength and the higher of the two corresponding rules would be selected. The area of interest for the general fuzzy rule base consequence matrix R_C is given by the activation array:

$$R_C = \begin{bmatrix} [+] & [+] & 0 & 0 & 0 \\ [+] & [+] & 0 & 0 & 0 \\ 0 & 0 & 0 & 0 & 0 \\ 0 & 0 & 0 & 0 & 0 \\ 0 & 0 & 0 & 0 & 0 \end{bmatrix} \tag{7-18}$$

where the '+' signs indicate the 2 x 2 activation array for the firing strengths of the fuzzy MAX and MIN operations, with all other elements being zero. When this is superimposed onto the rule base consequence matrix, the element with the highest value is selected. In this case, the feature matrix comprises a vector-matrix of three rule base consequence matrices, since each element of the feature matrix is a 3 x 1 vector. In this work, the rule base consequence matrix R_{δ_a} corresponding to peak deformation is the primary decision matrix since the design deformation is key to the developed algorithms. This leads to:

$$R_{\delta_a} = \begin{bmatrix} 0.2681 & 0.2801 & 0.2915 & 0.3024 & 0.3127 \\ \mathbf{0.4242} & 0.4421 & 0.4589 & 0.4748 & 0.4900 \\ 0.5632 & 0.5853 & 0.6060 & 0.6254 & 0.6437 \\ 0.6860 & 0.7108 & 0.7340 & 0.7555 & 0.7756 \\ 0.7934 & 0.8198 & 0.8441 & 0.8666 & 0.8874 \end{bmatrix} \tag{7-19}$$

with the element extracted being highlighted in bold. Hence, use of the fuzzy MAX operation yields the following values for peak deformation, peak head acceleration and peak chest acceleration being, respectively: $0.4242m, 36.37g$ and $28.70g$.

Subsequent refinements/improvements in the values of estimated AV laden mass and predicted collision velocity make use of the vectors of degrees of membership P_{m_a} and P_{v_a} to produce an updated matrix of firing strengths via the fuzzy MIN operation and a defuzzification method to obtain an updated, more accurate, weighted/interpolated feature vector, as used in (Dunlop, 1995). The fuzzy MIN operation is defined by:

$$P_{m_a} \cap P_{m_b} = Min\{P_{m_a} P_{m_b}\} \tag{7-20}$$

This leading to the following intersection:

$$P_{m_a} \cap P_{v_a} \tag{7-21}$$
$$= \begin{bmatrix} Min\left\{P_{m_{a_{1.00}}} P_{v_{a_{1.00}}}\right\} & Min\left\{P_{m_{a_{1.00}}} P_{v_{a_{1.25}}}\right\} & Min\left\{P_{m_{a_{1.00}}} P_{v_{a_{1.50}}}\right\} & \cdots & Min\left\{P_{m_{a_{1.00}}} P_{v_{a_{2.00}}}\right\} \\ Min\left\{P_{m_{1.25}} P_{v_{a_{1.00}}}\right\} & Min\left\{P_{m_{1.25}} P_{v_{a_{1.25}}}\right\} & Min\left\{P_{m_{1.25}} P_{v_{a_{1.50}}}\right\} & \cdots & Min\left\{P_{m_{1.25}} P_{v_{a_{2.00}}}\right\} \\ Min\left\{P_{m_{a_{1.50}}} P_{v_{a_{1.00}}}\right\} & Min\left\{P_{m_{a_{1.50}}} P_{v_{a_{1.25}}}\right\} & Min\left\{P_{m_{a_{1.50}}} P_{v_{a_{1.50}}}\right\} & \cdots & Min\left\{P_{m_{a_{1.50}}} P_{v_{a_{2.00}}}\right\} \\ \vdots & \vdots & \vdots & \ddots & \vdots \\ Min\left\{P_{m_{a_{2.00}}} P_{v_{a_{1.00}}}\right\} & Min\left\{P_{m_{a_{2.00}}} P_{v_{a_{1.25}}}\right\} & Min\left\{P_{m_{a_{2.00}}} P_{v_{a_{1.50}}}\right\} & \cdots & Min\left\{P_{m_{a_{2.00}}} P_{v_{a_{2.00}}}\right\} \end{bmatrix}$$

Similar to using the MAX operation, the MIN operation $P_{m_a} \cap P_{v_a}$ produces a 2 x 2 activation array (determining the firing strengths), which again, will be superimposed over the four 5 x 5 pre-calculated feature matrix. Using the above determined degrees of membership in the illustrative example, the matrix of firing strengths using the fuzzy MIN operation becomes:

$$P_{m_a} \cap P_{v_a} = \begin{bmatrix} 0.8103 \\ 0.1897 \\ 0 \\ 0 \\ 0 \end{bmatrix} \begin{bmatrix} 0.8103 & 0.1844 & 0 & 0 & 0 \\ 0.1897 & 0.1844 & 0 & 0 & 0 \\ 0 & 0 & 0 & 0 & 0 \\ 0 & 0 & 0 & 0 & 0 \\ 0 & 0 & 0 & 0 & 0 \end{bmatrix} \tag{7-22}$$

$$\begin{bmatrix} 0.8156 & 0.1844 & 0 & 0 & 0 \end{bmatrix}$$

7.2.1.5 DEFUZZIFICATION METHODS

A refinement to the initial fuzzy MAX operation is to use the fuzzy MIN operation combined with a defuzzification method. There are a number of defuzzification methods to obtain a crisp value from the 2 x 2 activation array when using the fuzzy MIN operation. These methods include:

Maxima: takes the highest entry in the 2 x 2 area of influence and fires the corresponding rule (selects the corresponding element in the feature matrix).

Middle of maxima: multiplies the rule obtained in the maxima case by the highest entry in the 2 x 2 area of influence.

Mean of maxima: multiplies all entries in the 2 x 2 area of influence with the corresponding rules and then takes the mean value (i.e. dividing by 4).

Centre of gravity method: as the mean of maxima but takes a weighted approach by dividing by the sum of the entries in the 2 x 2 area of influence.

In (Dunlop, 1995), the centre of gravity method is used and has been demonstrated to give the closest results in the context of the application considered here. Therefore, the centre of gravity method is used in this work and is given by:

$$u = \frac{\sum MIN\left\{P_{m_{a_i}} P_{v_{a_j}}\right\} r_{i_j}}{\sum MIN\left\{P_{m_{a_i}} P_{v_{a_j}}\right\}} \tag{7-23}$$

where $\sum MIN\left\{P_{m_{a_i}} P_{v_{a_j}}\right\}$ contains the ijth elements of $P_{m_a} \cap P_{v_a}$, which are obtained from $MIN\left\{P_{m_{a_i}} P_{v_{a_j}}\right\}$ see Equations(7-21) and (7-22), and r_{i_j} is the corresponding 2 x 2 rule base or, consequence sub-matrix, when considering the illustrative example, this is given by:

$$R_C = \begin{bmatrix} W & Y & 0 & 0 & 0 \\ X & Z & 0 & 0 & 0 \\ 0 & 0 & 0 & 0 & 0 \\ 0 & 0 & 0 & 0 & 0 \\ 0 & 0 & 0 & 0 & 0 \end{bmatrix} \tag{7-24}$$

The outputs of the key features (i.e. for each of δ_a, a_{a_H} and a_{a_C}) using the centre of gravity defuzzification method would yield:

$$\delta_a, a_{a_H}, a_{a_C} = \frac{\sum MIN\left\{P_{m_{a_i}} P_{v_{a_j}}\right\} r_{i_j}}{\sum MIN\left\{P_{m_{a_i}} P_{v_{a_j}}\right\}} \tag{7-25}$$

$$= \frac{0.8103W + 0.1844Y + 0.1897X + 0.1844Z}{0.8103 + 0.1844 + 0.1897 + 0.1844}$$

where r_{i_j} is the element in the ith row and jth column of R_C. Since the primary decision matrix in this work relates to peak deformation, when considering the rule base consequence matrix, R_{δ_a}, where $W = 0.2681$, $Y = 0.2801$, $X = 0.4242$ and $Z = 0.4421$, evaluation of Equation (7-25) yields:

$$\delta_a = \frac{0.8103(0.2681) + 0.1844(0.2801) + 0.1897(0.4242) + 0.1844(0.4421)}{0.8103 + 0.1844 + 0.1897 + 0.1844}$$

$$= 0.4509m$$

Applying the above weighted centre of gravity approach to occupant peak occupant head acceleration and peak occupant chest acceleration data gives rise to g-forces of $39.42g$ and $31.11g$, respectively.

The illustrative example has served to demonstrate how the look-up tables/surfaces, based on models developed in Chapter 5 (single AV collision model into an IRW), may be interpreted as a feature matrix and subsequently re-interpreted as stacked rule base consequence matrices within a fuzzy logic interpolation approach for use on-board an AV to pre-determine the key collision outcomes, thus allowing potential decisions to be made immediately prior to a collision scenario.

7.2.2 STAGE 2: PRE-DETERMINED COLLISION INJURY SEVERITY LEVELS

The outcomes (peak deformation, peak head acceleration and peak chest acceleration) from Stage 1 in Section 7.2.1 are used in Stage 2, along with the pedestrian impact

velocity, to pre-determine the collision injury severity levels. Details of the process to pre-determine collision injury severity levels are given in Algorithm 7-2.

Algorithm 7-2: *Process to Pre-determien the Collision Injury Severity Levels*

1. Define the upper and lower ranges for peak deformation δ_a, peak head acceleration a_{H_a}, peak chest acceleration a_{C_a} and pedestrian impact velocity p_{v_a}
2. Using the upper and lower ranges in Step 1., create fuzzy sets that are equally spaced crisp values between the minimum and maximum values for the 5 sets, where denoted A, B, C, D and E, where fuzzy set A corresponds to the highest injury severity and set E corresponds to the lowest injury severity.
3. The degrees of membership for the four component features to their pair-wise lower membership functions may be determined, respectively, from:
$$\mu_{f_l}(f) = \frac{p_{f_h} - \delta_a}{p_{f_h} - p_{f_l}}$$
where f is used as a general subscript to represent the four feature indices, i.e. for, δ_a, a_{H_a}, a_{C_a} and p_{v_a}
4. The degrees of membership for the four component features to the corresponding pair-wise higher membership functions may then be determined, respectively, from:
$$\mu_{f_h}(f) = 1 - \mu_{f_l}(f)$$
where f is used as a general subscript to represent the four feature indices, i.e. for, δ_a, a_{H_a}, a_{C_a} and p_{v_a}
5. The results of the injury severity from Steps 3 and 4, are represented by the row-partitioned 4 x 2 matrix, given by:
$$x_{S_{AV}} = \begin{bmatrix} \mu_{\delta_l}(\delta_a) & \mu_{\delta_h}(\delta_a) \\ \mu_{a_{H_l}}(a_{H_a}) & \mu_{a_{H_h}}(a_{H_a}) \\ \mu_{a_{C_l}}(a_{C_a}) & \mu_{a_{C_h}}(a_{C_a}) \\ \mu_{p_{v_l}}(p_{v_a}) & \mu_{p_{v_h}}(p_{v_a}) \end{bmatrix}$$

7.2.2.1 DEFINING THE RANGE OR UNIVERSE OF DISCOURSE

For a single AV, denoted Vehicle a, involving an IRW or a pedestrian(s), there are four features which correspond to the injury severity levels. These are peak deformation δ_a, peak head acceleration a_{H_a}, peak chest acceleration a_{C_a} and pedestrian impact velocity p_{v_a}. The four injury severity levels, denoted s_δ, $s_{H,}$ s_C and s_{p_v}, lie, respectively, within the upper and lower ranges:

$$s_{\delta_{1.00}} < s_{\delta_a} \leq s_{\delta_{5.00}} \tag{7-26}$$

$$s_{H_{1.00}} < s_{H_a} \leq s_{H_{5.00}} \tag{7-27}$$

$$s_{C_{1.00}} < s_{C_a} \leq s_{C_{5.00}} \tag{7-28}$$

$$s_{p_{v_{1.00}}} < s_{p_{v_a}} \leq s_{p_{v_{5.00}}} \tag{7-29}$$

in which $s_{\delta_{1.00}}$, $s_{H_{1.00}}$, $s_{C_{1.00}}$ and $s_{p_{v_{1.00}}}$ denote the lower bounds and $s_{\delta_{5.00}}$, $s_{H_{5.00}}$, $s_{C_{5.00}}$ and $s_{p_{v_{5.00}}}$ denote the upper bounds, respectively. The following arbitrary linguistic terms, detailed in Table 7-2, are used to describe the outcomes of peak deformation, peak head acceleration, peak chest acceleration and pedestrian impact velocity. As introduced in Section 7-1, the injury severity levels exist on a universe of discourse spanned by fuzzy sets denoted A, B, C, D and E, where fuzzy set A corresponds to the highest injury severity and set E corresponds to the lowest injury severity.

The ranges given in Equations (7-26) to (7-29) are spanned by equally spaced crisp values between the minimum and maximum values for the 5 sets, see Table 7-2. The universe of discourse for each of the four features are now defined.

The universe of discourse for peak deformation ranges from $0.2681m$ to $0.8874m$ and utilises five fuzzy sets, denoted E_δ to A_δ, respectively, with each fuzzy set D_δ, C_δ, and B_δ being identically triangular in shape, such that the peak for each fuzzy set is equally spaced and of magnitude unity. The peak deformation corresponding to the fuzzy sets is defined within the brackets for each case, as in Table 7-2. Note that $A_\delta(\delta_a)$ is $A_\delta(0.8874)$ and $E_\delta(\delta_a)$ is $E_\delta(0.2681)$, so that $C_\delta(\delta_a)$ is given by $(A_\delta(\delta_a) - E_\delta(\delta_a))/2$, similarly the intermediate cases for $B_\delta(\delta_a)$ and $D_\delta(\delta_a)$ are given by $(A_\delta(\delta_a) - C_\delta(\delta_a))/2$ and $(C_\delta(\delta_a) - E_\delta(\delta_a))/2$, respectively.

The universe of discourse for peak head acceleration ranges from $19.50g$ to $1150.50g$ and utilises five fuzzy sets, denoted E_H to A_H, respectively, again with each intermediate fuzzy set being identically triangular in shape, such that the peak for each fuzzy set is equally spaced and of magnitude unity. The peak head acceleration corresponding to the fuzzy sets is defined within the brackets for each case, as in Table 7-2. Note that $A_H(H_a)$ is $A_H(115.50)$ and $E_H(H_a)$ is $E_H(19.50)$, so that $C_H(H_a)$ is given by $(A_H(H_a) - E_H(H_a))/2$, similarly the intermediate cases for $B_H(H_a)$ and $D_H(H_a)$ are given by $(A_H(H_a) - C_H(H_a))/2$ and $(C_H(H_a) - E_H(H_a))/2$, respectively.

The universe of discourse for peak chest acceleration ranges from $15.39g$ to $91.18g$ and utilises five fuzzy sets, denoted E_C to A_C, respectively. Each of the intermediate fuzzy sets are identically triangular in shape, such that the peak for each fuzzy set is equally spaced and of magnitude unity. The peak chest acceleration corresponding to the fuzzy sets is defined within the brackets for each case, as in Table 7-2. Note that $A_C(C_a)$ is $A_C(91.18)$ and $E_C(C_a)$ is $E_C(15.39)$, so that $C_C(C_a)$ is given by $(A_C(C_a) - E_C(C_a))/2$, similarly the intermediate cases for $B_C(C_a)$ and $D_C(C_a)$ are given by $(A_C(C_a) - C_C(C_a))/2$ and $(C_C(C_a) - E_C(C_a))/2$, respectively.

The universe of discourse for pedestrian impact velocity ranges from $6.7056 m/s$ to $24.5872 m/s$ and utilises five fuzzy sets, denoted E_{p_v} to A_{p_v}, respectively, again with each intermediate fuzzy set being identically triangular in shape, such that the peak for each fuzzy set is equally spaced and of magnitude unity. The peak chest acceleration corresponding to the fuzzy sets is defined within the brackets for each case, as in Table 7-2. Note that $A_{p_v}(p_{v_a})$ is $A_{p_v}(91.18)$ and $E_{p_v}(p_{v_a})$ is $E_{p_v}(15.39)$, so that $C_{p_v}(p_{v_a})$ is given by $(A_{p_v}(p_{v_a}) - E_{p_v}(p_{v_a}))/2$, similarly the intermediate cases for $B(p_{v_a})$ and $D_{p_v}(p_{v_a})$ are given by $(A_{p_v}(p_{v_a}) - C_{p_v}(p_{v_a}))/2$ and $(C_{p_v}(p_{v_a}) - E_{p_v}(p_{v_a}))/2$, respectively.

It is noted that less than five fuzzy sets could have been used. However, when considering the levels of pedestrian injury severity, with reference to the literature, see Section 4.5.1 Chapter 4, it is convenient to use five fuzzy sets. In fact, it is the view of the author that the proposed fuzzy sets (A, B, C, D and E) for the impact velocity align well to the vehicle injury serveries. For example, when considering the vehicle, the fuzzy set 'C' for peak deformation, peak head acceleration and peak chest acceleration are considered not fatal but would result in injuries. Considering the fuzzy set 'B', the crisp values for the occupants of the vehicle and the pedestrians are considered to be venturing towards potentially fatal. As discussed in Section 4.5.1 in Chapter 4, Remark 4-1 states that a further detailed study is needed to explore in detail the intricacies of vehicle-pedestrian collisions, as there are many more variables to consider.

Table 7-2: *Stage 2: Fuzzy Sets of Peak Deformation, Peak Head Acceleration, Peak Chest Acceleration and Pedestrian Impact Velocity for Injury Severity*

Peak Deformation [m]		**Peak Head Acceleration [g]**		**Peak Chest Acceleration [g]**		**Pedestrian impact velocity [m/s]**	
$s_{\delta_{5.00}}$	$A_\delta(0.8874)$	$s_{H_{5.00}}$	$A_H(115.50)$	$s_{C_{5.00}}$	$A_C(91.18)$	$s_{p_{V_{5.00}}}$	A_{p_v} (24.5872)
$s_{\delta_{4.00}}$	$B_\delta(\delta_a)$	$s_{H_{4.00}}$	$B_H(H_a)$	$s_{C_{4.00}}$	$B_C(C_a)$	$s_{p_{V_{4.00}}}$	$B_{p_v}(p_{v_a})$
$s_{\delta_{3.00}}$	$C_\delta(\delta_a)$	$s_{H_{3.00}}$	$C_H(H_a)$	$s_{C_{3.00}}$	$C_C(C_a)$	$s_{p_{V_{3.00}}}$	$C_{p_v}(p_{v_a})$
$s_{\delta_{2.00}}$	$D_\delta(\delta_a)$	$s_{H_{2.00}}$	$D_H(H_a)$	$s_{C_{2.00}}$	$D_C(C_a)$	$s_{p_{V_{2.00}}}$	$D_{p_v}(p_{v_a})$
$s_{\delta_{1.00}}$	$E_\delta(0.2681)$	$s_{H_{1.00}}$	$E_H(19.50)$	$s_{C_{1.00}}$	$E_C(15.39)$	$s_{p_{V_{1.00}}}$	E_{p_v} (6.7056)

7.2.2.2 MEMBERSHIP FUNCTIONS

As in Section 7.2.1.2 and as discussed above, triangular fuzzy sets are used for each universe of discourse for the four features of peak deformation, peak head acceleration, peak chest acceleration and pedestrian impact velocity, see Figure 7-5, where f is used as a general subscript to represent the four feature indices, i.e. for, δ_a, a_{H_a}, a_{C_a} and p_{v_a}. So that the extended vector of features for Vehicle a becomes:

$$r_{f_a} = [r_{\delta_a} : r_{a_{H_a}} : r_{a_{C_a}} : r_{p_{v_a}}]^T$$

Consequently, when considering Table 7-2, the extended rule base consequence vector r_{f_a}, or feature vector, comprises the individual partitioned components for peak deformation δ_a, peak head acceleration a_{a_H}, peak chest acceleration a_{a_C} and pedestrian impact velocity v_a and these are given, respectively, by:

$$r_{\delta_a} = [E_\delta(0.2681) \quad D_\delta(\delta_a) \quad C_\delta(\delta_a) \quad B_\delta(\delta_a) \quad A_\delta(0.8874)] \tag{7-30}$$

$$r_{a_{H_a}} = [E_H(19.50) \quad D_H(H_a) \quad C_H(H_a) \quad B_H(H_a) \quad A_H(115.50)] \tag{7-31}$$

$$r_{a_{C_a}} = [E_C(15.39) \quad D_C(C_a) \quad C_C(C_a) \quad B_C(C_a) \quad A_C(91.18)] \tag{7-32}$$

$$r_{p_{v_a}} = \left[E_{p_v}(6.7056) \quad D_{p_v}(p_{v_a}) \quad C_{p_v}(p_{v_a}) \quad B_{p_v}(p_{v_a}) \quad A_{p_v}(24.5872)\right] \tag{7-33}$$

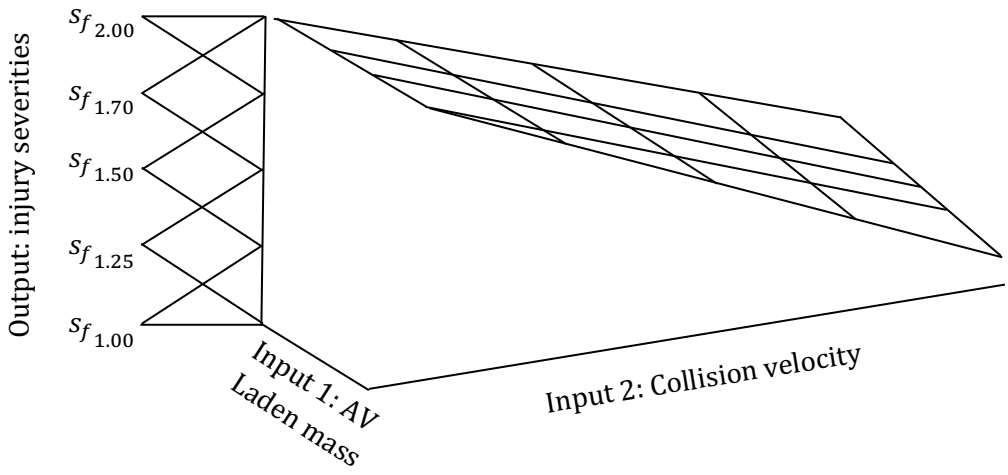

Figure 7-5: *Feature Matrix Formed of the Two Inputs (Autonomous Vehicle Laden Mass and Collision Velocity) and Fuzzy Sets for Collision Injury Severity on its Universe of Discourse*

To illustrate Stage 2, the same collision scenario is used as in the Stage 1 illustrative example, i.e. an AV with a laden mass $m_a = 1270kg$, travelling at a velocity $v_a = 11.60m/s$ $(25.9485mph)$ is considered. The collision outcome results in a peak deformation of $0.4509m$, peak head acceleration of $39.42g$ and peak chest acceleration of $31.11g$, respectively. The peak head acceleration and peak chest acceleration values are found to lie within their respective fuzzy sets D to E (the two lowest injury severities), the peak deformation and the pedestrian impact velocity are also found to lie within their respective fuzzy sets C to D. Refer to Table 7-2 and Figure 7-5.

As in Section 7.2.1.2, the degrees of membership to the two fuzzy sets can be calculated by making use of the following relationships. In each case the subscripts l and h correspond to the lower and higher adjacent membership functions, i.e. E to D, D to C, C to B and B to A. The degrees of membership for the four component features to their pair-wise lower membership functions may be determined, respectively, from:

$$\mu_{\delta_l}(\delta_a) = \frac{p_{\delta_h} - \delta_a}{p_{\delta_h} - p_{\delta_l}} \tag{7-34}$$

$$\mu_{a_{H_l}}(a_{H_a}) = \frac{p_{a_{H_h}} - a_{H_a}}{p_{a_{H_h}} - p_{a_{H_l}}} \tag{7-35}$$

$$\mu_{a_{C_l}}(a_{C_a}) = \frac{p_{a_{C_h}} - a_{C_a}}{p_{a_{C_h}} - p_{a_{C_l}}} \tag{7-36}$$

$$\mu_{p_{v_l}}(p_{v_a}) = \frac{p_{p_{v_h}} - p_{v_a}}{p_{p_{v_h}} - p_{p_{v_l}}} \tag{7-37}$$

The degrees of membership for the four component features to the corresponding pair-wise higher membership functions may then be determined, respectively, from:

$$\mu_{\delta_h}(\delta_a) = 1 - \mu_{\delta_l}(\delta_a) \tag{7-38}$$

$$\mu_{a_{H_h}}(a_{H_a}) = 1 - \mu_{a_{H_l}}(a_{H_a}) \tag{7-39}$$

$$\mu_{a_{C_h}}(a_{C_a}) = 1 - \mu_{a_{C_l}}(a_{C_a}) \tag{7-40}$$

$$\mu_{P_{v_h}}(P_{v_a}) = 1 - \mu_{P_{v_l}}(P_{v_a}) \tag{7-41}$$

The results of the injury severity from Equations (7-34) to (7-41), denoted x_S, are represented by the row-partitioned 4 x 2 matrix, given by:

$$x_{S_{AV}} = \begin{bmatrix} \mu_{\delta_l}(\delta_a) & \mu_{\delta_h}(\delta_a) \\ \mu_{a_{H_l}}(a_{H_a}) & \mu_{a_{H_h}}(a_{H_a}) \\ \mu_{a_{C_l}}(a_{C_a}) & \mu_{a_{C_h}}(a_{C_a}) \\ \mu_{p_{vl}}(p_{v_a}) & \mu_{p_{vh}}(p_{v_a}) \end{bmatrix} \tag{7-42}$$

where the injury severity will be represented by degrees of membership to two adjacent fuzzy sets at any point in time, i.e. E to D, D to C, C to B and B to A. When considering the AV only, the severity of injury of the occupant(s), denoted $x_{S_{AV}}$, are represented by the row-partitioned 3 x 2 matrix, given by:

$$x_{S_{AV}} = \begin{bmatrix} \mu_{\delta_l}(\delta_a) & \mu_{\delta_h}(\delta_a) \\ \mu_{a_{H_l}}(a_{H_a}) & \mu_{a_{H_h}}(a_{H_a}) \\ \mu_{a_{C_l}}(a_{C_a}) & \mu_{a_{C_h}}(a_{C_a}) \end{bmatrix} \tag{7-43}$$

When considering the pedestrian(s) only, the severity of injury of the pedestrian(s), denoted x_{S_P}, are represented by the 1 x 2 row matrix, given by:

$$x_{S_P} = \left[\mu_{p_{v_l}}(p_{v_a}) \quad \mu_{p_{v_h}}(p_{v_a})\right] \tag{7-44}$$

Returning to the illustrative example, the degrees of membership of the lower and higher pair-wise fuzzy sets D to E and C to D, are represented by the row-partitioned matrix, defined in Equation (7-42), and given by:

$$x_S = \begin{bmatrix} \mu_{\delta_l}(\delta_a) & \mu_{\delta_h}(\delta_a) \\ \mu_{a_{H_l}}(a_{H_a}) & \mu_{a_{H_h}}(a_{H_a}) \\ \mu_{a_{C_l}}(a_{C_a}) & \mu_{a_{C_h}}(a_{C_a}) \\ \mu_{p_{v_l}}(p_{v_a}) & \mu_{p_{v_h}}(p_{v_a}) \end{bmatrix} \coloneqq \begin{bmatrix} \mu_{\delta_D}(\delta_a) & \mu_{\delta_C}(\delta_a) \\ \mu_{a_{H_E}}(a_{H_a}) & \mu_{a_{H_D}}(a_{H_a}) \\ \mu_{a_{C_E}}(a_{C_a}) & \mu_{a_{C_D}}(a_{C_a}) \\ \mu_{p_{v_D}}(p_{v_a}) & \mu_{p_{v_C}}(p_{v_a}) \end{bmatrix} \tag{7-45}$$

The degree of membership for the four features that lie within the fuzzy sets D to E and C to D, corresponding to the row-partitioned matrix given by Equation (7-45) and the resulting matrix consisting of entries that correspond to the degrees of membership are given by:

$$x_S \coloneqq \begin{bmatrix} \mu_{\delta_D}(\delta_a) & \mu_{\delta_C}(\delta_a) \\ \mu_{a_{H_E}}(a_{H_a}) & \mu_{a_{H_D}}(a_{H_a}) \\ \mu_{a_{C_E}}(a_{C_a}) & \mu_{a_{C_D}}(a_{C_a}) \\ \mu_{p_{v_D}}(p_{v_a}) & \mu_{p_{v_C}}(p_{v_a}) \end{bmatrix} \coloneqq \begin{bmatrix} 0.819 & 0.181 \\ 0.170 & 0.830 \\ 0.170 & 0.820 \\ 0.905 & 0.095 \end{bmatrix} \tag{7-46}$$

The degrees of membership given in Equation (7-46) for the injury severity fuzzy sets for peak deformation, peak head acceleration, peak chest acceleration and pedestrian impact velocity are illustrated in Figure 7-6. The next Section will detail how this information is used to make decisions regarding the collision target.

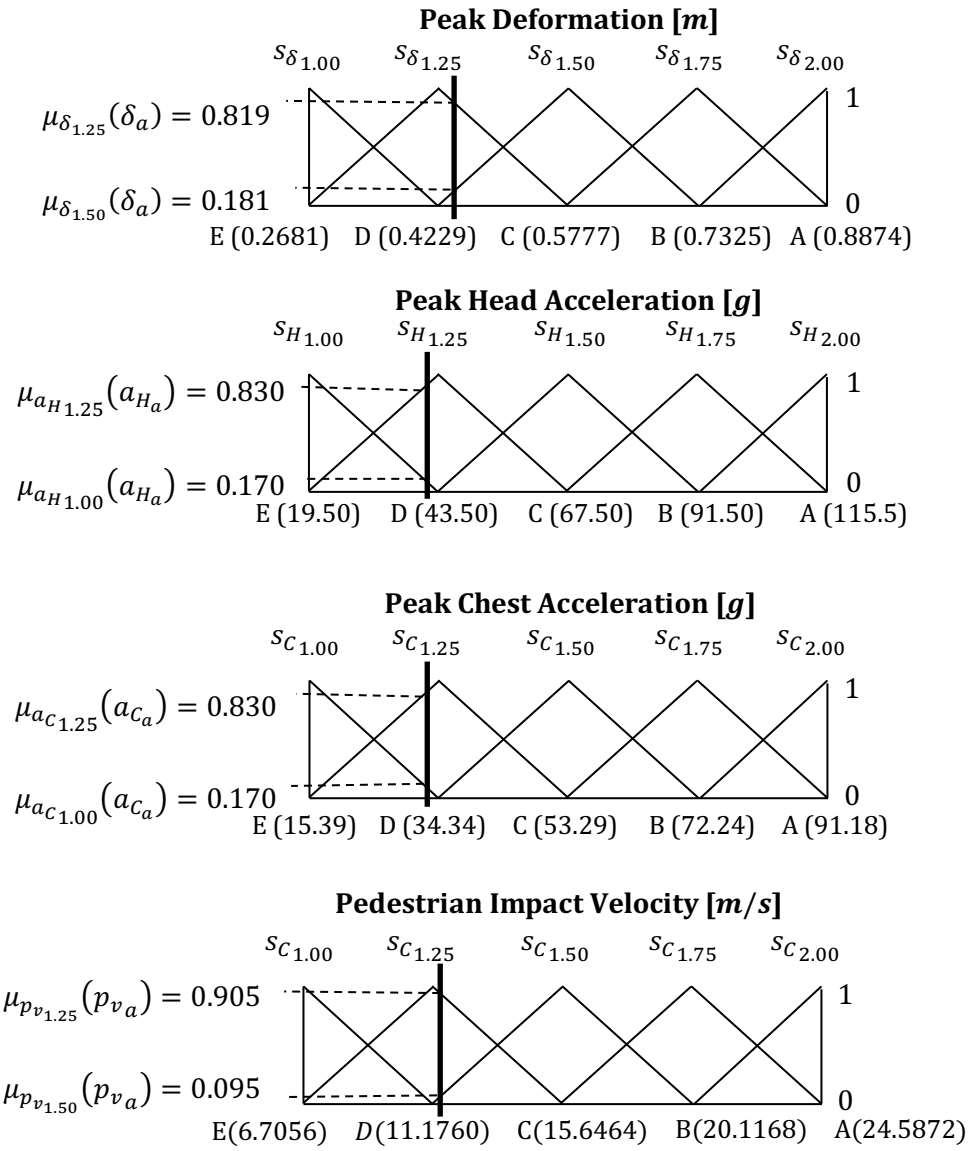

Figure 7-6: *Universe of Discourse for the Fuzzy Sets Corresponding to the Injury Severity for Peak Deformation δ_a, Peak Head Acceleration a_{a_H}, Peak Chest Acceleration a_{a_C} and Pedestrian Impact Velocity v_a*

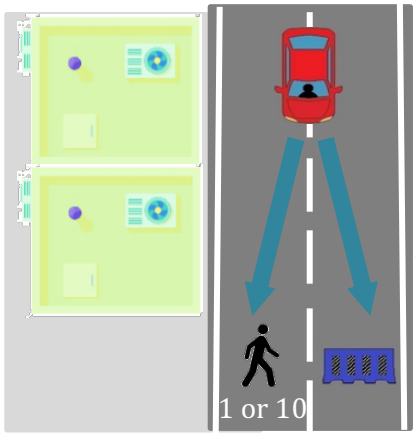

$$x_S := \begin{bmatrix} \mu_{\delta_D}(\delta_a) & \mu_{\delta_C}(\delta_a) \\ \mu_{a_{H_E}}(a_{H_a}) & \mu_{a_{H_D}}(a_{H_a}) \\ \mu_{a_{C_E}}(a_{C_a}) & \mu_{a_{C_D}}(a_{C_a}) \\ \mu_{P_{v_D}}(P_{v_a}) & \mu_{P_{v_C}}(P_{v_a}) \end{bmatrix} := \begin{bmatrix} 0.819 & 0.181 \\ 0.170 & 0.830 \\ 0.170 & 0.820 \\ 0.905 & 0.095 \end{bmatrix}$$

Figure 7-7: *Pre-Determined Injury Severities in the case of a Decision being made to Steer and Collide into the Immovable Rigid Wall or to Steer and Collide with the 1 or 10 Pedestrians*

7.3 STAGE 3: STIFFNESS CONTROLLER

Stage 3 evaluates whether an otherwise passive collision scenario of an AV colliding into an IRW can be improved. Such improvement may be achieved via an active structural stiffness change, as initially discussed in Section 4.4, Chapter 4. In the case of additional deformation capacity, i.e. the actual AV peak deformation has not exceeded a maximum design deformation length (i.e. $0.5900m$, see Table 4-1, Chapter 4), a decision could be made to soften the structure to take up the additional capacity, as disused in Section 4.2.3, Chapter 4. Taking such an action would reduce the peak head and chest acceleration g-forces experienced by the occupant(s). On the other hand, if it is found that the actual deformation might exceed the design deformation length, the structure may be stiffened. It may be possible to reduce the deformation to the design length, i.e. $0.5900m$ (or less), albeit with an increase in acceleration experienced by the occupant(s). The latter should, if possible, be achieved within the suggested maximum limits (see Section 4.2.4, Chapter 4), i.e. $80g$ and $60g$ for the head and chest accelerations, respectively.

7.3.1 STIFFNESS CONTROLLER OPERATION

This section considers the effect of changing the linear part of the bilinear stiffness function given by Equation (5-20), Section 5.3.4, Chapter 5, i.e. the coefficient defined by

$\gamma_a = \alpha_a k_a$ to affect deformation. Changing the value of this coefficient will also affect the peak deformation and peak acceleration. To investigate the effect of variation of γ_a, a scaling factor, denoted ϑ_a, is introduced such that the dynamic model becomes:

$$\ddot{x}_a + \left(\frac{\vartheta_a \gamma_a}{m_a} \pm \eta_a |\ddot{x}_a|\right) x_a = 0 \tag{7-47}$$

In the studies considered here, ϑ_a takes the following values: 0.50, 0.75 1.00, 1.25 and 1.50. The results obtained from using these values are plotted as the three multiple surfaces for peak deformation (upper), peak head acceleration (middle) and peak chest acceleration (lower) in Figures 7-8. The results in tabular form are presented in Appendix 8.0. In the upper subplot of Figure 7-8, corresponding to peak deformation, the five values of the scaling factor ϑ_a are such that the top deformation surface implies a reduced stiffness value related to $\vartheta_a = 0.5$ and the bottom surface corresponds to ϑ_a= 1.5 and implies an increased stiffness. The middle and lower sub-plots correspond, respectively, to the g-forces of occupant peak head and chest accelerations. The top g-force surface in both cases corresponds to an increased stiffness value related to ϑ_a= 1.5 and for the bottom surface $\vartheta_a = 0.5$. In all three cases, i.e. upper, middle and lower sub-plots, the central surface layers correspond to the nominal case where the scaling factor is unity, i.e. $\vartheta_a = 1.0$. As undertaken in Section 6.2.5, Chapter 6, a verification of the stiffness change was undertaken. Based on laws of physics in Sections 4.2.2 and 4.2.3, as the structural stiffness is changed, the model behaves as expected, i.e. for peak deformation, peak acceleration and collision energy.

As with the passive case (containing only one surface, i.e. $\vartheta_a = 1.00$), fuzzy logic will be used to interpolate between the five structural stiffness change surfaces, relating to incremental values of the scaling factor ϑ_a being either 0.50, 0.75, 1.00, 1.25 or 1.50. The corresponding values of estimated AV laden mass m_a and predicted collision

velocity v_a, are the same as in the passive case, see Section 4.2.3, Chapter 4. Again, linear interpolation is used to determine the desired stiffness value, i.e. a value to achieve the design deformation length of $0.5900m$ (as detailed in Table 4-1, Section 4.2.3, Chapter 4). The stiffness control algorithm is detailed in Algorithm 7-3. The algorithm essentially calculates the required active structural stiffness value to achieve a desired peak deformation value, i.e. the design value of $0.5900m$ (Note that desired peak head acceleration or peak chest acceleration could be configured as the primary decision factor instead of peak deformation). The modified outcomes due to the active stiffness controller for the values of peak deformation, peak head acceleration and peak chest acceleration are then determined, along with the collision injury severities. The active collision injury severities are then compared to the passive collision injury severities. If the severity values from the active case are higher, then no action is taken with a decision being made not to change the stiffness value of the collision structure (crumple zones).

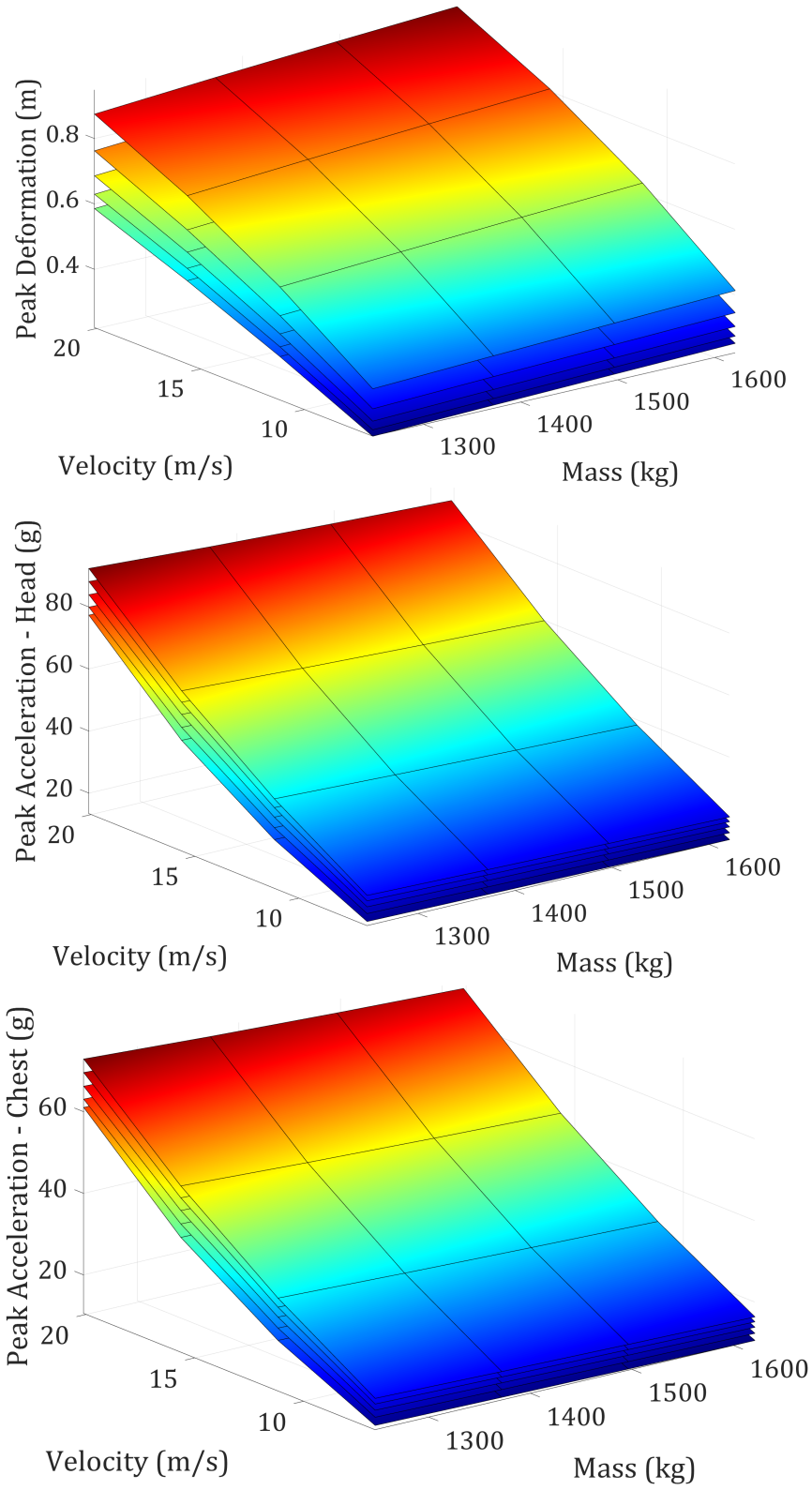

Figure 7-8: *Variations in Peak Deformation (Upper), Peak Head Acceleration (Middle) and Peak Chest Acceleration (Lower) Corresponding to Five Values of the Stiffness Scaling Factor (0.50, 0.75, 1.00, 1.25, 1.50)*

Algorithm 7-3: *Stiffness Controller Algorithm*

1. Use Algorithm 7-1 to determine the 3 vectors of stiffness change properties (see Section 7.2.1, Chapter 7) from the five layers of the look-up tables/surfaces, for a given AV laden mass and collision velocity, i.e.

$$\tilde{\delta}_a = \begin{bmatrix} \tilde{\delta}_{a_{0.50}} & \tilde{\delta}_{a_{0.75}} & \delta_{a_{1.00}} & \tilde{\delta}_{a_{1.25}} & \tilde{\delta}_{a_{1.50}} \end{bmatrix}$$
$$\tilde{a}_{C_a} = \begin{bmatrix} \tilde{a}_{C_{a_{0.50}}} & \tilde{a}_{C_{a_{0.75}}} & a_{C_{a_{1.00}}} & \tilde{a}_{C_{a_{1.25}}} & \tilde{a}_{C_{a_{1.50}}} \end{bmatrix}$$
$$\tilde{a}_{H_a} = \begin{bmatrix} \tilde{a}_{H_{a_{0.50}}} & \tilde{a}_{H_{a_{0.75}}} & a_{H_{a_{1.00}}} & \tilde{a}_{H_{a_{1.25}}} & \tilde{a}_{H_{a_{1.50}}} \end{bmatrix}$$

2. Based on the peak deformation vector in Step 1., determine the two values that the design deformation length ($i.e.\ \delta_{a_D} = 0.5900\text{m}$) is located between
3. Based on Step 2 and the determined two values, determine the 'set' lower value $\tilde{\delta}_{a_l}$ and higher value $\tilde{\delta}_{a_h}$
4. Run the following to determine the lower and higher degrees of membership:

$$\mu_{p_{\tilde{\delta}_{a_l}}}(p_{\tilde{\delta}_a}) = \frac{p_{\tilde{\delta}_{a_h}} - p_{\delta_{a_d}}}{p_{\tilde{\delta}_{a_h}} - p_{\tilde{\delta}_{a_l}}}$$
$$\mu_{p_{\tilde{\delta}_{a_h}}}(p_{\tilde{\delta}_a}) = 1 - \mu_{\delta_l}(\delta_a)$$

5. Considering the following stiffness scaling factors:

$$\vartheta_a = [0.50 \quad 0.75 \quad 1.00 \quad 1.25 \quad 1.50]$$

and based on Step 2, determine the corresponding two stiffness scaling factors and determine the 'set' lower ($\mu_{\vartheta_{a_l}}(p_{\vartheta_a})$) and higher ($\mu_{\vartheta_{a_h}}(p_{\vartheta_a})$) values.

6. The stiffness control change Δk_a value is given by:

$$\Delta k_a = \mu_{\vartheta_{a_l}}(p_{\vartheta_a}) + (0.25 * \mu_{P_{\tilde{\delta}_{a_h}}}(p_{\tilde{\delta}_a}))$$

and with the active stiffness value given by:

$$\tilde{k}_a = (k_a)(\Delta k_a)$$

7. Determine the actively modified peak deformation value based on the stiffness control change using:

$$\tilde{\delta}_a = p_{\tilde{\delta}_{a_h}} - ((p_{\tilde{\delta}_{a_h}} - p_{\tilde{\delta}_{a_l}})\mu_{P_{\tilde{\delta}_{a_h}}}(p_{\tilde{\delta}_a})$$

8. Based on the two sets that peak deformation belong to, repeat Step 3. for peak head acceleration and peak chest acceleration to determine the 'set' lower value $\tilde{a}_{C_{a_l}}/\tilde{a}_{H_{a_l}}$ and higher value $\tilde{a}_{C_{a_h}}/\tilde{a}_{H_{a_h}}$, and then determine an estimate of the 'new' peak chest and head acceleration based on the stiffness control change:

$$\tilde{a}_{C_a} = p_{\tilde{C}_{a_h}} - ((p_{\tilde{C}_{a_h}} - p_{\tilde{C}_{a_l}})\mu_{P_{\tilde{\delta}_{a_h}}}(p_{\tilde{\delta}_a})$$
$$\tilde{a}_{H_a} = p_{\tilde{H}_{a_h}} - ((p_{\tilde{H}_{a_h}} - p_{\tilde{H}_{a_l}})\mu_{P_{\tilde{\delta}_{a_h}}}(p_{\tilde{\delta}_a})$$

9. Use Algorithm 7-2 to determine the change in collision injury severities, subject to the stiffness controller change
10. Compare the peak deformation outcomes from this Algorithm (Algorithm 7.3) of the active case to the outcomes from Algorithm 7-2, i.e. the passive case. If the outcome from Algorithm 7-3 results in the highest injury severity levels, then do not change the stiffness of the structure.

7.3.2 SCENARIO 1: PRETERMINED PEAK DEFORMATION EXCEEDING THE DESIGN DEFORMATION

The illustrative example demonstrates a pre-determined collision outcome that exceeds the design value for the peak deformation. For this example, an AV with a laden mass m_a of $1396kg$ and a collision velocity v_a of $18.0604m/s$ ($40.40mph$) is considered. Using Algorithm 7-1, the passive collision properties were pre-determined and are given in Table 7-3 (Column 1). Using Algorithm 7-2, the collision injury severities are determined. For this example, the degrees of membership for the three features (occupant) lie within the fuzzy sets C to B (medium-high), and are given by:

$$x_{S_{AV}} := \begin{bmatrix} \mu_{\delta_C}(\delta_a) & \mu_{\delta_B}(\delta_a) \\ \mu_{a_{H_C}}(a_{H_a}) & \mu_{a_{H_B}}(a_{H_a}) \\ \mu_{a_{C_C}}(a_{C_a}) & \mu_{a_{C_B}}(a_{C_a}) \end{bmatrix} := \begin{bmatrix} 0.482 & 0.518 \\ 0.913 & 0.087 \\ 0.914 & 0.086 \end{bmatrix} \tag{7-48}$$

Using Algorithm 7-1 within Algorithm 7-3, the following three vectors of stiffness control properties are determined to be:

$$\tilde{\delta}_a = [0.8425 \quad 0.7322 \quad 0.6578 \quad 0.6032 \quad 0.5607]$$

$$\tilde{a}_{a_c} = [50.25 \quad 52.15 \quad 54.92 \quad 57.82 \quad 60.66]$$

$$\tilde{a}_{a_h} = [63.67 \quad 66.08 \quad 69.59 \quad 73.26 \quad 76.86]$$

The design value for the peak deformation value, $\delta_{a_d} = 0.5900m$ is located in between the peak deformation values of 0.6032 (higher value) and 0.5607 (lower value). The degree of membership to the lower membership function is determined to be 0.310 and to the higher membership function is determined to be 0.690. The two peak deformation values of $0.6032m$ (higher value) and $0.5607m$ (lower value) correspond to the stiffness scaling factors of 1.25 (lower value) and 1.50 (higher value), respectively. To achieve the design peak deformation value (i.e. $\delta_{a_D} = 0.5900m$), it is determined that a stiffness

scaling factor of 1.4224 is needed. As the passive stiffness value k_a of the crumple zones is $894{,}340 N/m$, multiplying this by the stiffness scaling factor gives a desired stiffness value of $1272{,}090 N/m$ for the active case. The following active collision properties were determined and are presented in Table 7-3 (Column 2). As desired, the peak deformation matches the design deformation length of $0.5900 m$. It is also worth noting that the peak head and chest accelerations are within their maximum limits of $80g$ and $60g$, respectively, for the US Federal Motor Vehicle Safety Standard (FMVSS) test limits (reference to Table 4-2, Section 4.2.4, Chapter 4). It is noted, however, that the peak chest acceleration is close to the maximum limit. Based on the results from this Scenario, Algorithm 7-3 could be extended such that the US FMVSS test limits are not exceeded. Using Algorithm 7-2, the collision injury severities are determined, these are given by:

$$\tilde{x}_{S_{AV}} \coloneqq \begin{bmatrix} \mu_{\tilde{\delta}_C}(\tilde{\delta}_a) & \mu_{\tilde{\delta}_B}(\tilde{\delta}_a) \\ \mu_{\tilde{a}_{H_C}}(\tilde{a}_{H_a}) & \mu_{\tilde{a}_{H_B}}(\tilde{a}_{H_a}) \\ \mu_{\tilde{a}_{C_C}}(\tilde{a}_{C_a}) & \mu_{\tilde{a}_{C_B}}(\tilde{a}_{C_a}) \end{bmatrix} \coloneqq \begin{bmatrix} 0.9204 & 0.0796 \\ 0.6565 & 0.3435 \\ 0.6575 & 0.3425 \end{bmatrix} \tag{7-49}$$

where the degrees of membership for the three features again lie within the fuzzy sets C to B (medium-high). Based on the above, the peak deformation injury severity has decreased, but the injury of severity for the peak head and peak chest accelerations have increased (as to be expected). Algorithm 7-3 is configured such that the peak deformation is the most important criteria and is used as the primary decision factor. It is noted, however, that peak head and chest acceleration could become the most important criteria and used as the primary decision factor, with peak deformation being less of an issue. For example, if Level 5 autonomy were to be implemented, it may well be the case that the occupant(s) are seated/located in the rear of the AV.

Table 7-3: *Output Collision Properties for the Passive Collision Structure Case (Algorithm 7-1) and the Active Collision Structure Case (Algorithm 7-3) for a Scenario Involving Excessive Peak Deformation*

Collision Output Properties	Passive (Algorithm 7-1)	Active (Algorithm 7-2)
Peak deformation, δ_a $[m]$	0.6578	0.5900
Peak chest acceleration, a_{a_C} $[g]$	54.92	59.78
Peak head acceleration, a_{a_H} $[g]$	69.59	75.74

7.3.2.1 COMPARISION OF RESULTS USING MODEL OF SINGLE AV COLLISION

This Section compares the results determined using Algorithms 7-1 and 7-3 to those directly obtained using the single AV bilinear dynamic collision nodal model developed in Chapter 5. The collision output properties for the passive case (Algorithm 7-1) and active case (Algorithm 7-3) are presented in Table 7-4, with reference to Columns 1 and 3, respectively. Columns 2 and 4 present the results obtained from the bilinear model directly, and correspond to the passive and active cases, respectively. Note that the values in square brackets in Columns 2 and 4 represent the use of Algorithms 7-1 and 7-3 expressed as a percentage difference to direct use of the bilinear models, with this being calculated using:

$$\left(\frac{A\ -B}{A}\right) * 100\%$$

where A and B denote the results obtained from Algorithm 7-1 and the bilinear model, respectively.

It is interesting to note that in the passive case in Column 2, the lowest percentage difference is that for the peak deformation (0.29%) and the highest percentage difference of (1.42%) is for the peak chest acceleration. The results presented in Column 4 of Table 7-4, which correspond to the active case when the stiffness value has been changed (increased) by a scaling factor of 1.4224 (as detailed in earlier Section 7.3.2)

show that the highest percentage difference is for the peak deformation (2.69%) with the lowest percentage difference (0.21%) being found for the peak head acceleration.

The above results justify the use of pre-calculated, pre-determined actions stored in look-up tables combined with interpolation using fuzzy logic, rather than direct online usage of the bilinear model with the potential risks of time-critical computations.

Table 7-4: *Comparing Collision Output Results from Using Algorithm 7-1 and Algorithm 7-3 to the Single Vehicle Bilinear Dynamic Collision Nodal Model*

Collision Output Properties	Passive (Algorithm 7-1)	Passive (Bilinear model)	Active (Algorithm 7-3)	Active (Bilinear model)
Peak deformation, δ_a $[m]$	0.6578	0.6597 [0.29%]	0.5900	0.5741 [2.69%]
Peak chest acceleration, a_{a_C} $[g]$	54.92	54.14 [1.42%]	59.78	59.49 [0.49%]
Peak head acceleration, a_{a_H} $[g]$	69.59	69.14 [0.65%]	75.74	75.58 [0.21%]

7.3.3 SCENARIO 2: PRETERMINED PEAK DEFORMATION LESS THAN THE DESIGN DEFORMATION

This illustrative example considers the potential softening of the stiffness value as opposed to the scenario that was presented in Section 7.3.2. In this case, there is a lower value for the AV laden mass m_a of $1270kg$ and a lower collision velocity v_a of $11.60m/s$ ($25.9485mph$). This leads to a pre-determined peak deformation value which is lower than the design deformation value. As in the previous example in Section 7.3.2, Algorithm 7-1 is used to pre-determine the passive collision properties, with the results presented in Column 1 of Table 7-5. Using Algorithm 7-2, the collision injury severities are determined, where for peak deformation, the degree of membership is within the fuzzy sets C and D, and for the peak head acceleration and peak chest acceleration, the degrees of membership lie within the fuzzy sets D and E. In this particular scenario, these are given by:

$$x_{S_{AV}} \coloneqq \begin{bmatrix} \mu_{\delta_D}(\delta_a) & \mu_{\delta_C}(\delta_a) \\ \mu_{a_{H_E}}(a_{H_a}) & \mu_{a_{H_D}}(a_{H_a}) \\ \mu_{a_{C_E}}(a_{C_a}) & \mu_{a_{C_D}}(a_{C_a}) \end{bmatrix} \coloneqq \begin{bmatrix} 0.819 & 0.181 \\ 0.170 & 0.830 \\ 0.170 & 0.830 \end{bmatrix} \tag{7-50}$$

Again, using Algorithm 7-1 within Algorithm 7-3, the following three vectors of stiffness control properties are determined to be:

$$\tilde{\delta}_a = [0.6002 \quad 0.5090 \quad 0.4509 \quad 0.4095 \quad 0.3780]$$

$$\tilde{a}_{a_c} = [25.3617 \quad 28.3726 \quad 31.1106 \quad 33.6102 \quad 35.9115]$$

$$\tilde{a}_{a_h} = [32.1370 \quad 35.9524 \quad 39.4218 \quad 42.5891 \quad 45.5053]$$

The design value for the peak deformation, $\delta_{a_d} = 0.5900m$, is located in between the peak deformation values of 0.6002 (higher value) and 0.5090 (lower value). The degree of membership to the lower membership function is determined to be 0.1115 and to the

higher membership function is determined to be 0.8885. The two peak deformation values of 0.6002 (higher value) and 0.5090 (lower value) correspond to stiffness scaling factors of 0.50 (lower value) and 0.75 (higher value), respectively. To achieve the design peak deformation value (i.e. $\delta_{a_d} = 0.5900m$), it is determined that a stiffness scaling factor of 0.5279 is required, i.e. a softening of the structure. As the passive stiffness value k_a of the crumple zones is $894{,}340N/m$, multiplying this by the stiffness scaling factor results in the desired stiffness value of $472{,}096N/m$ for the active case. The active collision properties are presented in Column 2 of Table 7-5. As desired, the peak deformation matches the design deformation length of $0.5900m$. Softening the structure has increased the peak deformation, but has had the desired positive benefit of reducing the peak accelerations experienced by the occupants. It is worth noting that the peak head and chest accelerations are well within the US FMVSS test limits of $80g$ and $60g$, respectively. Clearly, if the design deformation value of the AV was to be increased, the structure could be further softened, and the peak accelerations experienced by the occupants could be reduced even more. Again, using Algorithm 7-2, the collision injury severities for the active case are determined. These are given by:

$$\tilde{x}_{S_{AV}} \coloneqq \begin{bmatrix} \mu_{\tilde{\delta}_C}(\tilde{\delta}_a) & \mu_{\tilde{\delta}_B}(\tilde{\delta}_a) \\ \mu_{\tilde{a}_{H_E}}(\tilde{a}_{H_a}) & \mu_{\tilde{a}_{H_D}}(\tilde{a}_{H_a}) \\ \mu_{\tilde{a}_{C_E}}(\tilde{a}_{C_a}) & \mu_{\tilde{a}_{C_D}}(\tilde{a}_{C_a}) \end{bmatrix} \coloneqq \begin{bmatrix} 0.920 & 0.080 \\ 0.544 & 0.456 \\ 0.544 & 0.456 \end{bmatrix} \tag{7-51}$$

For peak deformation the degree of membership now lies within the fuzzy sets B and C, and for the peak head acceleration and peak chest acceleration, the degrees of membership remain within the fuzzy sets D and E, but with a higher degree of membership to the lower injury severity set E. As expected, the apparent injury severity is increased for peak deformation (without breaching the design deformation limit), and as desired, the peak head and chest accelerations have been reduced.

7.3.3.1 COMPARISION OF RESULTS USING MODEL OF SINGLE AV COLLISION

As in Section 7.3.2.1, this Section compares the results obtained using Algorithms 7-1 and 7-3 to those from direct use of the single bilinear dynamic collision nodal model developed in Chapter 5. The collision output properties for the passive case (Algorithm 7-1) and active case (Algorithm 7-3) are given in Columns 1 and 3 of Table 7-6, respectively. Columns 2 and 4 present the results obtained from the bilinear model directly, and correspond to the passive and active cases, respectively. Note that the values in square brackets in Columns 2 and 4 correspond, respectively, to the use of Algorithms 7-1 and 7-3 expressed as a percentage difference to the direct use of the bilinear model. It is interesting to note that for the passive case in Column 2 (as in the previous case in Section 7.2.3.1), the lowest percentage difference is for the peak deformation (2.06%) and the largest percentage difference of (3.78%) is for the peak chest acceleration. The results presented in Column 4 of Table 7-6 are for an active case, where the stiffness value has been reduced by a scaling factor of 0.5279, with this corresponding to softening of the structure. Referring to Column 4, Table 7-6, the largest percentage difference is for the peak chest acceleration (6.42%) with the lowest percentage difference (2.24%) being found for the peak deformation.

The percentage differences between the use of interpolation using fuzzy logic and the direct use of the bilinear model in this example is higher than in Section 7.3.2.1.

Table 7-5: *Output Collision Properties for the Passive Collision Structure Case (Algorithm 7-1) and the Active Collision Structure Case (Algorithm 7-3) for a Scenario Involving Excessive Peak Deformation*

Collision Output Properties	Passive (Algorithm 7-1)	Active (Algorithm 7-2)
Peak deformation, δ_a $[m]$	0.4509	0.5900
Peak chest acceleration, a_{a_C} $[g]$	31.11	28.04
Peak head acceleration, a_{a_H} $[g]$	39.42	35.53

Table 7-6: *Comparing Collision Output Results from Using Algorithm 7-1 and Algorithm 7-3 to the Single Vehicle Bilinear Dynamic Collision Nodal Model*

Collision Output Properties	Passive (Algorithm 7-1)	Passive (Bilinear model)	Active (Algorithm 7-3)	Active (Bilinear model)
Peak deformation, δ_a $[m]$	0.4509	0.4416 [2.06%]	0.5900	0.5768 [2.24%]
Peak chest acceleration, a_{a_C} $[g]$	31.11	29.93 [3.79%]	25.70	24.05 [6.42%]
Peak head acceleration, a_{a_H} $[g]$	39.42	37.93 [3.78%]	32.56	31.05 [4.64%]

7.4 STAGE 4: COLLISION TARGET SELECTION

The various EDM algorithms used for collision target selection are now introduced. These are based on the philosophical approaches (i.e. the deontological approach of Kant and the utilitarian approach of Bentham) and the social actions (i.e. altruism and selfishness) for the single AV collision case, i.e. determining between colliding into an IRW or 1 or 10 pedestrian(s), see Figure 3-1 in Section 3.2.1, Chapter 3.

7.4.1 COLLISION TARGET ALGORITHMS

The four collision target algorithms involving the philosophical approaches and social actions are outlined as follows. In the illustrative examples, the AV has two occupants.

7.4.1.1 COMMON UTILITY COST UNIT FOR COLLISION INJURY SEVERITY LEVELS

This sub-section deals with the proposal for and the creation of a common utility cost unit for collision injury severity levels. It is important to note that there is a need to address the problem of encompassing the attributes involved in dealing with deformation length in meters, acceleration experienced by occupants in g-force, and the severity as experienced by pedestrians in terms of collision impact velocity. There is a need, therefore, for a common utility cost unit. The common factor amongst these features is the collision injury severity level (see Section 7.2.2). Whilst each of the individual features exist on their universe of discourse with equally spaced membership functions on a linear range, it is important to distinguish the collision injury severity levels in a nonlinear manner, i.e. in an attempt to avoid severe to fatal collisions. Exploiting the fact that five membership functions span each universe of discourse, it is both convenient and helpful to map the linear crisp values for each feature on to a common function whereby the crisp values from the lowest to highest map linearly on to, $n = 1 - 5$ and postulate the functions N_{f_l} and N_{f_h}, given by:

$$N_{f_l} = \left(n_{f_l}!\right)^2 \tag{7-52}$$

where f is used as a general subscript to represent the four feature indices, to determine a common utility cost function of lives at risk for each feature and n_{f_l} is based on the membership to the lower bounds:

$$N_{f_h} = \left(n_{f_h}!\right)^2 \tag{7-53}$$

and where n_{f_h} is based on the membership to the upper bounds. An initial investigation of Equations (5-52) and (5-53) is given in Table 7-7, where it is clear that the higher

membership sets $n_{l/h}$ (i.e. values 4 and 5) give significantly higher values for $N_{f_{l/h}}$, hence emphasising (or amplifying) the collision injury severity levels of such collisions, with a view to avoid these collisions, hence reduce the utility cost to society.

The functions from Equations (7-52) and (7-53) are used together with the lower membership function, denoted $u_{f_l}(f)$, and the higher membership function, denoted $u_{f_h}(f)$, to define the general utility cost function of lives at risk that can be applied to each of the four collision features. This is given by the general function:

$$\acute{\eta}(f) = \left(N_{f_h}\left(u_{f_h}(f)\right) + N_{f_l}\left(u_{f_l}(f)\right)\right)N_{o/p} \tag{7-54}$$

where $N_{o/p}$ denotes the number of occupant(s)/pedestrian(s). Equation (7-54) is proposed here to define the utility cost function of lives at risk for each feature, peak deformation, peak head acceleration, peak chest acceleration and pedestrian impact velocity, respectively. These are given by:

$$\acute{\eta}(\delta_a) = \left(N_h\left(u_{\delta_h}(\delta_a)\right) + N_l\left(u_{\delta_l}(\delta_a)\right)\right)N_{o_a} \tag{7-55}$$

$$\acute{\eta}(a_{H_a}) = \left(N_h\left(u_{a_{H_h}}(a_{H_a})\right) + N_l\left(u_{a_{H_l}}(a_{H_a})\right)\right)N_{o_a} \tag{7-56}$$

$$\acute{\eta}(a_{C_a}) = \left(N_h\left(u_{a_{C_h}}(a_{C_a})\right) + N_l\left(u_{a_{C_l}}(a_{C_a})\right)\right)N_{o_a} \tag{7-57}$$

$$\acute{\eta}(p_{v_a}) = \left(N_h\left(u_{p_{v_h}}(p_{v_a})\right) + N_l\left(u_{p_{v_l}}(p_{v_a})\right)\right)N_{p_a} \tag{7-58}$$

Table 7-7: *Results of the Factorial-Squared Function used to Distinguish the Collision Injury Severity Levels in a Common Nonlinear Manner*

$n_{f_{l/h}}$	$N_{f_{l/h}}$
1	1
2	4
3	36
4	576
5	14400

7.4.1.2 DEONTOLOGICAL (KANT) ALGORITHM

As discussed in Section 2.3.2 Chapter 2, the deontological approach applied to an AV would ensure the AV follows its natural path without any intention to change paths to potentially save lives. Algorithm 7-4 describes the deontological (Kant) approach, with the AV continuing on its predetermined defined course/route.

7.4.1.3 UTILITARIAN (BENTHAM) ALGORITHM

The utilitarian approach is based on the views of Jeremy Bentham, as discussed in Section 2.3.2, Chapter 2. Recall that the development of the utilitarian approach is gathering support as was shown by the results from a survey (Bonnefon, J.F., Shariff, A. and Rahwan, I., 2016). The basic principle of this approach is to save as many lives as possible, even if this involves changing the path of the AV to potentially sacrifice the AV occupant(s) lives for the greater good. Algorithm 7-5 has been designed with the sole purpose of steering the AV into the collision path with the least severity, with this minimising the occupant/passenger injuries and potentially maximising the number of lives saved. Using Algorithm 7-2, information is fed through from Stage 2 (see Section 7.2.2), i.e. the collision injury severity of the occupant(s) and pedestrian(s) based on the properties of peak deformation δ_a, peak head acceleration a_{H_a}, peak chest acceleration a_{C_a} and pedestrian impact velocity v_a. Other additional information not determined in Stage 2 that is required, includes the number of pedestrians, denoted N_p and the number of occupants, denoted N_o. Recall that in this work, the number of pedestrians considered is either 1 or 10 and the number of occupants in the AV is 2.

Because potentially conflicting injury severities of the occupant(s) are captured (peak head and chest accelerations and peak deformation), use of two Euclidean metrics are applied to capture the overall utility cost. The utility of cost of lives at risk is given by the following Euclidean metric when peak deformation is 'low', i.e. less than or equal to the design deformation length:

$$\varepsilon_{low} = \sqrt{\acute{\eta}\left(a_{H_a}\right)^2 + \acute{\eta}\left(a_{C_a}\right)^2} \tag{7-59}$$

Conversely, when peak deformation is 'high', i.e. greater than the design deformation length the following Euclidean metric will capture the overall utility cost:

$$\varepsilon_{high} = \sqrt{\acute{\eta}(\delta_a)^2 + \acute{\eta}\left(a_{H_a}\right)^2 + \acute{\eta}\left(a_{C_a}\right)^2} \tag{7-60}$$

Based on the values determined from either Equation (7-59) or (7-60), the AV is commanded to steer into the path with the lowest value for the utility cost of lives at risk, i.e. the least overall utility cost to society.

Algorithm 7-4: *Deontological (Kant) Algorithm for Autonomous Vehicle Collision Target Selection*

i.	Regardless whether or not the AV is to be involved in an unavoidable collision, do not change the originally intended course/route

Algorithm 7-5: *Utilitarian (Bentham) Algorithm for Autonomous Vehicle Collision Target Selection*

i. Using Algorithm 7-2, obtain the collision injury severity, i.e. degree of membership to the fuzzy sets A, B, C, D and E for the four features, i.e. peak deformation δ_a, peak head acceleration a_{H_a}, peak chest acceleration a_{C_a} and pedestrian impact velocity p_{v_a} (Recall that $u_{f_l}(f)$ denotes the lower member function and $u_{f_h}(f)$ denotes the higher membership function, where f is used as a general subscript to represent the four feature indices: δ_a, a_{H_a}, a_{C_a} and p_{v_a})

ii. Determine number of pedestrians, denoted N_p and occupants, denoted N_o

iii. Assign an ID number, denoted n, where n is based on the membership to the higher, denoted n_h and lower bounds, denoted n_l (i.e. $A \rightarrow 5$, $B \rightarrow 4$, $C \rightarrow 3$, $D \rightarrow 2$ and $E \rightarrow 1$) for all of the occupant injury severity and also to the pedestrian impact velocity

iv. Determine the utility cost of life at risk for the AV occupant(s) and pedestrian(s) using the following general equation:

$$\acute{\eta}(f) = \left(N_{f_h}\left(u_{f_h}(f)\right) + N_{f_l}\left(u_{f_l}(f)\right)\right)N_{o/p}$$

$$\text{where } N_{f_h} = \left(n_{f_h}!\right)^2 \text{ and } N_{f_l} = \left(n_{f_l}!\right)^2$$

whereby the above expression for $\acute{\eta}(f)$ is used for the four collision features δ_a, a_{H_a}, a_{C_a} and p_{v_a} to give $\acute{\eta}(\delta_a)$, $\acute{\eta}(a_{h_a})$, $\acute{\eta}(a_{c_a})$ and $\acute{\eta}((p_{v_a})$.

v. Apply the following rules to obtain the overall utility cost:

- If the deformation is below or equal to the design deformation length (i.e. 0.5900m), the utility cost of lives at risk is determined using the following Euclidean cost metric: $\varepsilon_{softening} = \sqrt{\acute{\eta}(a_{H_a})^2 + \acute{\eta}(a_{C_a})^2}$
- If the deformation is above the design deformation length (i.e. 0.5900m), the utility cost of lives at risk is determined using the following Euclidean cost metric:

$$\varepsilon_{stiffening} = \sqrt{\acute{\eta}(\delta_a)^2 + \acute{\eta}(a_{H_a})^2 + \acute{\eta}(a_{C_a})^2}$$

vi. Steer into the path with the lowest value of the utility cost of lives at risk (i.e. the least cost to society)

7.4.1.4 ALTRUISTIC ALGORITHM (SOCIAL ACTION)

The altruistic algorithm is based on social actions, as discussed in Section 2.4, Chapter 2. For an AV collision, the AV (and corresponding occupant(s)) will be considered as the actor and the collision target (1 or 10 pedestrian(s)) will be considered as the recipient, see Figure 2-8 in Chapter 2. An act of altruism by the AV results in providing a benefit to the collision target at a cost to the AV occupant(s). Consequently, the AV utilising the altruistic algorithm will always steer into the IRW. (In contrast to the alternative of steering into the pedestrian(s) which would be an act of selfishness.) The altruistic algorithm is detailed in Algorithm 7-6.

7.4.1.5 SELFISH ALGORITHM (SOCIAL ACTION)

The act of selfishness was discussed in Section 2.4 Chapter 2, where such an act would involve the AV steering into the pedestrian(s). This is entirely due to the selfish benefit to the AV occupants and the disbenefit to the pedestrian(s). The selfish algorithm is detailed in Algorithm 7-7.

Algorithm 7-6: *Altruistic Algorithm for Autonomous Vehicle Collision Target Selection*

i.	Steer into the immovable rigid wall

Algorithm 7-7: *Selfish Algorithm for Autonomous Vehicle Collision Target Selection*

i.	Steer into the pedestrian(s)

7.4.2 DECISION TARGET AND STIFFNESS CONTROLLER RESULTS

The EDM algorithm which utilises a M2D approach is now presented, whereby the stiffness control algorithm (Algorithm 7-3) is combined with the four collision target selection algorithms (Algorithms 7-4 – 7-7). To demonstrate the EDM, the scenarios that are presented in Section 3.2.1, Chapter 3, will be used, i.e. an AV determining between colliding into an IRW or 1 or 10 pedestrians. The two illustrative examples for the stiffness controller, i.e. Scenarios 1 and 2, in Sections 7.3.2 and 7.3.3, respectively, are used to demonstrate the EDM, as such the AV properties are taken as follows:

- Scenario 1: m_a = 1396kg and $v_a =$ 18.0604m/s (40.40mph)
- Scenario 2: m_a = 1270kg and $v_a =$ 11.60m/s (25.9485mph)

Scenario 1 is typical of a situation when an element of increased structural stiffness is needed. Rather than showing several simulation examples, Scenario 1 is taken as being representative of such a situation. This scenario follows through to the decision making when considering the other situations in Sections 7.4.2.3, 7.4.2.4 and 7.4.2.5. Scenario 2 illustrates the advantages of softening the crumple structures in order to reduce the acceleration that the onboard occupants experience, whilst taking the available deformation up to (or just less than) the design deformation length.

7.4.2.1 QUANTIFYING THE OUTCOMES (PASSIVE AND ACTIVE)

Using the collision injury severities, a limit is applied to peak deformation, peak head acceleration, peak chest acceleration and pedestrian impact velocity relating to the above, i.e. the limit for each case when life is potentially lost/saved. The limit for peak deformation is based on the design deformation length (i.e. 0.5900m) and the limits for peak head and peak chest accelerations are based on the US new car assessment programme (NCAP) and US FMVSS tests, with the values being 80g and 60g, respectively. The limit for the pedestrian impact velocity has been determined based on the literature in Section 4.5, Chapter 4, where a value of 37.28m/s is adopted. Although, as stated in the Remark in Section 4.5, Chapter 4, further work is needed regarding a detailed study into pedestrian safety. Recall from Section 7.2, where the five levels of

collision injury severity were introduced, i.e. with the fuzzy sets A, B, C, D and E, where fuzzy set A represented the highest injury severity and set E the lowest injury severity. Considering Table 7-2, the limits outlined above are found to lie within the fuzzy sets B and C. Based on the limits and fuzzy sets, the degrees of membership to the fuzzy sets B and C for the four key features are determined as follows (in the same manner as previously introduced in Section 7.2.2), i.e.

$$x_{S_{AV}} := \begin{bmatrix} \mu_{\delta_C}(\delta_a) & \mu_{\delta_B}(\delta_a) \\ \mu_{a_{H_C}}(a_{H_a}) & \mu_{a_{H_B}}(a_{H_a}) \\ \mu_{a_{C_C}}(a_{C_a}) & \mu_{a_{C_B}}(a_{C_a}) \\ \mu_{P_{v_C}}(P_{v_a}) & \mu_{P_{v_B}}(P_{v_a}) \end{bmatrix} := \begin{bmatrix} 0.920 & 0.080 \\ 0.479 & 0.521 \\ 0.646 & 0.354 \\ 0.772 & 0.228 \end{bmatrix} \tag{7-61}$$

Considering Equation (7-61), Equations (7-55) to (5-58) have been used to determine the limits of the utility cost of lives at risk, see Table 7-8. As with the properties in Equation (7-61), it is undesirable to exceed the limits given in Table 7-8, as this may lead to highly severe and fatal collision outcomes.

Table 7-8: *Limits Applied to the Key Features for the Utility Cost of Life at Risk*

Key Feature	Limits - utility cost of lives at risk
Peak deformation [2 occupants]	158.4
Peak head acceleration [2 occupants]	634.7
Peak chest acceleration [2 occupants]	454.3
Pedestrian impact velocity [1 pedestrian]	159.1
Pedestrian impact velocity [10 pedestrians]	1591.2

When evaluating the utility cost of lives at risk, the peak deformation value is only considered when the limit is breached, i.e. above the design deformation length. This is implemented because deformation up to the design deformation length is neither viewed as a risk to the occupant(s) on-board the AV nor as a utility cost to society. However, beyond the design deformation length, deformation does represent a high risk to the occupant(s) and this then becomes a true utility cost to society. In contrast, all values up to and beyond the US FMVSS test limits for the peak head accelerations and peak chest accelerations values are considered, i.e. $80g$ and $60g$ for the peak head and chest accelerations, respectively.

When taking into account the above utility cost considerations, and comparing the passive and active cases, the following will be applied:

i. When an action is taken to soften the structure, the peak deformation value will be allowed to increase up to the design deformation length, therefore when assessing the benefit of active stiffness control only the reductions in the peak head acceleration and peak chest acceleration values are of interest
ii. When an action is taken to stiffen the structure, the peak deformation value will be reduced towards the design deformation length, therefore the resulting peak deformation, peak head acceleration and peak chest acceleration values are all of interest

Since the peak deformation is the primary decision feature, the active stiffness control system should ensure deformation does not exceed the design deformation length, hence the value of the utility cost due to deformation should ideally be zero.

Consequently, when comparing the passive and active cases for the utility cost of lives at risk, an overall utility cost metric based on the Euclidean norm will be used. In the

case of (i), above, the following Euclidean cost metric is used in the case of softening, denoted $\varepsilon_{softening}$, i.e.

$$\varepsilon_{softening} = \sqrt{\acute{\eta}\left(a_{H_a}\right)^2 + \acute{\eta}\left(a_{C_a}\right)^2} \tag{7-62}$$

and for (ii), above, the following Euclidean cost metric is used in the case of stiffening when comparing the passive and active cases for the utility cost of lives at risk, denoted $\varepsilon_{stiffening}$, i.e.

$$\varepsilon_{stiffening} = \sqrt{\acute{\eta}(\delta_a)^2 + \acute{\eta}\left(a_{H_a}\right)^2 + \acute{\eta}\left(a_{C_a}\right)^2} \tag{7-63}$$

where in general $\acute{\eta}\,(f)$ is defined as in Algorithm 7-5 for AV_a, etc, see Section 7.4.1.3.

Considering Scenario 1 in Section 7.3.2, the matrix containing the injury severities for the passive and active cases, respectively, are given by:

$$x_{S_{AV}} \coloneqq \begin{bmatrix} \boldsymbol{\mu_{\delta_C}(\delta_a)} & \boldsymbol{\mu_{\delta_B}(\delta_a)} \\ \mu_{a_{H_C}}(a_{H_a}) & \mu_{a_{H_B}}(a_{H_a}) \\ \mu_{a_{C_C}}(a_{C_a}) & \mu_{a_{C_B}}(a_{C_a}) \\ \boldsymbol{\mu_{P_{v_C}}(P_{v_a})} & \boldsymbol{\mu_{P_{v_B}}(P_{v_a})} \end{bmatrix} \coloneqq \begin{bmatrix} \mathbf{0.482} & \mathbf{0.518} \\ 0.913 & 0.087 \\ 0.914 & 0.086 \\ \mathbf{0.460} & \mathbf{0.540} \end{bmatrix}$$

and

$$\tilde{x}_{S_{AV}} \coloneqq \begin{bmatrix} \mu_{\tilde{\delta}_C}(\tilde{\delta}_a) & \mu_{\tilde{\delta}_B}(\tilde{\delta}_a) \\ \mu_{\tilde{a}_{H_C}}(\tilde{a}_{H_a}) & \mu_{\tilde{a}_{H_B}}(\tilde{a}_{H_a}) \\ \mu_{\tilde{a}_{C_C}}(\tilde{a}_{C_a}) & \mu_{\tilde{a}_{C_B}}(\tilde{a}_{C_a}) \end{bmatrix} \coloneqq \begin{bmatrix} 0.920 & 0.080 \\ 0.6565 & 0.3435 \\ 0.6575 & 0.3425 \end{bmatrix}$$

where it may be determined that the peak deformation of the AV exceeds the limit and the pedestrian impact velocity also exceeds the limit (both of these are in bold). Of interest, the active structural approach results in no AV properties exceeding the limit.

Considering Scenario 2 in Section 7.3.3, the matrix containing the injury severities for the passive and active cases, respectively, are given by:

$$x_{S_{AV}} \coloneqq \begin{bmatrix} \mu_{\delta_D}(\delta_a) & \mu_{\delta_C}(\delta_a) \\ \mu_{a_{H_E}}(a_{H_a}) & \mu_{a_{H_D}}(a_{H_a}) \\ \mu_{a_{C_E}}(a_{C_a}) & \mu_{a_{C_D}}(a_{C_a}) \\ \mu_{P_{v_D}}(P_{v_a}) & \mu_{P_{v_C}}(P_{v_a}) \end{bmatrix} \coloneqq \begin{bmatrix} 0.819 & 0.181 \\ 0.170 & 0.830 \\ 0.170 & 0.820 \\ 0.905 & 0.095 \end{bmatrix}$$

and

$$\tilde{x}_{S_{AV}} \coloneqq \begin{bmatrix} \mu_{\tilde{\delta}_C}(\tilde{\delta}_a) & \mu_{\tilde{\delta}_B}(\tilde{\delta}_a) \\ \mu_{\tilde{a}_{H_E}}(\tilde{a}_{H_a}) & \mu_{\tilde{a}_{H_D}}(\tilde{a}_{H_a}) \\ \mu_{\tilde{a}_{C_E}}(\tilde{a}_{C_a}) & \mu_{\tilde{a}_{C_D}}(\tilde{a}_{C_a}) \end{bmatrix} \coloneqq \begin{bmatrix} 0.920 & 0.080 \\ 0.544 & 0.456 \\ 0.544 & 0.456 \end{bmatrix}$$

where in the case of the passive and active cases, none of the properties exceed the limits.

Equations (7-55) to (7-58) are used to determine the individual contributions to the utility cost of life at risk for both Scenarios 1 and 2, see Table 7-9. When considering all of the AV key features, the overall Euclidean cost metric given in Equation (7-63) has been applied to the passive case in Scenario 1 and the overall Euclidean cost metric given in Equation (7-62) has been applied to the passive case in Scenario 2. Note that as peak deformation for Scenario 2 does not exceed the design deformation length, this is not considered in the Euclidean cost metric. Tables 7-10 and 7-11 detail the utility cost of life at risk (see Column 3) for the three different scenarios (see Column 1) and the collision target (see Column 2). Note that in the case of the AV occupants, the Euclidean

cost metric of either Equation (7-62) or Equation (7-63) is used in order to combine the contributing utility costs. In contrast, however, in the case of pedestrians, the function given by $\acute{\eta}\left(p_{v_a}\right)$, Equation (7-58), gives the overall utility cost directly.

Table 7-9: *Autonomous Vehicle Key Features for the Utility Cost of Lives at Risk for Scenarios 1 and 2*

Key Feature	Scenario 1: utility cost of lives at risk	Scenario 2: utility cost of lives at risk
Peak deformation [2 occupants]	631.4	19.6 (i.e. N/A)
Peak head acceleration [2 occupants]	166.0	7.0
Peak chest acceleration [2 occupants]	164.9	7.0

Table 7-10: *Utility Cost of Lives at Risk* for *Scenario 1, where the Euclidian Metric has been applied for the Autonomous Vehicle Properties (Passive)*

Scenario 1	Collision target	Utility cost of lives at risk
One pedestrian Immovable rigid wall (two occupants)	One pedestrian	327.6
Ten pedestrians Immovable rigid wall (two occupants)	Ten pedestrians	3276.0
One pedestrian Immovable rigid wall (two occupants)	Immovable rigid wall (two occupants)	673.4

Table 7-11: *Utility Cost of Lives at Risk for Scenario 2, where the Euclidian Metric has been applied for the Autonomous Vehicle Properties (Passive)*

Scenario 2	Collision target	Utility cost of lives at risk
One pedestrian Immovable rigid wall (two occupants)	One pedestrian	7.0
Ten pedestrians Immovable rigid wall (two occupants)	Ten pedestrians	70.4
One pedestrian Immovable rigidi wall (two occupants)	Immovable rigid wall (two occupants)	9.9

Using the results from the stiffness controller for Scenarios 1 and 2 in Sections 7.3.2 and 7.3.3, respectively, the utility cost of lives at risk for the active scenarios are determined for the AV (as was undertaken above). Tables 7-12 and 7-13 detail the active AV features (peak deformation δ_a, peak head acceleration a_{H_a} and peak chest acceleration a_{C_a}), where the passive cases given in Table 7-9 for Scenarios 1 and 2 make up Column 2 in Tables 7-12 and 7-13. Tables 7-14 and 7-15 detail the utility cost of lives at risk for the active case (see Column 3) for the three different scenarios (see Column 1) and the collision target (see Column 2). Using data from Tables 7-12 and 7-13, the overall Euclidean cost metric has been applied in Tables 7-14 and 7-15, when considering the AV features. As both Scenario 1 and 2 have resulted in a peak deformation equal to the design deformation length, these are now not applicable when using the Euclidean cost metric. In the case of Scenario 1, stiffening of the structure was achieved to reduce the peak deformation, with this increasing the accelerations. Scenario 2 involved softening the collision structure, with this utilising the deformation length and reducing the accelerations experienced by the occupants.

Table 7-12: *Autonomous Vehicle Key Features for the Utility Cost of Lives at Risk for Scenario 1 (Passive and Active)*

Key Feature	Utility cost of lives at risk (passive)	Utility cost of lives at risk (active)
Peak deformation [2 occupants]	631.4	158.4 (i.e. N/A)
Peak head acceleration [2 occupants]	166.0	443.0
Peak chest acceleration [2 occupants]	164.9	441.9

Table 7-13: *Autonomous Vehicle Key Features for the Utility Cost of Lives at Risk for Scenario 2 (Passive and Active)*

Key Feature	Utility cost of lives at risk (passive)	Utility cost of lives at risk (active)
Peak deformation [2 occupants]	19.6 (i.e. N/A)	158.4 (i.e. N/A)
Peak head acceleration [2 occupants]	7.0	4.7
Peak chest acceleration [2 occupants]	7.0	4.7

Table 7-14: *Utility Cost of Lives at Risk* for *Scenario 1, where the Euclidean Metric has been applied for the Autonomous Vehicle Properties (Active)*

Scenario 1	Collision target	Utility cost of lives at risk
One pedestrian Immovable rigid wall (two occupants)	One pedestrian	327.6
Ten pedestrians Immovable rigid wall (two occupants)	Ten pedestrians	3276.0
One pedestrian Immovable rigid wall (two occupants)	Immovable rigid wall (two occupants)	625.7

Table 7-15: *Utility Cost of Lives at Risk* for Scenario 2, *where the Euclidean Metric has been applied for the Autonomous Vehicle Properties (Active)*

Scenario 2	Collision target	Utility cost of lives at risk
One pedestrian Immovable rigid wall (two occupants)	One pedestrian	7.0
Ten pedestrians Immovable rigid wall (two occupants)	Ten pedestrians	70.4
One pedestrian Immovable rigidi wall (two occupants)	Immovable rigid wall (two occupants)	6.6

7.4.2.2 COLLISION SCENARIO RESULTS

The results from Scenarios 1 and 2 are detailed for the passive and active cases, with four situations considered. The same format of reporting the results follows through.

Scenarios 1 and 2 - Situation 1

This scenario involves the case where the AV with two occupants should decide between swerving to avoid one pedestrian or instead collide full frontal into an IRW, as illustrated

in Figure 3-1, Section 3.2.1, Chapter 3. The results from running the four collision target selection algorithms are given in Table 7-16 (passive) and Table 7-17 (active) for both Scenario 1 and Scenario 2. Considering Tables 7-16 and 7-17, Column 1 details the four algorithms (as detailed in Section 7.4.1), with the collision target results given in Columns 2 and 4 for Scenarios 1 and 2, respectively. The utility cost of lives at risk are given in Columns 3 and 5 for Scenarios 1 and 2, respectively, where the results are generated by the collision target algorithm selection and Tables 7-10 and 7-11, for Scenarios 1 and 2, respectively. Note that numbers given in square brackets in Tables 7-16 and 7-17 indicate the number of occupants or pedestrians.

Scenarios 1 and 2 - Situation 2

The results in Table 7-18 (passive) and Table 7-19 (active) involve the case where the AV should decide between swerving to avoid an IRW or instead collide into 1 pedestrian, as illustrated in Figure 3-1, Section 3.2.1, Chapter 3. The results from running the four collision target algorithms (passive) for both Scenarios 1 and 2 are given in Table 7-18 (passive) and Table 7-19 (active). Note that numbers given in square brackets in Tables 7-18 and 7-19 indicate the number of occupants or pedestrians.

Table 7-16: *Ethical Decision Maker Results for Scenarios 1 and 2 (Passive): AV Making a Decision Between Swerving to Avoid One Pedestrian and to Collide into an Immoveable Rigid Wall (Two Occupants On-Board the Autonomous Vehicle)*

	Scenario 1		Scenario 2	
Algorithm	**Target**	**Utility cost of lives at risk**	**Target**	**Utility cost of lives at risk**
Deontological	Pedestrian [1]	327.6	Pedestrian [1]	7.0
Utilitarian	Pedestrian [1]	327.6	Pedestrian [1]	7.0
Altruistic	Immovable rigid wall [2]	673.4	Immovable rigid wall [2]	9.9
Selfish	Pedestrian [1]	327.6	Pedestrian [1]	7.0

Table 7-17: *Ethical Decision Maker Results for Scenarios 1 and 2 (Active): AV Making a Decision Between Swerving to Avoid One Pedestrian and to Collide into an Immoveable Rigid Wall (Two Occupants On-Board the Autonomous Vehicle)*

	Scenario 1		Scenario 2	
Algorithm	**Target**	**Utility cost of lives at risk**	**Target**	**Utility cost of lives at risk**
Deontological	Pedestrian [1]	327.6	Pedestrian [1]	7.0
Utilitarian	Pedestrian [1]	327.6	Immovable rigid wall [2]	6.6
Altruistic	Immovable rigid wall [2]	625.7	Immovable rigid wall [2]	6.6
Selfish	Pedestrian [1]	327.6	Pedestrian [1]	7.0

Scenarios 1 and 2 - Situation 3

The results in Table 7-20 (passive) and Table 7-21 (active) involve the case where the AV should decide between swerving to avoid 10 pedestrians or instead collide full frontal into an IRW, as illustrated in Figure 3-1, Section 3.2.1, Chapter 3. The results from running the four collision target algorithms (passive) for both Scenarios 1 and 2 are given in Table 7-20 (passive) and Table 7-21 (active). Note that numbers given in square brackets in Tables 7-20 and 7-21 indicate the number of occupants or pedestrians.

Table 7-18: *Ethical Decision Maker Results for Scenarios 1 and 2 (Passive): AV Making a Decision Between Swerving to Avoid Immoveable Rigid Wall (Two Occupants On-Board the Autonomous Vehicle) and to Collide into One Pedestrian*

	Scenario 1		Scenario 2	
Algorithm	**Target**	**Utility cost of lives at risk**	**Target**	**Utility cost of lives at risk**
Deontological	Immovable rigid wall [2]	673.4	Immovable rigid wall [2]	9.9
Utilitarian	Pedestrian [1]	327.6	Pedestrian [1]	7.0
Altruistic	Immovable rigid wall [2]	673.4	Immovable rigid wall [2]	9.9
Selfish	Pedestrian [1]	327.6	Pedestrian [1]	7.0

Table 7-19: *Ethical Decision Maker Results for Scenarios 1 and 2 (Active): AV Making a Decision Between Swerving to Avoid Immoveable Rigid Wall (Two Occupants On-Board the Autonomous Vehicle) and to Collide into One Pedestrian*

	Scenario 1		Scenario 2	
Algorithm	**Target**	**Utility cost of lives at risk**	**Target**	**Utility cost of lives at risk**
Deontological	Immovable rigid wall [2]	625.7	Immovable rigid wall [2]	6.6
Utilitarian	Pedestrian [1]	327.6	Immovable rigid wall [2]	6.6
Altruistic	Immovable rigid wall [2]	625.7	Immovable rigid wall [2]	6.6
Selfish	Pedestrian [1]	327.6	Pedestrian [1]	7.0

Table 7-20: *Ethical Decision Maker Results for Scenarios 1 and 2 (Passive): AV Making a Decision Between Swerving to Avoid Ten Pedestrians and to Collide into an Immoveable Rigid Wall (Two Occupants On-Board the Autonomous Vehicle)*

	Scenario 1		Scenario 2	
Algorithm	**Target**	**Utility cost of lives at risk**	**Target**	**Utility cost of lives at risk**
Deontological	Pedestrians [10]	3276.0	Pedestrians [10]	70.4
Utilitarian	Immovable rigid wall [2]	673.4	Immovable rigid wall [2]	9.9
Altruistic	Immovable rigid wall [2]	673.4	Immovable rigid wall [2]	9.9
Selfish	Pedestrians [10]	3276.0	Pedestrians [10]	70.4

Table 7-21: *Ethical Decision Maker Results for Scenarios 1 and 2(Active): AV Making a Decision Between Swerving to Avoid Immoveable Rigid Wall (Two Occupants On-Board the Autonomous Vehicle) and to Collide into One Pedestrian*

	Scenario 1		Scenario 2	
Algorithm	**Target**	**Utility cost of lives at risk**	**Target**	**Utility cost of lives at risk**
Deontological	Pedestrians [10]	3276.0	Pedestrians [10]	70.4
Utilitarian	Immovable rigid wall [2]	625.7	Immovable rigid wall [2]	6.6
Altruistic	Immovable rigid wall [2]	625.7	Immovable rigid wall [2]	6.6
Selfish	Pedestrians [10]	3276.0	Pedestrians [10]	70.4

Scenarios 1 and 2 - Situation 4

The results in Table 7-22 (passive) and Table 7-23 (active) involve the case where the AV should decide between swerving to avoid an IRW or instead collide into 10 pedestrians, as illustrated in Figure 3-1, Section 3.2.1, Chapter 3. The results from running the four collision target algorithms (passive) for both Scenarios 1 and 2 are given in Table 7-22 (passive) and Table 7-23 (active). Note that numbers given in square brackets in Tables 7-22 and 7-23 indicate the number of occupants or pedestrians.

Table 7-22: *Ethical Decision Maker Results for Scenarios 1 and 2 (Passive): AV Making a Decision Between Swerving to Avoid Immoveable Rigid Wall (Two Occupants On-Board the Autonomous Vehicle) and to Collide into Ten Pedestrians*

	Scenario 1		Scenario 2	
Algorithm	**Target**	**Utility cost of lives at risk**	**Target**	**Utility cost of lives at risk**
Deontological	Immovable rigid wall [2]	673.4	Immovable rigid wall [2]	9.9
Utilitarian	Immovable rigid wall [2]	673.4	Immovable rigid wall [2]	9.9
Altruistic	Immovable rigid wall [2]	673.4	Immovable rigid wall [2]	9.9
Selfish	Pedestrians [10]	3276.0	Pedestrians [10]	70.4

Table 7-23: *Ethical Decision Maker Results for Scenarios 1 and 2 (Active): AV Making a Decision Between Swerving to Avoid Ten Pedestrians and to Collide into an Immoveable Rigid Wall (Two Occupants On-Board the Autonomous Vehicle)*

	Scenario 1		Scenario 2	
Algorithm	**Target**	**Utility cost of lives at risk**	**Target**	**Utility cost of lives at risk**
Deontological	Immovable rigid wall [2]	625.7	Immovable rigid wall [2]	6.6
Utilitarian	Immovable rigid wall [2]	625.7	Immovable rigid wall [2]	6.6
Altruistic	Immovable rigid wall [2]	625.7	Immovable rigid wall [2]	6.6
Selfish	Pedestrians [10]	3276.0	Pedestrians [10]	70.4

7.4.2.3 SUMMARY OF INITIAL RESULTS

The quantified results (passive and active) in terms of the utility cost of lives at risk are now evaluated from the simulation studies involving Scenarios 1 and 2 using the four algorithms detailed in Section 7.4.1. The utility cost of lives at risk for Scenarios 1 and 2 (considering the 4 situations) are given in Tables 7-24 and 7-25 for the passive and active cases, respectively.

Considering the results from the four situations in Table 7-24 for Scenarios 1 and 2, the selfish algorithm results in the most severe collision algorithm for the passive cases, with this resulting in the largest utility cost to society. Correspondingly, as expected, the selfish algorithm presents the largest utility cost to society when considering Situations 3 and 4 (when more pedestrians are considered), see Section 7.4.2.2. Considering the results in Tables 7-24, the deontological algorithm for the passive case 'sits' in the middle of the results in terms of the utility cost of lives at risk. The utilitarian algorithm is the most effective, giving rise to the lowest utility cost to society in the passive AV collisions considered, and the altruistic algorithm is a close runner-up , see Table 7-24.

Considering the active cases in Table 7-25, for Scenario 1 (stiffening the collision structure), the deontological, utilitarian and altruistic algorithms all result in a reduction to the utility cost to society. The selfish algorithm results in a utility cost of lives at risk which remains unchanged between the passive and active cases, as an AV with such an approach will always steer into the pedestrian(s). The utilitarian algorithm again provides the lowest utility cost to society, with the altruistic algorithm being again a close runner-up. Of interest, three situations changed when comparing between the passive and active cases, i.e. Situations 1, 2 and 4 for Scenario 2. Considering the active cases in Table 7-25, for Scenario 2 (softening the collision structure), the deontological, utilitarian and altruistic algorithms all result in a reduction to the utility cost to society, with the selfish algorithm remaining unchanged.

If occupants of AVs were to be allowed a buy-in option to decide on their EDM algorithm, it is the author's view that this would have to be done so at a premium cost. It is considered from an analysis of the results that the utilitarian and altruistic approaches should be considered as a basis for the standard algorithms for AVs. If a conservative approach was to be preferred, then the deontological algorithm could be an option for the standard EDM algorithm. The most undesirable option for any pedestrian or a group of pedestrians would be that of the selfish algorithm. It is considered that this option should be restricted to the transportation of relatively important occupants in e.g. a military vehicle in a war-zone situation surrounded by groups of enemy terrorists.

Table 7-24: *Quantified Results from the Simulation of Scenario 1 and 2 (Passive)*

	Scenario 1 (Passive)	Scenario 2 (Passive)
Algorithm	**Utility cost of lives at risk**	**Utility cost of lives at risk**
Deontological	4950.4	97.2
Utilitarian	2002.0	33.8
Altruistic	2693.6	39.6
Selfish	7207.2	154.8

Table 7-25: *Quantified Results from the Simulation of Scenario 1 and 2 (Active)*

	Scenario 1 (Active)	Scenario 2 (Active)
Algorithm	**Utility cost of lives at risk**	**Utility cost of lives at risk**
Deontological	4855.0	90.6
Utilitarian	1906.6	26.4
Altruistic	2502.8	26.4
Selfish	7207.2	154.8

7.4.2.4 QUANTIFICATION OF MEASUREMENT/ESTIMATION ERRORS

In this Section, a verification is undertaken to determine/quantify the effect of measurement/estimation errors. The effect of apparent changes in the AV laden mass m_a and collision velocity v_a is explored using the conservation of energy equation (see Equation (4-1), Section 4.2.2, Chapter 4). The nominal AV mass and collision velocity are given in bold in Tables 7-26 and 7-27 (Row 2). For this analysis, the AV laden mass is varied +/- 10% in Table 7-26 (Column 1) and the collision velocity is varied +/- 10% in Table 7-27 (Column 2). The resultant collision deformation energy for the variations in Tables 7-26 and 7-27 are presented in Columns 3, with the percentage difference from the nominal values given in Columns 4. The percentage difference being obtained from:

$$\left(\frac{nominal\ case - varied\ case}{nominal\ case}\right) * 100\%$$

From these results in Tables 7-26 and 7-27, it is clear that the collision velocity is significantly more important to have an accurate measure/estimate as it results in a larger change to the collision deformation energy (this is due to the squared influence of the velocity on the resulting deformation energy). The effect of this squared relationship is also clear when examining the look-up tables in Figure 5-18, Section 5.3.4.2 in Chapter 5. Further properties to explore in a detailed sensitivity analysis would include the structural stiffness value k_a, the occupant posture and seating position and the pedestrian impact location and kinematics.

Table 7-26: *Sensitivity Analysis of the Single Autonomous Vehicle Collision into an Immovable Rigid Wall when Considering the Autonomous Vehicle Laden Mass*

Mass $[kg]$	**Velocity** $[m/s]$	**Collision Deformation Energy** $[kJ]$	**Percentage difference** [%]
1.00*1247	**1.0*15.6464**	**152.6**	**---**
0.90*1247	1.0*15.6464	137.4	9.96
1.10*1247	1.0*15.6464	167.9	10.03

Table 7-27: *Sensitivity Analysis of the Single Autonomous Vehicle Collision into an Immovable Rigid Wall when Considering the Autonomous Vehicle Collision Velocity*

Mass $[kg]$	**Velocity** $[m/s]$	**Collision Deformation Energy** $[kJ]$	**Percentage difference** [%]
1.00*1247	**1.0*15.6464**	**152.6**	**---**
1.00*1247	0.9*15.6464	123.6	19.00
1.00*1247	1.1*15.6464	184.7	21.04

7.5 SUMMARY

In this Chapter, the four stages that comprise the ethical-decision maker (EDM) for collision target selection in the case of a single autonomous vehicle (AV) colliding into an immovable rigid wall (IRW) or into one or a group ten of pedestrians has been developed, namely: pre-determine collision outcomes; pre-determine collision injury severities; activate stiffness controller; and collision target selection.

In Stage 1, fuzzy logic was used to interpolate look-up tables (surfaces) to pre-determine the collision outcome of an AV colliding into an IRW. Using the information from Stage 1 and also considering the AV colliding into pedestrians, it has been demonstrated through illustrative examples that the severity of a collision can be pre-determined. The two-stages to the EDM have then been developed. In Stage 3, an active stiffness controller has been developed that can alter the collision severity, e.g. soften the structure to minimise occupant accelerations or stiffen the structure to minimise the peak deformation of the AV collision structures. It has also been shown that it is possible to reduce collision injury severity levels experienced by the occupants of an AV through the use of active collision structures. In Stage 4, considering the active collision structures, collision target selection algorithms have been explored. Through illustrative examples, it has been demonstrated that a utilitarian approach, closely followed by the altruistic approach produces the lowest utility cost to society. In contrast, the selfish approach, where the AV is programmed to prioritise occupant safety, has led (not surprisingly) to the largest cost to society. A sensitivity analysis has been undertaken, where it has been shown that it is more important to have an accurate estimation/measurement of the collision velocity of an AV over its laden mass value. Overall it has been demonstrated that an AV can be programmed to employ the philosophical doctrines and social actions to select a collision target based on an ethical model to decision (M2D) approach.

8. ETHICAL DECISION MAKER FOR MULTIPLE AUTONOMOUS VEHICLES

8.1 INTRODUCTION

This Chapter builds on Chapter 7 and focuses on the development of the ethical decision-maker (EDM) for the case of multiple autonomous vehicle (AV) collisions. Using the two-vehicle dynamic bilinear collision model developed in Chapter 6 and the corresponding 3D surfaces (look-up tables) of pre-determined passive full-frontal collision outcomes, in conjunction with interpolation using fuzzy logic, the following four Stages are detailed in this Chapter:

- Stage 1: pre-determine collision outcomes
- Stage 2: pre-determine collision injury severities
- Stage 3: activate stiffness controller
- Stage 4: collision target selection

In Stage 1, the two-vehicle dynamic bilinear collision model is also used directly and compared to the approach of using 3D surfaces and interpolation using fuzzy logic. In Stage 1, the colliding AVs (AV_a into AV_b/AV_c) properties are pre-determined, i.e. the three features of peak deformation, peak head acceleration and peak chest acceleration. As in the single AV collision case, the multiple AV collision case in Stage 2 uses the information from Stage 1 and applies the collision injury severities to the four potential outcomes (for the three AVs). In Stage 3, the two-vehicle collision model is used along

with the developed stiffness controller to assess whether the severity of a particular AV collision into another AV can be improved (i.e. severity reduced) via softening/stiffening the collision structures. Stage 4 then details the four potential collision target selection algorithms based on the two considered philosophical approaches (deontological and utilitarian) and the two considered social actions (altruism and selfishness). These algorithms make use of the injury severity levels and are assessed via the use of the overall utility cost to society as introduced in Chapter 7. As in Chapter 7, the general function, denoted $\acute{\eta}(f)$, see Equations (7-54) to (7-57), for each of the contributing collision features is utilised together with an overall Euclidean cost metric, denoted ε, see Equations (7-59) and (7-60) to accommodate a measure of the utility cost of lives at risk for the AV to AV collisions. This allows the results from the four algorithms to be evaluated and compared, i.e. to ascertain the most desirable ethical algorithm that provides the lowest utility cost to society.

8.2 STIFFNESS CONTROLLER

As with the single AV stiffness controller in Section 7.3, Chapter 7, Stage 3 of the AV to AV/AV scenario case involves evaluating whether a particular passive collision scenario can be improved, i.e. either by stiffening to reduce the peak deformations or softening to allow an increased deformation to reduce the peak acceleration. As with the single AV case, the AV to AV/AV stiffness controllers aim to achieve a peak deformation value matching, but not exceeding, the maximum design deformation length (i.e. $0.5900m$, see Table 4-1, Chapter 4). Activation of the stiffness controller (i.e. stiffening/softening) will lead to an increase/decrease in the peak head and chest acceleration g-forces experienced by the occupant(s). If possible, the peak head acceleration and peak chest acceleration should be kept within the suggested limits (see Section 4.2.4, Chapter 4), i.e. $80g$ and $60g$, respectively.

An alternative approach to that of the single-vehicle stiffness controller will be undertaken for the two-vehicle case. Recall in the single-vehicle stiffness controller case,

where this involved the interpolation of pre-determined surfaces containing collision outputs corresponding to stiffness changes. In the two-vehicle case, the bilinear one lumped mass (per vehicle) model (either nodal or modal) will be used, together with the stiffness control algorithm to achieve the desired outcome, i.e. the design deformation length. The use of the model directly (with a given AV laden mass and longitudinal collision velocity), allows for ease of investigation of the structural changes. Additional comparisons, including the clock time of the two-approaches, will allow accuracy versus complexity to be gauged, i.e. interpolation of pre-determined surfaces against the dynamic bilinear model.

The stiffness change is undertaken by varying the linear stiffness component within the bilinear stiffness function, denoted $\widetilde{K}_n$, see Equation (6-5, Chapter 6), in the bilinear model. In the case of a collision between two AVs, e.g. AV_a and AV_b, changing the values of the coefficients γ_a and γ_b (i.e. $\gamma_a = \alpha_a k_a$ and $\gamma_b = \alpha_b k_b$) will affect the peak deformation and the peak acceleration of both AVs. Introducing a scaling factor, denoted ϑ_a and ϑ_b, for AV_a and AV_b, respectively, the corresponding stiffness-to-mass ratio matrix, denoted $\overline{\mathrm{K}_{ab}}$, now becomes:

$$\overline{\mathrm{K}_{ab}} = -\begin{bmatrix} \left(\frac{\vartheta_a \gamma_a}{m_a} + \eta_a |\ddot{x}_a|\right) & -\frac{k_a}{m_a} & 0 \\ -\frac{k_a}{m_c} & \frac{(k_a + k_b)}{m_c} & -\frac{k_b}{m_c} \\ 0 & -\frac{k_b}{m_b} & \left(\frac{\vartheta_b \gamma_b}{m_b} + \eta_b |\ddot{x}_b|\right) \end{bmatrix} \tag{8-1}$$

In the studies undertaken in this research, the scaling factors ϑ_a and ϑ_b take values in the range between 0-50-1.50, as in the single vehicle case considered in Chapter 7.

8.2.1 SCENARIO 1: STAGES 1, 2 AND 3 - PREDETERMING COLLISION SEVERITY AND STIFFNESS CONTROLLER

The first scenario to be considered is the AV to AV/AV collision, as initially introduced in Figure 3-2, Section 3.2.1, Chapter 3, and further illustrated in Figure 8-1. The scenario involves three AVs: Vehicle a, denoted AV_a, Vehicle b, denoted AV_b and Vehicle c, denoted AV_c. Each of the three AVs (AV_a, AV_b and AV_c) have laden mass values, denoted m_a, m_b and m_c, respectively, and collision velocity values, denoted v_a, v_b and v_c, respectively. For this particular scenario, the properties of the three AVs are given in Table 8-1, with the number of occupants, denoted N_o, on-board each AV also included.

Algorithm 8-1: *Stiffness Controller Algorithm for the Two-Vehicle Case*

1. Estimate/measure the two colliding AV's collision velocities (v_a and $v_{b/c}$) and laden masses (m_a and $m_{b/c}$)
2. Use the two-vehicle bilinear model (or pre-stored values on surfaces and interpolated using fuzzy logic, as in Algorithm 7-1, in Chapter 7) to pre-determine the collision properties of each AV, i.e. peak deformation, peak head acceleration and peak chest acceleration
3. If the peak deformation of AV_a collision into AV_b/ $AV_c$are above the design deformation, then stiffen, and using the bilinear model, run ϑ_a and ϑ_b values of 1.0: 0.01: 1.5
4. If the peak deformation of AV_a collision into AV_b/ AV_c are below the design deformation, then soften, and using the bilinear model, run ϑ_a and ϑ_b values of 0.5: 0.01: 1.0
5. Find the ϑ_a and ϑ_b values that give the closest match (without exceeding) the design deformation value, i.e. $0.5900m$
6. Based on Step 5., determine the structural stiffness change values for each of the colliding AVs
7. Use Algorithm 7-2 (Chapter 7) to determine the collision injury severity levels between the colliding AVs for the passive and active cases

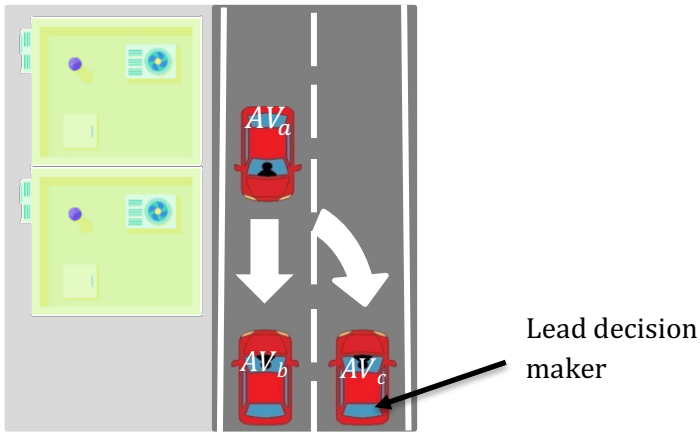

Figure 8-1: *Illustrating the Lead Decision Maker (Host) Autonomous Vehicle (on the bottom right AV_c) Making a Decision Between which AV, AV_a Collides into, i.e. itself AV_c or AV_b*

Table 8-1: *Scenario 1 - Multiple Autonomous Vehicle Collision Properties*

	Mass, m_a [kg]	**Velocity, v_a [m/s]**	**Number, N_o, of occupants on-board**
Vehicle a, AV_a	1247	15.6464 ($35mph$)	1
Vehicle b, AV_b	1402	16.5405($37mph$)	2
Vehicle c, AV_c	1532	12.5171 (28mph)	3

8.2.1.1 STAGE 1: PRE-DETERMINING COLLISION PROPERTIES

In Section 7.1, Chapter 7, the background into predetermining the collision properties for a single AV collision into an immovable rigid wall (IRW) was detailed. Here, the same process is now followed for the multiple AV collisions. Algorithm 7-1 (using fuzzy logic) detailed in Chapter 7, and the bilinear two-vehicle collision model detailed in Chapter 6, are used to pre-determine the collision properties for each AV, with the results obtained from both methods being compared. The pre-determined collision properties from Scenario 1 are detailed in Table 8-2 (AV_a collision into AV_b) and Table 8-3 (AV_a collision into AV_c). Considering Table 8-2, Rows 1 and 3 detail the results obtained from Algorithm 7-1 for AV_a and AV_b, respectively, and Rows 2 and 4 detail the results obtained directly from the two-vehicle bilinear collision model for AV_a and AV_b, respectively. Similarly, considering Table 8-3, Rows 1 and 3 detail the results obtained from

Algorithm 7-1 for AV_a and AV_c, respectively, and Rows 2 and 4 detail the results obtained directly from the two-vehicle bilinear collision model for AV_a and AV_c, respectively.

As discussed in Section 4.4.2.3, Chapter 4, the least vulnerable AV becomes the lead decision-maker, thus communicates with the other AVs to decide on the collision outcome. Consequently, based on the pre-determined collision properties for Scenario 1, detailed in Tables 8-2 and 8-3, it may be deduced that the least vulnerable AV is AV_c. It exhibits the properties of lowest peak deformation, peak chest acceleration and peak head acceleration. As such, AV_c is taken here, therefore, as the lead decision-maker, or host, as illustrated in Figure 8-1.

In Tables 8-2 and 8-3, the values given in the square bracket detail the percentage difference in results obtained from Algorithm 7-1 using fuzzy logic and those obtained from the two-vehicle bilinear collision model. As in Chapter 7, the percentage difference is obtained from:

$$\left(\frac{A - B}{A}\right) * 100\%$$

where A and B denote the results obtained from Algorithm 7-1 combined with fuzzy logic and the direct use of the bilinear model, respectively.

The lowest percentage difference is that of peak deformation (0.94%) involving the collision of AV_a and AV_c. The highest percentage difference is that of peak head acceleration (2.20%) involving the collision of AV_a and AV_b. The percentage difference between the results obtained from Algorithm 7-1 using fuzzy logic and the two-vehicle bilinear collision model are considered to be small, and therefore, support the justification of using either method.

Note from Tables 8-2 and 8-3, as to be expected, the peak deformations of the two colliding vehicles are identical. This is due to both vehicles having the same stiffness values and are subject to a common force which is identical in magnitude.

Table 8-2: *Use of the Fuzzy Logic (Algorithm 7-1) and the Bilinear Two Vehicle Collision Model to Determine the Pre-determined Collison Outcomes for* AV_a and AV_b

	Peak deformation, $\boldsymbol{\delta_a}$ $[\boldsymbol{m}]$	**Peak chest acceleration,** $\boldsymbol{a_{a_C}}$ $\boldsymbol{[g]}$	**Peak head acceleration,** $\boldsymbol{a_{a_H}}$ $\boldsymbol{[g]}$
AV_a Vehicle a (Fuzzy logic, Algorithm 7.1)	0.5954	50.30	63.74
AV_a Vehicle a (Bilinear model)	0.5896 [0.97%]	49.20 [2.19%]	62.34 [2.20%]
AV_b Vehicle b (Fuzzy logic, Algorithm 7.1)	0.5954	44.46	56.34
AV_b Vehicle b (Bilinear model)	0.5896 [0.97%]	43.76 [1.57%]	55.45 [1.58%]

Table 8-3: *Use of the Fuzzy Logic (Algorithm 7-1) and the Bilinear Two Vehicle Collision Model to Determine the Pre-determined Collison Outcomes for* AV_a and AV_c

	Peak deformation, $\boldsymbol{\delta_a}$ $[\boldsymbol{m}]$	**Peak chest acceleration,** $\boldsymbol{a_{a_C}}$ $\boldsymbol{[g]}$	**Peak head acceleration,** $\boldsymbol{a_{a_H}}$ $\boldsymbol{[g]}$
AV_a Vehicle a (Fuzzy logic, Algorithm 7.1)	0.5429	42.73	54.14
AV_a Vehicle a (Bilinear model)	0.5378 [0.94%]	41.82 [2.13%]	53.00 [2.11%]
AV_c Vehicle c (Fuzzy logic, Algorithm 7.1)	0.5429	34.57	43.80
AV_c Vehicle c (Bilinear model)	*0.5378* [0.94%]	*34.04* [1.53%]	*43.14* [1.51%]

8.2.1.2 STAGE 2: PRE-DETERMINED COLLISION INJURY SEVERITY LEVELS

In Section 7.2.2, Chapter 7, the background into predetermining the collision injury severity levels for a single AV collision into an IRW was detailed. Here the same process is again followed for the multiple AV collisions. Hence, Algorithm 7-2 in Chapter 7 is used to determine the collision injury severity levels, i.e. determining to which fuzzy sets the pre-determined collision properties lie within together with their corresponding degrees of membership.

Considering the collision properties in Table 8-2 (for the case of the bilinear model) between AV_a and AV_b, the collision injury severity levels for AV_a are given by:

$$x_{S_{AV_a}} := \begin{bmatrix} \mu_{\delta_C}(\delta_a) & \mu_{\delta_B}(\delta_a) \\ \mu_{a_{H_D}}(a_{H_a}) & \mu_{a_{H_C}}(a_{H_a}) \\ \mu_{a_{C_D}}(a_{C_a}) & \mu_{a_{C_C}}(a_{C_a}) \end{bmatrix} := \begin{bmatrix} 0.923 & 0.077 \\ 0.215 & 0.785 \\ 0.216 & 0.784 \end{bmatrix} \tag{8-2}$$

and the collision injury severity levels for AV_b are given by:

$$x_{S_{AV_b}} := \begin{bmatrix} \mu_{\delta_C}(\delta_b) & \mu_{\delta_B}(\delta_b) \\ \mu_{a_{H_D}}(a_{H_b}) & \mu_{a_{H_C}}(a_{H_b}) \\ \mu_{a_{C_D}}(a_{C_b}) & \mu_{a_{C_C}}(a_{C_b}) \end{bmatrix} := \begin{bmatrix} 0.923 & 0.077 \\ 0.502 & 0.498 \\ 0.503 & 0.497 \end{bmatrix} \tag{8-3}$$

In the case of the above, due to the differences in the laden mass values, the injury severity levels of AV_a (peak head acceleration and peak chest acceleration) are slightly higher than that of AV_b, although they do both belong to the same fuzzy sets, i.e. C to D.

Considering the collision properties in Table 8-3 between AV_a and AV_c, the collision injury severity levels for AV_a are given by:

$$x_{S_{AV_a}} \coloneqq \begin{bmatrix} \mu_{\delta_D}(\delta_a) & \mu_{\delta_C}(\delta_a) \\ \mu_{a_{H_D}}(a_{H_a}) & \mu_{a_{H_C}}(a_{H_a}) \\ \mu_{a_{C_D}}(a_{C_a}) & \mu_{a_{C_C}}(a_{C_a}) \end{bmatrix} \coloneqq \begin{bmatrix} 0.258 & 0.742 \\ 0.604 & 0.396 \\ 0.605 & 0.395 \end{bmatrix} \quad (8\text{-}4)$$

and the collision injury severity levels for AV_c are given by:

$$x_{S_{AV_c}} \coloneqq \begin{bmatrix} \mu_{\delta_D}(\delta_c) & \mu_{\delta_C}(\delta_c) \\ \mu_{a_{H_E}}(a_{H_c}) & \mu_{a_{H_D}}(a_{H_c}) \\ \mu_{a_{C_E}}(a_{C_c}) & \mu_{a_{C_D}}(a_{C_c}) \end{bmatrix} \coloneqq \begin{bmatrix} 0.258 & 0.742 \\ 0.015 & 0.985 \\ 0.016 & 0.984 \end{bmatrix} \quad (8\text{-}5)$$

In the case of the above, due to the differences in the laden mass values, the injury severity levels of AV_a (peak head acceleration and peak chest acceleration) are higher, and belong to the fuzzy sets C to D, whereas those for AV_c belong to fuzzy sets D to E.

Comparing collision injury severity levels from (AV_a colliding into V_b / AV_c), it is revealed that the collision outcomes for AV_aalways result in the highest injury severity.

8.2.1.3 STAGE 3: STIFFNESS CONTROLLER

Algorithm 8-1 (active stiffness controller) has been applied to this example to improve (i.e. reduce) the collision injury severity of all the AVs involved. The results which are obtained from Algorithm 8-1 for the AV_a collision into AV_b and for the AV_a collision into AV_c are given in Tables 8-4 and 8-5, respectively.

The results in Table 8-4 correspond to a case where the stiffness controller does not alter the stiffness (i.e. stiffness change coefficient, $\vartheta_a = \vartheta_b = 1$). Hence, the results are identical to those presented in Table 8-2 (Rows 2 and 4), and, as expected, the active and pre-determined passive collision injury severity levels for both vehicles also remain unchanged, i.e.

$$\tilde{x}_{S_{AV_a}} \coloneqq \begin{bmatrix} \mu_{\delta_C}(\delta_a) & \mu_{\delta_B}(\delta_a) \\ \mu_{a_{H_D}}(a_{H_a}) & \mu_{a_{H_C}}(a_{H_a}) \\ \mu_{a_{C_D}}(a_{C_a}) & \mu_{a_{C_C}}(a_{C_a}) \end{bmatrix} \coloneqq \begin{bmatrix} 0.923 & 0.077 \\ 0.215 & 0.785 \\ 0.216 & 0.784 \end{bmatrix} \tag{8-6}$$

$$\tilde{x}_{S_{AV_b}} \coloneqq \begin{bmatrix} \mu_{\delta_C}(\delta_b) & \mu_{\delta_B}(\delta_b) \\ \mu_{a_{H_D}}(a_{H_b}) & \mu_{a_{H_C}}(a_{H_b}) \\ \mu_{a_{C_D}}(a_{C_b}) & \mu_{a_{C_C}}(a_{C_b}) \end{bmatrix} \coloneqq \begin{bmatrix} 0.923 & 0.077 \\ 0.502 & 0.498 \\ 0.503 & 0.497 \end{bmatrix} \tag{8-7}$$

The alternative collision path is now detailed, i.e. AV_a colliding into AV_c, where the active results are given in Table 8-5 and compared to the passive results (given in Table 8-3). The active stiffness control algorithm has reduced the structural stiffness, giving a stiffness change coefficient, $\vartheta_a = \vartheta_b = 0.80$. Softening of the collision structures of both colliding AVs allows the additional design deformation capacity to be taken up, thus resulting in lower peak head and chest acceleration values.

This active control has resulted in a change to the pre-determined collision injury severity levels for AV_a, given by:

$$\tilde{x}_{S_{AV_a}} \coloneqq \begin{bmatrix} \mu_{C}(\delta_a) & \mu_{\delta_B}(\delta_a) \\ \mu_{a_{H_D}}(a_{H_a}) & \mu_{a_{H_C}}(a_{H_a}) \\ \mu_{a_{C_D}}(a_{C_a}) & \mu_{a_{C_C}}(a_{C_a}) \end{bmatrix} \coloneqq \begin{bmatrix} 0.928 & 0.072 \\ 0.739 & 0.261 \\ 0.740 & 0.260 \end{bmatrix} \tag{8-8}$$

and for AV_c given by:

$$\tilde{x}_{S_{AV_c}} \coloneqq \begin{bmatrix} \mu_{\delta_C}(\delta_c) & \mu_{\delta_B}(\delta_c) \\ \mu_{a_{H_E}}(a_{H_c}) & \mu_{a_{H_D}}(a_{H_c}) \\ \mu_{a_{C_E}}(a_{C_c}) & \mu_{a_{C_D}}(a_{C_c}) \end{bmatrix} \coloneqq \begin{bmatrix} 0.929 & 0.072 \\ 0.125 & 0.875 \\ 0.125 & 0.875 \end{bmatrix} \tag{8-9}$$

where, as discussed, the peak deformation collision injury severity has increased, but within the limits. Moreover, the peak head acceleration and peak chest acceleration values have been reduced. These results are evident by comparing Tables 8-3 and 8-5.

The clock time for the computations in Scenario 1 for the bilinear dynamic model and interpolation and fuzzy logic are compared, for the case of the AV_a collision into AV_b. The simulation is undertaken using an Intel Core i5-8350U processor (speed of $1.70GHz$). Algorithm 8-1 took 258 seconds to run the simulation using the bilinear model compared to the interpolation and fuzzy logic approach which took 0.9 seconds. This justifies using the fuzzy logic approach if used on-board an AV in real-time.

Table 8-4: *Scenario 1 Results (AV_a collision into AV_b) from Applying the Stiffness Controller Algorithm*

	Peak deformation, δ_a [m]	**Peak chest acceleration, a_{a_C} [g]**	**Peak head acceleration, a_{a_H} [g]**
AV_a, Vehicle a (Stiffness Controller, Algorithm 8-1)	0.5896	49.20	62.34
AV_b Vehicle b (Stiffness Controller, Algorithm 8-1)	0.5896	43.76	55.45

Table 8-5: *Scenario 1 Results (AV_a collision into AV_c) from Applying the Stiffness Controller Algorithm*

	Peak deformation, δ_a [m]	**Peak chest acceleration, a_{a_C} [g]**	**Peak head acceleration, a_{a_H} [g]**
AV_a Vehicle a (Stiffness Controller, Algorithm 8-1)	0.5888	39.2663	49.7562
AV_c Vehicle c (Stiffness Controller, Algorithm 8-1)	0.5888	31.9615	40.4999

8.2.2 SCENARIO 2: STAGE 1, 2 AND 3 - PREDETERMING COLLISION SEVERITY AND STIFFNESS CONTROLLER

In contrast to Scenario 1 in Section 8.2.1 of the AV to AV/AV collision investigations, a further scenario (Scenario 2) is now presented, as illustrated in Figure 8-2. For Scenario 2, the properties of the three AVs are given in Table 8-6, with the number of occupants on-board each AV also being included.

8.2.2.1 STAGE 1: PRE-DETERMINING COLLISION PROPERTIES

As with Scenario 1 in Section 8.2.1.1, Algorithm 7-1 (using fuzzy logic) and the two-vehicle collision bilinear model (developed in Chapter 6) are used to pre-determine the collision properties of each AV, with the results from both methods again being compared.

The pre-determined collision properties from Scenario 2 are detailed in Table 8-7 for (AV_a and AV_b) and Table 8-8 for (AV_a and AV_c). Table 8-7, Rows 1 and 3 detail the results obtained from Algorithm 7-1 using fuzzy logic for AV_a and AV_b, respectively, and Rows 2 and 4 detail the results obtained from the two-vehicle bilinear collision model for AV_a and AV_b, respectively. Similarly, considering Table 8-8, Rows 1 and 3 detail the results obtained from Algorithm 7-1 using fuzzy logic for AV_a and AV_c, respectively, and again Rows 2 and 4 detail the results obtained directly from the two-vehicle bilinear collision model for AV_a and AV_c, respectively.

In Scenario 2, AV_b is found to be the least vulnerable AV, see results in Tables 8-7 and 8-8, i.e. it has the lowest peak deformation, and lowest peak head and chest accelerations. Consequently, the least vulnerable AV, namely AV_b is taken as the lead decision maker in this scenario, as illustrated in Figure 8-2.

In Tables 8-7 and 8-8, the value in the square bracket details the percentage difference between the results obtained from Algorithm 7-1 using fuzzy logic and the results obtained from the two-vehicle bilinear collision model. The lowest percentage difference is that for peak deformation (0.81%) involving the collision of AV_a and AV_c , see Table 8-8. The highest percentage difference is that of peak chest acceleration (1.76%) involving the collision of AV_a and AV_b , see Table 8-7. Again with this scenario, the percentage differences between the use of Algorithm 7-1 using fuzzy logic and the two-vehicle bilinear collision model are considered to be small, and justify using either of these methods.

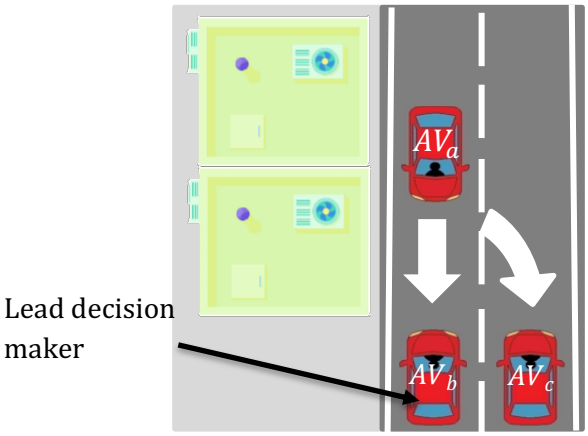

Figure 8-2: *Illustrating the Lead Decision Maker (Host) Autonomous Vehicle AV_b (on the bottom right) Making a Decision Between which AV, AV_a Collides into, i.e. either itself AV_b or AV_c*

Table 8-6: *Scenario 2: Multiple Autonomous Vehicle Collision Properties*

	Mass, m_a [kg]	**Velocity, v_a [m/s]**	**Number, N_o, of occupants on-board**
Vehicle a, AV_a	1247	15.6464 (35mph)	1
Vehicle b, AV_b	1632	11.6230 (26mph)	1
Vehicle c, AV_c	1684	23.6931 (53mph)	5

Table 8-7: *Use of the Fuzzy Logic (Algorithm 7-1) and the Bilinear Two Vehicle Collision Model to Determine the Pre-determined Collison Outcomes for AV_a and AV_b*

	Peak deformation, δ_a [m]	**Peak chest acceleration, a_{a_C} [g]**	**Peak head acceleration, a_{a_H} [g]**
AV_a, Vehicle a (Fuzzy logic, Algorithm 7-1)	0.5341	41.49	52.55
AV_a, Vehicle a (Bilinear model)	0.5297 [0.82%]	40.76 [1.76%]	51.65 [1.71%]
AV_b, Vehicle b (Fuzzy logic, Algorithm 7-1))	0.5341	31.53	39.95
AV_b, Vehicle b (Bilinear model)	0.5297 [0.82%]	31.15 [1.21%]	39.47 [1.20%]

Table 8-8: *Use of the Fuzzy Logic (Algorithm 7-1) and the Bilinear Two Vehicle Collision Model to Determine the Pre-determined Collison Outcomes for AV_a and AV_c*

	Peak deformation, δ_a [m]	**Peak chest acceleration, a_{a_C} [g]**	**Peak head acceleration, a_{a_H} [g]**
AV_a, Vehicle a (Fuzzy logic, Algorithm 7-1)	0.7049	70.52	89.36
AV_a, Vehicle a (Bilinear model)	0.7106 [0.81%]	71.50 [1.39%]	90.61 [1.40%]
AV_c, Vehicle c (Fuzzy logic, Algorithm 7-1))	0.7049	52.27	66.24
AV_c, Vehicle c (Bilinear model	0.7049 [0.81%]	52.95 [1.30%]	67.09 [1.28%]

8.2.2.2 STAGE 2: PRE-DETERMINED COLLISION INJURY SEVERITY LEVELS

As in Section 8.2.1.2, Algorithm 7-2 in Chapter 7 is now used to determine the collision injury severities for Scenario 2, i.e. determining in which fuzzy sets the pre-determined collision properties lie in and their corresponding degrees of membership.

Considering the collision properties in Table 8-7 involving AV_a and AV_b, the collision injury severity levels for AV_a are given by:

$$x_{S_{AV_a}} = \begin{bmatrix} \mu_{\delta_l}(\delta_a) & \mu_{\delta_h}(\delta_a) \\ \mu_{a_{H_l}}(a_{H_a}) & \mu_{a_{H_h}}(a_{H_a}) \\ \mu_{a_{C_l}}(a_{C_a}) & \mu_{a_{C_h}}(a_{C_a}) \end{bmatrix} := \begin{bmatrix} \mu_{\delta_D}(\delta_a) & \mu_{\delta_C}(\delta_a) \\ \mu_{a_{H_D}}(a_{H_a}) & \mu_{a_{H_C}}(a_{H_a}) \\ \mu_{a_{C_D}}(a_{C_a}) & \mu_{a_{C_C}}(a_{C_a}) \end{bmatrix} := \begin{bmatrix} 0.310 & 0.690 \\ 0.660 & 0.340 \\ 0.661 & 0.339 \end{bmatrix}$$

and the collision injury severity levels for AV_b are given by:

$$x_{S_{AV_b}} = \begin{bmatrix} \mu_{\delta_l}(\delta_b) & \mu_{\delta_h}(\delta_b) \\ \mu_{a_{H_l}}(a_{H_b}) & \mu_{a_{H_h}}(a_{H_b}) \\ \mu_{a_{C_l}}(a_{C_b}) & \mu_{a_{C_h}}(a_{C_b}) \end{bmatrix} := \begin{bmatrix} \mu_{\delta_D}(\delta_b) & \mu_{\delta_C}(\delta_b) \\ \mu_{a_{H_E}}(a_{H_b}) & \mu_{a_{H_D}}(a_{H_b}) \\ \mu_{a_{C_E}}(a_{C_b}) & \mu_{a_{C_D}}(a_{C_b}) \end{bmatrix} := \begin{bmatrix} 0.310 & 0.690 \\ 0.168 & 0.832 \\ 0.168 & 0.832 \end{bmatrix}$$

In Scenario 2, similar to Scenario 1, the injury severity levels for peak head and peak chest accelerations differ for AV_a and AV_b (i.e. they are higher, for AV_a and belong to the fuzzy sets C to D, whereas those for AV_b belong to the fuzzy sets D to E).

The collision properties in Table 8-8 detail the AV_a and AV_c collision injury severity levels. For AV_a, these are given by:

$$x_{S_{AV_a}} = \begin{bmatrix} \mu_{\delta_l}(\delta_a) & \mu_{\delta_h}(\delta_a) \\ \mu_{a_{H_l}}(a_{H_a}) & \mu_{a_{H_h}}(a_{H_a}) \\ \mu_{a_{C_l}}(a_{C_a}) & \mu_{a_{C_h}}(a_{C_a}) \end{bmatrix} := \begin{bmatrix} \mu_{\delta_C}(\delta_a) & \mu_{\delta_B}(\delta_a) \\ \mu_{a_{H_C}}(a_{H_a}) & \mu_{a_{H_B}}(a_{H_a}) \\ \mu_{a_{C_C}}(a_{C_a}) & \mu_{a_{C_B}}(a_{C_a}) \end{bmatrix} := \begin{bmatrix} 0.141 & 0.859 \\ 0.037 & 0.963 \\ 0.0385 & 0.9615 \end{bmatrix}$$

and the collision injury severity levels for AV_c are given by:

$$x_{S_{AV_c}} = \begin{bmatrix} \mu_{\delta_l}(\delta_c) & \mu_{\delta_h}(\delta_c) \\ \mu_{a_{H_l}}(a_{H_c}) & \mu_{a_{H_h}}(a_{H_c}) \\ \mu_{a_{C_l}}(a_{C_c}) & \mu_{a_{C_h}}(a_{C_c}) \end{bmatrix} := \begin{bmatrix} \mu_{\delta_C}(\delta_c) & \mu_{\delta_B}(\delta_c) \\ \mu_{a_{H_D}}(a_{H_c}) & \mu_{a_{H_C}}(a_{H_c}) \\ \mu_{a_{C_D}}(a_{C_c}) & \mu_{a_{C_C}}(a_{C_c}) \end{bmatrix} := \begin{bmatrix} 0.141 & 0.859 \\ 0.017 & 0.983 \\ 0.018 & 0.982 \end{bmatrix}$$

Again as in the case above, the injury severity levels in terms of peak head acceleration and peak chest acceleration differ between the occupants of the two AVs. The higher values of AV_abelong to the fuzzy sets B to C, whereas for AV_c they belong to sets C to D. It is observed that the peak accelerations (head and chest) for AV_a colliding into either AV_b *or* AV_c A are of a higher injury severity. This is due to the lower mass value of V_a.

8.2.2.3 STAGE 3: STIFFNESS CONTROLLER

Algorithm 8-1 (active stiffness controller) is again applied to improve (i.e. reduce) the collision injury severity of all the AVs involved. The results from the collision of AV_a into AV_b are given in Table 8-9, and can be compared to passive results in Table 8-7. Use of

active stiffness control has resulted in a softening of the structure (i.e. via a stiffness change coefficient, $\vartheta_a = \vartheta_b = 0.77$), giving the following active pre-determined collision injury severity levels for AV_a:

$$\tilde{x}_{S_{AV_a}} = \begin{bmatrix} \mu_{\delta_l}(\delta_a) & \mu_{\delta_h}(\delta_a) \\ \mu_{a_{H_l}}(a_{H_a}) & \mu_{a_{H_h}}(a_{H_a}) \\ \mu_{a_{C_l}}(a_{C_a}) & \mu_{a_{C_h}}(a_{C_a}) \end{bmatrix} \coloneqq \begin{bmatrix} \mu_{\delta_C}(\delta_a) & \mu_{\delta_B}(\delta_a) \\ \mu_{a_{H_D}}(a_{H_a}) & \mu_{a_{H_C}}(a_{H_a}) \\ \mu_{a_{C_D}}(a_{C_a}) & \mu_{a_{C_C}}(a_{C_a}) \end{bmatrix} \coloneqq \begin{bmatrix} 0.926 & 0.074 \\ 0.815 & 0.185 \\ 0.815 & 0.185 \end{bmatrix}$$

and for AV_b, given by:

$$\tilde{x}_{S_{AV_b}} = \begin{bmatrix} \mu_{\delta_l}(\delta_b) & \mu_{\delta_h}(\delta_b) \\ \mu_{a_{H_l}}(a_{H_b}) & \mu_{a_{H_h}}(a_{H_b}) \\ \mu_{a_{C_l}}(a_{C_b}) & \mu_{a_{C_h}}(a_{C_b}) \end{bmatrix} \coloneqq \begin{bmatrix} \mu_{\delta_C}(\delta_b) & \mu_{\delta_B}(\delta_b) \\ \mu_{a_{H_E}}(a_{H_b}) & \mu_{a_{H_D}}(a_{H_b}) \\ \mu_{a_{C_E}}(a_{C_b}) & \mu_{a_{C_D}}(a_{C_b}) \end{bmatrix} \coloneqq \begin{bmatrix} 0.926 & 0.074 \\ 0.286 & 0.714 \\ 0.286 & 0.714 \end{bmatrix}$$

where, again as expected, the peak deformation has increased, taking up the available capacity, with the peak head and chest accelerations reducing, hence reducing severity.

The active case results from the alternative collision path, i.e. AV_a colliding into AV_c, are given in Table 8-10 and compared to the passive results (given in Table 8-8). In this example, the peak deformation has exceeded the design deformation value, hence the active control algorithm has resulted in the stiffening of the collision structures of both colliding AVs (i.e. stiffness change coefficient, $\vartheta_a = \vartheta_c = 1.50$). The effect of stiffening the collision structures has resulted in a reduced peak deformation, but it has still breached the design deformation. The stiffness change has also resulted in peak head acceleration and peak chest acceleration of the occupant in AV_a going far beyond the US Federal Motor Vehicle Safety Standard (FMVSS) test limits (although this was also violated in the passive case). However, for AV_c the peak head acceleration and peak chest

acceleration of the five occupants are within the US FMVSS test limits. Overall, the collision scenario has been worsened for AV_a and improved for AV_c, as is evidenced by the active pre-determined collision injury severity levels, i.e. for AV_a given by:

$$\tilde{x}_{S_{AV_a}} = \begin{bmatrix} \mu_{\delta_l}(\delta_a) & \mu_{\delta_h}(\delta_a) \\ \mu_{a_{H_l}}(a_{H_a}) & \mu_{a_{H_h}}(a_{H_a}) \\ \mu_{a_{C_l}}(a_{C_a}) & \mu_{a_{C_h}}(a_{C_a}) \end{bmatrix} := \begin{bmatrix} \mu_{\delta_C}(\delta_a) & \mu_{\delta_B}(\delta_a) \\ \mu_{a_{H_B}}(a_{H_a}) & \mu_{a_{H_A}}(a_{H_a}) \\ \mu_{a_B}(a_{C_a}) & \mu_{a_{C_A}}(a_{C_a}) \end{bmatrix} := \begin{bmatrix} 0.803 & 0.197 \\ 0.685 & 0.315 \\ 0.686 & 0.314 \end{bmatrix}$$

and for AV_c given by:

$$\tilde{x}_{S_{AV_c}} = \begin{bmatrix} \mu_{\delta_l}(\delta_c) & \mu_{\delta_h}(\delta_c) \\ \mu_{a_{H_l}}(a_{H_c}) & \mu_{a_{H_h}}(a_{H_c}) \\ \mu_{a_{C_l}}(a_{C_c}) & \mu_{a_{C_h}}(a_{C_c}) \end{bmatrix} := \begin{bmatrix} \mu_{\delta_C}(\delta_c) & \mu_{\delta_B}(\delta_c) \\ \mu_{a_{H_C}}(a_{H_c}) & \mu_{a_{H_B}}(a_{H_c}) \\ \mu_{a_{C_C}}(a_{C_c}) & \mu_{a_{C_B}}(a_{C_c}) \end{bmatrix} := \begin{bmatrix} 0.803 & 0.197 \\ 0.756 & 0.244 \\ 0.757 & 0.243 \end{bmatrix}$$

Table 8-9: *Scenario 2 Results (AV_a collision into AV_b) from Applying the Stiffness Controller Algorithm*

	Peak deformation, δ_a $[m]$	**Peak chest acceleration, a_{a_C} $[g]$**	**Peak head acceleration, a_{a_H} $[g]$**
AV_a, Vehicle a (Stiffness Controller, Algorithm 8-1)	0.5892	37.8380	47.9464
AV_b, Vehicle b (Stiffness Controller, Algorithm 8-1)	0.5892	28.9118	36.6355

Table 8-10: *Scenario 2 Results (AV_a collision into AV_c) from Applying the Stiffness Controller Algorithm*

	Peak deformation, δ_a $[m]$	**Peak chest acceleration, a_{a_C} $[g]$**	**Peak head acceleration, a_{a_H} $[g]$**
AV_a, Vehicle a (Stiffness Controller, Algorithm 8-1)	0.6082	78.1813	99.0673
AV_c, Vehicle c (Stiffness Controller, Algorithm 8-1)	0.6082	57.8926	73.3585

8.3 STAGE 4: COLLISION TARGET SELECTON

The various EDM algorithms for collision target selection are now detailed in the case of AV to AV/AV collisions. The EDM philosophical algorithms to be evaluated are based on the deontological and utilitarian doctrines of Kant and Bentham, respectively, and those founded on the social actions based on altruism and selfishness.

8.3.1 COLLISION TARGET ALGORITHMS

The four collision target selection algorithms involving the philosophical approaches and social actions are outlined as follows.

8.3.1.1 UTILITARIAN (BENTHAM) ALGORITHM

The utilitarian algorithm for the AV to AV/AV approach involves saving as many lives as possible, as discussed in Section 2.4, Chapter 2. This may involve the AVs changing their own 'natural' path in order to potentially save a greater number of lives, this being for the greater good. The utilitarian approach is detailed in Algorithm 8-2, with the aim to save as many lives as possible in the case of AV to AV/AV collisions. Note that even in the case that no lives are lost, but lives are at risk, reducing the overall injury severity level, hence utility cost, becomes the goal of the utilitarian approach.

As with the single-vehicle utilitarian algorithm detailed in Section 7.4.1.3, Chapter 7, the algorithm begins by evaluating the number of occupants on-board the AVs. In the three

AV collision case, N_{a_o}, N_{b_o} and N_{c_o} denote the number of occupants on-board AVs, AV_a, AV_b and AV_c, respectively. Step 2 of Algorithm 8-2 then involves each AV evaluating the three injury severity features, e.g. of AV_a colliding into either AV_b or AV_c, and determining, e.g. for AV_a the peak deformation δ_a, peak head acceleration a_{H_a} and peak chest acceleration a_{C_a}. Steps 2 to 5 then involve determining the overall utility cost of lives at risk for each of the contributing collision features of the three colliding AVs. Step 6 then involves obtaining an overall utility cost combining the three injury severities of the occupant(s), i.e. peak head and chest accelerations and peak deformation. This is achieved by utilisation of a Euclidean norm-based approach to determine an overall utility cost metric. The utility of cost of lives at risk (in this example, for AV_A) is given by the following Euclidean cost metric when the peak deformation is less than or equal to the design deformation length ($0.5900m$), and potential for active softening is possible, as introduced in Chapter 7, Equation (7-59):

$$\varepsilon_{softening} = \sqrt{\acute{\eta}\left(a_{H_a}\right)^2 + \acute{\eta}\left(a_{C_a}\right)^2} \tag{8-10}$$

and when the peak deformation is above the design deformation length ($0.5900m$), and potential for active stiffening is possible, see Chapter 7, Equation (7-60)

$$\varepsilon_{stiffening} = \sqrt{\acute{\eta}(\delta_a)^2 + \acute{\eta}\left(a_{H_a}\right)^2 + \acute{\eta}\left(a_{C_a}\right)^2} \tag{8-11}$$

Step 7, then involves the lead decision-maker AV either commanding the other AVs or itself to steer into the path resulting in the lowest utility cost to society.

As highlighted in the single-vehicle utilitarian algorithm, a further detailed study of the occupants should be taken into account, e.g. sex, age, health and social status. It is expected that such properties would significantly influence the final target selection.

8.3.1.2 DEONTOLOGICAL (KANT) ALGORITHM

As discussed in Section 2.3.2, Chapter 2, the deontological approach applied to the selection of an AV to AV/AV collision would ensure the AV follows its natural path. This is undertaken without any intention to change paths nor to potentially save lives. Algorithm 8-3 describes the deontological approach.

Algorithm 8-2: *Utilitarian (Bentham) Algorithm for Autonomous Vehicle Collision Target*

1. Determine number of occupants, denoted N_o on-board AVs: AV_a, AV_b and AV_c (i.e. N_{o_a}, N_{o_b} and N_{o_c})
2. For AVs AV_a, AV_b and AV_c, use Algorithm 7-2 (Chapter 7), to obtain the collision injury severity, i.e. degree of membership to the fuzzy sets A, B, C, D and E for the four features, i.e. peak deformation δ_a, peak head acceleration a_{H_a} and peak chest acceleration $a_{C_a}(u_{f_l}(f)$ denotes the lower member function and $u_{f_h}(f)$ denotes the higher membership function, where f is used as a general subscript to represent the four feature indices).
3. For each AV (AV_a, AV_b and AV_c), assign an ID number, denoted n, where n is based on the membership to the higher, denoted n_h and lower bounds, denoted n_l (i.e. $A \rightarrow 5$, $B \rightarrow 4$, $C \rightarrow 3$, $D \rightarrow 2$ and $E \rightarrow 1$) for each of the contributing occupant injury severities
4. For each AV (AV_a, AV_b and AV_c), determine the overall utility cost of lives at risk for the three AVs using the following equations:

$$\acute{\eta}_f = \left(N_{f_h}\left(u_{f_h}(f)\right) + N_{f_l}\left(u_{f_l}(f)\right)\right)N_o$$

where $N_{f_h} = \left(n_{f_h}!\right)^2$ and $N_{f_l} = \left(n_{f_l}!\right)^2$

in which $\acute{\eta}_f$ takes the form $\acute{\eta}(\delta_a)$, $\acute{\eta}(a_{h_a})$ and $\acute{\eta}(a_{c_a})$.

5. Apply the following rules:
   - If the deformation is less than or equal to the design deformation length (i.e. 0.5900m), and there is potential for softening to take up available capacity the utility cost of lives at risk is determined using the following Euclidean metric: $\varepsilon_{softening} = \sqrt{\acute{\eta}\left(a_{H_a}\right)^2 + \acute{\eta}\left(a_{C_a}\right)^2}$
   - If the deformation is above the design deformation length (i.e. 0.5900m), and there is potential for stiffening to reduce deformation the utility cost of lives at risk is determined using the following Euclidean metric: $\varepsilon_{stiffening} = \sqrt{\acute{\eta}(\delta_a)^2 + \acute{\eta}\left(a_{H_a}\right)^2 + \acute{\eta}\left(a_{C_a}\right)^2}$
6. Steer into the path to avoid the largest overall utility cost of lives at risk – i.e. command AVs to steer into the path of least utility cost to society.

Algorithm 8-3: *Deontological (Kant) Algorithm for Autonomous Vehicle Collision Target*

1. Whether or not an AV is to be involved in an unavoidable collision with another AV, do not change the existing course/route

8.3.1.3 ALTRUISTIC (SOCIAL ACTION) ALGORITHM

The altruistic algorithm is based on social actions, as discussed in Section 2.4, Chapter 2. In terms of the altruistic algorithm, the lead decision-maker must take action towards other AVs that places others at a benefit. By its very nature, the altruistic lead decision-maker must not gain from the action. Such a scenario is implausible in the three-way AV collision cases considered in this Chapter, as there would be no benefit to be gained. Consequently, as in a three-way human conflict scenario, the altruistic approach proves to be a non-trivial case and is not considered in this Chapter.

The above prompts an interesting area for further work which could involve an additional layer of ethical decision making to combine an altruistic approach with the active stiffness controller. In realising a further layer to the EDM an altruistic host AV could be programmed to 'sacrifice its own performance' to help another target AV in an AV to AV collision.

8.3.1.4 SELFISH (SOCIAL ACTION) ALGORITHM

As discussed in Section 2.4, Chapter 2, an act of selfishness would involve the lead decision-maker to command and implement a collision between the two other AVs involved in a potential collision. This collision scenario would be of a benefit to the lead decision-maker and of a dis-benefit to the two other AVs, hence being an act of selfishness. The selfish algorithm is detailed in Algorithm 8-4.

Algorithm 8-4: *Selfish Algorithm for Autonomous Vehicle Collision Target*

1. Always command the other two involved AVs to align for a collision

8.3.2 DECISION TARGET AND STIFFNESS CONTROLLER RESULTS

The EDM algorithm which utilises a M2D approach is now presented, whereby the stiffness control algorithm (Algorithm 8-1) is combined with the three collision target selection algorithms (Algorithms 8-2 to 8-4). To demonstrate the EDM, the scenarios are used as detailed in Table 8-1, Section 8.2.1 for Scenario 1 and Table 8-2, Section 8.2.2 for Scenario 2.

Scenarios 1 and 2 have been designed to illustrate the effectiveness of active stiffness control (both softening/stiffening being undertaken to increase/decrease the peak deformation of the design deformation value). Consequently, rather than showing several simulation examples, Scenarios 1 and 2 are taken as being representative.

8.3.2.1 QUANTIFYING THE OUTCOMES (PASSIVE AND ACTIVE)

As in Chapter 7, Section 7.4.2.1, a limit has been applied to the peak deformation, peak head acceleration and peak chest acceleration, where for each case life is potentially lost/saved. Recall that from Chapter 7, the limit for peak deformation is based on the design deformation length (i.e. $0.5900m$) and the limits for peak head and peak chest accelerations are based on the US new car assessment programme (NCAP) and US FMVSS tests, with the values being $80g$ and $60g$, respectively. Also recall from Chapter 7, Section 7.4.2.1, where, for the nominal case of an AV (Vehicle a), the limits relate to the key severity features, giving the following corresponding degrees of membership:

$$x_{S_{AV}} \coloneqq \begin{bmatrix} \mu_{\delta_C}(\delta_a) & \mu_{\delta_B}(\delta_a) \\ \mu_{a_{H_C}}(a_{H_a}) & \mu_{a_{H_B}}(a_{H_a}) \\ \mu_{a_{C_C}}(a_{C_a}) & \mu_{a_{C_B}}(a_{C_a}) \end{bmatrix} \coloneqq \begin{bmatrix} 0.920 & 0.080 \\ 0.479 & 0.521 \\ 0.646 & 0.354 \end{bmatrix}$$

Recall the above severity features, and the common utility cost unit for collision injury severity levels in Table 7-8, Section 7.4.1.1 (where previously only two occupants on-board the AV were considered). The utility cost is now to be scaled up to accommodate

for 1 – 5 occupants, see Section 8.2.1, Table 8-1 for Scenario 1 and Section 8.2.2, Table 8-6 for Scenario 2, as given in Table 8-11. Equations (7-55) to (7-57) as detailed in Chapter 7, have been used to determine the utility cost of lives at risk for the three collision features for occupants on-board each AV. Note that it is undesirable to exceed the limits, as this may lead to highly severe or fatal collision outcomes. If these limits are exceeded when considering Scenarios 1 and 2, for the three EDM algorithms, the outcomes are highlighted in bold.

Table 8-11: *Limits Applied to the Three Key Features for the Utility Cost of Lives at Risk for Two Vehicle Collisions involving 1-5 occupants*

Key Feature	**Limits - utility cost of lives at risk (1 - 5 Occupants)**				
	1	**2**	**3**	**4**	**5**
Peak deformation, $N(\delta_a)$	79.2	158.4	237.6	316.8	396.0
Peak head acceleration, $N(a_{H_a})$	317.5	634.7	952.0500	1269.4	1586.8
Peak chest acceleration, $N(a_{C_a})$	227.2	454.3	681.5	908.6	1135.8

The results for Scenario 1 in Section 8.2.1, are given in Tables 8-12 and 8-13, respectively. For this, Equations (8-2) and (8-3) have been used to determine the utility cost of lives at risk for the collisions, AV_a to AV_b and AV_a to AV_c.

Referring to Table 8-11, the three key features for AV_a collisions into AV_b and AV_c are detailed in Tables 8-12 and 8-13, respectively. Note that all these values are within the limits and so are not in bold. The active case for Scenario 1 uses Equations (8-6) to (8-7), and the resulting utility cost of lives at risk for the collisions AV_a to AV_b and AV_a to AV_c are detailed in Tables 8-14 and 8-15, respectively. Note that in the case of the AV_a to AV_b collision in Table 8-14, there is no stiffness change; with reference to Table 8-2 the deformation is already at the design value. Note that N/A (i.e. not applicable) is applied to all the peak deformation results in Tables 8-12 to 8-15, as the design deformation length has not been breached. The active stiffness control has allowed for softening of the structures in the case of collision AV_a to AV_c, with the results presented in Table 8-15.

Table 8-12: *Autonomous Vehicle Key Features for the Utility Cost of Lives at Risk for Scenario 1 Collision Between AV_a and AV_b (Passive Case) and N(Overall)*

Key Consideration/Feature	Vehicle *A*: utility cost of lives at risk	Vehicle *B*: utility cost of lives at risk
N_o – Number of pedestrians	1	2
ή (δ) – Peak deformation	N/A	N/A
ή (H_a) – Peak head accel	29.1	39.9
ή (C_a) – Peak chest accel	29.1	39.8

Table 8-13: *Autonomous Vehicle Key Features for the Utility Cost of Lives at Risk for Scenario 1 Collision Between AV_a and AV_c (Passive Case) and N(Overall)*

Key Consideration/Feature	Vehicle *A*: utility cost of lives at risk	Vehicle *C*: utility cost of lives at risk
N_o – Number of pedestrians	1	3
ή (δ) – Peak deformation	N/A	N/A
ή (H_a) – Peak head accel	16.7	11.9
ή (C_a) – Peak chest accel	16.6	11.9

Table 8-14: *Autonomous Vehicle Key Features for the Utility Cost of Lives at Risk for Scenario 1 Collision Between AV_a and AV_b (Active Case) and N(Overall)*

Key Consideration/Feature	Vehicle *A*: utility cost of lives at risk	Vehicle *B*: utility cost of lives at risk
N_o – Number of pedestrians	1	2
ή (δ) – Peak deformation	N/A	N/A
ή (H_a) – Peak head accel	29.1	39.9
ή (C_a) – Peak chest accel	29.1	39.8

Table 8-15: *Autonomous Vehicle Key Features for the Utility Cost of Lives at Risk for Scenario 1 Collision Between AV_a and AV_c (Active Case) and N(Overall)*

Key Consideration/Feature	Vehicle *A*: utility cost of lives at risk	Vehicle *C*: utility cost of lives at risk
N_o – Number of pedestrians	1	3
ή (δ) – Peak deformation	N/A	N/A
ή (H_a) – Peak head accel	12.4	10.9
ή (C_a) – Peak chest accel	12.3	10.9

The results of Scenario 2 in Section 8.2.2 are detailed in Tables 8-16 and 8-17, respectively. For this, Equations (8-4) and (8-5) have been used to determine the utility cost of lives at risk for the collisions, AV_a to AV_b and AV_a to AV_c,

Whilst it is noted that the key collision features in Table 8-16 are well within the limits given in Table 8-11, those in Table 8-17 indicate that the occupant of AV_a is at high risk of severe/fatal injury levels for all key features. The five occupants within AV_c are not at the same level of risk, however, the peak deformation does exceed the limit. The active case for Scenario 2 uses Equations (8-8) to (8-9), and the resulting utility cost of lives at

risk for the collisions AV_a to AV_b and AV_a to AV_c are detailed in Tables 8-18 and 8-19, respectively. The results of the collision between AV_a *and* AV_b are detailed in Table 8-18. This has involved the active softening of the structure, with this decreasing the peak head acceleration and peak chest accelerations. This has bought about an improvement to the collision case without exceeding the design deformation, where the overall utility cost has been reduced.

Now considering the AV_a *and* AV_c collision in Table 8-19, active stiffening has significantly reduced the peak deformation of both AV_a and AV_c, however the peak accelerations experienced by the occupants have significantly increased. Whilst deformation has decreased for AV_c it does remain excessive. The stiffness change to both AVs has resulted in an increase to the occupant's peak head accelerations and peak chest accelerations. It is interesting to note that the injury severity levels of the 5 occupants on-board of AV_c have been significantly reduced, however, this is at the expense of AV_a effectively sacrificing one occupant. Note that in the cases of Tables 8-17 and 8-19, the deformation utility cost is required to be taken into account. It is also again, noted that N/A (i.e. not applicable) is applied to the peak deformation results in Tables 8-16 and 8-18, as the design deformation length has not been exceeded.

Table 8-16: *Autonomous Vehicle Key Features for the Utility Cost of Lives at Risk for Scenario 2 Collision Between AV_a and AV_b (Passive Case)*

Key Consideration/Feature	Vehicle *A*: utility cost of lives at risk	Vehicle *B*: utility cost of lives at risk
N_o – Number of pedestrians	1	1
ή (δ) – Peak deformation	N/A	N/A
ή (H_a) – Peak head accel	14.9	3.5
ή (C_a) – Peak chest accel	14.9	3.5

Table 8-17: *Autonomous Vehicle Key Features for the Utility Cost of Lives at Risk for Scenario 2 Collision Between AV_a and AV_c (Passive Case)*

Key Consideration/Feature	Vehicle *A*: utility cost of lives at risk	Vehicle *C*: utility cost of lives at risk
N_o – Number of pedestrians	1	5
ή (δ) – Peak deformation	**499.9**	**2499.3**
ή (H_a) – Peak head accel	**556.0**	177.3
ή (C_a) – Peak chest accel	**555.2**	177.1

Table 8-18: *Autonomous Vehicle Key Features for the Utility Cost of Lives at Risk for Scenario 2 Collision Between AV_a and AV_b (Active Case)*

Key Consideration/Feature	Vehicle *A*: utility cost of lives at risk	Vehicle *B*: utility cost of lives at risk
N_o – Number of pedestrians	1	1
ή (δ) – Peak deformation	N/A	N/A
ή (H_a) – Peak head accel	9.9	3.1
ή (C_a) – Peak chest accel	9.9	3.1

Table 8-19: *Autonomous Vehicle Key Features for the Utility Cost of Lives at Risk for Scenario 2 Collision Between AV_a and AV_c (Active Case)*

Key Consideration/Feature	Vehicle A: utility cost of lives at risk	Vehicle C: utility cost of lives at risk
N_o – Number of pedestrians	1	5
ή (δ) – Peak deformation	**142.4**	**711.9**
ή (H_a) – Peak head accel	**4930.6**	838.8
ή (C_a) – Peak chest accel	**4916.7**	836.1

8.3.2.2 COLLISION SCENARIO RESULTS

The results arising from Scenarios 1 and 2 (with particular details including the number of occupants on-board each AV are given in Tables 8-1 and 8-6, respectively) are presented for the passive and active cases in Tables 8-20 and 8-21, respectively. The collision targets when considering the three EDM algorithms for Scenarios 1 and 2 are given in first sub-columns of Columns 1 and 2, respectively. The utility cost of lives at risk for each of the AV to AV collisions is given in the second sub-columns of Columns 1 and 2 for Scenarios 1 and 2, respectively, where the outcomes are generated by the collision target algorithm selected.

It is interesting to note that the stiffness controller has either reduced the utility cost of lives at risk or made no change for all but one of the cases considered in Tables 8-20 and 8-21. This case involves Scenario 2 and the collision between AV_a and AV_c, see Table 8-19. This is due to the initial injury severity of the collision being high, especially for AV_a. Upon stiffening the structure, the peak head acceleration and peak chest acceleration values become excessive, i.e. to the point where an extremely severe/fatal collision may be experienced. However, via the active stiffness control the utility cost for AV_c is reduced by 45%, i.e. is almost halved.

Table 8-20: *Ethical Decision Maker Results for Scenarios 1 and 2 (Passive): AV_a Making a Decision Between Swerving to Avoid AV_b and to Collide into AV_c*

	Scenario 1		Scenario 2	
Algorithm	**Target**	**Overall utility cost of lives at risk**	**Target**	**Overall utility cost of lives at risk**
Deontological	$AV_a -> AV_b$	AV_a: 41.2 AV_b: 56.4	$AV_a -> AV_b$	AV_a: 21.1 AV_b: 4.9
Utilitarian	$AV_a -> AV_c$	AV_a: 23.5 AV_c: 16.8	$AV_a -> AV_b$	AV_a: 21.1 AV_b: 4.9
Selfish	$AV_a -> AV_b$	AV_a: 41.2 AV_b: 56.4	$AV_a -> AV_c$	AV_a: 931.3 AV_c: 2511.8

Table 8-21: *Ethical Decision Maker Results for Scenarios 1 and 2 (Active): AV_a Making a Decision Between Swerving to Avoid AV_b and to Collide into AV_c*

	Scenario 1		Scenario 2	
Algorithm	**Target**	**Overall utility cost of lives at risk**	**Target**	**Overall utility cost of lives at risk**
Deontological	$AV_a -> AV_b$	AV_a: 41.2 AV_b: 56.4	$AV_a -> AV_b$	AV_a: 14.0 AV_b: 4.4
Utilitarian	$AV_a -> AV_c$	AV_a: 17.5 AV_b: 15.4	$AV_a -> AV_b$	AV_a: 14.0 AV_b: 4.4
Selfish	$AV_a -> AV_b$	AV_a: 41.2 AV_b: 56.4	$AV_a -> AV_c$	AV_a: 6964.6 AV_c: 1381.8

8.3.2.3 SUMMARY OF INITIAL RESULTS

The quantified results (passive and active) in terms of the utility cost of lives at risk are now evaluated from the simulation studies involving Scenarios 1 and 2 using the three algorithms detailed in Section 8.3.1. The utility cost of lives at risk for Scenarios 1 and 2 are given in Tables 8-22 and 8-23 for the passive and active cases, respectively. Tables 8-22 and 8-23 detail the utility cost of lives at risk for each scenario (Columns 1 and 2) and the sum of the utility cost of lives at risk for the two scenarios (Column 3). The results from the three algorithms are given in Table 8-22 for Scenarios 1 and 2, where the selfish algorithm results in the highest collision severities, hence resulting in the largest utility cost to society. However, with reference to Scenario 1 only, the

deontological and selfish algorithms have equal costs to society, this is due, in part, to the deontological collision following its 'naturally' intended path. The combined sum of Scenarios 1 and 2 for the deontological algorithm (passive case) 'sits' in the middle of the results in terms of the overall utility cost of lives at risk. The utilitarian algorithm is the most effective algorithm for Scenario 1 and 2, as it gives the lowest overall utility cost to society for the passive AV collisions considered.

Table 8-22: *Ethical Decision Maker Results for Scenarios 1 and 2 (Passive): AV_a Making a Decision Between Swerving to Avoid AV_b and to Collide into AV_c*

	Overall utility cost of lives at risk		
Algorithm	**Scenario 1**	**Scenario 2**	**Scenarios 1 and 2**
Deontological	97.6	26.0	123.6
Utilitarian	40.3	26.0	66.3
Selfish	97.6	3443.1	3540.7

Table 8-23: *Ethical Decision Maker Results for Scenarios 1 and 2 (Active): AV_a Making a Decision Between Swerving to Avoid AV_b and to Collide into AV_c*

	Overall utility cost of lives at risk		
Algorithm	**Scenario 1**	**Scenario 2**	**Scenarios 1 and 2**
Deontological	97.6	18.4	116.0
Utilitarian	32.9	18.4	51.3
Selfish	97.6	8346.4	8444.0

The active results are given in Table 8-23, where the active stiffness controller results in either no change or an improvement to most of the cases. As mentioned in Section 8.3.2.2, this is due to the severe/fatal collision in Scenario 2 between AV_a and AV_c, see Table 8-19, where the stiffness controller results in extremely high accelerations experienced by the occupants in AV_a. Scenario 1, involves the collision between AV_a and AV_b, with this resulting in no change, as the peak deformation is on the limit of the design deformation length, see Tables 8-12 and 8-14. However, the collision between AV_a and AV_c results in the softening of the collision structures, with this decreasing the utility cost of lives at risk (i.e. softening the structure uses the available deformation capacity and reduces the accelerations experienced by the occupant(s)), see Tables 8-13 and 8-15. A similar result is obtained for Scenario 2 involving the collision between AV_a and AV_b, see Tables 8-16 and 8-18.

For Scenario 2, the active case between AV_a and AV_c results in a significant decrease in deformation through stiffening of the structures. As expected, the peak head accelerations and peak chest accelerations have increased, see Tables 8-17 and 8-19. However, it should be noted that the peak accelerations (head and chest) are only fatal for the single occupant in AV_a. As discussed initially in Section 8.3.2.1, the 5 occupants contained within AV_c are at a much lower risk of severe and fatal injuries. The peak deformation in Table 8-19 for AV_c is above the limit by a factor of 1.8 in terms of the utility cost of lives at risk, i.e. 711.9 compared to the limit of 396.0 given in Table 8-1. Compared to the passive case, where a utility cost of lives at risk value of 2499.3 was determined, this represents a significant improvement. This result suggests it is likely that the five occupants in the active case may not experience severe or fatal injuries, whereas it is highly likely they would have been fatal in the passive case. However, it is interesting to note that it is only when the selfish algorithm becomes the lead decision-maker that this particular the AV_a to AV_c collision target is selected.

The overall outcome from the multiple vehicle collision scenarios result in similar results to the single-vehicle cases considered in Chapter 7. However, further work is needed for the multiple AV collisions, with more scenarios needing to be considered. Different permutations of AV location and the number of occupants on-board each AV would be worth considering and an area of further work could be a Monte Carlo simulation.

8.4 SUMMARY

In this Chapter, the four stages that comprise the ethical decision-maker (EDM) for collision target selection in the case of autonomous vehicle (AV) to AV/AV collision scenarios have been developed, these are: pre-determine collision outcomes; pre-determine collision injury severities; activate stiffness controller; and collision target selection.

Stage 1, used fuzzy logic to interpolate look-up tables (surfaces) to pre-determine the collision outcomes of the AV to AV/AV collisions, with the results compared to the two-vehicle bilinear model. The differences between the models were determined to be small, with a maximum percentage difference of 2.2%. The information from Stage 1 was used to pre-determine the injury severity of the AV to AV/AV collision outcomes. Stage 3 then involved the development of the active stiffness controller, where the two-AV dynamic bilinear model was used (this was to facilitate a comparison between the computational clock-time of fuzzy logic interpolation approach with direct use of the two-AV dynamic collision model). As in the single AV case, the stiffness controller has been developed so that it can alter the collision severity, e.g. soften the structure to minimise occupant accelerations or stiffen the structure to minimise the peak deformation of the AV collision structures. It was determined at this stage that the fuzzy logic interpolation method was significantly faster to compute than the two-AV dynamic collision model when using the active stiffness control algorithm (0.9 seconds compared

to 258.0 seconds). It was found that the stiffness controller resulted in improvements to collision scenarios, with the most significant results being evidenced when stiffening was required. In Scenario 2, the stiffening of the structure led to the potential for 5 lives to be saved. In Stage 4, as in the single AV case, various collision target selection algorithms have been explored. Through illustrative examples, it has been demonstrated that a utilitarian approach produces the lowest overall utility cost to society. In contrast, the selfish approach, where the AV is programmed to prioritise its occupant safety, led (not surprisingly) to the largest cost to society. The altruistic approach was deemed not to be a viable option for AV to AV/AV collisions, as it is viewed to be implausible for the lead decision-maker to act in an altruistic manner.

This Chapter has extended upon Chapter 7, for the single AV collision case, to encompass what are considered to be the first steps towards the multiple AV collision case. This has focussed on considering three AVs (AV_a, AV_b and AV_c), with attention focussed on collision target selection from an ethical viewpoint. It has been shown that, through two specifically designed scenarios that an active stiffness control system can lead to benefit in terms of reduced utility cost to society. It is considered that the outcome of this Chapter will form the basis of further work in a number of directions. One such area being to explore the benefit of the utilitarian approach in secondary and tertiary collision scenarios.

9. CONCLUSIONS AND FURTHER WORK

9.1 CONCLUSION

It is well known that fully autonomous vehicles (AVs) are being developed, with testing taking place on public roads, such as in Coventry, UK. This piece of research has been driven by the desire to improve the road safety of future AVs, and has taken a radical view of what might be a future 'blueprint'. The original motivation for the research was that of developing a system that minimises the number of serious injuries and fatalities of the occupants on-board an AV in the event of an unavoidable collision. This involved the development of an active stiffness controller for the crumple zones of future AVs. The research was further motivated by the work of (Goodall, 2014), where AVs need to make ethical decisions in terms of collision target selection. Initial solutions to the ethical dilemma include the deontological approach of Kant and the utilitarian approach of Bentham, with social actions also being considered, namely those of the altruistic and selfish actions. With specific simplifications and working assumptions in place, the thesis has attempted to reach the core of the issue and provide some directions towards achieving a future fleet of ethical and 'safer' AVs through the use of computer simulation.

The AVs considered in this research have identical structures and are based on a finite element (FE) simulation of a specific vehicle collision into an immovable rigid wall (IRW). Then, based on the FE simulation, mathematical models, or lumped parameter

models (LPMs), of the collision into an IRW have been developed. The mathematical models aim to capture the key features from the FE collision data, i.e. peak deformation, peak acceleration and collision energy absorption. Initially, linear models were considered as well as linear models with multiple sections, i.e. piecewise linear models. Whilst the piecewise linear models were difficult to tune, hence not taken further, they did highlight the phenomenon of departure from linearity. To develop a model that achieved a 'better' fit to the FE data, nonlinear models were investigated. A novel proposal presented in this thesis is based on a bilinear model, with attention initially being placed on a novel spatial quasi-static bilinear model to capture the force versus deformation characteristic. For practical purposes, where it is desirable to vary the model parameters (i.e. AV laden mass and collision velocity), a novel dynamic bilinear model has been developed. The model developed was able to capture the dynamic response up to the first quarter cycle of a second-order dynamic equation. Key within the dynamic bilinear model is a nonlinear product term involving the two factors of force and progressive deformation. It has been shown through simulation that the dynamic bilinear model is effective in capturing the key features of an AV colliding into an IRW. It is also emphasised that the tuning process of the dynamic bilinear model is straightforward and has been demonstrated to be very effective. The dynamic bilinear model for the single AV collision case was then extended to the two-vehicle AV to AV collision case, where again, the efficacy of the model has been demonstrated. To gain an understanding of occupant collision properties, the acceleration versus time data from FE simulation is fed into an occupant sled model. Based on the sled model simulation, the occupant peak head acceleration and peak chest acceleration were extracted. The relationship between peak acceleration and peak head acceleration and peak chest acceleration have been determined using scaling factors. These are used in conjunction with the bilinear dynamic model to replicate single AV into an IRW and AV to AV collisions. The dynamic bilinear model allowed the three key collision features of peak

deformation, peak head acceleration and peak chest acceleration to be investigated over a range of values for the AV laden mass and collision velocity.

The main contribution presented in the thesis has been the development of an ethical decision-maker (EDM) for collision target selection. The EDM has been developed for both single AV collisions into IRW and AV to AV collisions, to facilitate decisions in the event of an inevitable collision scenario. Embedded within the EDM is a novel model-to-decision (M2D) approach. The EDM was designed as a framework to evaluate four potential algorithms, namely those based on deontological, utilitarian, altruistic and selfish approaches. These four approaches each have well established origins and based on sound philosophical and societal tenets, hence justifiably worthy of investigation. The EDM uses pre-calculated data corresponding to a range of AV laden mass values and collision velocity values. This data is generated from the bilinear dynamic models (single AV collisions into an IRW and multiple AV to AV collisions) and stored in the form of look-up tables (surfaces). Immediately prior to an inevitable collision, the surfaces are interpolated using fuzzy logic and used to pre-determine estimates of the three key features, i.e. peak deformation, peak head acceleration and peak chest acceleration. Based on the three key features, collision injury severity levels are pre-determined. The injury severity levels exist on a universe of discourse spanned by fuzzy sets denoted A, B, C, D and E, where fuzzy set A corresponds to the highest injury severity and set E corresponds to the lowest injury severity. Based on the degrees of membership to the fuzzy sets for the three key features, a common utility cost unit for collision injury severity levels has been developed. A function has been developed that distinguishes the collision injury severity levels in a nonlinear manner, i.e. in an attempt to avoid severe to fatal collisions. To allow the collision scenarios to be compared, and to accommodate the key features, an overall Euclidean cost metric is proposed. The Euclidean cost metric has emerged as a 'better way' to present and compare the outcomes in terms of a

common currency, hence a utility cost to society. It is worth noting that the notion of a utility cost to society and the use of a Euclidean norm to portray this was not an original objective as detailed in Section 1.3, Chapter 1. It is, however, another minor contribution within the developed EDM.

A further additional contribution to the above EDM is that of a novel stiffness controller. The developed LPMs have been developed to capture the effect of altering the structural stiffness (i.e. softening, no change and stiffening) over a range of values for AV laden mass and collision velocity. The captured effects are stored within look-up tables (surfaces) and interpolated using fuzzy logic. With the development of a stiffness control algorithm, the stiffness change is determined such that peak deformation is as close as possible to the design deformation length, (in this work $0.5900m$). This could lead to softening the structure to increase the peak deformation, thus reducing the peak head acceleration and peak chest acceleration. Alternatively, stiffening the structure would reduce the peak deformation, but would lead to increased peak head acceleration and peak chest acceleration. The performance of the stiffness controller is evaluated in the same manner as the EDM for the collision target selection. Hence, collision properties are pre-determined, thus allowing collision injury severity levels to be known for the passive case (no change in stiffness applied). A common utility cost unit for injury severity levels is then evaluated using the overall Euclidean cost metric based on the collision features. This allows the passive cases for the collision target selection to be compared to the active cases of collision target selection for the four algorithms based on the deontological, utilitarian, altruistic and selfish approaches. A UK provisional and full US Patent has been granted for the active stiffness control system, see Appendix 1.0.

The results from the EDM collision target selection and stiffness controller suggest that it is possible to achieve a future fleet of ethical and 'safer' AVs. Through illustrative

examples of the AV to IRW collision cases, it has been demonstrated that a utilitarian approach, closely followed by the altruistic approach produces the lowest utility cost to society. In contrast, the selfish approach, where the AV is programmed to prioritise occupant safety, leads (not surprisingly) to the largest cost to society. Similarly, when considering AV to AV/AV collisions, through illustrative examples, it has been demonstrated that a utilitarian approach produces the lowest overall utility cost to society. In contrast, the selfish approach, where the AV is programmed to prioritise its occupant safety, leads (not surprisingly) to the largest cost to society. The altruistic approach was deemed not to be a viable option for AV to AV/AV collisions, as it is viewed implausible for the lead decision-maker to act in an altruistic manner. It was found that the stiffness controller resulted in improvements to collision scenarios, with the most significant results being evidenced when stiffening was required in the case of an AV to AV/AV collision. In one of the scenarios, stiffening of the structure leads to the potential for 5 lives to be saved.

From a practical viewpoint of implementation, it has been verified that it is more important to have an accurate estimation/measurement of the collision velocity of an AV over its laden mass value. Another point of interest, when operating the stiffness controller, the computation time of the fuzzy logic interpolation method was compared to the use of the bilinear dynamic model. For the AV to AV collision, it was determined that the fuzzy logic interpolation method was significantly faster to compute than the two-AV dynamic collision model when using the active stiffness control algorithm (0.9 seconds compared to 258.0 seconds). The quasi-static spatial bilinear model, which represents a minor novelty in this work, might offer a practical compromise between accuracy and computational complexity.

An additional minor contribution is the development of a simulation tool which provides a design framework for investigating AV collisions, involving pedestrians, IRWs and other AVs. The simulation design tool has been designed specifically using the industry standard MATLAB and Simulink, which is widely adopted in the automotive industry.

Overall it has been demonstrated that an AV can be programmed to employ the philosophical doctrines and social actions to select a collision target based on an ethical M2D approach. Furthermore, a stiffness controller can be applied to reduce the injury severity of collisions, hence reduced the overall utility cost to society.

As the work has evolved some of the topics have been published at International Conferences and in relevant special issues arising from events dealing with intelligent transport systems, see Appendix 9.0.

9.2 FURTHER WORK

As with any interesting research, the work is never quite complete and the most important aspects are inevitably yet to be done. This section highlights several such avenues which have been identified as further work.

The ECS requires significant further work to consider the practical aspects of the operation. The current study has proposed that all collision scenarios are of full-frontal into other AVs or an IRW. Consideration is needed regarding the AV steering dynamics, thus the capability of a vehicle to steer into a given collision target. It may be determined in certain scenarios that the AV can only steer into the target with an offset collision, i.e. not full frontal. This introduces a new layer of pre-collision decision making that is likely to involve the AV making decisions between colliding into an AV full frontal or potentially into another AV off-set. The additional layer included within the EDM would enable the AV to pre-determine if a collision outcome is likely to be a full-frontal or an

offset collision. Further to this, with in-built look-up tables containing off-set AV to AV/IRW collision data, decisions can then be made regarding the collision target. Further considerations built into the ECS could be the ability of the ECS to accurately estimate the AV laden mass and predict the collision velocity. It would also be of interest to investigate the post-collision scenarios, i.e. secondary and tertiary collisions, such as multiple-lane motorway collisions.

With consideration given to the limited scenarios explored within this research, i.e. AV to IRW/pedestrian(s) and AV to AV/AV collisions, further scenarios could be explored. Possibilities include an AV to IRW/AV as well as AV to pedestrian(s)/AV. Further details could be built into the EDM to specify details on the AV and pedestrians. The age, sex, health, relationship between occupant(s) and pedestrian(s) and social status are factors that may influence the EDM, i.e. the AV target. A detailed study is required into pedestrian and occupant safety, where more FE studies are required (e.g. occupant properties, impact velocity and orientation), and, if possible correlating these to accident reports. In the case of occupants and pedestrians age, it could be questioned e.g. whether it is ethically worth saving a 65-year-old male over a 15-year-old female. Many such AV ethical questions remain unanswered and potentially could be answered with the use of computational ethics, as has been initially demonstrated in this research. Although the premise of this research considered all future AVs to be identical (e.g. structural crumple zone stiffness and baseline mass), this is perhaps over-simplified and it may be worth considering a further investigation into a fleet of mixed AVs of different structural crumple zone stiffness and baseline mass values, this forms another layer that could potentially be incorporated in to the EDM. Such added complexity could render the altruistic approach a viable option, as alluded to in Chapter 8.

The foundations of this research are grounded in the use of finite element (FE) collision outputs from a conventional vehicle containing an engine located at the front of the vehicle. In future work, it is believed that redesigned crumple zone structures consisting of no additional components would allow for a better control environment. Thus, it would allow for results that are perhaps more accurately predictable (and repeatable). A standardised structure for AVs to be investigated using FE would also allow for the effect of stiffening/softening the crumple zones to be further interrogated, i.e. effects of peak deformation and peak head acceleration and peak chest acceleration.

The mathematical modelling in this work proved to be successful, with the key features captured with sufficient accuracy, i.e. peak deformation, peak acceleration (and corresponding peak head acceleration and peak chest acceleration) and collision deformation energy. Whilst only two-degree of freedom models were investigated in this research, it is considered that the use of models containing higher degrees of freedom may provide better results. However, more complex tuning methods would be required to be developed, as has been demonstrated in this research, models with greater degrees of freedom are more difficult to tune.

The EDM algorithms have the potential to be further developed. An approach which appears to be potentially promising is that of game theory and more specifically that of Nash equilibrium. Nash equilibrium is an approach motivated by the social actions of mutualism and altruism, and it operates in such a manner whereby the action is to do what is best for oneself and also what is best for the group. Consequently, the developed approach would present an equilibrium point for the common good, i.e. a point whereby no one potentially loses.

An interesting development would be that of a scaled laboratory-based version of the crumple zone for investigation of the use of currently available actively controlled materials, including shape memory alloys and piezoelectric devices. This would present an interesting stepping-stone towards developing, demonstrating and evaluating the potential of a stiffness controller onboard a future AV. Further scaled-down AVs could be developed with collision target algorithms on-board within the ECS to determine the effectiveness of AVs' communicating information pre-collision and then making informed 'split-second' decisions, i.e. choice of AV target and stiffness controller.

It would be interesting to determine the general view of the public on the ECS, via the use of a survey. This could be achieved by demonstrating the benefits of the two constituent parts of the system, i.e. collision target selection and the stiffness controller, and determining whether the quantifiable benefits in terms of utility cost to society is realistic and that the state of technology-readiness is sufficiently well developed.

REFERENCES

Alghamdi, A., (2001). Collapsible impact energy absorbers: an overview. Thin-Walled Structures, 39(2), pp. 189–213.

Anderson, M., Anderson, S.L. and Armen, C., (2004). Towards Machine Ethics. In Proceedings of the AOTP'04-The AAAI-04 Workshop on Agent Organizations: Theory and Practice.

Anderson, M., Anderson, S.L. and Armen, C., (2005). Towards Machine Ethics: Implementing Two Action-Based Ethical Theories. In Proceedings of the AAAI 2005 Fall Symposium on Machine Ethics, Arlington, VA.

Anderson, M., Anderson, S.L. and Armen, C., (2006). MedEthEx: A Prototype Medical Ethics Advisor. In Proceedings of the 18th Conference on Innovative Applications of Artificial Intelligence, Boston, Massachusetts, pp. 1759–1765.

Appel, H. and Tomasd, J., (1973). The energy management structure for the Volkswagen. In *Proc. International Technical Conference on Enhanced Safety of Vehicles (ESV)*. SAE Paper No. 730078.

Ashton, S.J., (1980). A preliminary assessment of the potential for pedestrian injury reduction through vehicle design. SAE Technical Paper No. 801315.

Ashton, S.J. and Mackay, G.M., (1979). Some characteristics of the population who suffer trauma as pedestrians when hit by cars and some resulting implications. In *4th IRCOBI International Conference,* Gothenburg.

Ballesteros, M.F., Dischinger, P.C. and Langenberg, P., (2004). Pedestrian injuries and vehicle type in Maryland, 1995–1999. *Accident Analysis & Prevention*, 36(1), pp.73-81.

Barlas, T.K., and Van Kuik, G.A.M., (2010). Review of state of the art in smart rotor control research for wind turbines. *Progress in Aerospace Sciences*, 46(1), pp.1-27.

Bastien, C., (2014). The prediction of kinematics and injury criteria of unbelted occupants under autonomous emergency braking. PhD Thesis, Coventry University, UK.

Bennett, J.A., Lust, R.V, and Wang, J.T., (1991). Optimal design strategies in crashworthiness and occupant protection, Crashworthiness and Occupant Protection in Transport Systems, 126, ASME, New York, pp. 51-66.

Belmonte, F.J., Martín, S., Sancristobal, E., Ruiperez-Valiente, J.A. and Castro, M., 2020. Overview of embedded systems to build reliable and safe ADAS and AD systems. *IEEE Intelligent Transportation Systems Magazine*.

Bhuiyan, J., (2016) After two million miles, Google's robot car now drives better than a 16-year-old [online]. Available at: https://www.recode.net/2016/10/5/13167364/google-self-driving-cars-2-million-miles [Accessed 10 June 2017].

Bhuyan A, Ganilova, O., (2012). Crush can behaviour as an energy absorber in a frontal impact. In Journal of Physics: Conference Series, 382 (Conference 1), paper 012009. Bristol: IOP Publishing.

Bonnefon, J.F., Shariff, A. and Rahwan, I., (2015). Autonomous vehicles need experimental ethics: are we ready for utilitarian cars? arXiv preprint arXiv:1510.03346.

Bonnefon, J.F., Shariff, A. and Rahwan, I., (2016). The social dilemma of autonomous vehicles. Science, 352(6293), pp.1573-1576.

Bonnefon, J.F., Shariff, A. and Rahwan, I., (2019). The trolley, the bull bar, and why engineers should care about the ethics of autonomous cars [point of view]. Proceedings of the IEEE, 107(3), pp.502-504.

Bruni, C., DiPillo, G. and Koch, G., (1974). Bilinear systems: an appealing class of nearly linear systems in theory and applications. IEEE Trans. Automat. Contr., 19(4), pp.334 - 348.

Burnham, K. J., (1991). Self-tuning Control for Bilinear Systems. PhD Thesis, Coventry Polytechnic, UK.

Burns, J.H. and Hart, H.L.A., (1998). The collected works of Jeremy Bentham: An introduction to the principles of morals and legislation, Oxford University Press.

Centre for Collision Safety and Analysis., (2017). Centre for Collision Safety and Analysis – 2010 Toyota Yaris. [online] Available at: https://www.ccsa.gmu.edu/models/2010-toyota-yaris/ [Accessed 14 April 2017].

Cheva, W., Yasuki, T., Gupta, V. and K. Mendis., (1996). Vehicle development for frontal/offset crash using lumped parameter modeling, Technical Paper. In International Society of Automotive Engineering (SAE International), Warrendale, PA, USA.

Clark, C., (1994). The crash anticipating extended airbag bumper system. *Proc. Fourteenth International Technical Conference on Enhanced Safety of Vehicles (ESV)*, Munich, Germany, US Department of Transportation, National Highway Traffic Safety Administration, Washington, DC. USA, pp.1468-1480.

Crandall, J.R., Bhalla, K.S. and Madeley, N.J., (2002). Designing road vehicles for pedestrian protection. *BMJ: British Medical Journal*, 324(7346), p.1145.

Crew, B., (2015). Driverless cars could reduce traffic fatalities by up to 90%, says report [online]. Available at: https://www.sciencealert.com/driverless-cars-could-reduce-traffic-fatalities-by-up-to-90-says-report [Accessed 10 June 2017].

Cuerden, R., Richards, D. and Hill, J., (2007). Pedestrians and their survivability at different impact speeds. In *Proceedings of the 20th International Technical Conference on the Enhanced Safety of Vehicles,* Lyon, France, Paper (No. 07-0440).

Davis, G., (2001). Relating severity of pedestrian injury to impact speed in vehicle-pedestrian crashes: Simple threshold model. *Transportation Research Record: Journal of the Transportation Research Board*, (1773), pp.108-113.

Dawkins, R., (2006). The Selfish Gene, 4th Edition, Oxford, Oxford University Press.

Deb, A. and Srinivas, K.C., (2008). Development of a new lumped parameter model for vehicle side-impact safety simulation, Proceedings of the Institution of Mechanical Engineers, Part D: Journal of Automobile Engineering, 222 (10), pp. 1793-1811.

Department of Transport (DOT)., (2017). Available at: https://www.gov.uk/government/organisations/department-for-transport [Accessed 26th June 2017].

Desapriya, E., Subzwari, S., Sasges., D., Basic, A., Alidina, A., Turcotte, K. and Pike, I., (2010). Do light truck vehicles (LTV) impose greater risk of pedestrian injury than passenger cars? A meta-analysis and systematic review. *Traffic injury prevention*, 11(1), pp.48-56.

Deshpande, R., Kutty, K. and Mani, S., (2015). Detection of visual saliency region for ADAS applications. SAE Technical Paper No. 10.4271/2015-01-0214.

Dhani, A., 2019. Reported Road Casualties in Great Britain: Provisional Estimates Year Ending June 2019.

Dischinger, P.C., Ryb, G.E., Kufera, J.A. and Ho, S.M., (2013). Declining statewide trends in motor vehicle crashes and injury-related hospital admissions. Annals of advances in automotive medicine, 57, p.247.

Dogan, E., Chatila, R., Chauvier, S., Evans, K., Hadjixenophontos, P., and Perrin, J., (2016). Ethics in the Design of Automated Vehicles: The Ethics Project. In *22th European Conference on Artificial Intelligence (ECAI)* [Online], Holland, pp. 10-13.

Dokoupil, T., (2008). Autos: Doing away with hood ornaments [online]. Available at:

http://www.newsweek.com/autos-doing-away-hood-ornaments-88375 [Accessed 4 April 2017].

Du Bois, P., Chou, C.C., Fileta, B.B., Khalil, T.B., King, A.I., Mahmood, H.F., Mertz, H.J., Wismans, J., Prasad, P. and Belwafa, J.E., (2004). Vehicle crashworthiness and occupant protection. Washington D.C, American Iron and Steel Institute.

Dunoyer, A. P., (1996). Bilinear Self-Tuning Control and Bilinearisation of Nonlinear Industrial Systems, Ph.D. Thesis, Coventry University, UK.

Eckermann, E., (2001). World history of the automobile. Society of Automotive Engineers.

Ekambaram, K., (2016). The potential benefit of SMART load limiters in European frontal impacts, Doctoral dissertation, Loughborough University, UK.

Ekambaram, K. and Frampton, R., (2016). Effect of age on injury outcome in passenger car frontal crashes. At European conference on human centred design for intelligent transport systems, Loughborough, UK.

Ekman, M., (2005). Modelling and Control of Bilinear Systems: Applications to the Activated Sludge Process. PhD Thesis, Uppsala University, Sweden.

Elmarakbi, A.M. and Zu, J.W., (2004). Dynamic modeling and analysis of vehicle smart structures for frontal collision improvement. International journal of automotive technology, 5(4), pp.247-255.

Elmarakbi, A. and Zu, J., (2007). Mathematical modelling of a vehicle crash with emphasis on the dynamic response analysis of extendable cubic nonlinear dampers using the incremental harmonic balance method. Proceedings IMechE Part D: Journal of Automobile Engineering, 221(2), pp.143-156.

Euro NCAP., (2017a). Full width rigid barrier [online]. Available at: https://www.euroncap.com/en/vehicle-safety/the-ratings-explained/adult-occupant-protection/full-width-rigid-barrier/ [Accessed 17th June 2017].

Euro NCAP., (2017b). Pedestrian Protection [online]. Available at: https://www.euroncap.com/en/vehicle-safety/the-ratings-explained/pedestrian-protection/. [Accessed 10 July 2017].

Federal Highway Administration., (2016). U.S. Department of Transportation Federal Highway Administration [online]. Available at: https://www.fhwa.dot.gov/ohim/onh00/bar8.htm. [Accessed 10 June 2017].

Foot, P., (1967). The problem of abortion and the doctrine of the double effect. *Oxford Review*, 5, pp.5–15.

Ford., (2020). Available at: https://corporate.ford.com/articles/products/autonomous-2021.html [Accessed 9th January 2020].

Foster, K.R., Wenseleers, T. and Ratnieks, F.L., (2001). Spite: Hamilton's unproven theory. Annales Zoologici Fennici, 38 (3/4), pp. 229-238.

Friedrich, B., (2016). The effect of autonomous vehicles on traffic. In M. Maurer et al. *Autonomous Driving.* Belin, Springer, pp. 317-334.

Fredriksson, R., Rosén, E. and Kullgren, A., (2010). Priorities of pedestrian protection—A real-life study of severe injuries and car sources. *Accident analysis & prevention*, 42(6), pp.1672-1681.

Gandhi, U.N. and Hu, J.S., (1995). Data-based approach in modeling automobile crash, International Journal of Impact Engineering 16(1), pp. 95-118.

Gawronski, W. K., (2004). Advanced Structural Dynamics and Active Control of Structures. New York, Springer.

Gerónimo, D., Vázquez, D., de la Escalera, A., López, A.M., Imiya, A., Pajdla, T. and Álvarez, J.M., (2017). Vision-Based Advanced Driver Assistance Systems. In Computer Vision in Vehicle Technology: Land, Sea & Air. Wiley, pp.100-121.

Goodall, N.J., (2014). Machine ethics and automated vehicles. In G. Meyer and S. Beiker, Road Vehicle Automation. Springer International Publishing, pp. 93-102.

Goodall, N.J., (2016). Can you program ethics into a self-driving car? IEEE Spectrum, 53(6), pp.28-58.

Google., (2016). Google Self-Driving Cars Incidents [online]. Available at: https://google-self-driving-car-incidents.silk.co/ [Accessed 12th June 2017].

Goriely, A., Vandiver, R. and Destrade, M., 2008. Nonlinear euler buckling. Proceedings of the Royal Society A: Mathematical, Physical and Engineering Sciences, 464(2099), pp.3003-3019.

Graczykowski, C., (2016). Mathematical models and numerical methods for the simulation of adaptive inflatable structures for impact absorption. *Computers & Structures*, 174, pp.3-20.

Greene, G., (2013). *Moral tribes: emotion, reason, and the gap between us and them*. New York, Penguin.

Gupta, P. and Srivastava, R. K., (2010). Overview of multi-functional materials. In M Joo Er, *New Trends in Technologies: Devices, Computer, Communication and Industrial Systems*. InTech, pp.1-14.

Gustafsson, S. and Thulin, H., Gawronski 2003). Pedestrians and cyclists-exposure and injury risks in different traffic environments for different age groups. Results from TSU92-the years of 1998 to 2000. *VTI MEDDELANDE*, (928).

Hamilton, W. D., (1963). The Evolution of altruistic behaviour, American Naturalist, (97) 896, pp.354-356.

Hamilton, W. D., (1964a). The genetical evolution of social behaviour, Part I, Journal of Theoretical Biology 7(1), pp.1-16.

Hamilton, W. D., (1964b). The genetical evolution of social behaviour, Part II, Journal of Theoretical Biology, 7(1), pp.17-52.

Hamilton, W.D., (1970). Selfish and spiteful behaviour in an evolutionary model. Nature, 228(5277), pp.1218-1220.

Hamilton, W.D., (1971). Geometry for the selfish herd. Journal of theoretical Biology, 31(2), pp.295-311.

Hardin, G., (1968). The tragedy of the commons, Science, 162(3859), pp.1243-1248.

Hartl, D.J. and Lagoudas, D.C., (2007). Aerospace applications of shape memory alloys. *Proceedings of the Institution of Mechanical Engineers, Part G: Journal of Aerospace Engineering*, 221(4), pp..535-552.

Hawkins, J. A., (2019). Uber is at fault for fatal-self driving crash, but it's not alone. Available at: https://www.theverge.com/2019/11/19/20972584/uber-fault-self-driving-crash-ntsb-probable-cause (assessed 1 June 2020).

Henary, B.Y., Ivarsson, J. and Crandall, J.R., (2006). The influence of age on the morbidity and mortality of pedestrian victims. *Traffic injury prevention*, 7(2), pp.182-190.

Hobbs, C A. and McDonough P J., (1998). Development of the European New Car Assessment Programme (Euro NCAP). In *Proceedings of the Sixteenth International Technical Conference on the Enhanced Safety of Vehicles*, Windsor.

Hollowell, W.T., Gabler, H.C., Stucki, S.L., Summers, S. and Hackney, J.R., (1998). Review of potential test procedures for FMVSS No. 208. National Highway Traffic Safety Administration.

Honda Motor Co., Ltd., Tokyo (JP). (2001). *Control device for controlling rigidity and deformation of car body.* United States Patent: US 6,286,895 B1.

Honda Motor Co., Ltd., Tokyo (JP). (2004). *Chassis frame buckling control device and chassis frame deformation control device.* United States Patent: US 7,202,588 B2.

Howard, D. and Dai, D., (2014). Public perceptions of self-driving cars: The case of Berkeley, California. In *93rd Annual Meeting TRB*, Washington DC.

Howard, B., (2019). Tesla: we'll have full self-driving by 2020. Robo-taxis, too. Available at: https://www.extremetech.com/extreme/290029-tesla-well-have-full-self-driving-by-2020-robo-taxis-too. [Accessed 9th January 2020].

Hsia, T.C., 1977. System identification: least-squares methods.

James, K. R., Haritos, N. and Ades, P. K., (2006). Mechanical stability of trees under dynamic loads, American Journal of Botany, 93(10), pp.1522-1530.

Jawad, S., (2002). Smart structures for frontal collision mitigation. SAE Technical Paper No. 2002-01-0247.

Kamal, MM., (1970) Analysis and simulation of vehicle to barrier impact. In International Society of Automotive Engineering (SAE International), Warrendale, PA, USA.

Kamm, F., (2015). *The trolley problem mysteries.* 1st Ed. Oxford, Oxford University Press.

Kant, I., (2007). Critique of pure reason, Revised Edition, Penguin Classics.

Katahira, S., Shibata, E. and Monji, T., (2007). Development of an advanced stereo camera system, SAE Technical Paper No. 10.4271/2007-01-3591.

Keeler, S. and Kimchi, M., (2015). Advanced high-strength steels application guidelines V5, WorldAutoSteel.

Keller, L., Milinski, M., Frischknecht, M., Perrin, N., Richner, H. and Tripet, F., (1994). Spiteful animals still to be discovered. Trends in Ecology & Evolution, 9(3), p.103.

Kim, C.H. and Arora, J.S., (2003). Nonlinear dynamic system identification for automotive crash using optimization: a review, Structural and Multidisciplinary Optimization, 25(1), p. 218.

King, A.I., (2017). Biomechanics of Automotive Safety Restraints. In the Biomechanics of Impact Injury. Springer, Cham, pp.597-628.

Kröyer, H.R., Jonsson, T. and Várhelyi, A., (2014). Relative fatality risk curve to describe the effect of change in the impact speed on fatality risk of pedestrians struck by a motor vehicle. *Accident Analysis & Prevention*, 62, pp.143-152.

Kumar, S., 2008. A Numerical Study on the Axial Crush Characteristics of Thin Walled Rectangular Tubes Subjected to Dynamic Impact (No. 2008-01-0242). SAE Technical Paper.

Kun, W., Haibin, L. and Yang, W., (2016). Study on Head Impact Injury Evaluation Index of Vehicle Interior Fittings. In Measuring Technology and Mechatronics Automation (ICMTMA), 2016 Eighth International Conference, China, pp. 643-648.

Kuwabara, G. and Kono, K., (1987). Restitution coefficient in a collision between two spheres. Japanese Journal of Applied Physics, 26(8R), p.1230.

Lambert., F, 2016. Another fatal Tesla crash reportedly on autopilot emerges, Model S hits a streetsweeper truck – caught on dashcam. Available at: https://electrek.co/2016/09/14/another-fatal-tesla-autopilot-crash-emerges-model-s-hits-a-streetsweeper-truck-caught-on-dashcam/ (Assessed 11/06/2020).

Laris, M., (2018). Waymo launches nation's first commercial self-driving taxi service in Arizona. The Washington Post. Available at: https://www.washingtonpost.com/local/trafficandcommuting/waymo-launches-nations-first-commercial-self-driving-taxi-service-in-arizona/2018/12/04/8a8cd58a-f7ba-11e8-8c9a-860ce2a8148f_story.html [Accessed 9th January 2020].

Leaf, W.A. and Preusser, D.F., (1999). *Literature review on vehicle travel speeds and pedestrian injuries*. US Department of Transportation, National Highway Traffic Safety Administration.

Lee, D., 2019. Uber self-driving crash 'mostly caused by human error'. Available at: https://www.bbc.co.uk/news/technology-50484172 [Accessed 11/06/2020].

Lefler, D.E. and Gabler, H.C., (2004). The fatality and injury risk of light truck impacts with pedestrians in the United States. *Accident Analysis & Prevention*, 36(2), pp.295-304.

Li, T. and Cheer, L., (2016). Mercedes Benz admits automated driverless cars would run over CHILD rather than serve and risk injuring the passengers inside [online]. Available at: http://www.dailymail.co.uk/news/article-3837453/Mercedes-Benz-says-driverless-cars-hit-child-street-save-passengers-inside.html (Accessed 14th February 2017).

Li, G., Yang, J. and Simms, C., (2017). Safer passenger car front shapes for pedestrians: a computational approach to reduce overall pedestrian injury risk in realistic impact scenarios. *Accident Analysis & Prevention*, 100, pp.97-110.

Lim, J., (2015). A Consideration on the Offset Frontal Impact Modeling Using Spring-Mass Model. International Journal of Mechanical, Aerospace, Industrial, Mechatronic and Manufacturing Engineering 9(8), p.7.

Lim, J.M., (2017). Lumped mass-spring model construction for crash analysis using full frontal impact test data. International Journal of Automotive Technology, 18(3), pp.463-472.

Lin, P., (2013). The Ethics of Autonomous Cars [online]. Available at:https://www.theatlantic.com/technology/archive/2013/10/the-ethics-of-autonomous-cars/280360/ [Accessed 2nd July 2017].

Lin, P., (2016). Why ethics matters for autonomous cars. In M. Maurer et al. Autonomous Driving. Berlin, Heidelberg, Springer, pp. 69-85.

Litman, T., (2014). Autonomous vehicle implementation predictions. Victoria Transport Policy Institute, 28.

Lloyd, W. F., (1833). Two Lectures on the Checks to Population. Oxford, Oxford University Press.

LSTC., (2017). Available at: http://www.lstc.com/products/models/dummies [Accessed 22nd May 2017].

Lu, M., Wevers, K. and Van Der Heijden, R., (2005). Technical feasibility of advanced driver assistance systems (ADAS) for road traffic safety. Transportation Planning and Technology, 28(3), pp.167-187.

Magee, C.L., (1988). Design for Crash Energy Management present and Future Developments. In Proceedings of the Seventh International Conference on Vehicle structural mechanics, Detroit, Michigan, USA.

Martineau, S., Burnham, K. J., Haas, O. C. L., Andrews, G. and Heeley, A., (2004). Four-term Bilinear PID Controller, Journal Control Engineering Practice, 12(4), pp. 457–464.

Marzougui, D., Samaha, R.R., Cui, C., Kan, C.D. and Opiela, K.S., (2012). Extended validation of the finite element model for the 2010 Toyota Yaris Passenger Sedan. Report, National Crash Analysis Centre, George Washington University, Washington, DC, USA.

McAleer, M., (2017). Audi's self-driving A8: drives can watch Youtube or check emails at 60km/h. The Irish Times. Available at: https://www.irishtimes.com/life-and-style/motors/audi-s-self-driving-a8-drivers-can-watch-youtube-or-check-emails-at-60km-h-1.3150496 [Accessed 9th January 2020].

M-city, (2017). Mcity Test Facility [online]. Available at: https://mcity.umich.edu/ [Accessed 10 June 2017].

McLaren, M.B., (2006) Computational Models of Ethical Reasoning: Challenges, Initial Steps, and Future Directions, IEEE Intelligent Systems, 21 (4), pp. 29–37.

Mizuno, K. and Kajzer, J., (1999). Compatibility problems in frontal, side, single car collisions and car-to-pedestrian accidents in Japan. *Accident Analysis & Prevention*, 31(4), pp.381-391.

Mladenović, M.N., Abbas, M. and McPherson, T., (2014). Development of socially sustainable traffic-control principles for self-driving vehicles: the ethics of anthropocentric design. In *Ethics in Science, Technology and Engineering, 2014 IEEE International Symposium*. Chicago, USA, pp. 1-8.

Moaveni, B., Abad, M. K. R. and Nasiri, S., (2015). Vehicle longitudinal velocity estimation during the braking process using unknown input Kalman filter. *Vehicle System Dynamics: International Journal of Vehicle Mechanics and Mobility,* 53(10), pp.1373-1392.

Mohler, R. R., (1973). Bilinear control processes: with applications to engineering, ecology and medicine. In Mathematics in Science and Engineering (Volume 106), Academic Press.

Mohler, R. R. and Kolodziej, W. J., (1980). An overview of bilinear system theory and applications, IEEE Transactions on Systems., Man and Cybernetics, 10, pp.683-688.

Mologni, J.F., Nunes, A.S., Siqueira, C.L., Figueiredo, D.L., Ribas, J.C., Junior, A.C. and Alves, M.A., (2014). Challenges on the Design of Automotive Radar Systems and V2V Technology . SAE Technical Paper No. 2014-36-0356.

Munyazikwiye, B.B., Karimi, H.R. and Robbersmyr, K.G., 2013, October. Mathematical modeling of vehicle frontal crash by a double spring-mass-damper model. In 2013 XXIV International Conference on Information, Communication and Automation Technologies (ICAT) (pp. 1-6). IEEE.

Munyazikwiye, B.B., Karimi, H.R. and Robbersmyr, K.G., (2017). Optimization of Vehicle-to-Vehicle Frontal Crash Model Based on Measured Data Using Genetic Algorithm. *IEEE Access*, 5, pp.3131-3138.

Murphy, M. (2016)., Coming in 2021: A self-driving Ford car with no steering wheels or pedals [online]. Available at: https://qz.com/759643/ford-self-driving-car-2012-no-steering-wheels-or-pedals-or-handover-function [Accessed 10 June 2017].

NHTSA., (2019). Automated Vehicles for Safety. Available at: https://www.nhtsa.gov/technology-innovation/automated-vehicles-safety [Accessed 15th October 2019].

Ni, C.M, and Song, J.O., (1986). Computer-aided Design Analysis Methods for Vehicle Structural Crashworthiness. In Symposium on Vehicle Crashworthiness Including Impact Biomechanics, ASME, Anaheim, CA, USA.

Nyholm, S. and Smids, J., (2016). The ethics of accident-algorithms for self-driving cars: an applied trolley problem?. Ethical Theory and Moral Practice, 19(5), pp.1275-1289.

O'Neill, B., (2009). Preventing passenger vehicle occupant injuries by vehicle design—a historical perspective from IIHS. Traffic injury prevention, 10(2), pp.113-126.

O'Kane, S., (2019). Uber debuts a new self-driving car with more fail safes. Available at: https://www.theverge.com/2019/6/12/18662626/uber-volvo-self-driving-car-safety-autonomous-factory-level (Accessed 1 June 2020).

Ostrowski, M., Griskevicius, P. and Holnicki-Szulc, J., 2005, June. Feasibility study of an adaptive energy absorbing system for passenger vehicles. In *Proceedings of the 16th international conference on „Computer Methods in Mechanics "Czestochowa, Poland*.

Pawlus, W., Karimi, H.R. and Robbersmyr, K.G., 2014. Investigation of vehicle crash modeling techniques: theory and application. *The International Journal of Advanced Manufacturing Technology*, *70*(5-8), pp.965-993.

Peng, R.Y. and Bongard, F.S., (1999). Pedestrian versus motor vehicle accidents: an analysis of 5,000 patients. *Journal of the American College of Surgeons*, *189*(4), pp.343-348.

Penning, D.A., Sawvel, B. and Moon, B.R., (2016). Debunking the viper's strike: harmless snakes kill a common assumption. Biology letters, 12(3).

Pitt, R., Guyer, B., Hsieh, C.C. and Malek, M., (1990). The severity of pedestrian injuries in children: an analysis of the Pedestrian Injury Causation Study. *Accident Analysis & Prevention*, *22*(6), pp.549-559.

Posadzki, A., (2016). Ethics to pose difficult challenge for self-driving, Audi executive says [online]. Available at: http://toronto.citynews.ca/2016/02/12/ethics-to-pose-difficult-challenge-for-self-driving-audi-executive-says/ [Accessed 10 June 2017].

Rosén, E., Källhammer, J.E., Eriksson, D., Nentwich, M., Fredriksson, R. and Smith, K., (2010). Pedestrian injury mitigation by autonomous braking. *Accident Analysis & Prevention*, 42(6), pp.1949-1957.

Rosén, E. and Sander, U., (2009). Pedestrian fatality risk as a function of car impact speed. *Accident Analysis & Prevention*, 41(3), pp.536-542.

Prasad, P., (2015). Injury criteria and motor vehicle regulations. In N.Yoganandan et al. Accidental Injury, New York, Springer, pp. 793-809.

Rawls, J., (1971). *A Theory of Justice*. Cambridge, Harvard University Press.

Rawls, J., (1999). A Theory of Justice, Revised Edition. Cambridge, Harvard University Press.

Reed, G.S and Jones, N (2013). Toward Modelling and Automating Ethical Decision Making: Design, Implementation, Limitations, and Responsibilities, Topoi, 32(2), pp. 237–250.

Richards, D.C., (2010). Relationship between speed and risk of fatal injury: pedestrians and car occupants (No. 16), Department for Transport: London.

Richards, D., Cookson, R., Smith, S., Ganu, V. and Pittman, M., (2010). The characteristics of speed-related collisions (No. 117), Department for Transport: London.

Ross, W.D., (1930). The Right and the Good, Oxford University Press.

Schuster, D.H.P., Fels, A.G. and Akzo Nobel NV, (1998). *Material for antiballistic protective clothing*. United States Patent 5,854,143.

Roudsari, B.S., Mock, C.N., Kaufman, R., Grossman, D., Henary, B.Y. and Crandall, J., (2004). Pedestrian crashes: higher injury severity and mortality rate for light truck vehicles compared with passenger vehicles. *Injury Prevention*, 10(3), pp.154-158.

Serway, R. and Jewett, J., (2012). Principles of physics: a calculus-based text (Volume 1). Brooks Cole, p.171.

Smith, B.W., (2013). Human error as a cause of vehicles crashes [online]. Available at: http://cyberlaw.stanford.edu/blog/2013/12/human-error-cause-vehicle-crashes [Accessed 4th April 2017].

Stapp, J.P., (1970). Voluntary Human Tolerance Levels. In E.S Gurdjian et al, Impact Injury and Crash Protection, Charles C. Thomas.

Sutcliffe, M., (2019). Autodrive Project Lays Foundation for Future CAV use, Fleet News. Available at: https://www.fleetnews.co.uk/smart-transport/features/autodrive-project-lays-foundation-for-future-cav-use [Accessed 9th January 2019].

Sze, N.N. and Wong, S.C., (2007). Diagnostic analysis of the logistic model for pedestrian injury severity in traffic crashes. *Accident Analysis & Prevention*, 39(6), pp.1267-1278.

Tefft, B.C., (2013). Impact speed and a pedestrian's risk of severe injury or death. *Accident Analysis & Prevention*, 50, pp.871-878.

TeslaDeaths, 2020. Tesla Deaths is a record of Tesla accidents that involved a driver, occupant, cyclist, motorcyclist, or pedestrian death, whether or not the Tesla or its driver were at fault. Available at: https://www.tesladeaths.com/ (Assessed 11/06/2020).

Thomas, P., Charles, J. and Fay, P., (1995). Lower limb injuries-The effect of intrusion, crash severity and the pedals on injury risk and injury type in frontal collisions. SAE Technical Paper No. 952728.

Thomson, J.J., (1985). The trolley problem. *The Yale Law Journal*, 94(6), pp.1395-1415.

US NCAP., (2017). Available at: https://www.nhtsa.gov/ratings [Accessed 25th July 2017].

Vahidi, A., Stefanopoulou, A. and Peng, H., (2005). Recursive least squares with forgetting for online estimation of vehicle mass and road grade: theory and experiments, *Vehicle System Dynamics*, 41(1), pp.31-55.

Van Ratingen, M., Williams, A., Lie, A., Seeck, A., Castaing, P., Kolke, R., Adriaenssens, G. and Miller, A., (2016). The European new car assessment programme: a historical review, Chinese journal of traumatology, 19(2), pp.63-69.

Wiggers, K., (2020). Waymo's autonomois cars have driven 20 million miles on public roads. Available at: https://venturebeat.com/2020/01/06/waymos-autonomous-cars-have-driven-20-million-miles-on-public-roads/ [Accessed 9th January 2020].

Wilkinson, J. H., (1965). *The Algebraic Eigenvalue Problem,* Oxford, Clarendon Press.

Wilson, E. 0., (1975). Sociobiology. The New Synthesis, Belknap of Harvard University Press.

Witteman, W., (1999). Improved Vehicle Crashworthiness Design by Control of the Energy Absorption for Different Collision Situations. PhD Thesis, Eindhoven University of Technology, Eindhoven, The Netherlands.

Witteman, W., (2005). Adaptive frontal structure design to achieve optimal deceleration pulses In *Proceedings of the Nineteenth International Technical Conference on Enhanced Safety of Vehicles (ESV)*, Washington DC, USA.

Witteman, W. J. and Kriens, R. F. C., (2001). The necessity of an adaptive vehicle structure to optimize deceleration pulses for different crash velocities. In *Proceedings in the Seventeenth International Technical Conference on Enhanced Safety of Vehicles (ESV),* Amsterdam, Netherlands.

Wragge-Morley, R. T., Herrmann, G., Barber, P. and Burgess, S. C., (2015). Gradient and mass estimation from CAN based data for a light passenger car, *SAE International Journal of Passenger Cars - Mechanical Systems*, 8, pp.137-145.

Yang, X., Liu, L., Vaidya, N.H. and Zhao, F., (2004). A vehicle-to-vehicle communication protocol for cooperative collision warning. In Mobile and Ubiquitous Systems: Networking and Services, 2004: The First Annual International Conference, Boston, USA.

Zaikin, O., Korablin, A., Dyulger, N. and Barnenkov, N., (2017). Model of the Relationship between the Velocity Restitution Coefficient and the Initial Car Velocity during Collision. Transportation Research Procedia, 20, pp.717-723.

Zaseck, L.W., Orton, N.R., Gruber, R., Rupp, J., Scherer, R., Reed, M. and Hu, J., (2017). The influence of personal protection equipment, occupant body size, and restraint system on the frontal impact responses of Hybrid III ATDs in tactical vehicles. Traffic injury prevention, 18(6) pp.642-649.

APPENDIX 1.0
LIST OF ASSUMPTIONS

Throughout the development of the ethical collision system (ECS) proposed in this thesis, a number of key working assumptions have been made. Some of these have already been alluded to above in the foregoing Sections. The main assumptions are documented in the following three sub-sections.

A.1.1 VEHICLE STUCTURE MODELLING

- Autonomous vehicles (AVs) are identically structured (here based on the 2010 Toyota Yaris Sedan)
- Full-frontal collision (i.e. no angle offset and 100% overlap)
- Longitudinal members are geometrically aligned (i.e. same height)
- Collision heat and sound energy are negligible
- Longitudinal road gradient and lateral camber is zero
- AV modelled as a point mass acting at centre of gravity
- Mechanical structure of crumple zones modelled as mass-spring model (damping was initially considered and then removed)
- AV's design deformation is based on testing methods, i.e. United States New Car Assessment Programme (US NCAP)

A.1.2 ASSUMED AUTONOMOUS VEHICLE SYSTEM ATTRIBUTES

- AVs will be fully automatically controlled with compatible advanced driver assisted systems (ADAS) systems
- AVs will have robust vehicle to anything (V2X) communication
- Desired stiffness change for each AV is achievable through the use of smart materials (i.e. active stiffening/softening)

- AV laden masses are known/predicted pre-collision
- AV longitudinal velocities are known/predicted pre-collision
- Weather conditions (e.g. temperature and road friction) are not considered
- No human intervention i.e. human is out of the loop as AVs are driver-less
- Collision has been deemed to be unavoidable and AVs are already aligned for a full-frontal collision
- The smart materials are activated at a short time, denoted Δt, prior to collision and fixed thereafter (i.e. there is no further adjustment of the smart materials during the collision)
- All AVs have identical/compatible ECS

APPENDIX 2.0
INTERNATIONAL PATENT

Summary: A method of managing collisions between a plurality of vehicles in an active collision management system, wherein one or more the of the vehicles has a crash structure whose stiffness can be adjusted, the method comprising the steps of: determining whether a collision event between the plurality of vehicles is to occur based on data measured by one or more object detection sensors; and in the event that a collision event is to occur, for each vehicle: identifying a first crash structure and determining an initial stiffness of the crash structure; determining the mass and/or velocity of the and predicting the amount of energy which would be absorbed by each vehicle in the collision at the determined masses and/or velocities and crash structure stiffness; and subsequently determining a level of aggressivity of the collision based on the predicted energy absorption for each vehicle; identifying a first crash structure whose stiffness can be adjusted, and determining a subsequent stiffness value for the crash structure based on the determined amount of energy to be absorbed by each of the vehicles such that the energy absorbed by the crash structure is changed and the level of aggressivity is reduced; and stiffening the first crash structure to the determined stiffness value.

Details overleaf.

Note: Author name change from James Trollope to James Pickering.

(19) World Intellectual Property Organization
International Bureau

(43) International Publication Date
28 May 2015 (28*05.2015)

WIPOIPCT

WO 2015/075461 A1

(10) International Publication Number
WO 2015/075461 A1

(51) International Patent Classification:
G08G 2/16 (2006.01)

(21) International Application Number:
PCT/GB2014/053442

(22) International Filing Date:
20 November 2014 (20.11.2014)

(25) Filing Language: English

(26) Publication Language: English

(30) Priority Data:
1320489.6 20 November 2013 (20.11.2013) GB

(71) Applicant: COVENTRY UNIVERSITY [GB/GB]; Priory Street, Coventry CV1 5FB (GB).

(72) Inventors: TROLLOPE, James; c/o Coventry University, Priory Street, Coventry, West Midlands CV1 5FB (GB). BURNHAM, Keith; c/o Coventry University, Priory Street, Coventry, West Midlands CV1 5FB (GB).

(74) Agent: WITHERS & ROGERS LLP; 4 More London Riverside, London, Greater London SE1 2AU (GB).

(81) Designated States *(unless otherwise indicated, for every kind of national protection available):* AE, AG, AL, AM, AO, AT, AU, AZ, BA, BB, BG, BH, BN, BR, BW, BY, BZ, CA, CH, CL, CN, CO, CR, CU, CZ, DE, DK, DM, DO, DZ, EC, EE, EG, ES, FI, GB, GD, GE, GH, GM, GT, HN, HR, HU, ID, IL, IN, IR, IS, JP, KE, KG, KN, KP, KR, KZ, LA LC, LK, LR, LS, LU, LY, MA, MD, ME, MG, MK, MN, MW, MX, MY, MZ, NA, NG, M, NO, NZ, OM, PA PE, PG, PH, PL, PT, QA, RO, RS, RU, RW, SA, SC, SD, SE, SG, SK, SL, SM, ST, SV, SY, TH, TJ, TM, TN, TR, TT, TZ, UA UG, US, UZ, VC, VN, ZA ZM, ZW.

(84) Designated States *(unless otherwise indicated, for every land of regional protection available):* ARIPO (BW, GH, GM, KE, LR, LS, MW, MZ, NA, RW, SD, SL, ST, SZ, TZ, UG, ZM, ZW), Eurasian (AM, AZ, BY, KG, KZ, RU, TJ, TM), European (AL, AT, BE, BG, CH, CY, CZ, DE, DK, EE, ES, FI, FR, GB, GR, HR, HU, IE, IS, IT, LT, LU, LV, MC, MK, MT, NL, NO, PL, PT, RO, RS, SE, SL SK, SM, TR), OAPI (BF, BJ, CF, CG, CI, CM, GA GN, GQ, GW, KM, ML, MR, NE, SN, TD, TG).

Published:

— *with international search report (Art. 21(3))*

— *with amended claims and statement (Art. 19(1))*

WO 2015/075461 A1

(54) Title: METHOD OF MANAGING COLLISIONS BETWEEN A PLURALITY OF VEHICLES AND VEHICLE APPLYING SUCH A METHOD

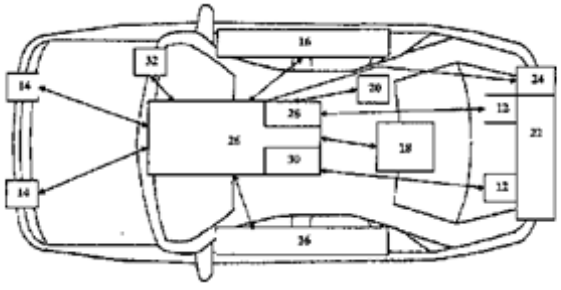

Figure 6

(57) Abstract: A method of managing collisions, the method comprising: identifying a first crash structure 22 and determining an initial stiffness of the crash structure; determining a level of aggressivity of the collision based on the predicted energy absorption for each vehicle; identifying a first crash structure whose stiffness can be adjusted, and determining a subsequent stiffness value for the crash structure based on the determined amount of energy to be absorbed by each of the vehicles such that the energy absorbed by the crash structure is changed and the level of aggressivity is reduced; and stiffening the first crash structure to the determined stiffness value.

APPENDIX 3.0
DEVELOPMENT OF LINEAR NODAL ONE LUMPED PARAMETER MODEL

To begin, consideration is given to a single vehicle, denoted Vehicle a, represented by a point mass, denoted m_a, and moving at an initial velocity, denoted $\vec{v}_a$, as illustrated in Figure A-3-1. Also illustrated in Figure A-3-1, is the coordinate system corresponding to longitudinal and lateral motion, denoted x and y. Note that consideration is limited here to longitudinal motion only. For this single vehicle LPM, it is assumed that the vehicle collides into an immovable rigid wall, i.e. to represent the US NCAP full frontal impact test, as described in Section 3.2.1, Chapter 3. Newton's First Law of Motion states that an object will continue in motion at the same velocity, unless acted upon by a force. In the case of the vehicle of laden mass m_a colliding into the immovable rigid wall at a given velocity, the vehicle will exert a force, denoted f_a applied to the rigid wall, as illustrated in Figure A-3-1. The rigid wall will exert a force equal in magnitude and opposite in sign or direction to that produced by the vehicle. This natural phenomenon is described by Newton's Third Law of Motion, i.e. every action has an equal and opposite reaction. Newton's Second Law of Motion states that the force on an object is proportional to the rate of change of the momentum, i.e. changing velocity, as described in Equation (3-1), Chapter 3. Therefore, the force on the vehicle will be proportional to the rate of change of the velocity (or equivalently the acceleration/deceleration).

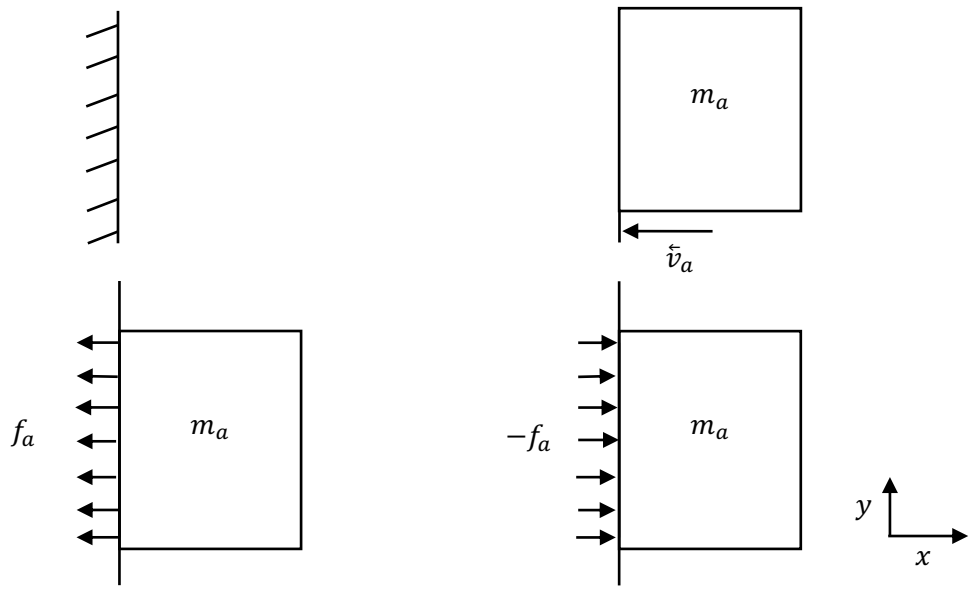

Figure A-3-1: *Vehicle Mass Travelling at a Constant Velocity with a Rigid Wall in Sight (Top) and Vehicle Mass Striking the Rigid Wall Producing a Force (Bottom - Left) and the Rigid Wall Exerting an Equal and Opposite Force (Bottom - Right)*

Figure A-3-2 (top) illustrates a schematic plan view of a vehicle consisting of two symmetrical longitudinal crumple zones about the x-axis, where the spring stiffness elements are denoted k_{a_l} and k_{a_r} for the left and right crumple zones. Since consideration is given to full frontal collisions only and acknowledging the fact that the spring elements are in parallel, each supporting half of the mass, i.e. $\frac{m_a}{2}$, these can be combined such that a single spring stiffness element, i.e. $k_a = k_{a_l} + k_{a_r}$ supports the whole mass, m_a, as illustrated in Figure A-3-2 (middle). The free body diagram of the mass spring model is illustrated in Figure A-3-2 (bottom), where the reaction forces are represented as vectors, i.e. f_{k_a} being the spring stiffness reaction force, with this acting against the force due to acceleration. As a consequence of Newton's Third Law, the reaction force from the rigid wall acting through the longitudinal crumple zones is given by $f_{k_a} = -f_a(t)$, where $f_a(t)$ is proportionally related to the deformation, via $k_a x_a(t)$, i.e.

$$f_a(t) = m_a \frac{dv_a(t)}{dt} = m_a \frac{d^2x_a(t)}{dt^2} = -k_a x_a(t) \tag{A-3-1}$$

giving the following differential equation representation:

$$m_a \frac{d^2x_a(t)}{dt^2} + k_a x_a(t) = f_a(t) \tag{A-3-2}$$

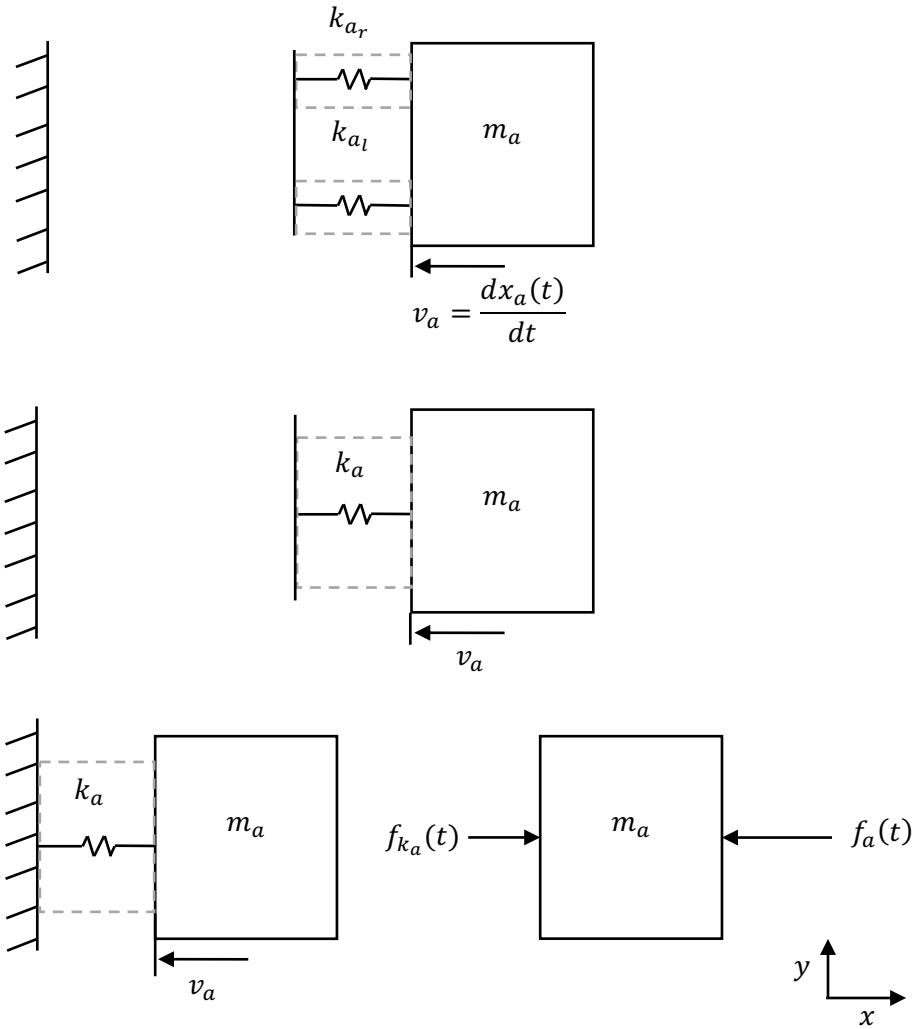

Figure A-3-1: *Vehicle Mass Travelling at a Constant Velocity Consisting of Crumple Zones with a Rigid Wall in Sight (Top), Vehicle Mass Travelling at a Constant Velocity Consisting of Combined Crumple Zones (i.e. $k_a = k_{a_l} + k_{a_r}$) with a Rigid Wall in Sight (Middle) and Single Mass Spring and Damper (Bottom - Left) Indicating Forces (Bottom - Right)*

APPENDIX 4.0
INVESTIGATION INTO VARYING THE MASS DISTRIBUTION OF THE TWO-LINKED MASS SPRING MODEL

A.4.1 TWO LUMPED MASS NODAL MODEL

The two-lumped mass vehicle configuration is illustrated in Figure A-4-1, where m_{a_1} and m_{a_2} correspond to the two masses (such that $m_a = m_{a_1} + m_{a_2}$), k_{a_1} and k_{a_2} correspond to the two stiffness values and v_a corresponds to the initial velocity of the two mass system. The form of the differential equation is given by:

$$M_a \ddot{x}_a + K_a x_a = 0 \tag{A-4-1}$$

where M_a and K_a are matrix quantities, defined such that:

$$\begin{bmatrix} m_{a_1} & 0 \\ 0 & m_{a_2} \end{bmatrix} \ddot{x}_a + \begin{bmatrix} k_{a_1} + k_{a_2} & -k_{a_2} \\ -k_{a_2} & k_{a_2} \end{bmatrix} x_a = 0 \tag{A-4-2}$$

and x_a is now a vector quantity $x_a = \begin{bmatrix} x_{a_1} \\ x_{a_2} \end{bmatrix}$.

Figure A-4-2 corresponds to the vehicle striking the rigid immovable wall at the point where deformation commences beyond the failure point. The free body diagram of the two-lumped mass model is illustrated in Figure A-4-3.

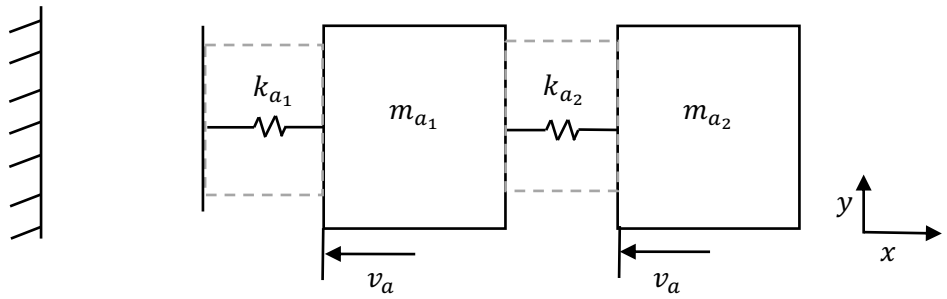

Figure A-4-1: *Two Lumped Mass Vehicle Model Travelling at a Constant Velocity Consisting of Crumple Zones with a Wall in Sight*

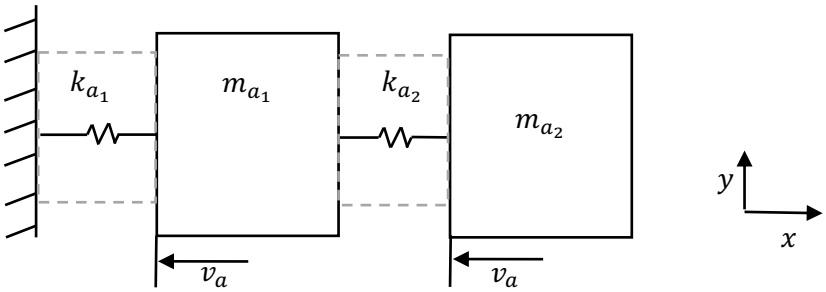

Figure A-4-2: *Two Lumped Mass Vehicle Model Colliding into a Wall*

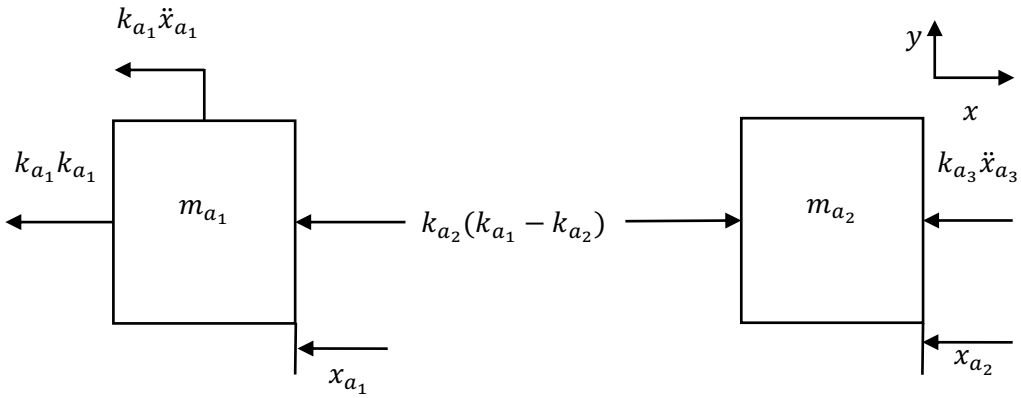

Figure A-4-3: *Two Lumped Mass Vehicle Model Colliding into a Wall and Indicating the Forces*

The two-lumped mass system is now represented by a fourth order dynamic model, which can be configured in the state space form. Setting $\chi_1 = x_a$ and $\chi_2 = \dot{x}_a$, the state space form becomes:

$$\begin{bmatrix} \dot{\chi}_1 \\ \dot{\chi}_2 \end{bmatrix} = \begin{bmatrix} 0 & I \\ \widetilde{K}_a & 0 \end{bmatrix} \begin{bmatrix} \chi_1 \\ \chi_2 \end{bmatrix} \tag{A-4-3}$$

where

$$\widetilde{K}_a = -\begin{bmatrix} \frac{k_{a_1} + k_{a_2}}{m_{a_1}} & \frac{-k_{a_2}}{m_{a_1}} \\ \frac{-k_{a_2}}{m_{a_2}} & \frac{k_{a_2}}{m_{a_2}} \end{bmatrix}$$

and I is the identity matrix of appropriate dimensions (in this case 2 x 2). Note that χ_1, $\chi_2 = \dot{\chi}_1$ and $\dot{\chi}_2$ contain the deformations, velocities and accelerations of the vehicle represented by the two mass system.

A.4.2 INVESTIGATING THE MASS DISTRIBUTION

An investigation into the mass distribution of the two-linked mass-spring model was undertaken, as in (Munyazikwiye, Karimi and Robbersmyr, 2013). The simulation was undertaken using the same procedure as detailed in Section 5.4.3 Chapter 5. The mass distribution is detailed in column one of Table A-4-1, where $m_{a_1} : m_{a_2}$ denotes the mass distribution, with $m_a = m_{a_1} + m_{a_2}$. The results from the study where a zero offset for buckling are detailed in Table A-4-1.

Table A-4-1: *Values of Maximum Deformation Corresponding to Mechanical Damping*

Mass ratio ($m_{a_1} : m_{a_2}$)	**Peak Deformation [m]**	**Peak Acceleration [g]**	**Collision Deformation Energy [kJ]**
FE Simulation	0.5625	51.9269	140.66
10:90	0.7306	57.6433	254.10
20:80	0.7459	46.0875	304.63
30:70	0.7552	43.4370	317.55
40:60	0.7597	48.6349	310.97
50:50	0.7608	53.5351	300.52
60:40	0.7587	56.8901	291.40
70:30	0.7527	50.6641	285.56
80:20	0.7403	62.9307	283.80
90:10	0.7159	60.7108	283.20

APPENDIX 5.0
ONE VEHICLE LOOK-UP TABLES

A.5.1 PEAK DEFORMATION

Vehicle laden mass $[kg]$

$m_a =$

Velocity $[mph]$	1247	m_a x 1.1	$m_a\ x$ 1.2	$m_a\ x$ 1.3	$m_a\ x$ 1.4
15	0.2681	0.2801	0.2915	0.3024	0.3127
25	0.4242	4.42E-01	0.4589	0.4748	0.49
35	0.5632	0.5853	6.06E-01	0.6254	0.6437
45	0.686	0.7108	0.734	0.7555	7.76E-01
55	0.7934	0.8198	0.8441	0.8666	8.87E-01

A.5.2 PEAK ACCELERATION

Vehicle laden mass $[kg]$

$m_a =$

Velocity $[mph]$	1247	m_a x 1.1	$m_a\ x$ 1.2	$m_a\ x$ 1.3	$m_a\ x$ 1.4
15	18.521	17.8021	17.175	16.6239	16.133
25	34.5391	33.4072	32.4271	31.5704	30.8149
35	54.5262	53.1082	51.9095	50.8857	49.9922
45	79.7307	78.2716	77.131	76.182	75.4256
55	111.8175	110.8275	110.1965	109.8417	109.7245

A.5.3 COLLISION ENERGY

Vehicle laden mass $[kg]$

Velocity $[mph]$	$m_a =$ 1247	m_a x 1.1	$m_a\ x$ 1.2	$m_a\ x$ 1.3	$m_a\ x$ 1.4
15	2.80E+04	3.08E+04	3.36E+04	3.64E+04	3.92E+04
25	7.79E+04	8.57E+04	9.35E+04	1.01E+05	1.09E+05
35	1.53E+05	1.68E+05	1.83E+05	1.98E+05	2.14E+05
45	2.52E+05	2.78E+05	3.03E+05	3.28E+05	3.53E+05
55	3.77E+05	4.15E+05	4.52E+05	4.90E+05	5.28E+05

APPENDIX 6.0
DEVELOPMENT OF LINEAR NODAL TWO LPM

As a convenient starting point, each vehicle of the two-vehicle nodal model is modelled with a one-lumped mass and linear spring element, thus each vehicle is effectively modelled as a second order system, with the overall system being of 6th order. Figure A-6-1 (upper) illustrates such a two-vehicle full frontal collision scenario and Figure A-6-1 (lower) illustrates the corresponding free body diagram. Each vehicle is modelled by a single mass, denoted m_a and m_b, and a corresponding spring stiffness, denoted k_a and k_b, with a combined arbitrarily small mass, denoted m_c, representing the contact connection between the two vehicles. Subscripts a and b correspond to Vehicle a and Vehicle b, respectively. Under a full-frontal collision, both spring sections are under compression, where the centre of the mass m_c is basically the datum point, i.e. the point of reference for the two vehicle deformations. Note that the datum point will move within its own reference frame, depending on the final momentum of the combined two-vehicle structure. The degrees of freedom denoted by the deformations are given by x_a, x_c and x_b, corresponding to Vehicle a and b Vehicle and the combined frontal-end mass, which is a datum point with respect to the deformations.

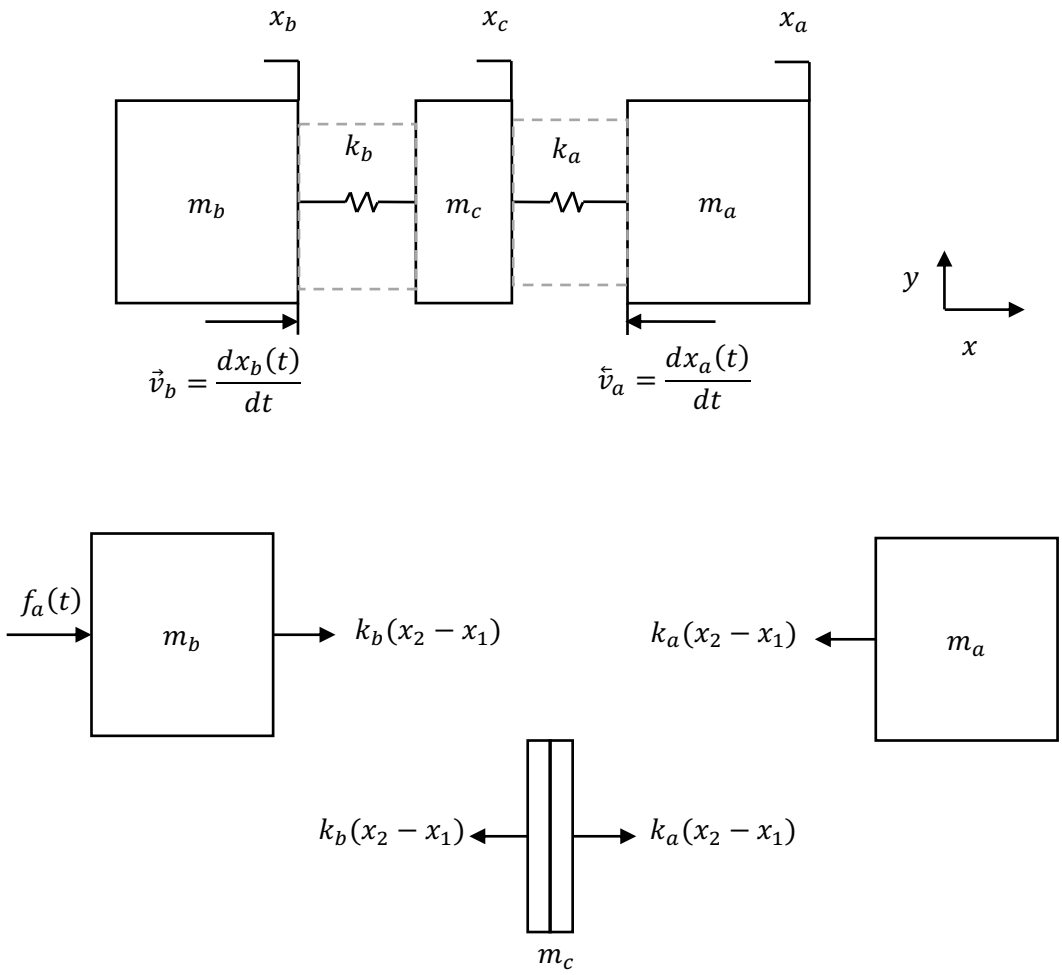

Figure A-6-1: *Illustrating the Two Vehicle Full-Frontal Collision Scenario (Top) and the Two Mass Spring Damper Model Free Body Diagram (Bottom)*

The two-vehicle full frontal collision configuration consisting of the three-mass system of Figure A-6-1 is described by the following coupled differential equations:

$$m_a\ddot{x}_a + k_a(x_a - x_c) = 0 \qquad \text{(A-6-1)}$$

$$m_c\ddot{x}_c + k_a x_a + (k_b - k_a)x_c + k_b x_b = 0 \qquad \text{(A-6-2)}$$

$$m_b\ddot{x}_b + k_b(x_b - x_c) = 0 \qquad \text{(A-6-3)}$$

APPENDIX 7.0
TWO VEHICLE LOOK-UP TABLES

A.7.1 PEAK DEFORMATION: VEHICLE A AND VEHICLE B

Peak Deformation - Vehicle A

		Velocity $[m/s]$				
		6.7056	11.176	15.6464	20.1168	24.5872
Vehicle laden mass $[kg]$	m_a = 1247	0.4243	0.4958	0.5632	0.6266	0.6861
	m_a x 1.1	0.4329	0.5056	5.74E-01	0.6381	0.6982
	m_a x 1.2	0.4406	0.5142	0.5834	0.6482	0.7088
	m_a x 1.3	0.4474	0.5219	0.5918	0.6572	0.7182
	m_a x 1.4	0.4535	0.5288	0.5993	0.6652	0.7265

Peak Deformation - Vehicle B

		Velocity $[m/s]$				
		6.7056	11.176	15.6464	20.1168	24.5872
Vehicle laden mass $[kg]$	m_a = 1247	0.4243	0.4958	0.5632	0.6266	0.6861
	m_a x 1.1	0.4329	0.5056	5.74E-01	0.6381	0.6982
	m_a x 1.2	0.4406	0.5142	0.5834	0.6482	0.7088
	m_a x 1.3	0.4474	0.5219	0.5918	0.6572	0.7182
	m_a x 1.4	0.4535	0.5288	0.5993	0.6652	0.7265

A.7.2 PEAK ACCELERATION: VEHICLE A AND VEHICLE B

Peak Acceleration - Vehicle A

		Velocity $[m/s]$				
		6.7056	11.176	15.6464	20.1168	24.5872
Vehicle laden mass $[kg]$	m_a = 1247	34.55	4.40E+01	54.533	66.3923	79.7436
	m_a x 1.1	35.6065	45.3965	56.3918	68.7849	82.7829
	m_a x 1.2	36.5575	46.6783	58.0754	70.9586	85.5537
	m_a x 1.3	37.4188	47.8419	59.6083	72.9431	88.0907
	m_a x 1.4	38.203	48.9037	61.0104	74.7626	90.4225

Peak Acceleration - Vehicle B

		Velocity $[m/s]$				
		6.7056	11.176	15.6464	20.1168	24.5872
Vehicle laden mass $[kg]$	$m_a =$ 1247	34.55	43.9774	54.533	66.3923	79.7436
	m_a x 1.1	32.3695	41.2696	51.2653	62.5317	75.2573
	m_a x 1.2	30.4646	38.8985	48.3962	59.1321	71.2947
	m_a x 1.3	28.7838	36.8015	45.8526	56.1101	67.762
	m_a x 1.4	27.2878	34.9312	43.5789	53.4019	64.5875

A.7.3 COLLISION ENERGY: VEHICLE A AND VEHICLE B

Collision Energy - Vehicle A

		Velocity $[m/s]$				
		6.7056	11.176	15.6464	20.1168	24.5872
Vehicle laden mass $[kg]$	$m_a =$ 1247	7.79E+04	1.12E+05	1.53E+05	1.99E+05	2.52E+05
	m_a x 1.1	8.16E+04	1.18E+05	1.60E+05	2.09E+05	2.64E+05
	m_a x 1.2	8.50E+04	1.22E+05	1.67E+05	2.18E+05	2.75E+05
	m_a x 1.3	8.81E+04	1.27E+05	1.73E+05	2.25E+05	2.85E+05
	m_a x 1.4	9.09E+04	1.31E+05	1.78E+05	2.33E+05	2.94E+05

Collision Energy - Vehicle B

		Velocity $[m/s]$				
		6.7056	11.176	15.6464	20.1168	24.5872
Vehicle laden mass $[kg]$	$m_a =$ 1247	7.79E+04	1.12E+05	1.53E+05	1.99E+05	2.52E+05
	m_a x 1.1	8.16E+04	1.18E+05	1.60E+05	2.09E+05	2.64E+05
	m_a x 1.2	8.50E+04	1.22E+05	1.67E+05	2.18E+05	2.75E+05
	m_a x 1.3	8.81E+04	1.27E+05	1.73E+05	2.25E+05	2.85E+05
	m_a x 1.4	9.09E+04	1.31E+05	1.78E+05	2.33E+05	2.94E+05

APPENDIX 8.0
STIFFNESS CONTROLLER LOOK-UP TABLES

A.8.1 PEAK DEFORMATION STIFFNESS CHANGES

$0.50 * k_a, where\ k_a = 8323{,}33 k/N$

Velocity $[mph]$	$m_a = 1247$	$m_a * 1.1$	$m_a * 1.2$	$m_a * 1.3$
15	0.3671	0.383	0.398	0.4122
25	0.5678	0.5901	0.6109	0.6304
35	0.7362	0.7619	0.7856	0.8077
45	0.8747	0.9016	0.9259	0.9482

$0.75 * k_a$

Velocity $[mph]$	$m_a = 1247$	$m_a * 1.1$	$m_a * 1.2$	$m_a * 1.3$
15	0.3059	0.3194	0.3322	0.3444
25	0.4799	0.4996	0.5181	0.5356
35	0.6316	0.6554	0.6775	0.6983
45	0.7624	0.7884	0.8125	0.8347

$1.00 * k_a$

Velocity $[mph]$	$m_a = 1247$	$m_a * 1.1$	$m_a * 1.2$	$m_a * 1.3$
15	0.2681	0.2801	0.2915	0.3024
25	0.4242	0.4421	0.4589	0.4748
35	0.5632	0.5853	0.606	0.6254
45	0.686	0.7108	0.734	0.7555

$1.25 * k_a$

Velocity [mph]	$m_a = 1247$	$m_a * 1.1$	$m_a * 1.2$	$m_a * 1.3$
15	0.2417	0.2527	0.2631	0.273
25	0.3847	0.4011	0.4167	0.4315
35	0.5138	0.5345	0.5539	0.5722
45	0.6296	0.6534	0.6755	0.6961

$1.5 * k_a$

Velocity [mph]	$m_a = 1247$	$m_a * 1.1$	$m_a * 1.2$	$m_a * 1.3$
15	0.222	0.2321	0.2417	0.2509
25	0.3547	0.3701	0.3847	0.3985
35	0.4759	0.4954	0.5138	0.5311
45	0.5857	0.6084	0.6296	0.6495

A.8.2 PEAK HEAD ACCELERATION STIFFNESS CHANGES

$0.50 * k_a$

Velocity [mph]	$m_a = 1247$	$m_a * 1.1$	$m_a * 1.2$	$m_a * 1.3$
15	14.7759	14.2556	13.8041	13.4082
25	29.1299	28.381	27.7477	27.2041
35	49.0641	48.3702	47.8433	47.4481
45	77.3567	77.3809	77.6102	78.0316

$0.75 * k_a$

Velocity [mph]	$m_a = 1247$	$m_a * 1.1$	$m_a * 1.2$	$m_a * 1.3$
15	17.3264	16.6755	16.1094	15.6118
25	32.9653	31.968	31.1063	30.3613
35	53.2487	52.0881	51.1193	50.3177
45	79.9426	78.9867	78.3102	77.8328

$1.00 * k_a$

Velocity [mph]	$m_a = 1247$	$m_a * 1.1$	$m_a * 1.2$	$m_a * 1.3$
15	19.5026	18.7456	18.0852	17.505
25	36.3697	35.1778	34.1458	33.2436
35	57.416	55.923	54.6607	53.5827
45	83.9565	82.42	81.2189	80.2197

$1.25 * k_a$

Velocity [mph]	$m_a = 1247$	$m_a * 1.1$	$m_a * 1.2$	$m_a * 1.3$
15	21.434	20.5834	19.8401	19.1862
25	39.4478	38.0823	36.9024	35.8707
35	61.3534	59.599	58.0939	56.7878
45	88.2039	86.2674	84.6557	83.294

$1.5 * k_a$

Velocity [mph]	$m_a = 1247$	$m_a * 1.1$	$m_a * 1.2$	$m_a * 1.3$
15	23.1892	22.2503	21.434	20.7157
25	42.2664	40.7557	39.4478	38.3009
35	65.0444	63.0509	61.3534	59.8701
45	92.4046	90.1268	88.2039	86.5466

A.8.3 PEAK CHEST ACCELERATION STIFFNESS CHANGES

$0.50 * k_a$

Velocity $[mph]$	$m_a = 1247$	$m_a * 1.1$	$m_a * 1.2$	$m_a * 1.3$
15	11.6608	11.2501	10.8938	10.5814
25	22.9886	22.3975	21.8978	21.4688
35	38.7201	38.1725	37.7567	37.4448
45	61.0479	61.067	61.2479	61.5805

$0.75 * k_a$

Velocity $[mph]$	$m_a = 1247$	$m_a * 1.1$	$m_a * 1.2$	$m_a * 1.3$
15	13.6735	13.1598	12.7132	12.3204
25	26.0153	25.2283	24.5483	23.9603
35	42.0225	41.1066	40.342	39.7094
45	63.0886	62.3343	61.8003	61.4236

$1.00 * k_a$

Velocity $[mph]$	$m_a = 1247$	$m_a * 1.1$	$m_a * 1.2$	$m_a * 1.3$
15	15.3909	14.7935	14.2724	13.8145
25	28.702	27.7614	26.947	26.235
35	45.3112	44.133	43.1368	42.2861
45	66.2562	65.0437	64.0958	63.3073

$1.25 * k_a$

Velocity $[mph]$	$m_a = 1247$	$m_a * 1.1$	$m_a * 1.2$	$m_a * 1.3$
15	16.9151	16.2439	15.6573	15.1412
25	31.1311	30.0535	29.1224	28.3082
35	48.4185	47.034	45.8462	44.8155
45	69.6082	68.08	66.8081	65.7335

$1.5 * k_a$

Velocity $[mph]$	$m_a = 1247$	$m_a * 1.1$	$m_a * 1.2$	$m_a * 1.3$
15	18.3003	17.5593	16.9151	16.3483
25	33.3555	32.1633	31.1311	30.2261
35	51.3313	49.7581	48.4185	47.2479
45	72.9233	71.1257	69.6082	68.3003

APPENDIX 9.0
LIST OF PUBLICATIONS

Note: Author name change from James Trollope to James Pickering.

Pickering, J.E., Podsiadly, M. and Burnham, K.J., 2019. A Model-to-Decision Approach for the Autonomous Vehicle (AV) Ethical Dilemma: AV Collision with a Barrier/Pedestrian (s). *IFAC-PapersOnLine*, *52*(8), pp.257-264.

Pickering, J.E., Ashman, P., Gilbert, A., Petrovic, D., Warwick, K. and Burnham, K.J., 2018, September. Model-to-Decision Approach for Autonomous Vehicle Convoy Collision Ethics. In *2018 UKACC 12th International Conference on Control (CONTROL)* (pp. 301-308). IEEE.

Pickering, J.E., Podsiadly, M., Ashman, P. and Burnham, K.J., 2018. Machine Ethics for Autonomous Vehicle Collisions. In *IACAP–Annual Meeting*.

Trollope, J. Burnham, K. (8 – 10th September 2015). Altruistic Decision-Making Algorithm for Controlled Collisions. Proc. 24th International Conference on Systems Engineering, Coventry, UK

Trollope, J. Burnham, K. (24 - 29th August 2014). Modelling Vehicle Body Structures for Active Buckling Control. Proc. The 19th World Congress of the International Federation of Automatic Control (IFAC), Cape Town, South Africa

Trollope, J. Burnham, K. (19-21st August 2014). Hybrid identification of bilinear model in the presence of uncertainty and absence of sufficient data. Proc. 23rd International Conference on Systems Engineering, Las Vegas, USA

Trollope, J. Burnham, K. (8 - 11th July 2014). Active Buckling Control for Vehicle Body Structures: A Fuzzy Logic Approach for Collision Energy Distribution. Proc. UKACC 10th International Conference on Control (Control 2014), Loughborough, UK

Trollope, J. Burnham, K. (29th – 31st July 2013). Collision Energy Mitigation through Active Control of Future Lightweight Vehicle Architectures. Proc. 10th International Conference on Informatics in Control, Automation and Robotics, Reykjavik, Iceland

Trollope, J. Burnham, K. (1st - 4th July 2013). An Operational Research Approach to Active Control for Mechanical Structures. Proc. 26th European Conference on Operational Research, Rome, Italy

Trollope, J. Burnham, K. (6 - 9th June 2013). Actively Controlled Materials for Structures. Proc. 13th British Polish Workshop, Srebrna Gora, Poland

Trollope, J. Burnham, K. (2013). Active Buckling Control for Future Lightweight Vehicle Body Structures. Journal of Measurement and Control. 46 (10), 315-320